HIGHWAY RESEARCH
RECORD

Number 60

Rigid Pavement Design
1963
10 Reports

HIGHWAY RESEARCH BOARD
OF THE
NATIONAL ACADEMY OF SCIENCES —
NATIONAL RESEARCH COUNCIL

HIGHWAY RESEARCH RECORD 60
RIGID PAVEMENT DESIGN: 1963

This 168-page book contains ten papers presented at the 43rd Annual Meeting of the Highway Research Board, as follows:

"An Extension of Rigid Pavement Design Methods," by W. R. Hudson and B. F. McCullough.

"Temperature Variations in a Cement Concrete Pavement and the Underlying Subgrade," by V. Venkatasubramanian.

"Evaluating Subgrade Friction-Reducing Mediums for Rigid Pavements," by A. G. Timms.

"Tests of Concrete Pavement Slabs on Cement-Treated Subbases," by L. D. Childs.

"Moving Load Test on Experimental Prestressed Concrete Highway Slab," by John R. Smith and Richard K. Lightholder.

"Load Tests on Thin Pretensioned Pavement Slabs," by A. P. Christensen and R. L. Janes.

"Load Tests on Post-Tensioned Pavement Slabs," by A. P. Christensen.

"Tests of Reinforcement Splices for Continuously-Reinforced Concrete Pavement," by Henry A. Lepper, Jr., and Jai B. Kim.

"Behavior of Experimental Continuously-Reinforced Concrete Pavements in Mississippi," by Silvio J. Spigolon.

"Construction of a Continuously-Reinforced Concrete Pavement in South Dakota," by Robert A. Crawford and Donald W. Anderson.

Price: $3.00   December 1964

Contents

An Extension of Rigid Pavement Design Methods

W. R. HUDSON and B. F. MC CULLOUGH

Respectively, Supervising Design Research Engineer and Design Research Engineer, Texas Highway Department

This paper verifies and extends certain developments in the AASHO Interim Pavement Design Guide. A choice of mathematical models is made based on studies of the AASHO and Maryland Road Tests' stress data as well as data from in-service pavements.

As an extension of the initial work, the design thickness equation is expanded to include the concrete modulus of elasticity, total traffic, and pavement continuity (jointed or continuous). A nomograph is presented that allows a quick solution to the expanded equation.

A new design chart is presented for design of the reinforcing steel in jointed reinforced pavements. In addition, a nomograph for solving bar spacing and bar size is included.

•IN 1920, A. I. Goldbeck and Clifford Older independently developed formulas for approximating the stresses in concrete pavements. The best known of these formulas is generally called the "corner formula" and was the basis for rigid pavement design for many years. Results of the Bates Road Test in 1922-23 appeared to confirm the original corner formula. In 1926, H. M. Westergaard completed his treatise on the analysis of stresses in concrete pavements (1). It was concerned with the determination of maximum stresses in slabs of uniform thickness for three load conditions under several limiting assumptions (2). The Westergaard equation for corner stresses has become the definitive design equation for portland cement concrete pavements. In this equation, Westergaard includes the following variables:

P = wheel load, in lb;
h = the thickness of the concrete slab, in in.;
μ = Poisson's ratio for concrete;
E = Young's modulus of elasticity for the concrete in psi;
k = subgrade modulus in pci; and
a = radius of area of load contact, in in.

Using this same general equation form, slightly different design equations have been developed by Spangler (3), Kelly (4), and Pickett (5). These equations are empirical or semi-empirical, but all retain the basic form of the Westergaard simplified theory.

All of these design equations are based on static loading. This is necessary because very little theory exists to describe time dependent variables such as dynamic loads.

Road Test Results Used in Design

Three large-scale road tests have been conducted involving portland cement concrete pavement—the Bates Road Test, 1922; the Maryland Road Test, 1950; and the AASHO Road Test, 1958-61. All three have added valuable information to our knowledge of concrete pavement performance. Only the AASHO Road Test, however, was large

enough to provide us with adequate information on which to base dynamic design equations. The first objective of the Road Test as outlined by the Advisory Committee (6) was:

> To determine the significant relationship between the number of repetitions of specified axle loads of different magnitude and arrangement and the performance of different thicknesses and uniformly designed and constructed asphaltic concrete, plain portland cement concrete, and reinforced portland concrete surfaces. ....

In addition to basic performance data, the AASHO Road Test also provided an opportunity to measure strains in concrete pavements under dynamic loads, and thus provide a mechanistic tie from these pavements to future designs.

Development of AASHO Design Guide

The AASHO Operating Committee on Design appointed a working subcommittee on pavement design. The job of the subcommittee was to adapt the data from the AASHO Road Test to use in design procedures for asphaltic concrete pavements and portland cement concrete pavements.

It was the unanimous opinion of the subcommittee that there are substantial factors to be considered in a design procedure that are not available as variables in the AASHO Road Test results. Four of these factors are (a) the length of test time relative to the normal life of the pavement being designed; (b) climatic and geologic differences between the conditions at the Road Test site and other geographic regions; (c) the need for a guide in designing pavement types not included in the Road Test, such as continuously-reinforced portland cement concrete pavements; and (d) expansion of the Road Test results to various other materials such as low-modulus concrete and stabilized bases.

It was decided that the AASHO Road Test performance equations should form the basis for the AASHO Rigid Pavement Interim Design Guide to add these additional factors.

The Interim Design Guide was developed as a guide for use in developing more exact design procedures. The committee was very deliberate in its efforts to provide for future improvements in the work as additional information became available. The guide (7) states that:

> The above design equations are based on fixed values for certain elements that are obviously important in the design of rigid pavement. These elements include thickness and quality of subbase environmental effects, variations in the amount of load transfer at transverse joints, and the effects of joint elimination through continuous reinforcement. It is expected the design equations will be further modified in the future as experience is gained and these elements are evaluated.

PRESENTATION OF GUIDE

Scope

It is felt that a detailed list of parameters should be incorporated into a rigid pavement structure analysis. The Rigid Guide presents a procedure that encompasses most of these parameters and allows the engineer to design the pavement structure from the subgrade up. Basically the Guide separates the design into four phases—slab dimensions, reinforcement, joints, and slab support control. The first two phases are handled by formulas and will be discussed; the latter two are not discussed.

Slab Dimensions.—The Guide's approach to pavement structure design is a combination of theoretical and empirical relations. The design parameters covered by the various theoretical analyses previously discussed are loading factor magnitude and tire pressure; support media strength; concrete properties—strength, modulus of elasticity, Poisson's ratio; and continuity (load transfer). Whereas, the final equation for the rigid pavement research phase of the AASHO Road Test encompassed the load applica-

tion factor as well as the following parameters: loading factor magnitude, repetitions, and axle type. In this case, the concrete properties, subgrade support and other design factors were fixed parameters and their effect cannot be evaluated by the AASHO Road Test equation.

The AASHO Subcommittee for Rigid Pavement Design combined the two approaches into one equation. The parameters encompassed by the combined methods are loading factor magnitude, repetitions, tire pressure, and axle type; support media strength; concrete properties' strength, modulus of elasticity, and Poisson's ratio; continuity (load transfer); support media friction; and regional factors, i.e., weather, temperature, etc.

Reinforcement.—Steel reinforcement is placed in the slab for the purpose of holding any cracks that form in the pavement tightly closed, enabling the pavement to perform as an integral structural unit. The Guide covers the design of two basic types of reinforced concrete pavement, i.e., jointed-reinforced and continuously-reinforced. Each requires an individual procedure.

The reinforcement for the jointed concrete pavement is determined by the application of the conventional "subgrade drag theory." In essence, the formula is based on the principle of balancing the slab's resistance to movement against the tensile strength of the steel.

The design method for continuously-reinforced concrete pavement is based on the concept of balancing the internal concrete stresses developed by temperature and shrinkage against the tensile strength of steel (10).

Development of Thickness Equation

Two general approaches were open for use in the Guide to combine the Road Test equation and theory, (a) use of theoretical formuli as the basic design form modified by the load term in the final answer for repetitions, and (b) use of the Road Test equation as a valid basis adding modifications from theory for variations in physical constants.

The second approach was selected as the more valid because it depends on the Road Test results for its starting point and uses theory for determining variations in the basic equation. Also at the Road Test, failure was not defined as cracking (overstress), but as a specific reduction in serviceability that usually did not occur until after initial cracking.

After a cursory examination of the available information, the Spangler equation was selected for use in the design equation because of its simplicity and because it showed a good correlation with Road Test measurements. It was stated in the Guide that, "one point of merit in this approach is that if a better stress equation is found, it can be incorporated into the design method with very little revision. ...."

After selecting the Spangler equation for modifying concrete properties, there were two possible choices for inserting it into the general AASHO equation, (a) obtaining a ratio of the selected concrete properties to those at the AASHO Road Test and making it an additive term to the AASHO equation, or (b) modifying the term in general equation to include various concrete properties. The committee selected the first alternative and derived the following equations:

When the terminal serviceability index (p) = 2.0:

$$\log W_t = 7.35 \log (D_2 + 1) + \frac{G_t}{\beta} - 0.06 +$$
$$3.58 \log \left[\frac{S_c' (D_2^{0.75} - 1.132)}{690 \left(D_2^{0.75} - \frac{18.416}{Z^{0.25}} \right)} \right] \qquad (1)$$

When the terminal serviceability index (p) = 2.5:

$$\log W_t = 7.35 \log (D_2 + 1) + \frac{G_t}{\beta^7} - 0.06 +$$
$$3.42 \log \left[\frac{S_c (D_2^{0.75} - 1.132)}{690 \left(D_2^{0.75} - \frac{18.416}{z^{0.25}} \right)} \right] \quad (2)$$

Discussion of Design Charts

Design nomographs that solve for the thickness of jointed-concrete pavement and the reinforcement requirements for both jointed and continuous-concrete pavement are presented in the Guide.

Thickness. — In deriving the nomograph for pavement thickness, the AASHO Road Test values for the modulus of elasticity and load transfer characteristics were fixed to solve the equation. This eliminates these factors as variables, hence the chart has variable scales only for traffic, working stress, and subgrade support. The chart, therefore, is not applicable to continuous concrete pavements or low modulus concrete pavements. Furthermore, the traffic scale is in terms of equivalent daily 18-kip single-axle load applications for a 20-yr traffic analysis. The daily traffic approach is restricting because the analysis is for fixed time period, and is difficult to use for other time periods or for evaluating the life of an existing pavement structure.

Reinforcement. — The chart solution for reinforcement in jointed pavements is in graphic rather than nomographic form. The graphic solution has variable scales for pavement thickness, slab length, and working stress; but the graph is limited to the solution for a fixed friction factor.

The chart solution for reinforcement in continuously-reinforced concrete pavement is flexible in that all the parameters involved in the design equation are included as variables on the nomograph.

DEVELOPMENT OF NEW EQUATION

The design equation developed for the AASHO Design Guide was a first attempt to utilize the AASHO Road Test data in pavement design. The equation is cumbersome and several assumptions were made early in its development (7). Other refinements were omitted from the equation that would make it a more useable formula under actual conditions.

The purposes of this investigation are to (a) simplify the design equation if possible, (b) investigate and clarify several of the assumptions made in the early development, and (c) include any additional refinements in the equation that can be developed from present data.

The equation developed herein has the following variations from the original equation: (a) the Road Test stress data are used to verify the selection of a theoretical model, (b) traffic is used as the total expected number of equivalent 18-kip application (Σ L) over the life of the pavement (design period), (c) the term for pavement continuity is evaluated and extended to continuously reinforced pavements, and (d) the use of terms for both modulus of elasticity and subgrade modulus is encouraged.

Model Selection

In order to select a model for combining theory with Road Test performance data, the Road Test strain data (2) were compared with various modifications of the Westergaard theory. The table in Figure 1 gives the equations that were examined and the correlation obtained. It can be seen that Spangler's equation fits the data as well as any of the more complicated equations.

It should be noted that the data fitting does not support nor deny the theoretical formulation of ℓ (radius of relative stiffness), because none of the factors involved in the radius of relative stiffness, because none of the factors involved in the radius of rela-
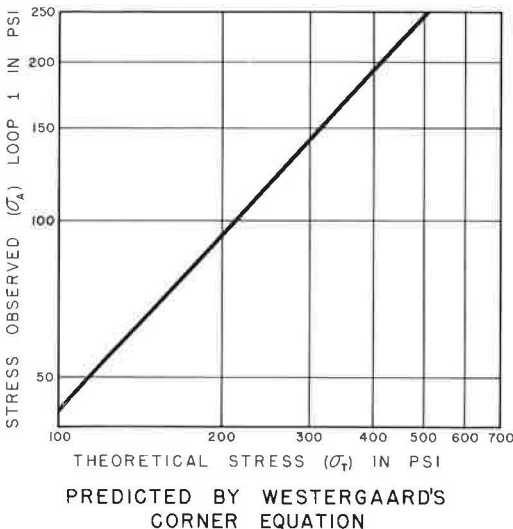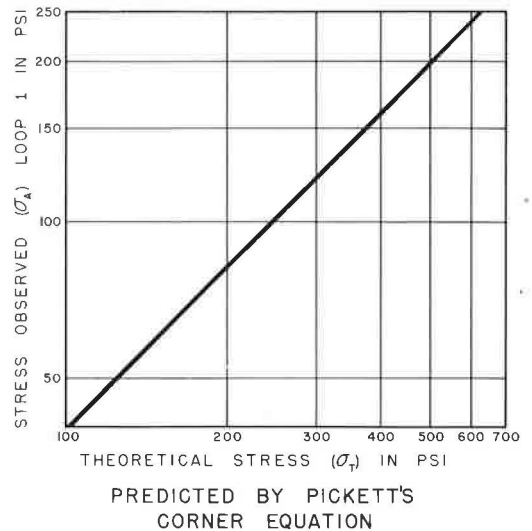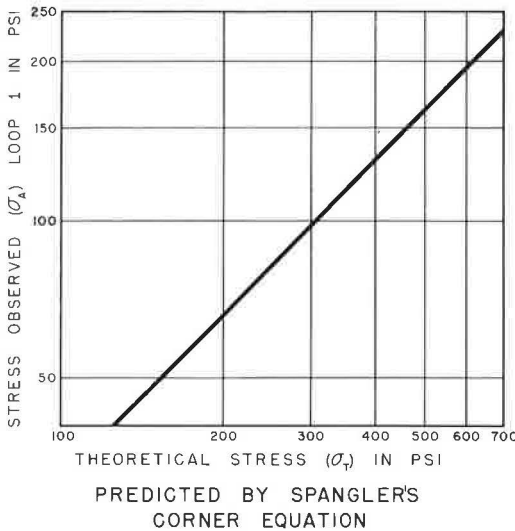
tive stiffness, i.e., E, k, or μ, were varied at the Road Test in a manner allowing proper analysis.

After considering the fit of the data, the Spangler equation was selected. Figure 1 shows the correlation between Spangler, Westergaard, Pickett, and the Road Test stresses as calculated from corner load strains, Loop 1, AASHO Road Test (2). The following equation was selected as a result of the correlation.

$$\log \sigma_{18} = 1.010 \log \sigma_{sp} - 0.521 \tag{3}$$

in which:

σ_{18} = stress calculated from strains measured under an 18-kip single-axle vibratory load on Loop 1, AASHO Road Test, psi.

PREDICTED BY SPANGLER'S
CORNER EQUATION

PREDICTED BY PICKETT'S
CORNER EQUATION

PREDICTED BY WESTERGAARD'S
CORNER EQUATION

EQUATION FOR PREDICTING CORNER STRESS OBSERVED AT THE AASHO ROAD TEST IN TERMS OF A THEORETICAL STRESS:

$$\sigma_A = A\sigma_T{}^B$$

WHERE:
σ_A = STRESSES OBSERVED LOOP 1 - AASHO ROAD TEST
σ_T = THEORETICAL STRESSES
A & B = CORRELATION CONSTANTS
r^2 = CORRELATION COEFFICIENT

	A	B	r^2
SPANGLER'S EQUATION	.301	1.010	0.999
PICKETT'S EQUATION	.389	1.006	0.999
WESTERGAARD'S CORNER EQUATION	.309	1.078	0.999

Figure 1. Theoretical stresses compared with observed stresses on Loop 1, AASHO Road Test.

σ_{sp} = stress predicted by the Spangler equation for a 9,000-lb wheel load (18-kip single-axle), psi.

Modifying the Road Test Equation

A study by W. R. Hudson and F. Scrivner (8) showed excellent correlation between observed stresses at the Road Test, slab thickness, and log W, i.e., the number of load applications carried. To extend the study and obtain a correlation of the form needed in this work, a correlation of the term $(D + 1)$ with observed corner load stresses on the Road Test Loop 1 was developed (Fig. 2). The resulting equation (Eq. 4) has a coefficient of determination (r^2) of 0.999.

$$\log (D + 1) = 1.995 - 0.517 \log \sigma_{18} \tag{4}$$

Substituting Eq. 3 into Eq. 4 gives:

$$\log (D + 1) = 1.995 - 0.517 (1.010 \log \sigma_{sp} - 0.521) = 2.264 - 0.522 \log \sigma_{sp} \tag{5}$$

In a preliminary report (11) the Road Test equation is developed in terms of ΣL (accumulated equivalent 18-kip single-axle loads).

The equation becomes:

$$\log \Sigma L = 7.35 \log (D + 1) - 0.06 + \frac{G}{\beta'} \tag{6}$$

in which

$$G = \frac{4.5 - P_t}{3.0}$$

$$\beta' = 1 + \frac{1.624 \times 10^7}{(D + 1)^{8.46}}$$

$$\log \rho = 7.35 \log (D + 1) - 0.06$$
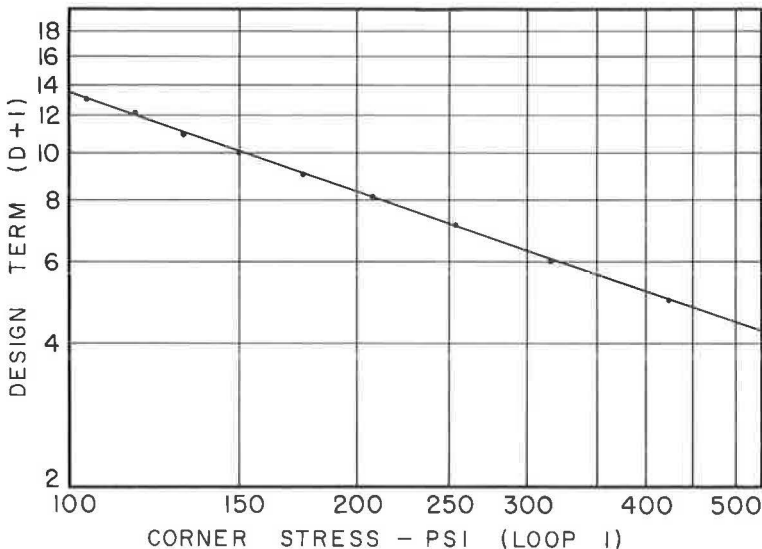
P_t = serviceability at end of time, t.

Figure 2. Correlating design term (D+1) with corner load stresses on Loop 1.

In this equation β' is a curvature parameter, and ρ is a design function as shown when the equation is in the form:

$$G = \beta' \left[\log \Sigma L - \log \rho \right] \tag{7}$$

This being the case, and because $(D + 1)$ exerts a large influence on $\log \Sigma L$ through the ρ term and only a weak influence through the β term, it was decided to substitute σ for $(D + 1)$ in the ρ term only. Therefore, substituting Eq. 5 into Eq. 6 gives:

$$\log \Sigma L = 7.35 \left[2.264 - 0.522 \log \sigma_{sp} \right] - 0.06 + \frac{G}{\beta} \tag{8}$$

This equation obtains for pavements of a fixed strength, S_C, (28 day) for AASHO Road Test pavements was constant at 690 psi ± random variations. Previous design equations have relied on the σ/S_C ratio as the measure of adequate design. Work done for the AASHO Interim Rigid Pavement Design Guide related this ratio to pavement life in terms of $\log \Sigma L$. This can be stated as follows:

It can be assumed that $\log \Sigma L$ is a function of the σ/S_C ratio; and that when an increased σ is matched by an increased S so that the ratio $\sigma x/S_x$ remains equal to the ratio σ/S_C, no change in ΣL would result. Therefore, the rate of change of ΣL as S_C changes is inversely proportional to the rate of change of $\log \Sigma L$ as σ changes.

Inserting strength into Eq. 8 as such an inverse ratio with the fixed strength of the Road Test pavements (690 psi) the following is obtained:

$$\log \Sigma L = 7.35 \left[2.264 - 0.522 \log \left(\frac{\sigma_{sp}^{690}}{S_x} \right) \right] - 0.06 + \frac{G}{\beta} \tag{9}$$

The Spangler equation for stress has the form,

$$\sigma_{sp} = \frac{J P}{D^2} \left(1 - \frac{a_1}{\ell} \right) \tag{10}$$

Substituting the full Spangler equation, σ_{sp}, expanding and combining terms obtains:

$$\log \Sigma L = -9.483 - 3.837 \log \left(\frac{J}{S_x D^2} \left[1 - a_1/\ell \right] \right) + \frac{G}{\beta} \tag{11}$$

in which

$$\ell = \left[\frac{Z D^3}{12 (1 - \mu^2)} \right]^{0.25}$$

In order to simplify the design equation and without damage to the theory, Poisson's ratio (μ) is fixed at a value of 0.20, resulting in a simplied form for the radius of relative stiffness: $\ell = (Z D^3/11.52)^{0.25}$. Taking $a_1 = a \sqrt{2}$ and substituting for ℓ and a_1, Eq. 11 becomes

$$\log \Sigma L = -9.483 - 3.837 \log \left(\frac{J}{S_x D^2} \left[1 - \frac{2.61a}{Z^{1/4} D^{3/4}} \right] \right) + \frac{G}{\beta} \tag{12}$$

in which

ΣL = number of accumulated equivalent 18-kip single-axle loads
J = a coefficient dependent on load transfer characteristics or slab continuity

S_X = modulus of rupture of concrete at 28 days (psi)
D = nominal thickness of concrete pavement (inches)
Z = E/k
E = modulus of elasticity for concrete (psi)
k = modulus of subgrade reaction (psi/inch)
a = radius of equivalent loaded area = 7.15 for Road Test 18-kip axles

$$G = \frac{P_0 - P_t}{3} = \frac{4.5 - P_t}{3}$$

$$\beta = 1 + \frac{1.624 \times 10^7}{(D + 1)^{8.46}}$$

At this point, a so-called life term must be inserted into the design equation. The life term will simply serve to modify the life of a pavement section as predicted by Road Test equation (a 2-yr test). Studies of existing pavements in Texas and Illinois, among others, have established this fact. A substitution of the Road Test values for parameters in Eq. 12 would reduce it back to the basic Road Test equation. Performance studies now being conducted in Texas have indicated that the logarithm of the predicted applications obtained by the Road Test equation must be reduced by a factor of 0.896. The AASHO Subcommittee on Rigid Pavement Design in effect reduced the logarithm of the predicted applications by a factor of 0.935 by using a safety factor (0.75 of the concrete strength for a working stress). Although the use of a safety factor to reduce the working stress is satisfactory, the use of a life term was adopted because future results of performance studies will undoubtedly provide a better estimate of the true factor and such values can be used to replace the trial value.

In determining the magnitude of the life factor both the Design Guide and the Texas performance studies were given equal consideration and an average factor of 0.9155 was selected.

Application of the life factor to the right side of Eq. 12 gives:

$$\log \Sigma L = -8.682 - 3.513 \log \left(\frac{J}{S_X D^2} \left[1 - \frac{2.61a}{Z^{1/4} D^{3/4}} \right] \right) + 0.915 \frac{G}{\beta} \tag{13}$$

Only one term in Eq. 13 has not been evaluated adequately, the continuity or J term. The selection of a value, J, for design purposes must now be postulated on the basis of limited data. The J value for the jointed pavements on the Road Test is automatically fixed at the value of 3.2 that was used in all correlation work. For the present, this value shall be assumed to apply for all jointed-concrete pavements with adequate load transfer. A J value of 2.2 was selected for continuously-reinforced concrete pavements based on comparisons of previous design procedures and performance studies. This value also gives answers that are compatible with the recommendations in the AASHO Design Guide.

Graphical Solution

Using this equation, it is particularly hard to solve for concrete pavement thickness D. It is a very simple matter, however, to program this equation on a computer and solve for ΣL using all combinations of the other variables. The resulting output is useful in the form of tables. These tables can be combined graphically into a very useful nomograph (Fig. 3). The nomograph is for a final serviceability level of 2.5. Evaluation of terminal serviceability throughout the United States has shown that an acceptable level for the final or terminal condition of an Interstate pavement is 2.2 - 2.5. The Texas Highway Department has settled on 2.5 for use in design of such pavements. For design of lower class roads a terminal serviceability of 1.5 is felt to be satisfactory.

Use of the Nomograph. — The examples on the chart show how typical design problems may be handled. Certain information is normally fixed by the conditions at the site or by arbitrary choice.
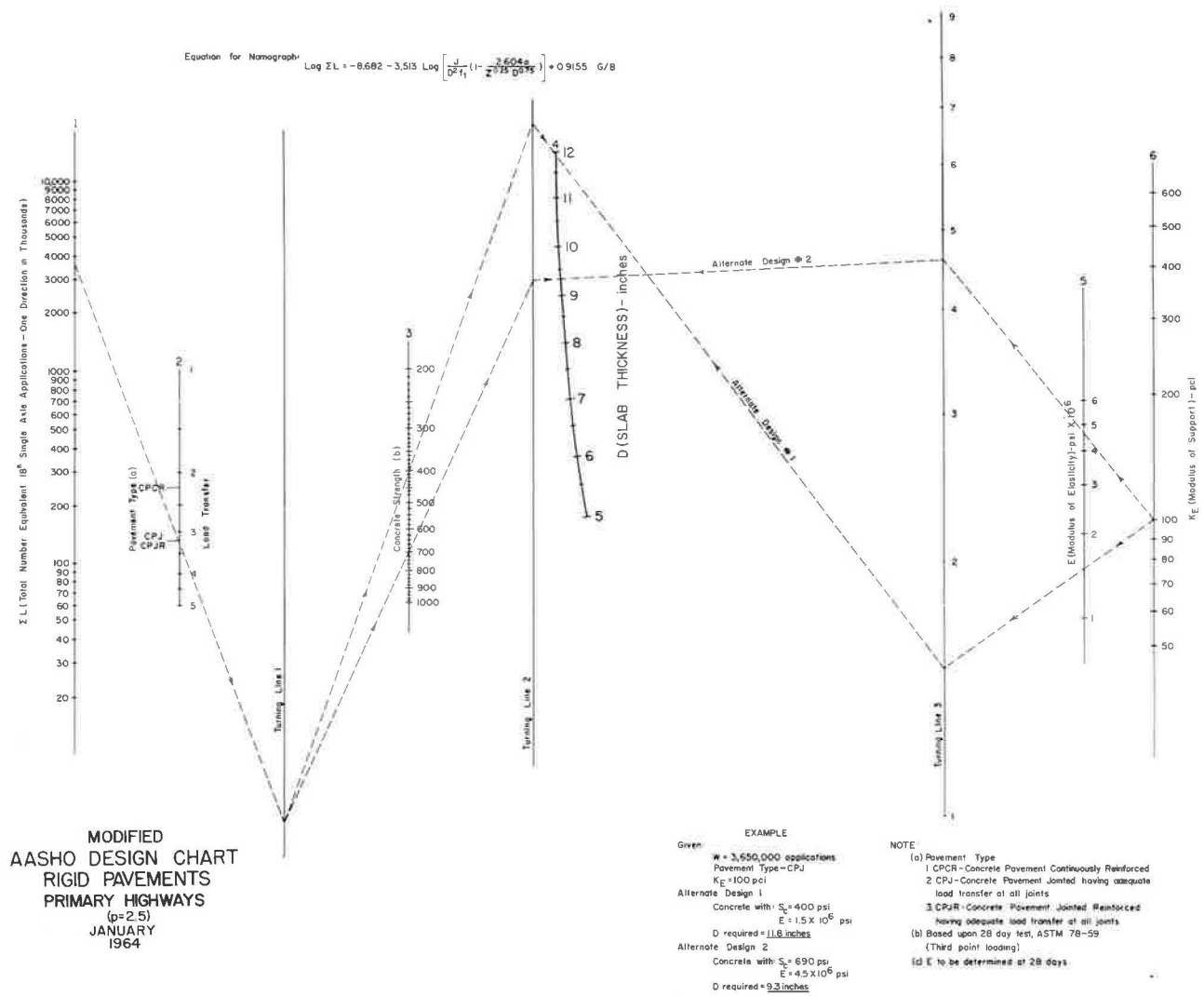
Equation for Nomograph

$$\text{Log } \Sigma L = -8.682 - 3.513 \text{ Log} \left[\frac{J}{D^2 f_t} \left(1 - \frac{3.604 s}{Z^{0.25} D^{0.75}} \right) \right] + 0.9155 \ G/B$$

ΣL (Total Number Equivalent 18" Single Axle Applications — One Direction in Thousands)

10,000
9000
8000
7000
6000
5000
4000
3000
2000

1000
900
800
700
600
500
400
300

200

100
90
80
70
60
50

40

30

20

Turning Line 1

Pavement Type (a)

Load Transfer

CPCR

CPJ
CPJR

Concrete-Strength (b)

Turning Line 2

D (SLAB THICKNESS) — inches

Alternate Design # 2

Alternate Design # 1

Turning Line 3

E (Modulus of Elasticity) — psi X 10⁶

K_E (Modulus of Support) — pci

MODIFIED
AASHO DESIGN CHART
RIGID PAVEMENTS
PRIMARY HIGHWAYS
(p=2.5)
JANUARY
1964

EXAMPLE

Given:
  W = 3,650,000 applications
  Pavement Type — CPJ
  K_E = 100 pci
Alternate Design 1
  Concrete with: S_c = 400 psi
    E = 1.5 X 10⁶ psi
  D required = 11.8 inches
Alternate Design 2
  Concrete with: S_c = 690 psi
    E = 4.5 X 10⁶ psi
  D required = 9.3 inches

NOTE
  (a) Pavement Type
    1 CPCR — Concrete Pavement Continuously Reinforced
    2 CPJ — Concrete Pavement Jointed having adequate
      load transfer at all joints
    3 CPJR — Concrete Pavement Jointed Reinforced
      having adequate load transfer at all joints
  (b) Based upon 28 day test, ASTM 78-59
    (Third point loading)
  (c) E to be determined at 28 days

Figure 3. Rigid pavement design nomograph.

1. ΣL = 3,650,000 applications is an estimate of the traffic to be carried during the life of the proposed pavement. It should be established by statistical prediction procedures from study of past loadometer and traffic count data. Texas Highway Department methods may be found in (9).

2. k_E = 100 pci is established by the existing subgrade plus some evaluation of the improvement that will be gained by the subbase (12).

3. Pavement type, CPJ, jointed plain concrete pavement with load transfer at the joints. This factor may be chosen by the designers and varied for several different designs. Often, however, the choice is dictated by other existing factors as assumed for this example.

With these factors provided, it is appropriate to establish the value of each factor on its respective scale and proceed as follows: (a) mark ΣL on scale 1; (b) mark pavement type on scale 2; (c) mark k_E value on scale 6; (d) taking E = 1.5 in anticipation of using low-modulus shell concrete for the first trial, mark 1.5 on scale 5 as shown; (e) connect the points on scale 1 and scale 2 projecting the line to a point on turning line 1; (f) select a trial concrete strength (400 psi) and mark it on scale 3; (g) connect this point on scale 3 to the intersection on turning point 1 and extend it to a point on turning line 2; (h) transferring over the scales 5 and 6, connect the points on these scales and project to turning line 3; and (i) connect turning points 2 and 3 to establish the required thickness D = 11.8 in. on scale 4.

It may be desirable to check alternate designs. Another example is shown on the design chart, which using different concrete characteristics and following the same procedures yields D = 9.3 in.

MODIFICATION OF REINFORCEMENT DESIGN

Jointed-Reinforced Concrete Pavement

The friction factor was not included as a variable in the Design Guide nomograph for determining the reinforcement in jointed-concrete pavement. The nomograph was solved for a fixed friction factor of 1.5. This was an adequate premise during the period when sand cushion blankets were used between the pavement and the subbase, but the current trend toward crushed stone or stabilized subbase emphasizes the need for considering friction factor in design. Experiments performed by the Texas Highway Department have shown friction factors in excess of two, therefore, if the Guide's nomograph were used to design the reinforcement for a high friction subbase, an inadequate design would result.

In addition to inserting friction factor into design, it is felt that the solution for the reinforcing requirements could best be expressed as a percentage in lieu of the current concept of using the area of steel per ft of slab width. The latter designation is satisfactory for estimating purposes, but is difficult to comprehend from a design standpoint. Furthermore, when the solution is expressed as a percentage, the values are comparable and compatible with the solutions obtained with continuously-reinforced concrete pavement. By simply changing the designation of several expressions in the Guide, the answer for "subgrade drag" would be in percentages as follows (7):

$$P_S = \frac{L\,F}{2\,f_S} \times 100 \tag{14}$$

in which

P_S = required steel percentage, percent.
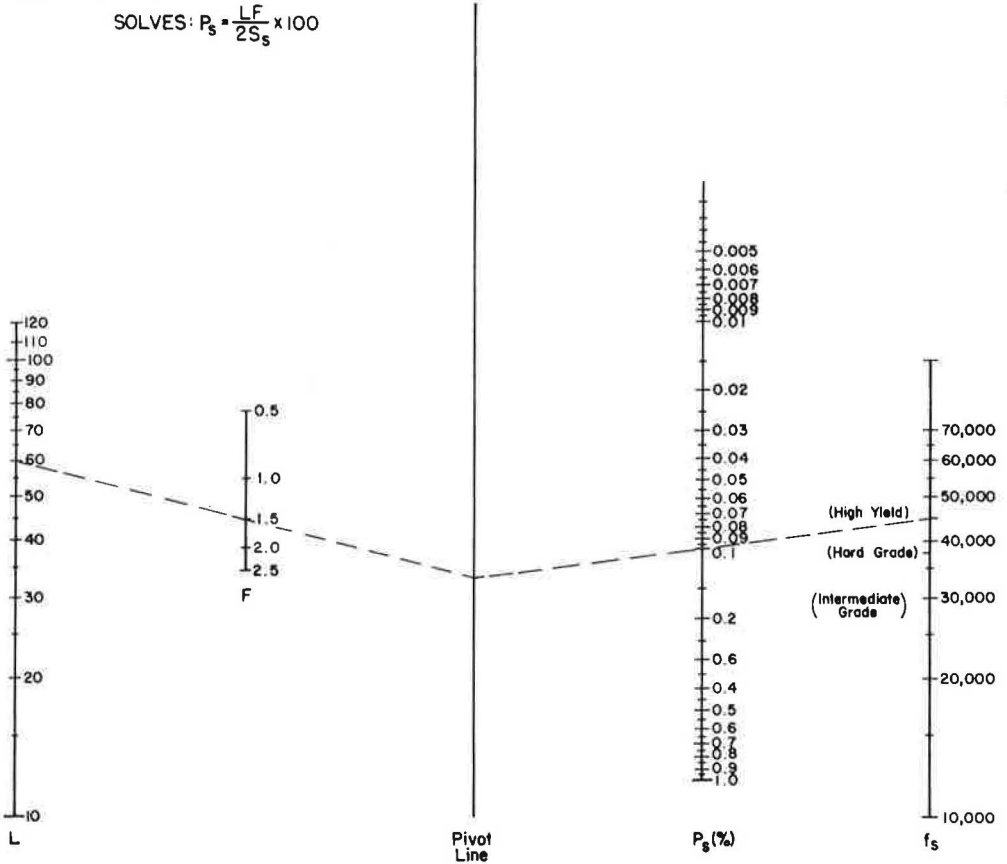L = length of slab between joints, ft.
F = friction factor of subbase.
f_S = allowable working stress in steel, psi.

Figure 4 shows a nomograph for solving Eq. 14. Note the flexibility provided, in that the working stress can be varied between wide limits in addition to including friction factor as a variable. The inclusion of a complete scale for working stress in lieu of several fixed values allows the designer to apply any desired value.

Figure 4. Distributed steel requirement for light reinforced jointed-concrete pavements.

In addition, the designer has added flexibility using the two scales on the right to either select the steel type or grade and determine the resulting required steel percentage, or select an optimum steel percentage and determine the steel type.

Steel Size and Spacing Requirements

The solution for jointed-reinforced concrete pavement is expressed as a percentage. The next step in design after determining the steel percentage is to determine the bar spacing and size needed to fulfill the required percentage. The equation for solving for bar spacing is as follows:

$$y = \frac{A_b}{D \ P_s} \times 100 \tag{15}$$
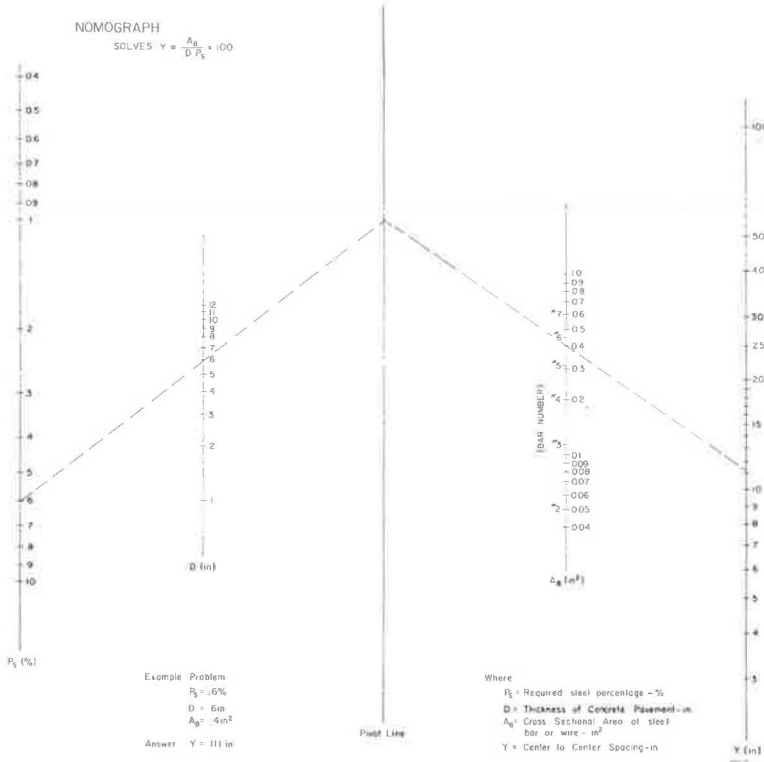
Figure 5. Steel spacing for reinforced concrete pavement.

in which

> y = bar or wire spacing, center to center, in.
> A_b = cross-sectional area of bar or wire, sq in.
> D = pavement thickness, in.
> P_S = required steel percentage, percent.

Figure 5 shows a nomograph solution of this equation. Using the variable scales on the right side of the nomograph, several combinations of bar spacings and sizes that meet the steel percentage requirements can be readily obtained.

SUMMARY

Conclusions

The following conclusion can be draw from this work: (a) Based on an analysis of stresses "observed" at the AASHO Road Test, the Spangler simplification of the Westergaard stress equations fits the Road Test pavements. The use of this equation as a stress model in design is therefore justified. (b) A design equation relating load applications to pavement design factors including modulus of elasticity and slab continuity can be developed through the relationship of stress to slab thickness and load applications observed at the Road Test. (c) The complicated design equation involving load applications, modulus of rupture, modulus of elasticity, slab continuity, modulus of subgrade reaction, thickness of slab, and pavement performance can be usefully displayed as a nomograph using general computer solutions of the equations. (d) The evaluation of all variables and constants are reasonably well founded except for the value of life term and slab continuity. Continued observations on existing pavements

will help verify these effects. (e) By use of a series of nomographs, the steel rein-forcing requirements, i.e., bar size and spacing, for the design conditions of either jointed-reinforced concrete pavement or continuously-reinforced concrete pavement can be determined with several simple manipulations. (f) The design charts developed herein allow the designer to consider numerous variables that were not accounted for in previous design methods. Hence, more flexibility is afforded the designer.

Needed Research

The design methods reported herein are intended to represent the best use of available knowledge concerning portland cement concrete pavements. They are presented as empirical approximations of the true phenomena involved. Continuing research into various aspects of this problem is being carried on.

Powerful computational techniques along with the wealth of experimental data that is being accumulated should advance pavement performance knowledge. Specifically, additional information is needed to evaluate a variable termed "subbase quality" (Q). This variable is related to the load carrying capacity, but must also evaluate the ability of the subgrade to maintain its integrity under repeated load applications. The search should also continue to develop a meaningful environment factor $(\overline{RF})$, a function of weather and other environmental conditions. This term would of course include the curling and warping effects of temperature and moisture differentials.

In addition to these two variables, not included in the design equation developed herein, a great amount of work remains for the verification of the following parameters:

1. J, a function of slab continuity, load conditions, and jointing procedures.

2. ℓ, radius of relative stiffness, a function of E, K, and D. The present application of these factors is based on elastic theory. It can immediately be noted that K is far from elastic and additional study is warranted.

3. Log ΣL, several satellite studies designed to extend and verify the AASHO Road Test equations are in various stages of planning at the present time. Such studies are vital to the solution of this problem.

Method of Proposed Research

In addition to Road Test satellite studies, which are considered to be vital to the solution of this problem, at least two other avenues of research must be exploited.

There is an immediate need for the development of more adequate and versatile methods of analysis permitting the extension of the available solutions past the simpli-fied special-case solutions developed by Westergaard in 1925. Particular attention is needed on dynamic loadings.

A second need is that of developing additional information concerning the effects of dynamic loads on the so-called elastic material properties. There is sufficient proof available from the Road Test to indicate that such a study is both physically and economically feasible by employing a vibrating loader similar to that introduced at the Road Test (2, 8).

The Road Test strain-performance studies provide a basis for extending the Road Test performance equations to include additional design variables, for example: (a) modulus of elasticity of concrete (E), (b) flexural strength of concrete (S_C), (c) joint type and arrangment, (d) subbase and subgrade characteristics (k), and (e) slab loading conditions (continuity).

REFERENCES

1. Westergaard, H. M., "Computation of Stresses in Concrete Roads." HRB Proc. 5(Pt. 1):90-112 (1925).
2. Hudson, W. R., "Comparison of Concrete Pavement Load-Stresses at AASHO Road Test with Previous Work." HRB Highway Res. Rec. 42, pp. 57-98 (1963).
3. Spangler, M. G., "Stresses in the Corner Region of Concrete Pavements." Iowa Eng. Exp. Sta. Bull. 157 (1942).

4. Kelly, E. F., "Application of the Results of Research to the Structural Design of Concrete Pavements." Public Roads, 20 (1939).
5. Portland Cement Assoc., "Concrete Pavement Design." Chicago (1951).
6. "The AASHO Road Test—History and Description of Project." HRB Spec. Rept. 61A (1961).
7. "AASHO Interim Guide for the Design of Rigid Pavement Structures." AASHO Comm. on Des. (Apr. 1962).
8. Hudson, W. R., and Scrivner, F., "AASHO Road Test Principal Relationships—Performance with Stress, Rigid Pavements." HRB Spec. Rept. 73 (1962).
9. Derdeyn, C. J., "A New Method of Traffic Evaluation for Use in Pavement Design." HRB Highway Res. Rec. 46, pp. 1-10 (1964).
10. McCullough, B. F. and Ledbetter, W. B., "LTS Design of Continuously Reinforced Concrete Pavements." Jour. of the Highway Div., ASCE Proc., 86(HW4) (Dec. 1960).
11. HRB AASHO Road Test staff, "Second Preliminary Report on the AASHO Road Test." Presented to U. S. Bureau of Public Roads (May 8, 1961).
12. Murray, W. M., and Stein, P. K., "Strain Gage Techniques." M.I.T., Cambridge, pp. 537-548 (1956).
13. Timashenko, S., and Goober, J. N., "Theory of Elasticity." McGraw-Hill, p. 24 (1951).
14. "The AASHO Road Test—Pavement Research." HRB Spec. Rept. 61E, pp. 139-286 (1962).

Temperature Variations in a Cement Concrete Pavement and the Underlying Subgrade

V. VENKATASUBRAMANIAN
Civil Engineering Department, Indian Institute of Technology, Kharagpur
(S.E.Rly.), India

This paper presents the results of temperature observations carried out for slightly more than 2 yr on a 6-in. thick portland cement concrete slab at Kharagpur, India. Temperature studies were also made on the water bound macadam base and the natural subgrade beneath the slab. The observed time-temperature variations are compared with existing theories of temperature distribution in a concrete slab. Based on the observed data, an empirical equation to estimate the amplitude of surface temperature variation in the 6-in. slab from the air temperature data is given.

•DESIGN OF cement concrete pavements has not appreciably advanced from the prevailing empirical methods in spite of the immense development in concrete design and technology. The main reason for this is that from the standpoint of stress analysis the concrete pavement, a long and thin slab resting on a shallow foundation, is a highly complex structure. Any study of pavement stresses must take into account the varying characteristics of the subgrade on which the slab rests. Of the many factors that induce stresses in a concrete pavement, the wheel loads and the temperature variations in the slab are important. Because the effects of moisture differential counteract the more harmful effects of temperature differential, the effect of moisture as a stress producer in a pavement slab is generally neglected. Also, no simple and satisfactory method of precisely measuring the moisture gradient in a slab has been evolved. Extensive observations by the U. S. Corps of Engineers (1) have revealed that the dynamic effect of wheel loads can be handled by a coefficient of impact. Therefore, it is comparatively easy to fairly accurately estimate the wheel load stresses using Westergaard's or Pickett's analysis. These wheel load stresses by themselves may be well within the permissible stresses. However, it is quite possible that the wheel load stresses combined with temperature stresses may lead to slab failures.

The effect of temperature on a cement concrete pavement can be divided into two parts (a) the daily variation of the slab temperature, the top surface being hotter or cooler than the bottom and (b) the yearly or seasonal variation in the average concrete temperature. The former variation causes the slab to curl, thereby creating "curling stresses." The latter gives rise to friction forces between the slab and the base. Generally, the slab will adjust itself to the slowly changing seasonal temperature conditions without causing excessive stresses. Of the two, the effect of daily variation in temperature with its consequent curling is more serious. Apart from the development of curling stresses, it leads to a partial loss of the subgrade support at the corners and edges (critical areas as far as the wheel load dispositions are concerned).

The temperature variation in a concrete slab depends on the meteorological characteristics of the area. Published data on temperature distribution in a concrete road slab has, so far, been confined to subtropical countries. No temperature data appear to be available for concrete roads in humid tropical areas. To gather such data, temperature observations were carried out on a 6-in.-thick cement concrete slab 5 by 4 ft

at the Indian Institute of Technology, Kharagpur, India for the past 3 yr. The test area was 72 mi southeast of Calcutta, and its geographical location is given as 87.5° East longitude and 22° North Latitude. To simulate the common practice of stage construction generally adopted in India, the 6-in. slab was cast on a 4-in.-thick water bound macadam base laid over a 6-in.-thick laterite stone subbase. The subgrade of sandy clay loam, the stone subbase, and the macadam base were thoroughly rolled before each succeeding layer was laid. The concrete used for the test slab had an average 28-day cube strength of 5,550 psi, modulus of elasticity in flexure of 2.95×10^6 psi, and a modulus of rupture of 533 psi. When laying the concrete, copper-constantan thermocouples were installed at the surface of the concrete at depths of 1, 2, 4, and 6 in. Prior to laying the concrete slab, the subgrade and the interior of the macadam base were carefully exposed in two places. Thermocouples were placed 2 in. inside the base (8 in. from the top of the slab) and 4.5 in. inside the subgrade (20.5 in. from the top of the slab).

No automatic temperature recorders of the continuous type were available except at a prohibitive cost; therefore, a mirror galvanometer was used to measure the e.m.f. set up by the thermocouple junctions. The observations were usually started at 7 A.M. in the summer and 8 A.M. in the winter. Readings were taken at 2-hr intervals. However, between 11 A.M. and 2 P.M., and 4 and 7 A.M., the readings were recorded at 1-hr intervals so the maximum and minimum surface and air temperatures could be obtained. The temperature readings are not continuous, but were planned so as to develop full information covering both daily and yearly temperature cycles. The average temperature of the slab was obtained by averaging the temperatures measured at the different points along its depth. Figures 1 and 2 show the prevailing weather conditions of the test slab area.

From the data obtained, it was possible to find the critical temperature conditions for each of the days; and because the observations were made during all the months of the different seasons, it was possible to get a reasonably accurate picture regarding the daily as well as yearly concrete temperature variations. Table 1 gives a summary of the data obtained in this manner. On a careful study of the table, the following observations appear evident. The average slab temperature varies about 33.7 C (60 F) during the year. This variation controls the magnitude of yearly change in the pavement length caused by temperature changes. The maximum recorded surface temperature of the slab was 51.0 C (124 F). This occurred on May 17, 1961, a clear rainless day.
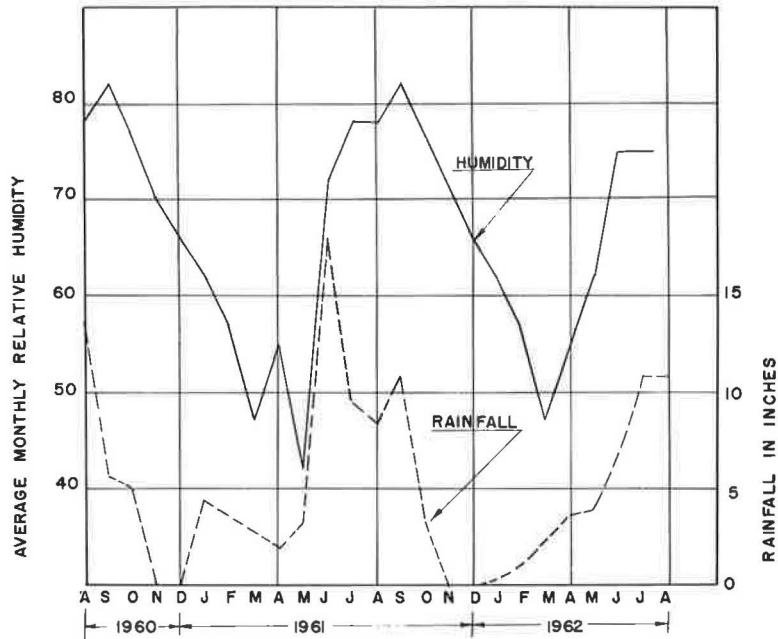

Figure 1.   Annual air temperature variation.
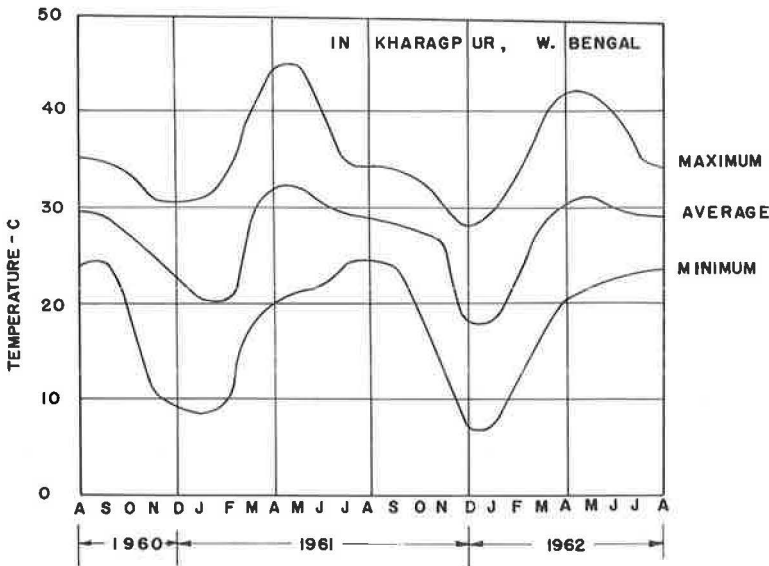
Figure 2. Annual variations in relative humidity and rainfall.

The maximum positive gradient was 12.0 C (21.6 F) on April 11, 1961; and the maximum negative gradient of 6.3 C (11.3 F) on May 2, 1961. This high negative gradient was caused by heavy freak thunderstorms that occurred on the evenings of May 1, 2, 1961. This negative gradient occurred at about 8 P.M. on May 2; it was transient in nature, and rapidly disappeared restoring normal conditions in about 6 hr.

On the same day, the surface temperature of the slab dropped from 44.5 C at 3 P.M. to 27.5 C at 8 P.M. The maximum negative gradient of 5.0 C, due to seasonal variation, occurred at about 5 A.M. on November 29, 1960. It is interesting to recall that the maximum surface temperature recorded by Teller and Sutherland (2) was 112.5 F (44.5 C) and 31.0 C by Bergstrom (3). Swanberg (4) has reported a maximum surface temperature of 122 F for a 7-in. slab in the Minneapolis area. Also the Arlington tests by Teller and Sutherland indicate that the maximum value of the day temperature differential is about three times the maximum value of the night differential. The present observations indicate that under humid tropical conditions the day differential is only slightly more than thice the night differential value. Further more, the observed night temperature differential varies within very narrow limits between winter and summer. Based on the Arlington tests, for purposes of design computations, Kelly (5) recommends a maximum positive temperature differential of 3 F per in. slab thickness. From

TABLE 1

SUMMARY OF OBSERVED TEMPERATURES IN A 6-INCH-THICK CONCRETE SLAB, I.I.T., KHARAGPUR, WEST BENGAL

Date	Avg. Temp. (°C)		Max. Temp. (°C)		
			Day		Night
	Max.	Min.	Surface	Gradient (+)	Gradient (-)
Aug. 31, 1960	34.7	25.8	38.0	7.7	2.8
Sept. 7, 1960	35.5	27.0	37.5	4.1	3.0
Sept. 22, 1960	40.0	28.9	39.3	7.2	4.0
Oct. 26, 1960	36.5	24.1	39.5	7.2	2.3
Nov. 2, 1960	33.6	25.4	36.5	7.1	3.2
Mar. 8, 1961	37.6	23.4	42.0	10.0	4.6
Mar. 24, 1961	39.9	28.4	46.3	10.4	4.7
Apr. 5, 1961	42.4	28.7	47.2	11.5	4.1
Apr. 11, 1961	43.3	28.0	48.0	12.0	4.8
Apr. 17, 1961	45.3	29.2	49.5	10.3	4.5
May 2, 1961	42.4	26.8	45.5	8.0	6.3
May 17, 1961	46.2	32.1	51.0	11.9	4.8
June 4, 1961	42.9	31.5	46.8	9.6	4.5
Feb. 15, 1962	33.3	19.2	37.0	9.5	4.5
Feb. 27, 1962	35.6	23.1	39.2	8.7	3.7

the data available for the 6-in. slab in this study, the maximum positive temperature differential may be assumed to be 2.0 C (4 F) per in. slab thickness and the maximum negative gradient of 1 C (2 F) per in. slab thickness.

Figures 3 to 8 plot the daily temperature variations at different depths for the different yearly seasons. From these graphs, the temperature gradients for six time periods are interpolated and plotted in Figures 9 to 14. A study of these curves reveals
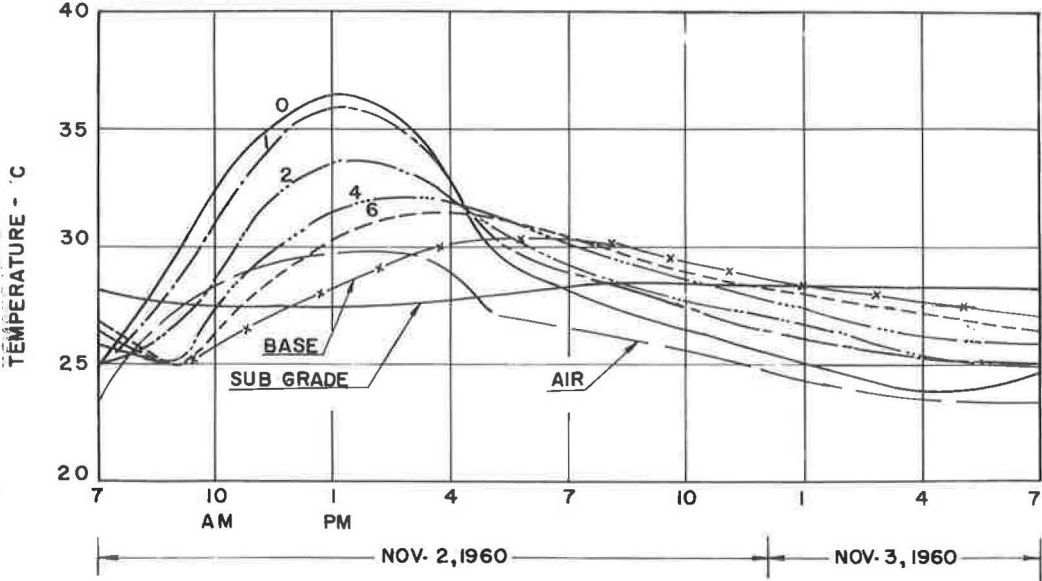

Figure 3. Variation of temperature with time at various depths.
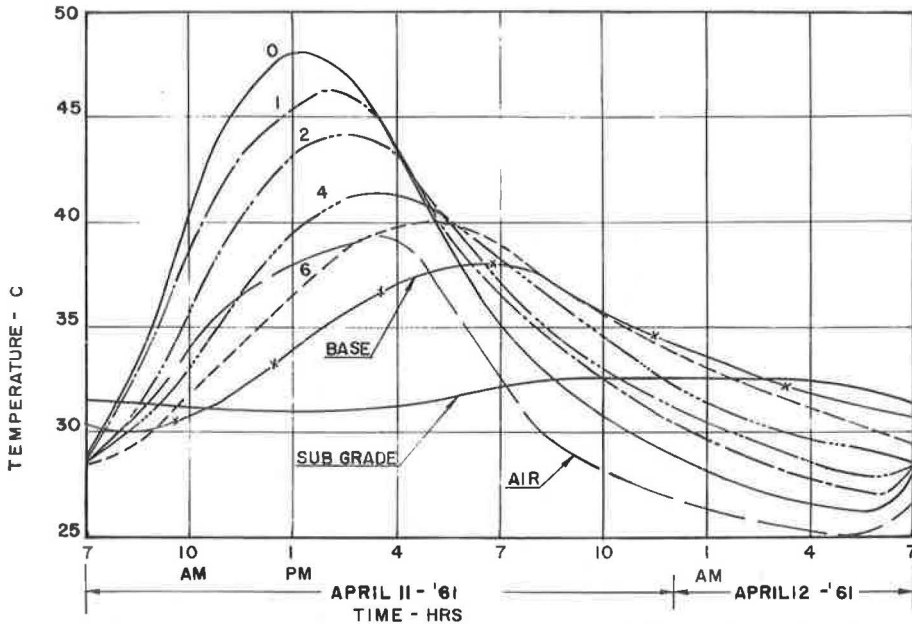
Figure 4. Variation of temperature with time at various depths.
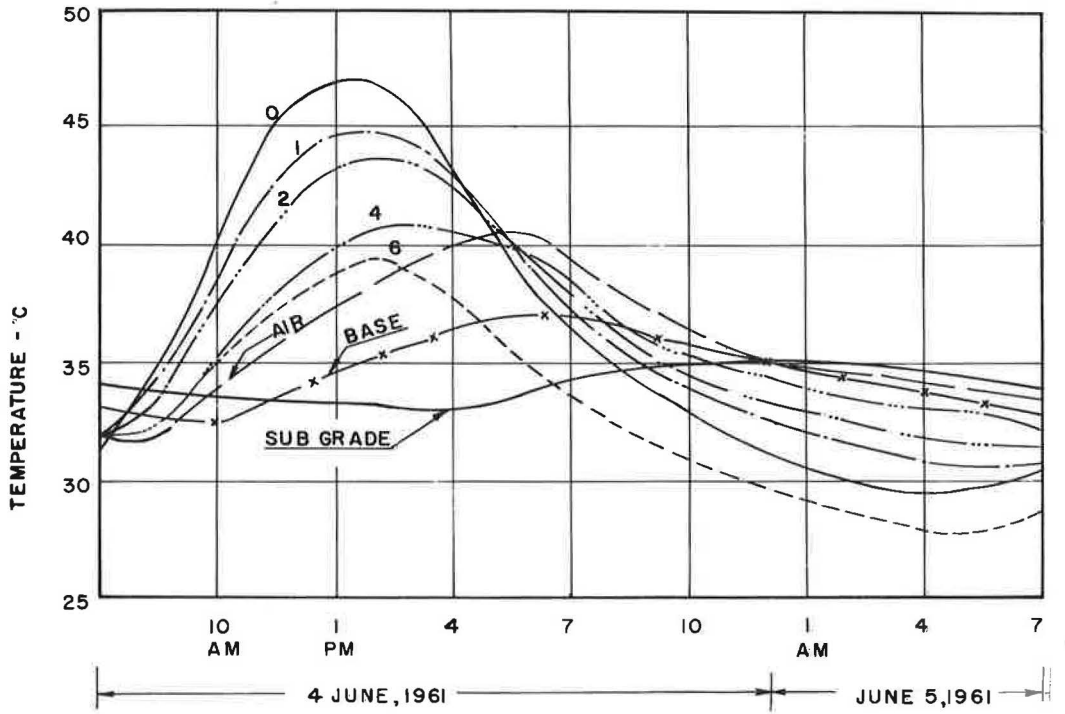
Figure 5. Variation of temperature with time at various depths.
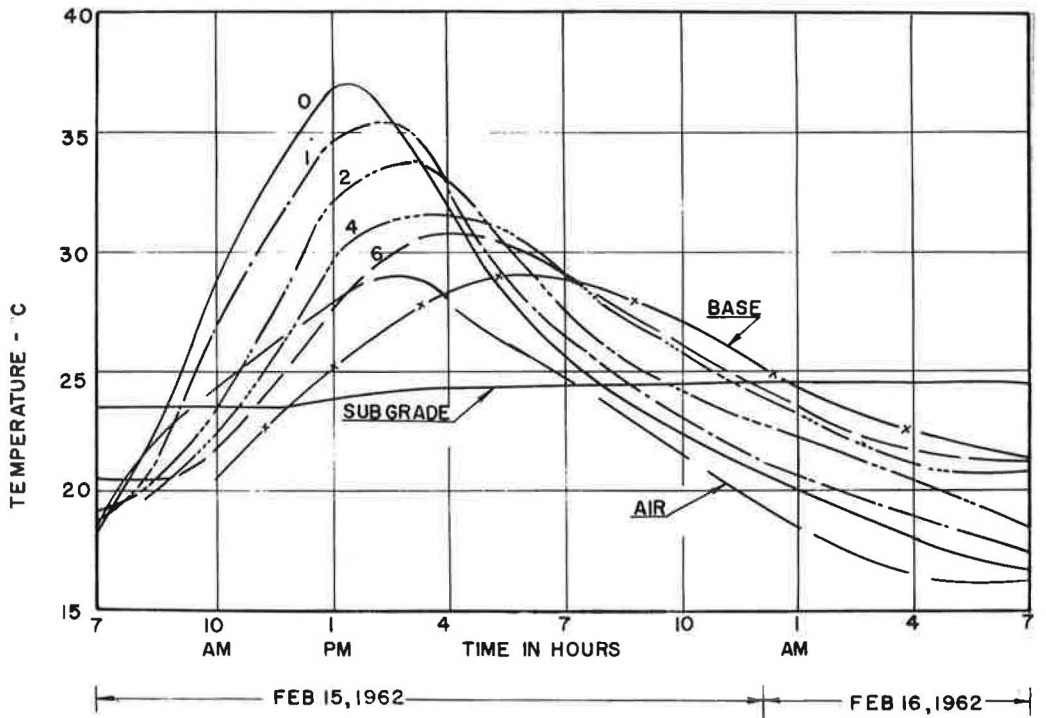
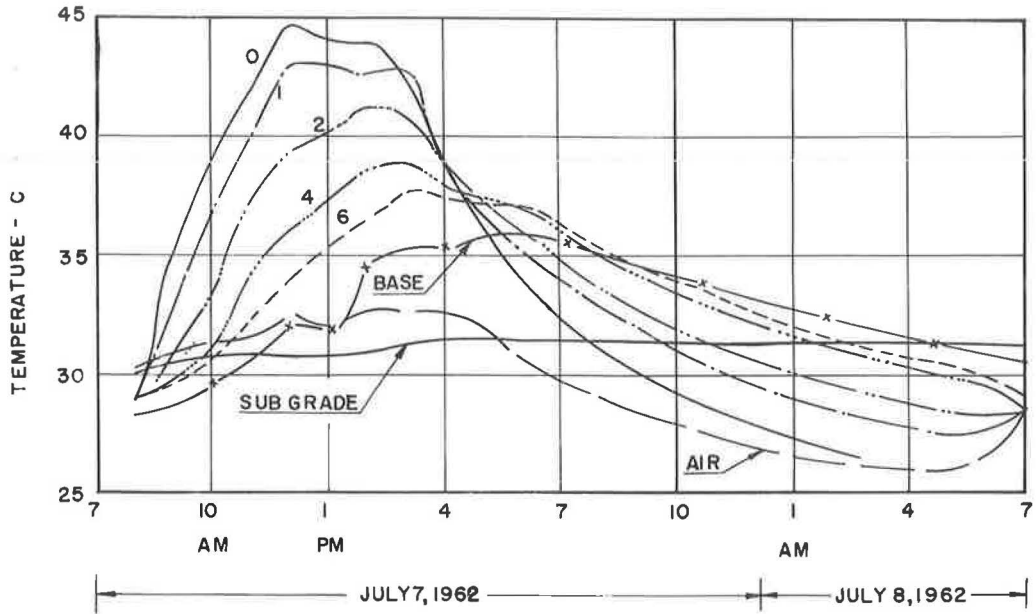Figure 6. Variation of temperature with time at various depths.

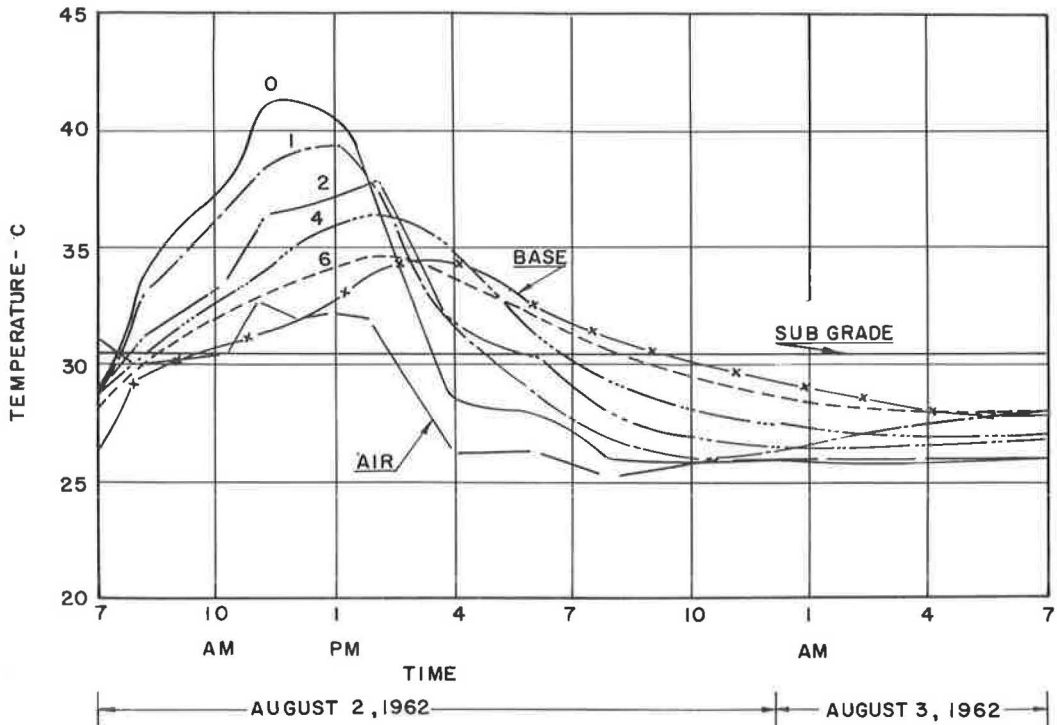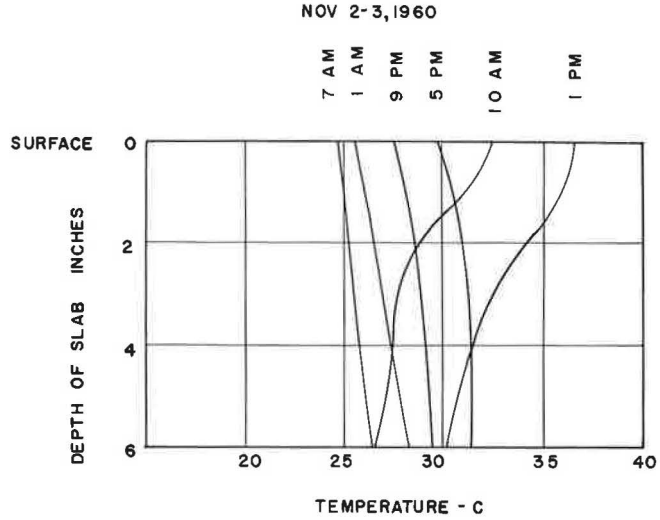Figure 7. Variation of temperature with time at various depths.

Figure 8. Variation of temperature with time at various depths.

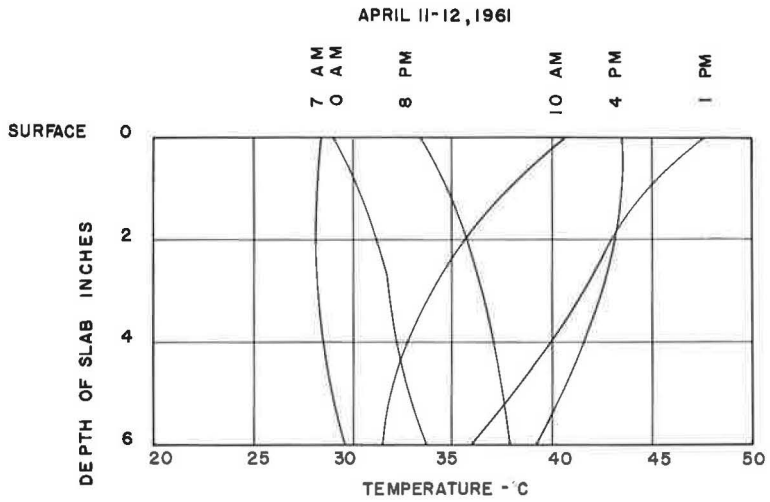Figure 9. Variation of temperature with depths at various times.

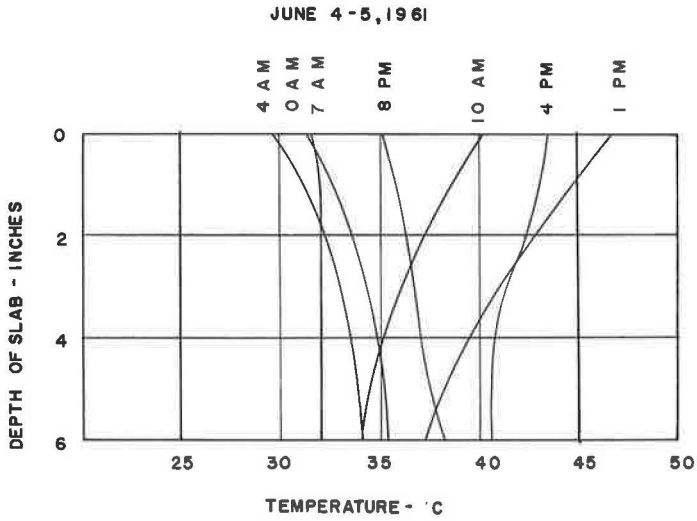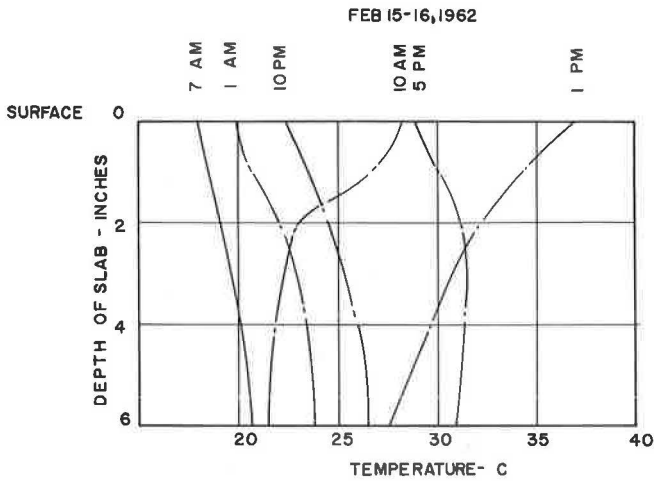Figure 10. Variation of temperature with depths at various times.

JUNE 4-5, 1961

4 AM
0 AM
7 AM
8 PM
10 AM
4 PM
1 PM

Figure 11.   Variation of temperature with depths at various times.

FEB 15-16, 1962

7 AM
1 AM
10 PM
10 AM
5 PM
1 PM

SURFACE

Figure 12.   Variation of temperature with depths at various times.
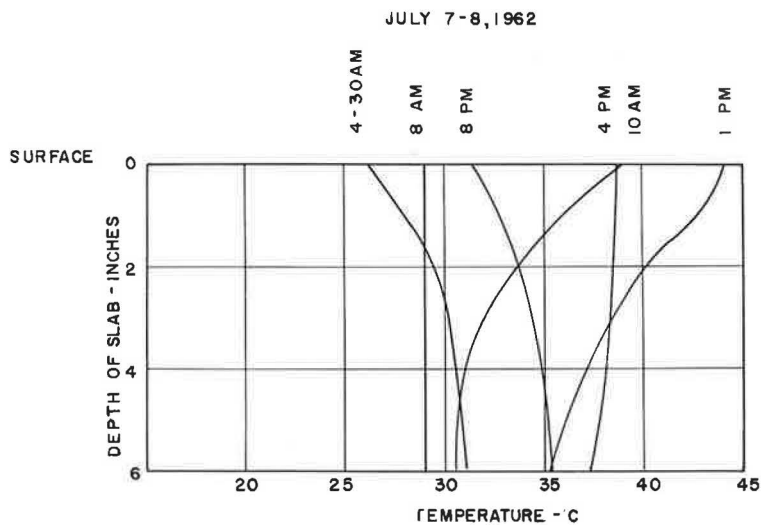
JULY 7-8,1962

Figure 13. Variation of temperatures with depths at various times.
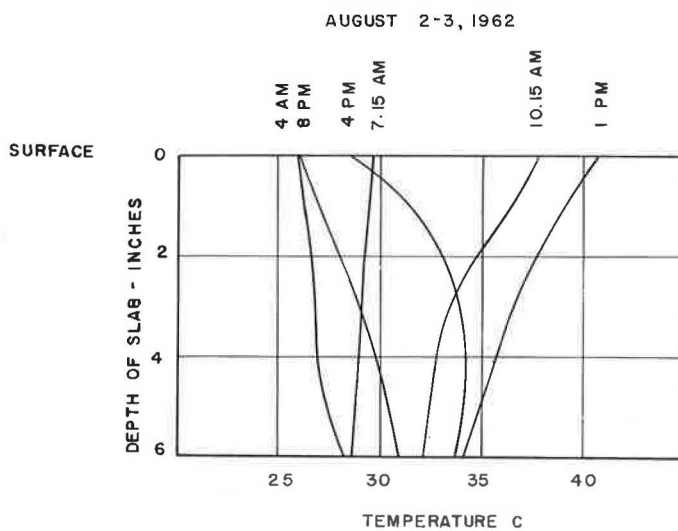
AUGUST 2-3, 1962

Figure 14. Variation of temperature with depths at various times.

that the daily variation curves approximate a wave form only during the nonmonsoon months. During the monsoon months, July and to September, the curves appear to be very erratic. During these months the sky is rarely clear and direct solar radiation on the slab is not continuous; also, the subgrade and the slab are very wet, if not saturated. Under such circumstances it is safe to assume that the temperature curling stresses will not be critical. The prevailing temperature conditions during the monsoon months also can be disregarded without much error in the development of design criteria for concrete slab temperature stresses in humid tropic areas.

The steepest positive temperature gradient occurs at the time of maximum surface temperature (about 1 P.M.), and the maximum negative gradient occurs between 4 and 5 A.M. Also the maximum gradient curves causing the maximum curling stresses are very nearly linear justifying Westergaard's assumption. Thus, Westergaard's concept of a linear temperature gradient, while it is not valid for the general case, is true for the critical condition in which the designer is interested. These findings are in close agreement with the Arlington test results.

The maximum and minimum observed values of subgrade temperatures underneath the slab are given in Table 2. The daily variation of subgrade temperature is almost negligible, but there is appreciable seasonable variation. The temperature of the subgrade by itself may not be important, but a study of Figures 3-8 referred to previously indicates that in the early hours of the morning when there is no direct solar radiation on the slab and when the temperature gradient in the concrete slab is negative, the subgrade temperature is always higher than the temperatures at the bottom face of the slab, and the stone subbase. Being in contact with them, the subgrade is able to transmit heat in the reverse direction. This phenonemon may be partly responsible for the difference between the observed and theoretical temperature distribution within the slab.

At present there are two elastic theories available for the estimation of curling stresses in a concrete road slab due to temperature variation. Both the theories depend on the coefficients of restraint for their ultimate use. These are very difficult to evaluate precisely during the service behavior of the slab. As such, from a practical point of view, one theory is not superior to the other. However, the variation limits of the curling stresses can be set down from the temperature distribution data. Westergaard's theory, developed as early as 1927, assumes a linear temperature gradient through the slab (6). The other theory was presented by Thomlinson of the Road Research Laboratory, U. K. in 1938 (7). Thomlinson's theory is favored on the continent. He assumes the surface temperature of the slab to vary according to a simple harmonic law. The temperature θ at any given depth x below the surface at any time t is given by the relation:

$$\theta = \theta_0 \, e^{-\frac{x}{h}\sqrt{\frac{\pi}{T}}} \sin\left(\frac{2\pi}{T}\, t - \frac{x}{h}\sqrt{\frac{\pi}{T}}\right) \qquad (1)$$

in which

θ_0 = amplitude of the temperature cycle at the free surface of the slab

e = the base of the Naperian system of logarithms

h^2 = diffusivity of the concrete in sq in. per hour

$$= \frac{\text{thermal conductivity}}{\text{heat capacity per unit volume}}$$

T = periodic time of the temperature cycle (24 hours for the daily cycle)

It should be noted that Bergstrom (3) also accepts the above relationship, but assumes θ_0 to be a constant, and determines its value so as to insure close agreement between the maximum values of the theoretical and observed temperature gradients. Sparkes (8) and Bergstrom (3) state that close agreement exists between the observed and com-

TABLE 2

EXTREME SUBGRADE
TEMPERATURES

Date	Subgrade Temp. (°C)	
	Max.	Min.
Aug. 31, 1960	29.5	28.0
Sept. 7, 1960	31.3	29.0
Sept. 15, 1960	30.7	29.0
Sept. 22, 1960	33.7	29.0
Oct. 26, 1960	30.2	28.2
Nov. 2, 1960	28.7	27.5
Mar. 8, 1961	29.0	27.5
Mar. 24, 1961	33.0	31.4
Apr. 5, 1961	33.5	31.4
Apr. 11, 1961	32.6	30.6
Apr. 17, 1961	35.0	33.8
May 2, 1961	33.8	31.4
May 17, 1961	36.0	33.8
June 4, 1961	35.0	33.5
Feb. 15, 1962	24.5	22.8
Feb. 27, 1962	27.5	26.0

puted temperature distribution in concrete pavements. As already mentioned, the temperature variation at the surface approximates a simple harmonic law only during the dry months of the year and furthermore, this approximation is valid in the morning before the surface temperature has reached its peak value. In the afternoon deviation from the sinusoidal variation is more prominent. The result being that during the day the measured positive temperature differential is always greater than the computed differential, and during the night the maximum measured differential is always less than the computed value. This is clearly shown in Table 3. However, in the evaluation of the curling stresses, this discrepancy can be accounted for by harmonic analysis as suggested by Champion (9). Therefore, it appears that if one is able to establish a reasonably accurate and simple method to estimate the amplitude of the surface temperature variation in a slab, Thomlinson's theory can be used to evaluate the curling stresses expected in the slab.

In most of the developed areas, the meteorological data like the maximum and minimum daily air temperature and daily rainfall will be available. Therefore, if an experimental relationship can be established between the amplitudes of the daily variations of the concrete's surface temperature, and the prevailing air temperature variation in that area, the surface temperature amplitude at a similar locality can be easily estimated. An attempt has been made in this direction for the 6-in. slab under study, and the results are given in Table 4, and Figure 15. It can be seen that for design purposes, the maximum value of the surface temperature for the 6-in. slab can be taken as 1.5 times the maximum value of the air temperature recorded that day. Also the minimum value of the surface temperature is almost equal to the minimum air temperature recorded. It is suggested, therefore, that the amplitude of the surface temperature variation θ_O can be given by the empirical relationship:

$$\theta_O = \frac{1.5\,\theta_{a_{max}} - \theta_{a_{min}}}{2} \tag{2}$$

in which

$\theta_{a_{max}}$ and $\theta_{a_{min}}$ are the maximum and minimum air temperature values on a particular day on which the amplitude of the surface temperature variation for a 6-in.

TABLE 3

COMPARISON BETWEEN MAXIMUM
MEASURED AND CALCULATED
TEMPERATURE GRADIENTS

Diffusivity of concrete $= h^2 = 6.48$ sq in./hr[a]

Date	Max. Temp. Gradient			
	Measured		Calculated	
	Day (+ve)	Night (-ve)	Day (+ve)	Night (-ve)
Nov. 2, 1960	6.3	2.7	4.5	4.5
Feb. 15, 1962	9.5	3.8	7.5	7.5
Apr. 15, 1962	12.0	4.5	8.0	8.0
June 4, 1962	9.6	4.0	6.3	6.3

[a]"Thermal Properties of Concrete." Bull. 1, Boulder Canyon Project Final Reports, U. S. Bureau of Reclamation.

TABLE 4

RATIOS OF EXTREME VALUES OF SURFACE
AND AIR TEMPERATURES

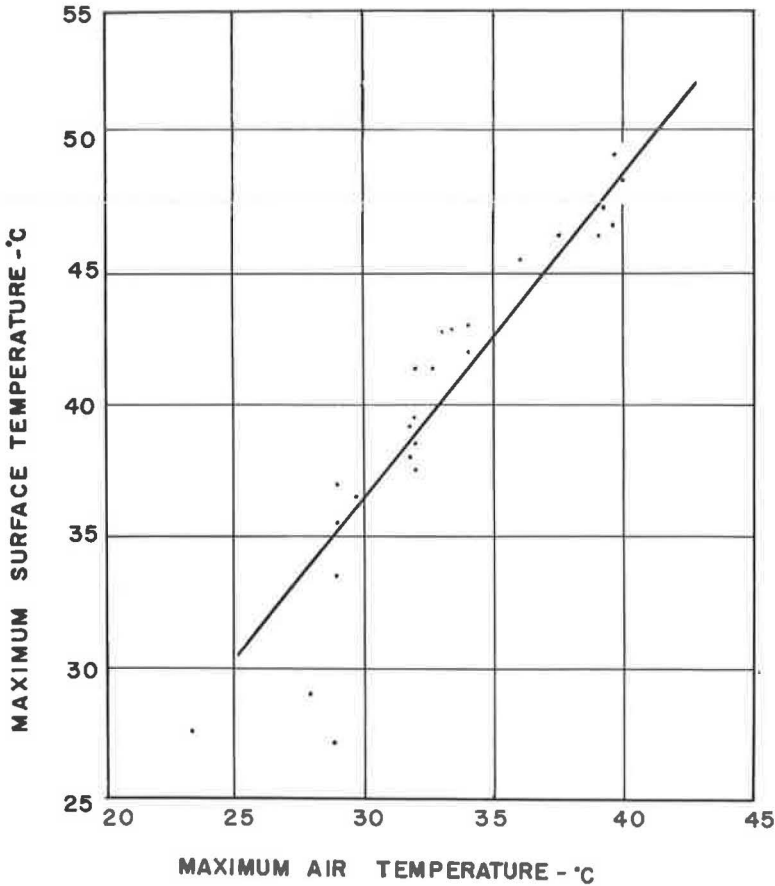| Date	Maximum Air Temp. $\theta_{a_{max}}$	Maximum Surface Temp. $\theta_{o_{max}}$	$\dfrac{\theta_{o_{max}}}{\theta_{a_{max}}}$	Minimum Air Temp. $\theta_{a_{min}}$	Minimum Surface Temp. $\theta_{o_{min}}$	$\dfrac{\theta_{o_{min}}}{\theta_{a_{min}}}$
Aug. 31, 1960	31.8	38.0	1.19	25.5	27.0	1.06
Sept. 2, 1960	32.0	39.0	1.21	27.0	25.7	0.95
Sept. 8, 1960	32.0	41.4	1.29	25.8	25.5	1.00
Sept. 14, 1960	32.0	38.5	1.20	25.5	25.5	1.00
Sept. 15, 1960	33.0	42.8	1.28	26.5	25.5	0.96
Sept. 22, 1960	34.0	43.0	1.27	27.0	28.0	1.04
Oct. 26, 1960	32.0	39.5	1.23	22.5	22.5	1.00
Nov. 2, 1960	29.8	36.5	1.22	23.5	24.0	1.02
Mar. 8, 1961	34.0	42.0	1.23	21.0	21.5	1.02
Mar. 24, 1961	37.5	46.3	1.23	25.2	26.5	1.05
Apr. 5, 1961	39.0	46.3	1.19	24.8	26.5	1.07
Apr. 11, 1961	39.2	47.5	1.21	25.0	26.3	1.05
Apr. 17, 1961	39.8	49.5	1.24	24.6	27.0	1.10
May 2, 1961	36.0	45.5	1.27	23.8	25.0	1.05
May 17, 1961	41.6	51.0	1.23	28.2	29.8	1.06
June 4, 1961	39.6	46.8	1.18	27.7	29.5	1.06
Feb. 15, 1962	29.0	37.0	1.27	16.2	17.0	1.05
Feb. 27, 1962	31.8	39.2	1.23	20.5	22.3	1.09
July 7, 1962	32.8	44.8	1.36	26.2	26.2	1.00
Aug. 2, 1962	32.6	41.3	1.27	25.2	26.0	1.03
Nov. 15, 1962	29.2	32.0	1.10	18.2	16.0	0.88
Dec. 13, 1962	25.5	28.8	1.13	14.0	14.0	1.00

Figure 15. Maximum surface temperature vs maximum air temperature.

slab will be θ_O. It must be noted that there is a phase different between the times at which the peak values occur. Furthermore, this relationship is applicable only to the 6-in. slab laid in the climatic conditions referred to previously. Once the amplitude of the surface temperature variation can be established, the curling stresses can be evaluated from Thomlinson's analysis.

ACKNOWLEDGMENTS

REFERENCES

1. "Rigid Pavement for Roads, Streets, Walks and Open Storage Areas." U. S. Army Corps of Engineers Manual, EM 1110-345-202 (June 30, 1961).
2. Teller, L. W. and Sutherland, E. J., "The Structural Design of Concrete Pavements—Part 2." Public Roads, 16(9) (1935).
3. Bergstrom, S. G., "Temperature Stresses in Concrete Pavements." Stockhlm (1950).
4. Swanberg, J. H., "Temperature Variation in a Concrete Pavement and the Underlying Subgrade." Proc. HRB 25:169-180 (1945).

5. Kelly, E. F., "Applications of the Results of Research to the Structural Design of Pavements." Public Roads, 20(5-6) (1939).

6. Westergaard, H. M., "Analysis of Stresses in Concrete Roads Caused by Variations of Temperature." Public Roads, 8(3) (1927).

7. Thomlinson, J., "Temperature Variations and Consequent Stress Produced by Daily and Seasonal Temperature Cycles in Concrete Slabs." Concrete and Constructional Engineering (June-July 1940).

8. Sparkes, F. N., "Stresses in Concrete Road Slabs." The Structural Engineer (Feb. 1939).

9. Champion, S., "The Technical Aspects of the Design of Roads." Technical Press Ltd., London (1950).

Evaluating Subgrade Friction-Reducing Mediums for Rigid Pavements

A. G. TIMMS
Structural Research Division, U. S. Bureau of Public Roads

As early as 1924 the U. S. Bureau of Public Roads conducted studies to determine the magnitude of the resistance offered by the subgrade to the horizontal movement of concrete pavement slabs. These early studies clearly showed that this resistance varies considerably with the type of material on which the pavement rests. In recent years increased interest in prestressed concrete pavements indicates a need for mediums that offer a low resistance to slab movement.

This paper presents the results of a study of several friction-reducing mediums that have been proposed by designers of prestressed pavements. The data on these mediums were developed by moving 6-ft sq slabs horizontally, alternately forward and backward several times. The thrust necessary to cause horizontal movement of the slab and the magnitude of displacement caused by the thrust were measured from the time that the first detectable movement took place until free sliding began.

●FOR MANY YEARS pavement designers have known that low-friction mediums will substantially reduce the direct tensile stresses induced in concrete slabs by subgrade resistance. However, because these stresses are generally quite small for the relatively short slabs of conventional concrete pavements, little use was made of such mediums until the advent of prestressed pavements.

Prestressed pavement, with slab lengths ranging upward to 800 ft, requires low-friction mediums for the most efficient use of the applied prestressing force. A 50 percent reduction in the frictional resistance of the material on which the pavement rests could result in a 30 to 40 percent reduction in the prestressing force.

Previous investigations have established that the resistance offered to slab movement by the subgrade can be decreased by a variety of means. In 1924, Goldbeck (1) reported that the elimination of ridges and depressions in the subgrade or the introduction of a sand layer between the subgrade and the pavement causes an appreciable decrease in the coefficient of friction. Recently, Stott (2) of the Road Research Laboratory of Great Britain presented the results of a comprehensive investigation of various materials used as sliding layers, including polyethylene sheeting, paraffin wax, bitumen, and lubricating oil.

In the past, a thin sand layer has been the most commonly used medium to reduce friction between the slab and the subgrade. However, many engineers now believe that sand layers should not be used under the relatively thin prestressed highway pavements because of the possible aggravation of edge pumping.

The importance of friction-reducing mediums to prestressed pavement led the U. S. Bureau of Public Roads to undertake a study designed to develop comparative data on several types of mediums that have been proposed for such pavement.

SCOPE OF STUDY

In this study the resistance to slab movement was determined for the seven following conditions: (a) subgrade soil consisting of micaceous clay loam and referred to in

TABLE 1

PHYSICAL PROPERTIES OF SUBGRADE AND SUBBASE
MATERIALS, SHEET AND EMULSIFIED ASPHALTS

Property	Subgrade Soil	Granular Subbase	Blend Washed Sand and Gravel	Sand in Sheet Asphalt	Sand in Emulsified Asphalt
Mechanical analysis (% passing sieve size):					
3-in.		100			
2-in.		98			
1½-in.		96			
1-in.		91			
¾-in.		84			
⅜-in.	100	70			100
No. 4	99	61		100	95
No. 10	98	54		98	87
No. 40	94	36		68	37
No. 80	-	-		30	9
No. 200	78	15		12.5	4
Liquid limit	40	33			
Plasticity index	15	16			
Classification	A-6(10)	A-2-6(0)		-	-
Penetration				60-70	60-70
Asphalt content, %				8.8	7.5

(Blend Washed Sand and Gravel column: No information available.)

Figure 1.   (a) Slabs between abutments, and (b) 5-in. slab loaded to weight equivalent
of 11-in. slab.

this report as "plastic soil," (b) granular subbase consisting of material meeting the U. S. Bureau of Public Roads grading and plasticity requirements for Federal highway projects (3), (c) granular subbase consisting of a blend of washed sand and gravel, (d) granular subbase, same as (b), with 1-in. sand layer covered by one-ply building paper, (e) granular subbase, same as (b), with a layer of emulsified sand asphalt about 1 in. thick, (f) granular subbase, same as (b), with a thin leveling course of sheet asphalt covered by a double layer of polyethylene sheeting containing a special friction-reducing additive, and (g) granular subbase, same as (b), with a layer of sheet asphalt about ½ in. thick.

The physical properties and AASHO classification of the subgrade and subbase materials together with information on the sheet and emulsified asphalts are given in Table 1.

For each condition, force-displacement curves were developed from data obtained by moving six-ft sq concrete slabs horizontally, alternately forward and backward several times to simulate the behavior of pavements in service. The force or thrust necessary to cause horizontal movement of the slab and the magnitude of displacement caused by the thrust were measured from the time that the first detectable movement took place until free sliding began.

The testing program was divided into a winter-spring study and a summer study, at which times the absorbed moisture in the subbase and subgrade was at the maximum and minimum of the annual cycle of moisture change, respectively.

All slabs were 5 in. thick. In order to develop data for force-displacement curves for 8- and 11-in. thick slabs, 100-lb weights were dispersed uniformly on top of the 5-in. slabs to provide the proper weight equivalency. A general view of the test slabs and a 5-in. slab loaded to the weight equivalency of an 11-in. slab are shown in Figure 1.

TEST PROCEDURE

Figure 2 shows the arrangement of the test slabs and the testing apparatus. Five, 1-ft sq wooden posts were set in the ground, 3 ft deep and 9 ft on centers, to serve as abutments for the thrusting force. The subbases and sliding mediums were placed symmetrically in 8-ft squares between the wooden posts. The 6-ft sq, 5-in. thick con-
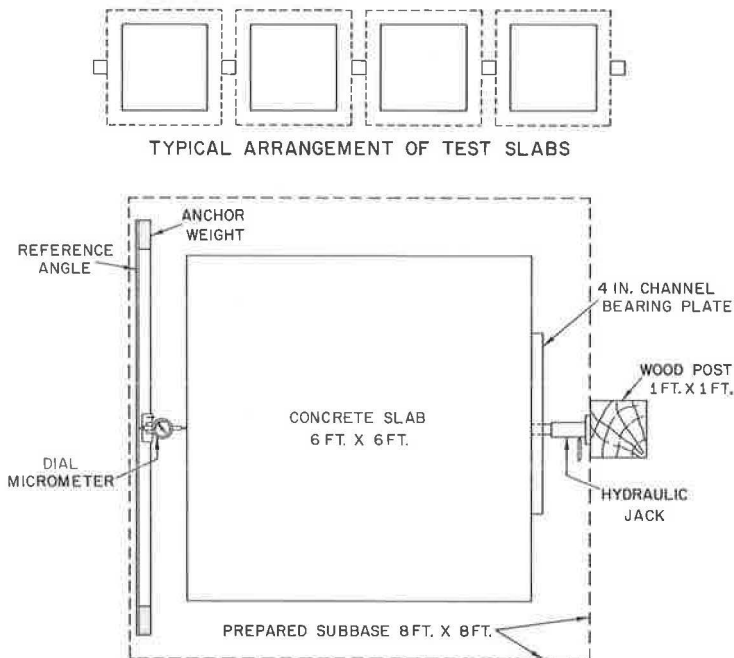

Figure 2. Arrangement of test slabs and testing apparatus.

crete slabs were cast in place, concentric with the 8-ft squares. A hydraulic jack applied the thrusting force to the concrete slab through a 3-ft long, 4-in. channel bearing plate. Horizontal displacement was measured with a micrometer dial on the side of the slab opposite to the thrusting force.

In most of the tests the thrusting force was applied continuously in increments at 5-min intervals as follows: 5-in. slab—200 lb, 8-in. slab—320 lb, and 11-in. slab—440 lb.

The thrusting force was held constant during the 5-min interval between the added increments. The displacement of the slab was measured immediately after the application of each increment of force and again just before the next increment was applied. These two readings were averaged to give a single value. Incremental loading was continued until the slab was sliding freely and the magnitude of the thrusting force could no longer be increased.

The thrusting force was removed every five minutes in load decrements as follows: 5-in. slab—400 lb, 8-in. slab—640 lb, and 11-in. slab—880 lb.

On release of the thrusting force, the slab tended to reverse direction. This return movement was also recorded in certain tests, being measured immediately after the removal of each decrement of force and just before the removal of the next decrement.

Force-displacement diagrams were also developed for the 5-in. slab on the granular subbase with a sand layer at two rates of loading other than the rate described above. One rate was very fast, in which 200 lb of force were applied every 10 sec and the other was twice as slow as the described rate, or 200 lb every 10 min.

In general, the slabs were moved back and forth three times or a total of six instrumented runs. The slab under test was protected from the elements by a canvas shelter.

TEST RESULTS

The data obtained in the testing of the slabs are shown in various ways in Figures 3-11. These figures illustrate certain characteristics of force-displacement behavior that have been reported by other investigators (2, 4).

Typical Data

Figure 3 shows typical data resulting from two of the tests. Each point on the curves represents an average value of six displacement tests, three in a forward and three in a backward direction. As the increments of force were applied, the successive increments of displacement increased in magnitude in a ratio that closely approximates a parabola. After free sliding occurred, the thrusting force could not be increased beyond that which initially caused the slab to slide. The slab returned slightly toward its original position on release of the thrusting force. This return movement is believed to be the result of elastic deformation of the soil and was measured in only a few of the tests, because it is of little value to the purpose of this study.

Rate of Application of Thrusting Force

The effect of the rate of loading on the displacement of a slab cast on the granular subbase with a sand layer is shown in Figure 4. The total thrusting force was applied in approximately $1\frac{1}{2}$, 45, and 90 min for the fast, medium, and slow loading rates, respectively. From these data it is apparent that rate of loading has no appreciable effect on the displacement of slabs on sand layers. This finding agrees with that of Stott (2) who observed that restraint offered by a friction-reducing layer of sharp sand was not markedly affected by variations in the rate of slab movement between 0.08 and 0.5 in. per hour.

Successive Slab Movements

Examples of data obtained from these successive movements are shown in Figure 5 for 5-in. thick slabs cast on a sand layer, polyethylene sheeting, and emulsified sand asphalt. Once free sliding occurred at first movement, the slabs moved so rapidly under the accumulated thrusting force that accurate force-displacement measurements
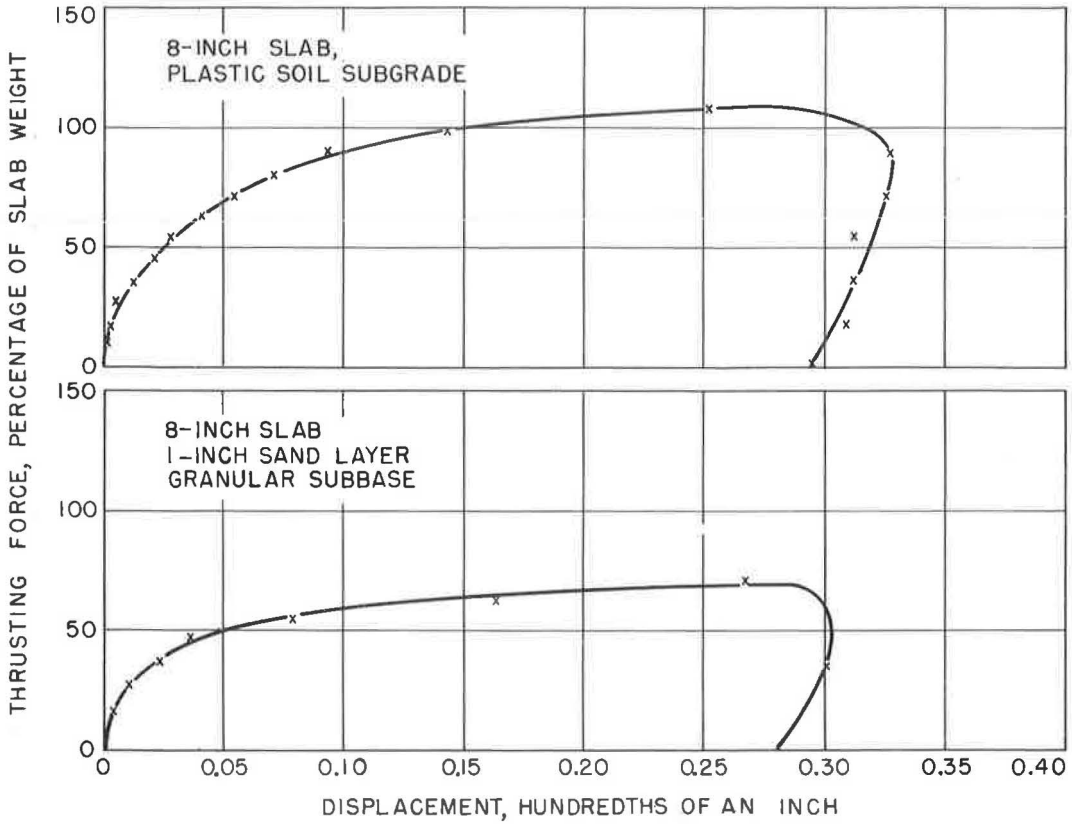
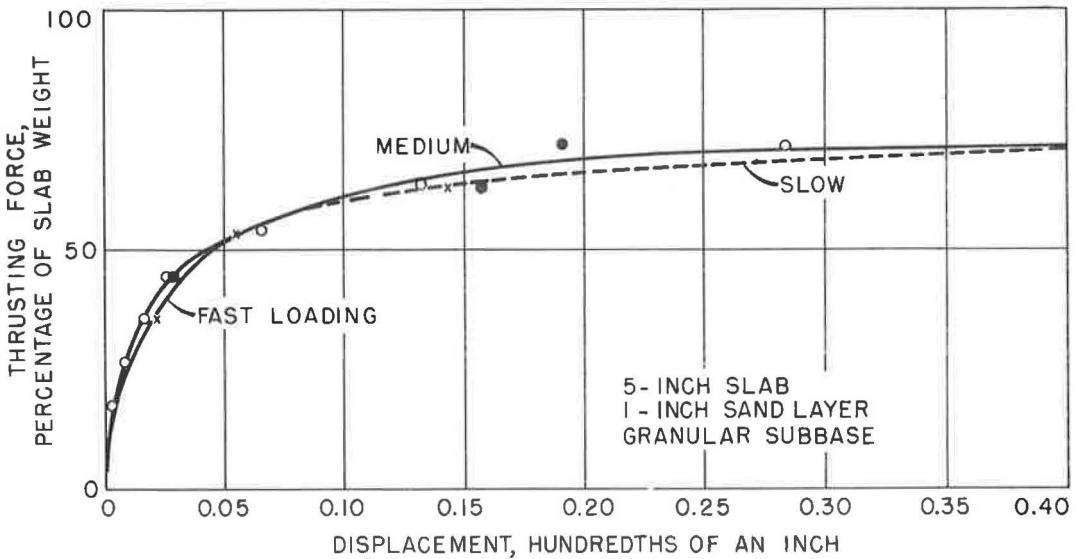Figure 3.   Typical force-displacement curves.

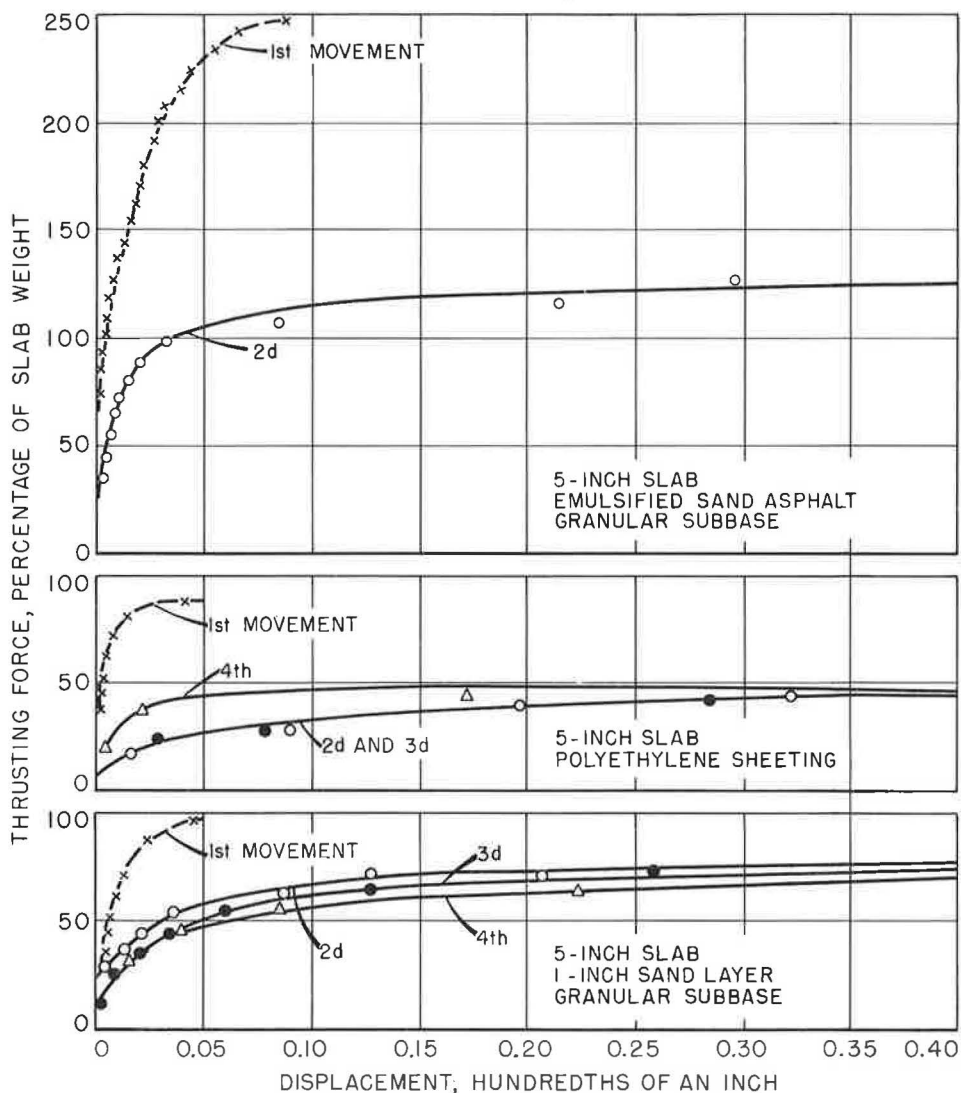Figure 4.   Effect of rate of loading on force-displacement relations.

Figure 5. Effect of successive slab movements on force-displacement relations.

were unattainable. This accounts for the plotted data on the first-movement curves being terminated at the point where free sliding began.

Figure 5 shows that all three of the proposed friction-reducing mediums produced, as expected, greater resistance to slab displacement for the first movement than for the following movements. It is evident, however, that a condition of essential stability of resistance is obtained after only two or three movements. The data also show that the magnitude of the coefficient of friction or thrusting force at free sliding (expressed in terms of percentage of slab weight) is considerably greater for the emulsified sand asphalt than for the polyethylene sheeting and the sand layer.

Tests of the emulsified sand asphalt were discontinued after the second movement of the slab because of the large thrusting force necessary to cause free sliding. Likewise, tests of the sheet asphalt were concluded after the first movement because the thrusting force required to start free sliding was three times the weight of the slab. Both of the materials bonded themselves to the bottom of the slab, thus indicating the need for an intermediate sliding medium if used beneath prestressed pavements.

Winter-Summer Comparisons

Force-displacement relations were obtained in the summer and again in the winter-spring period for 5-, 8-, and 11-in.-thick slabs on the plastic subgrade soil, granular subbase, blend of washed sand and gravel, and the sand layer. The foregoing mediums are identified previously as conditions 1 through 4, respectively. A 5-in. slab was cast on each of the mediums and, in turn, weighted to the equivalent of 8- and 11-in. slabs. The data developed in these tests are shown in Figures 6-9, with each plotted value being the average of five slab movements. The first movement of the slab in a test series was not included in the average. Consequently, the values represent a condition of essential stability of resistance to slab movement. The subgrade was not frozen at the time of the winter-spring tests.

The force-displacement relations for the slabs on the plastic subgrade soil are shown in Figure 6. For a displacement up to about 0.1 in., it is evident that less thrusting force was required to move the slabs in the winter than in the summer. However, in the free-sliding range, the thrusting force necessary to move the slabs in the winter was at least equal to that required for summer movement. The moisture in the top $\frac{1}{2}$ in. of the subgrade soil was 22 and 25 percent, respectively, at the time of the summer and the winter-spring tests.

There is a tendency for the coefficient of friction to decrease in magnitude with an increase in slab thickness. This same tendency was observed by Teller and Sutherland (4) who noted that it may be related to resistance to movement caused by an elastic or semi-elastic deformation within the soil itself.

Figure 7 presents the force-displacement relations for those slabs on the granular subbase. Experience has shown that the surface of granular subbases may vary considerably in roughness with the type of granular material and construction practices. In this study the surface of the granular subbase was considered to be relatively smooth and quite sandy in texture.

The relations observed indicate that (a) the magnitude of the friction coefficient for the granular subbase, unlike that for the plastic subgrade, tends to remain constant with an increase in slab thickness, and (b) the shape of the force-displacement curve for the granular material, again unlike that for the plastic soil, is unaffected by moisture conditions related to the season of the year.

Figures 8 and 9 present the summer and winter-spring relations for the slabs on the blend of washed sand and gravel and for the slabs on the 1-in. sand layer, respectively. Except for the winter data of the 5-in. slab, the relations for the blend of washed sand and gravel are quite similar to those found for the granular subbase. The data of Figure 9 show conclusively that the coefficient of friction for the slabs on the 1-in. sand layer is unaffected by seasonal variations in subgrade moisture or by slab thicknesses. These conditions appear to be typical for slabs on granular materials.

Force-displacement relations were obtained only in the summer for the slabs on the double layer of special polyethylene sheeting used to cover a thin leveling course of sheet asphalt. From these relations, shown in Figure 10, it is evident that slab thickness has little effect on the magnitude of the coefficient of friction.

Summary of Friction Coefficients for 5-In. Slabs

Coefficient of friction data for the 5-in. thick slabs on each of the seven different mediums included in this study are summarized in Figure 11. The seven mediums are arranged from left to right in the descending order of the magnitude of related coefficient of friction values. The numbers in parentheses identify the mediums with the seven conditions mentioned earlier in this report. These values are the maximum developed in the tests at free sliding, regardless of the season of the year.

Two significant facts are apparent from the data shown in Figure 11. First, the friction coefficient for the initial movement of a slab is appreciably greater than that for the average of subsequent movements, ranging from approximately 35 percent greater for the 1-in. sand layer to about 90 percent for the emulsified asphalt. Secondly, the polyethylene sheeting produced the lowest coefficient of friction values, about 0.9 for first movement and 0.5 for subsequent movements, followed by the 1-in. sand layer with nearly 1.0 for first movement and about 0.7 for subsequent movements.
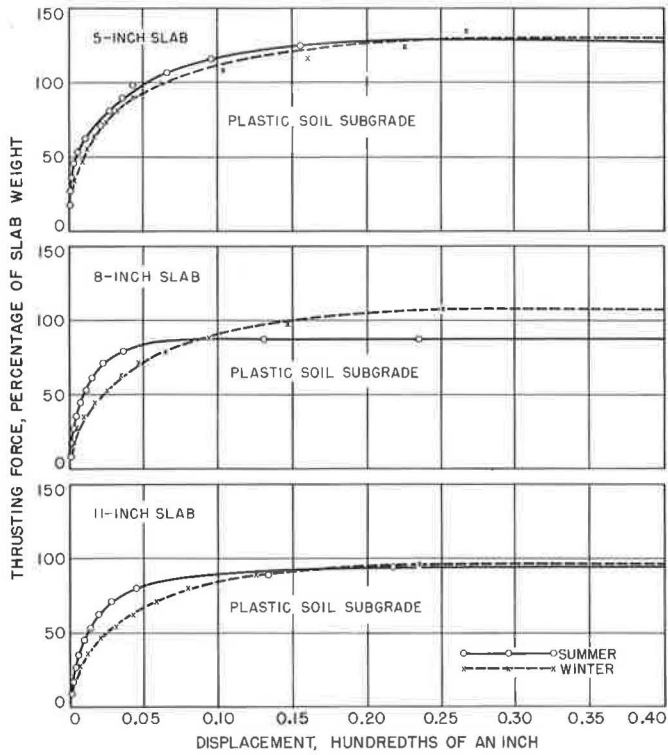
35

Figure 6. Force-displacement curves for concrete slabs on plastic soil.
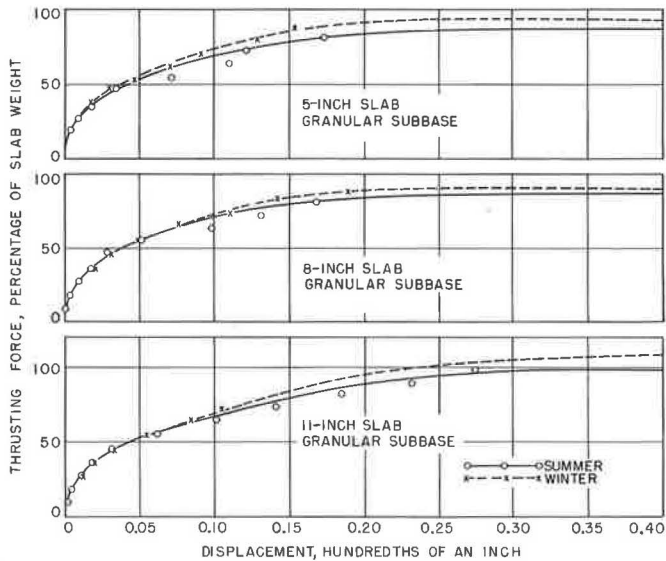

Figure 7. Force-displacement curves for concrete slabs on granular subbase, BPR grading
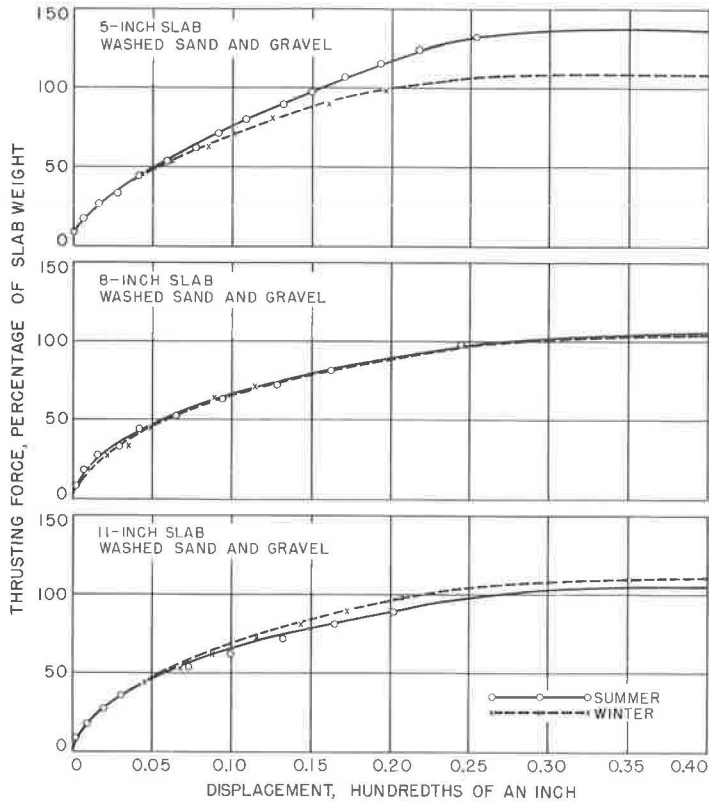and plasticity requirements.

Figure 8. Force-displacement curves for concrete slabs on blend of washed sand and gravel subbase.
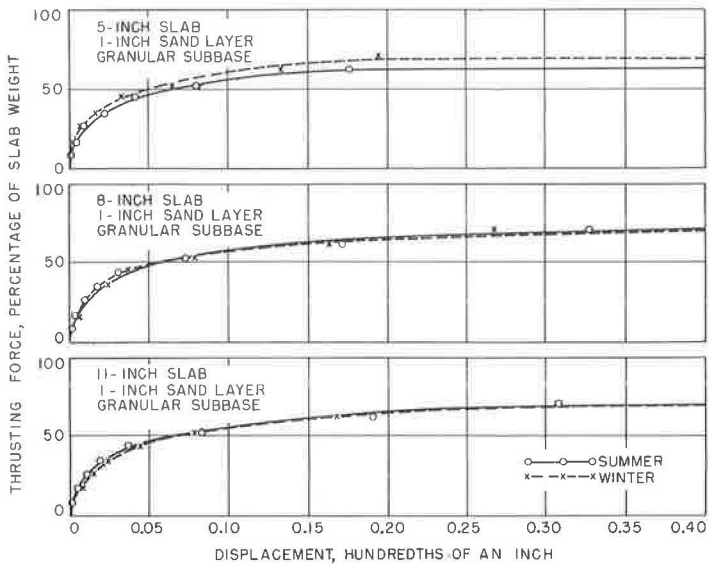

Figure 9. Force-displacement curves for concrete slab on granular subbase plus 1-in. sand layer.
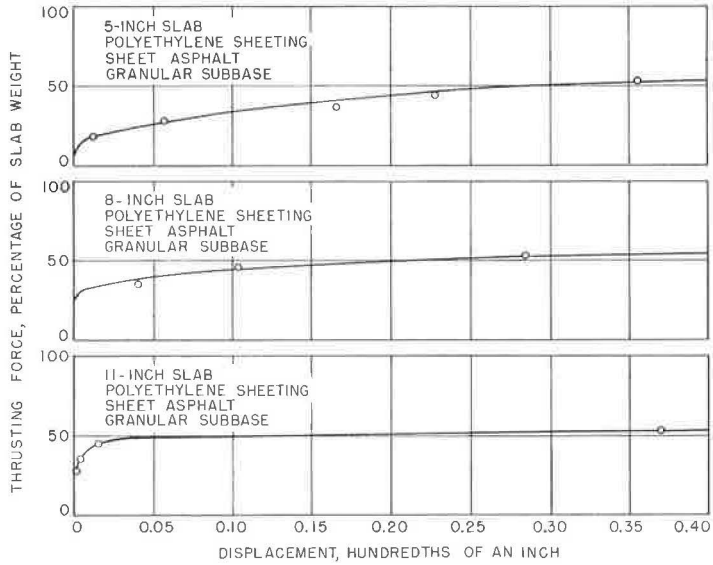
Figure 10.   Force-displacement curves for leveling course of asphalt covered with
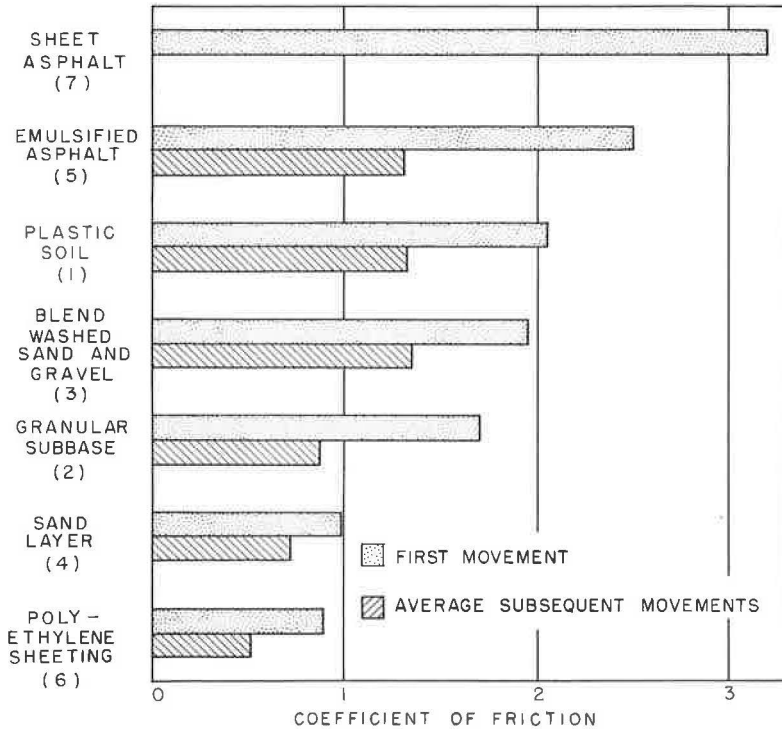a double layer of polyethylene sheeting.

Figure 11. Summary of coefficients of friction for 5-in. slabs.

CONCLUSIONS

The following conclusions are based on the analysis of the data developed in this study.

1. For granular materials, the magnitude of the coefficient of sliding friction is unaffected by slab thicknesses ranging from 5 to 11 in. and by seasonal variations in subgrade moisture content. For the double layer of polyethylene sheeting on the thin leveling course of sheet asphalt, the magnitude of the coefficient of friction is unaffected by slab thickness. The effect of seasonal variations in subgrade moisture on the friction coefficient for the polyethylene sheeting was not determined in this study.

2. For sand layers, the coefficient of friction is unaffected by rate of application of the thrusting force (rate of loading), ranging from $1\frac{1}{2}$ min to 90 min for total applied force. The effect of rate of loading was not determined for the other mediums included in this study.

3. The coefficient of friction for the initial movement of a slab is appreciably greater than for subsequent movements, with a condition of essential stability of resistance being obtained after only two or three cycles of movement.

4. A thin sand layer and a double layer of polyethylene sheeting on a thin leveling course of sheet asphalt are effective friction-reducing mediums.

REFERENCES

1. Goldbeck, A. T., "Friction Tests of Concrete on Various Subbases." Public Roads, 5(5) (July 1924).
2. Stott, J. P., "Tests on Materials for Use in Sliding Layers Under Concrete Road Slabs." Civil Engineering, 56(663-665) (1961).
3. "Standard Specifications for Construction of Roads and Bridges on Federal Highway Projects." FP-61, Section 200, U. S. Bureau of Public Roads.
4. Teller, L. W. and Sutherland, E. C., "The Structural Design of Concrete Pavements." Public Roads, 16(8-10) (Oct., Nov., Dec. 1935).

Tests of Concrete Pavement Slabs on Cement-Treated Subbases

L. D. CHILDS
Development Engineer, Research and Development Laboratories, Portland Cement
Association, Skokie, Ill.

Concrete pavement slabs were built on cement-treated subbases
and tested to determine deflection, strain, and pressure re-
sponse to static loads. Concrete thickness varied from 3 to 8
in. and subbase thickness from 3 to 9 in. Subbase surface treat-
ments were (a) cement-sand grout to produce bond; (b) a polye-
thylene film to prevent bond; and (c) in one instance, an asphalt
emulsion.

The pavements were evaluated relative to 8-in. concrete on
a 5-in. gravel subbase by measuring deflections, slab strains,
and subgrade pressures when loads were applied at interiors,
edges, and joints. Based on equal edge deflections, the ability
to carry loads ranged from 200 percent of the standard for 8-in.
concrete bonded to 5-in. cement-treated subbases, to 45 percent
for 3-in. concrete on a 3-in. cement-treated subbase with an
asphalt emulsion treatment. It was shown that bonded interlayers
increased the ability to carry load as much as an additional $\frac{1}{2}$
to 1 in. of concrete.

Experimental deflections at interiors and edges were in good
agreement with those computed by the Westergaard formulas
when the bearing value of the cement-treated subbase was meas-
ured by a 30-in. plate.

•THE SERVICEABILITY of a concrete pavement depends largely on the stability and
uniformity of the material on which it is built. Because highway systems traverse
areas with different soils and corresponding differences in bearing capacity and volume
change characteristics, it is often necessary to temper the effects of these variations
on serviceability by building subbases of stable material.

Granular materials, ranging from a maximum size compatible with layer thickness
to a minimum where not more than ten percent passes the No. 200 sieve, have proven
successful for subbases for primary pavements. Laboratory tests on both open-graded
and dense-graded materials in this category have shown that if the materials were
placed according to standard density and moisture conditions, there was negligible
densification under repetitive loads (1), and pressures on the subgrade were small for
all thicknesses tested (2). It was also found that the slight increase in bearing value
achieved by thickening the subbase layers did not significantly improve the ability of 8-
in. concrete slab pavement systems to support loads.

Because granular materials suitable for subbases are not readily available in all
parts of the country, marginal soils of low plasticity have been treated with cement and
compacted on the subgrade to serve as pavement subbases. The success of this method
prompted an extension of the laboratory study of subbases to include a study of the load-
deflection, strain, and pressure response of pavements incorporating concrete on
cement-treated subbases.

OBJECTIVES AND SCOPE

Studies by Abrams (4) have shown that cement-treated bases offer considerable resistance to deflection under load. As the load that can be carried by a concrete pavement increases with the improved bearing value of the foundation, it follows that concrete slabs on cement-treated subbases should be capable of carrying greater loads than those on granular subbases.

The tests had a threefold objective: (a) to measure the deflection, strain, and pressure response of loaded concrete slabs on cement-treated subbases; (b) to investigate the feasibility and desirability of developing full interface friction between the concrete and the cement-treated subbase by establishing interlayer bond; and (c) to study the adaptability of current design methods to concrete pavements on cement-treated subbases.

The program includes pavements of 3, 5, 7 and 9 in. of concrete on 3, 6, 9 and 12 in. of cement-treated subbase, in addition to pavements of 8-in. concrete on 5-in. cement treatment which were built and tested for direct comparison with pavements of 8-in. concrete on 5-in. granular subbases. Tests were scheduled to permit the reporting of data on pavements of concrete less than 9 in. thick prior to completion of the total program. Tests on thicker slabs were deferred for later study.

This progress report is restricted to an evaluation of nine pavements. In addition to the data from tests of 8-in. concrete on 5-in. cement-treated subbase (CTS), results are shown for combinations of 3-, 5-, and 7-in. concrete slabs on 3- and 6-in. CTS; and 3- and 5-in. concrete on 9-in. CTS. For this phase of the study the concrete and CTS materials were not varied, and the subbase material contained sufficient cement to meet minimum requirements for soil-cement as determined from ASTM test procedures and PCA weight-loss criteria.

Load-deflection and strain responses of the various combinations were measured when the slabs were subjected to static loads. A limited repetitive load study was made on two bonded structures to explore early bond failure, but equipment was not available for complete fatigue tests.

MATERIALS

Subgrade.—A silty clay soil was placed in a 4-ft deep waterproofed pit to form the subgrade for the pavements. Gradation and moisture-density relations are shown in Figure 1. The soil was compacted in 6-in. lifts to standard conditions as determined by AASHO method T99 or ASTM Method D698 with mechanical tampers. To maintain a low subgrade bearing value, it was necessary to rework the surface each time a new pavement was placed. This value, k, measured with a 3-in. diameter plate at 0.05-in. deflection, ranged from 70 to 90 psi per in. of deflection.

Cement-Treated Material.—A nonplastic soil with a gradation curve labeled cement-treated material in Figure 1 was mixed with 5.5 percent cement by weight and 11 percent water in a pug mill and compacted on the subgrade. The cement requirement was determined from ASTM Standard Methods D559 and D560 and the Portland Cement Association criterion for weight loss (5). The moisture-density curve, determined by ASTM Method D558 (Fig. 1) indicated standard conditions to be 125 pcf at 10.5 percent moisture.

The cement-treated material was compacted by mechanical tamper and vibrating sled as shown in Figures 2 and 3, and moist cured until concrete was cast. In-place densities, moistures after compaction, and bearing values measured at age 14 days with a 30-in. diameter plate at 0.05-in. deflection are given in Table 1.

The pavement code is made up of two numbers and a letter. The first number is the concrete thickness; the letter denotes interface treatment (as shown by Column 3); and the last number is CTS thickness. The reference for these tests is 8-in. concrete on 5 in. of compacted open-graded gravel (8G5) (3).

Specimens were molded as suggested by Felt and Abrams (6) from samples of the material during placement. These were tested in compression and flexure and for sonic modulus at ages 7, 28, and 60 days. The results are given in Table 2.
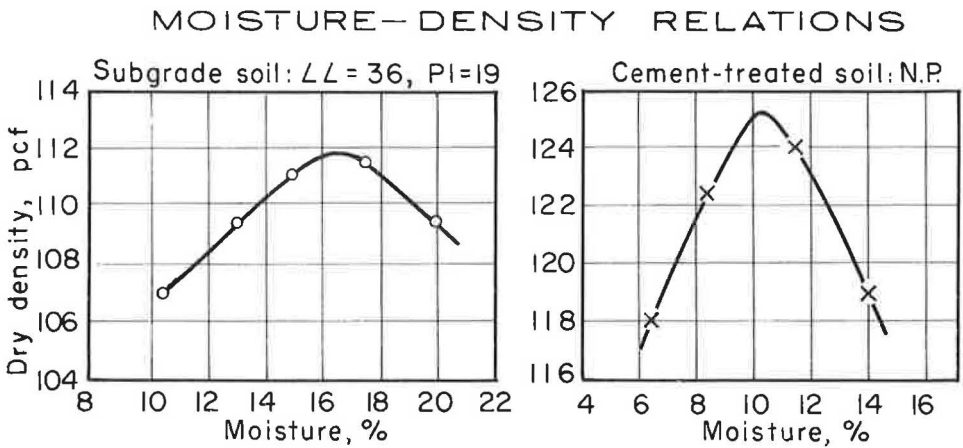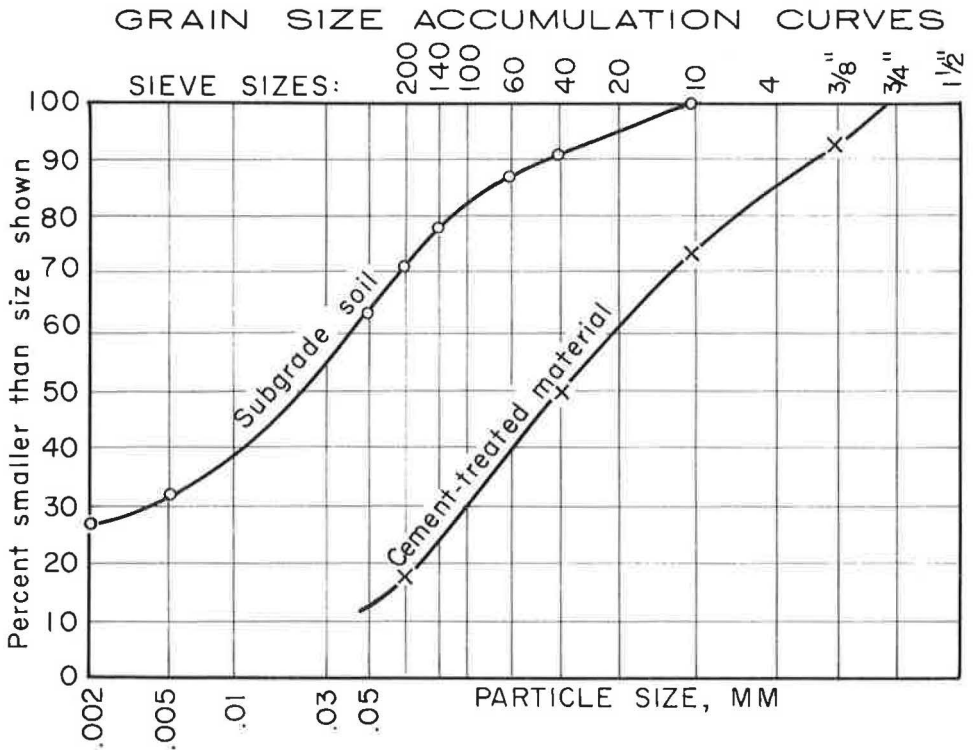
GRAIN SIZE ACCUMULATION CURVES

MOISTURE–DENSITY RELATIONS

Figure 1. Foundation materials.

Figure 2.   Consolidation of subbase with
             mechanical tamper.

Figure 3.   Final consolidation and level-
             ing with vibrating sled.

TABLE 1

IDENTITY AND PROPERTIES OF SUBBASE AND SUBGRADE

Identity				Subbase in Place Data			
Layer Thickness		Upper Interface Condition	Pave- ment Code	Dry Density (pcf)	Mois- ture (%)	30-In. Plate Bearing, k (pci)	
Concrete	Subbase					Subgrade	Subbase
8	5 in. gravel	—	8G5	135	7.3	75	130
8	5 in. s/c	No bond	8N5	127	9.8	88	350
8	5 in. s/c	Bond	8B5	131	10.6	90	360
7	6 in. s/c	No bond	7N6	129	10.2	80	405
7	3 in. s/c	Bond	7B3	130	10.3	70	200
5	9 in. s/c	No bond	5N9	126	10.0	66	540
5	6 in. s/c	No bond	5N6	124	11.3	74	410
5	3 in. s/c	No bond	5N3	119	11.2	75	203
5	3 in. s/c	Bond	5B3	122	11.4	65	188
3	9 in. s/c	Bond	3B9	118	11.6	69	510
3	6 in. s/c	Bond	3B6	123	10.6	75	378
3	6 in. s/c	No bond	3N6	119	9.7	71	365
3	3 in. s/c	Bond	3B3	121	10.8	68	190
3	3 in. s/c	SS-1[a]	3S3	119	10.5	78	210

[a]CTS surface coated with asphaltic emulsion SS-1.

TABLE 2

CTS SPECIMEN PROPERTIES

Pave-ment[a]	Cylinders, Comp. (psi)			Beams, Flex. (psi)			28-Day Sonic Modulus (10^6 psi)
	Days			Days			
	7	28	60	7	28	60	
8N5	330	420	490	65	105	160	1.42
8B5	320	505	610	75	110	170	1.62
7N6	280	380	470	68	112	165	1.65
7B3	350	520	630	77	119	177	1.68
5N9	290	410	500	60	95	150	1.36
5N6	305	515	610	73	120	170	1.70
5N3	355	530	640	68	98	146	1.47
5B3	330	500	615	78	103	180	1.55
3B9	270	390	480	73	100	145	1.49
3B6	310	480	590	70	113	166	1.67
3N6	340	520	625	66	108	153	1.60
3B3	300	490	580	80	120	158	1.50
3S3	280	460	550	97	123	172	1.52

[a]Identifying code in Table 1.

TABLE 3

CONCRETE SPECIMEN DATA

Pave-ment[a]	Cylinders, Comp. (psi)			Beams, Flex. (psi)			28-Day Sonic Modulus (10^6 psi)
	Days			Days			
	7	28	60	7	28	60	
8G5	4,400	5,200	5,500	500	580	640	5.2
8N5	3,920	4,850	5,420	510	590	695	5.9
8B5	3,700	4,450	5,100	545	605	710	6.0
7N6	3,860	4,710	5,330	560	670	750	5.9
7B3	4,085	4,625	5,220	600	720	790	6.0
5N9	3,690	4,580	5,270	520	650	720	5.8
5N6	3,390	4,525	4,960	555	635	690	5.5
5N3	4,160	4,505	5,135	608	706	740	5.6
5B3	4,090	4,800	5,450	586	680	722	5.6
3B9	3,750	4,530	5,265	563	605	760	5.9
3B6	3,780	4,690	5,100	536	675	790	5.8
3N6	3,520	4,380	5,150	510	610	700	5.7
3B3	3,630	4,160	4,825	520	570	660	5.3
3S3	3,980	4,660	5,070	490	565	655	5.5

[a]Identifying code in Table 1.

Concrete. — The concrete was made with 1-in. maximum gravel aggregate and was mixed in the laboratory plant. The cement factor was 6 sk per cu yd, water-cement ratio 0.50, slump 2.5 to 3.5 in., and air content 4 to 5 percent. Standard 6- × 12-in. cylinders and 6- × 36-in. beams were molded when the slabs were cast. Compressive and flexural strengths and sonic modulus values of fog cured specimens are given in Table 3.

The slabs were cured with wet burlap until mortar dikes could be constructed to contain water on the surface and protect the areas designated for application of strain gages. When these were completed, the slabs were flooded and water was retained on the surface throughout the first series of tests to prevent upward curl due to differential changes in moisture content. Later, 8 to 10 weeks, the water was removed for the second series of tests on curled slabs.

INSTRUMENTATION AND OPERATIONS

The pavements were constructed and tested in an area where temperatures were maintained between 65 and 75 F. Loads were applied by hydraulic jacks reacting against an overhead frame. Circular steel plates on rubber pads distributed the load to the concrete (Fig. 4).

The first two pavements tested were 8-in. concrete on 5-in. CTS. These slabs were 12 × 18 ft and were cast with a doweled $\frac{3}{8}$-in. wide butt joint connecting the slabs along the 18-ft edges. The subbase extended 1 ft beyond the edge of the concrete on all pavements except a duplicate 8N5 that was built without the ledge (Fig. 5).

Two treatments were used at the interlayer between the concrete and subbase. In one case, the CTS was covered with 4-mil polyethylene film prior to concreting to prevent bond; and in the second case, a grout of equal parts of fine sand and cement was brushed onto the subbase to assure bond. At the end of test the shear strengths at the bonded surface, measured by direct shear tests on 6-in. diameter cores, ranged from 100 to 200 psi. Figure 6 shows a sawed and broken section of pavement illustrating the composite bonded construction.

The 8-in. slabs were instrumented with SR-4 type A-9 gages and pressure cells as shown in Figure 7. Deflections were measured with 0.001-in. dial indicators at the edges of the 12- and 16-in. plates, and at intervals on a transverse line in the vicinity of the load.

For the remaining combinations of concrete on the cement-treated subbase, the pavements were altered to include two types of transverse joints. The slab dimensions were reduced from 12 × 18 ft to 10 × 14 ft, and 5-ft slabs were built at each end to provide joints that could be tested for load transfer effectiveness when loads were placed at the joints. The test slab and one end slab were connected by a smooth-faced construction joint with no provision for load transfer. This was formed by casting fresh concrete
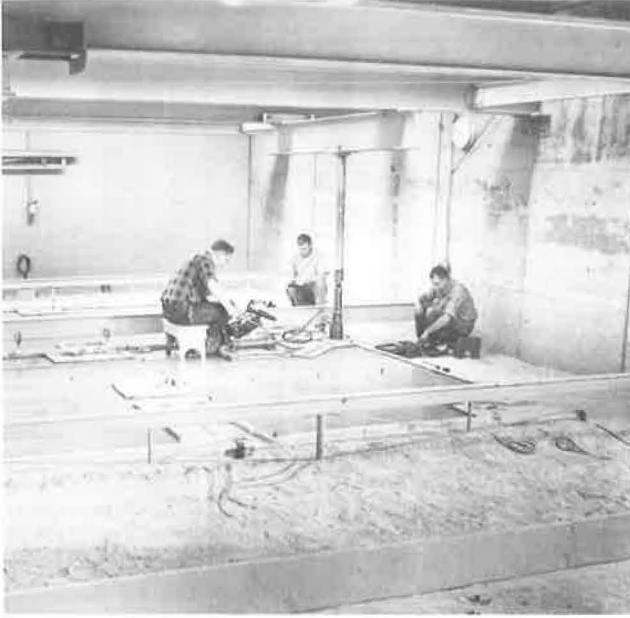
44

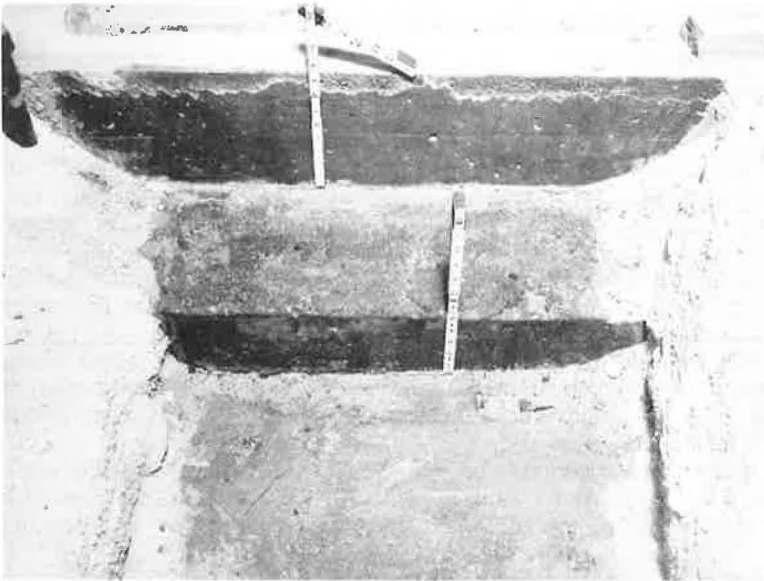Figure 4. Static load tests at doweled corner of flat slab.

Figure 5. Ledge of 5-in. cement-treated subbase (CTS) 1-ft beyond edge of 8-in. concrete slab.
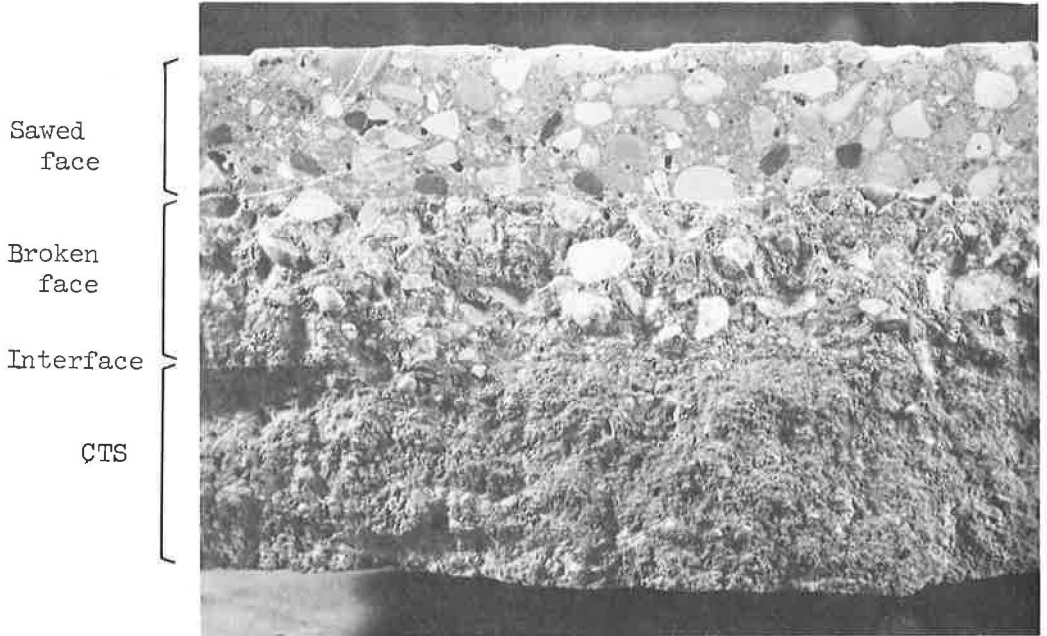
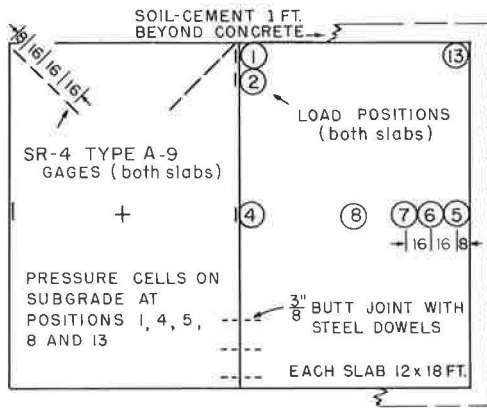Figure 6. Efficacy of bond between concrete and cement-treated subbase.

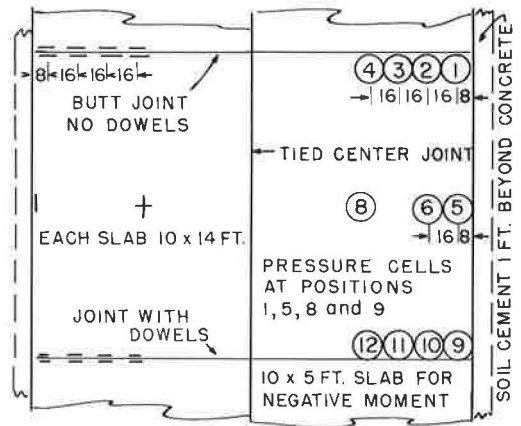

Figure 7. Gage and load locations for 8-in. concrete.

Figure 8. Gage and load locations for 10-x 14-ft slabs.

against the hardened concrete of the test slab. On the opposite end, the same casting procedure was followed, but round steel dowels extended through the joint. These joints differed from the usual contraction joint because there was no interlock of aggregate. Dowel diameters were $\frac{1}{8}$ in. for each in. of concrete thickness, and spacing was 12 in. except that dowels in 3-in. concrete were $\frac{1}{4}$ in. diameter and 6 in. on centers. All joint openings remained less than 0.02 in. throughout the tests. The interlayer treatments were the same as those described for 8-in. concrete on 5-in. CTS and are designated N or B except for combination 3S3, on which an asphalt emulsion was applied to the 3-in. subbase.

Loads on 10- × 14-ft slabs were distributed by 16-in. diameter plates. The area under the 16-in. plate was equivalent to the effective contact area of a pair of 7.00-20 dual truck tires. Maximum loads varied with load position and pavement response. On the thinner combinations, edge loads rarely exceeded 9,000 lb. Load positions are shown in Figure 8.

TEST RESULTS

Deflections, strains, and pressures for all load increments were recorded for eleven positions on the 8-in. concrete and for 13 positions on the other thicknesses. From these data, trends were established and the influence of specific variables was determined.

Flat Slabs

Data from Tests at Interiors, Edges, and Joint Corners.—The effect of load intensity on slab deflections, strains, and subgrade pressures for three combinations are shown in Figure 9. Curves for 8-in. concrete on 5-in. gravel, 8G5, are included for comparison. The small deviations from linearity are typical of all combinations tested. Due to this the deflections, strains, and pressures caused by loads were compared at a 9-kip load because it is the legal wheel load limit in many States, and all unrestricted roads and streets must be capable of carrying a limited number of loads of this intensity.

Relative Response of Test Pavements to Load.—The deflection, strain, and pressure responses to 9-kip loads at interior and free edge positions on all combinations are shown in Figure 10. The ability to support loads is an inverse function of these measurements, therefore low magnitudes indicate high load capacity. The order of increasing magnitude of deflection, strain, and pressure is not always the same; but if the 8-in. slab on 5-in. gravel is ignored, the order is well established for combinations of
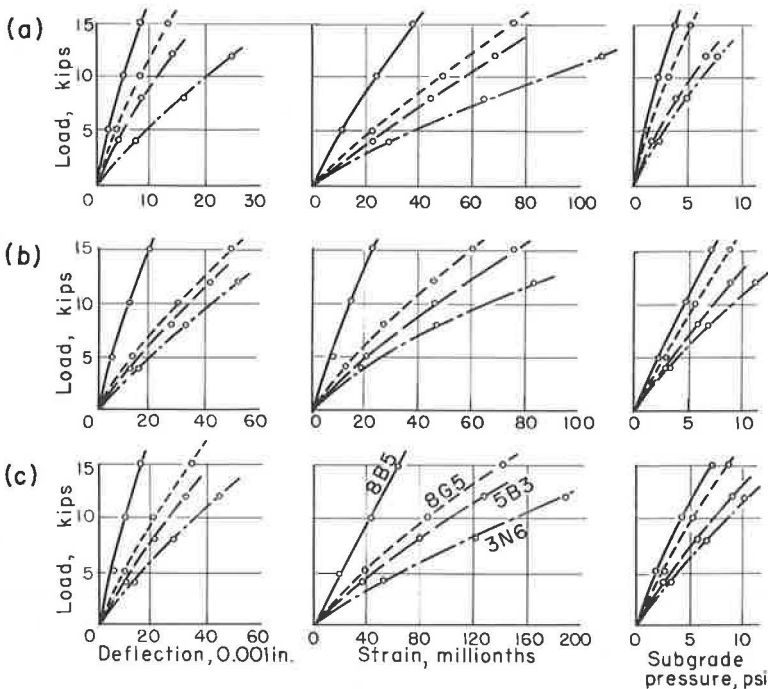

Figure 9. Representative data: (a) interior, (b) joint corner, and (c) free edge (8B5 and 8G5, doweled; 5B3 and 3N6, undoweled).
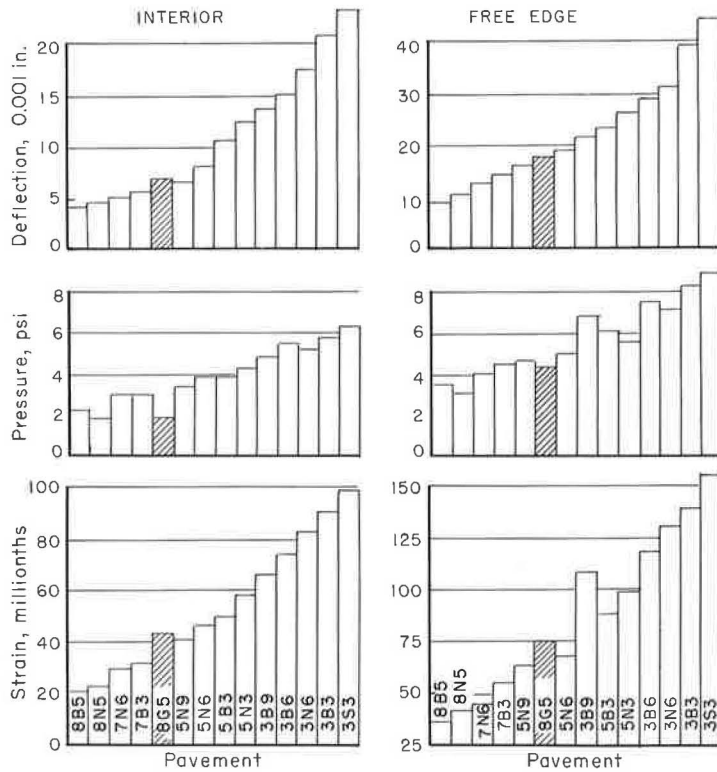
Figure 10. Deflections, strains, and pressures for all pavement combinations at 9 kips.

low response or high response and there is some variation in the middle range. When deflections and strains of the concrete pavements on CTS are compared with those of the standard 8G5, it is evident that combinations 8B5, 8N5, 7N6, 7B3, and 5N9 are stronger than the standard.

Loads causing edge deflection of the test pavements equal to that of 8G5 at 9 kips were computed and are as follows: 8B5, 18 kips; 8N5, 15 kips; 7N6, 13 kips; 7B3, $11\frac{1}{2}$ kips; 5N9, 10 kips; 5N6, $8\frac{1}{2}$ kips; 3B9, $7\frac{1}{2}$ kips; 5B3, 7 kips; 5N3, $6\frac{1}{2}$ kips; 3B6, $5\frac{1}{2}$ kips; 3N6, 5 kips; 3B3, $4\frac{1}{2}$ kips; and 3S3, 4 kips. It was assumed for this computation that load varied inversely as deflection. The 9-kip load for the standard 8G5 pavement is justified by the fact that the edge stress on this pavement at 9 kips was one half the modulus of rupture. The previous values may be modified in practice because all pavements are not designed for the same traffic life and higher loads are tolerated when the number of applications is limited.

Estimates of loads that would produce equal critical stress were not made because the strains measured in these tests were in the top fibers of the concrete, and on bonded pavements there is evidence of a shift in the neutral axis position away from the midplane of the concrete. Supplementary tests are needed to locate the position of critical tensile stress in these bonded pavements. It is noted that the 9-kip loads produced low compressive strains on the concrete surface of the stronger combinations and high strains in the concrete of the weaker pavements. However, during a checkout test of a repetitive load machine, more than 50,000 9-kip loads were applied to the 3S3 structure without evidence of concrete failure.

Effect of Load Placement on Measurements at Slab Edge. —Sensitivity of pavements to transverse location of load was explored by measuring edge deflections, strains, and pressures when loads were positioned inward from the free edge. Figure 11a compares data for 8-in. concrete slabs on 5-in. CTS with those for the standard 8-in. concrete on 5-in. gravel. The 8N5 structure was tested near an edge (a) without a subbase ledge,
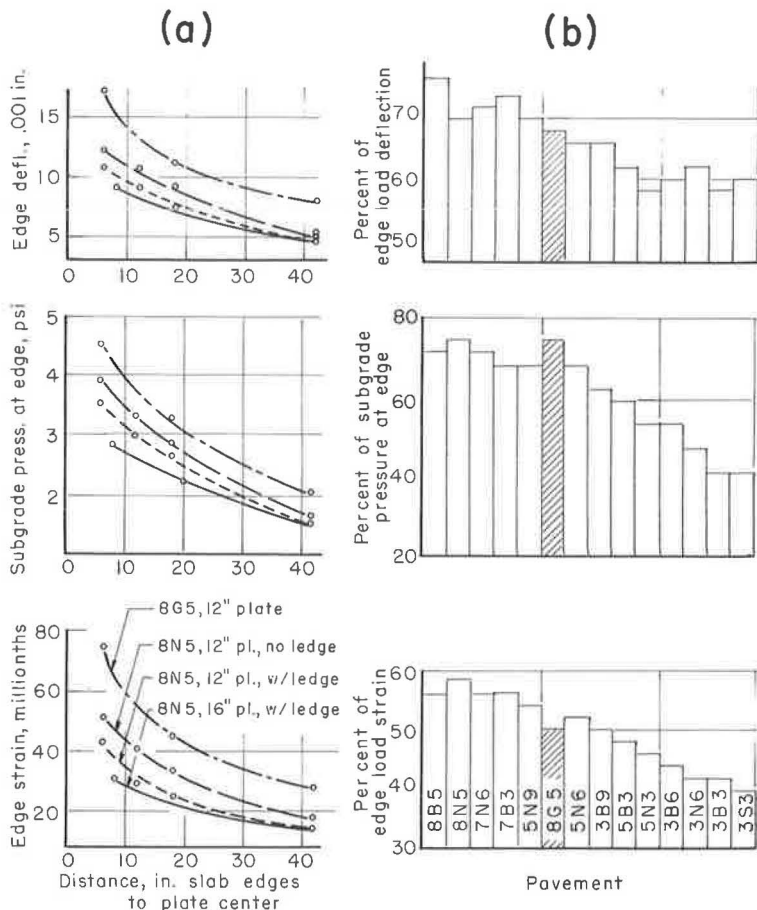
Figure 11. Slab response to 9-kip load near edge: (a) effect of lateral load placement on edge measurement, and (b) percent of edge load measurement developed when load center was 24 in. from edge.

i.e., the edge of the CTS was directly beneath the edge of the concrete, and (b) with a ledge of CTS extending 1 ft beyond the slab edge. Loads were applied with a 12-in. plate for direct comparison of the two types of edge construction with the granular subbase and repeated with a 16-in. plate on the treatment with a ledge to show the change in response to edge loads when the distribution area was increased to that of a pair of dual tires.

Plate Size and Ledge Effect—When loads were applied with 12-in. plates tangent to slab edges, deflections and strains for the 8N5 structure without the subbase ledge were about 70 percent of those for the standard. The 1-ft ledge caused further reduction, and edge deflections and strains were about 60 percent of those for 8G5. Additional relief was achieved by enlarging the bearing area, and values recorded with a 16-in. plate on the 8N5 structure with the ledge were about half those measured in the 8G5 standard. The effect of plate size and ledge diminished as the load position moved inward from the slab until at the 42-in. position no advantage was apparent.

Response to Load 2 Ft from Edge —Figure 11b shows the effect of inward placement of load on measurements at the slab edge for all combinations. The data, obtained when a 16-in. plate was placed with its center 2 ft from the slab edge and loaded to 9 kips, are expressed as percent of the value recorded when the plate was tangent to the edge.

Strains were more sensitive than deflections to lateral load placement. When loads were in from the edge, pressures and deflections for combinations having a greater ability to support loads than the standard 8G5 were approximately 70 percent of those due to edge loads; but as the pavements became more sensitive to deflection and strain, the ability to distribute a load also was reduced as evidenced by the lower strains, deflections, and pressures measured at the edge due to the inward load. Although longitudinal strains at slab edge due to inward loads on the thinner pavements are much less than those caused by loads on plates tangent to the edge, the reduced rigidity of these pavements results in higher transverse strains at the load, and longitudinal cracking is imminent.

Effect of Load Along Joint. —All combinations except the 8-in. concrete on 5-in. CTS were built with a butt joint with no mechanical interlock on one end of the test slab and a joint with dowels on the other. The slabs were tested under static loads at four locations along each joint as shown in Figure 8. Strain gages and deflection dials were located to read maximum compressive strains in the upper surface of the concrete and maximum deflections. In most cases the maximum tensile strain due to a load at the corner (position 1) was read on the gage at position 3 which was 40 in. in from the slab edge, although on occasion the gage located 56 in. from the edge indicated the largest strain.

There was no undoweled joint investigation for the 8-in. concrete on 5-in. CTS. At the doweled joints of these slabs, loads were placed at corners and also placed with plate centers 24 in. inward, as shown in Figure 7. Compressive strains were measured at the load, and tensile strains were measured along the corner bisector.

Strain and Deflection Profile at Transverse Joint—Transverse profiles of deflections and strains produced by 9-kip loads for each of the four load positions along a joint are shown for the undoweled joint of pavement 5N6 in Figure 12. The solid lines represent measurements on the loaded side of the joint, and measurements on the opposite side are shown as dashed lines.

When the loading plate was at the corner, tangent to the free edge, a maximum tensile strain parallel to the joint developed in the top fibers about 40 in. inward from the free edge. This strain was close in magnitude to the transverse compressive strain at the joint edge directly at the plate. As the load was moved inward along the joint from the slab edge, the compressive strain at the load increased until the load was 40 in. from the free edge, and deflection decreased until the load was 56 in. from the edge.

Summary of Joint Test Data—Figure 13 exhibits maximum deflections and strains on both the loaded and opposite sides of undoweled joints for each of four load positions when 9-kip loads were applied. Similar strains are shown in an order approximating increasing magnitude.

The trends exhibited for combination 5N6 in Figure 12 are corroborated by the measurements on the remaining combinations. In all cases the maximum deflections occurred under corner loading and diminished as the load was moved away from the longitudinal edge. Maximum measured strains occurred at the joint edge tangent to the plate when the load was 40 or 56 in. from the free edge.

When loads were applied at positions 1, 5, and 9, representing truck wheels along slab edges, strains at joint edges were always less than those at free edges. However, when the load plate was placed inward from the free edge at position 6, representing a more frequent wheel position, joint edge strains for positions 2, 3, and 4 exceeded those at free edges (Figure 11b). Thus, the area of critical strain in pavements depends on the path of a wheel with respect to the slab edge.

Doweled vs Undoweled Joint—Data from tests at doweled joints are shown in Figure 14. In most cases measurements for the same magnitude and load position were slightly lower at doweled joints than those at undoweled joints. However, doweled joints rated about the same as undoweled joints in load transfer effectiveness. Deflection differences and load transfer effectiveness are shown for the two 9-kip load locations on each of three slabs in Table 4.

Ratings for the remaining combinations may be computed from the data in Figures 13 and 14. Effectiveness is the Teller and Sutherland (7) ratio of deflection of the unloaded slab to the average deflection of both slabs. With one exception, effectiveness
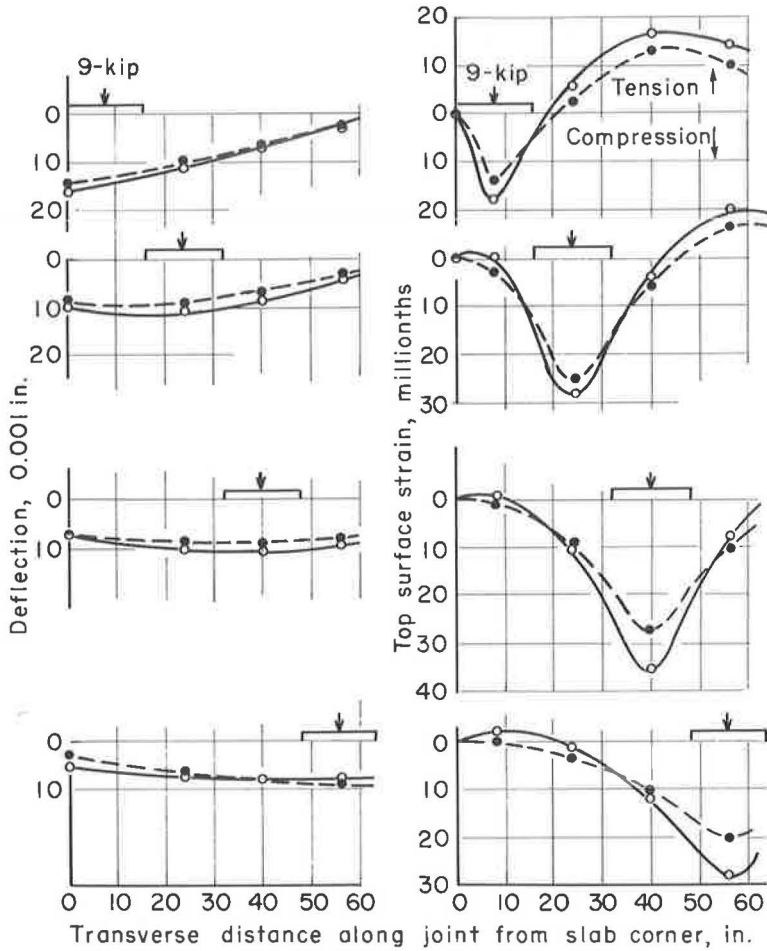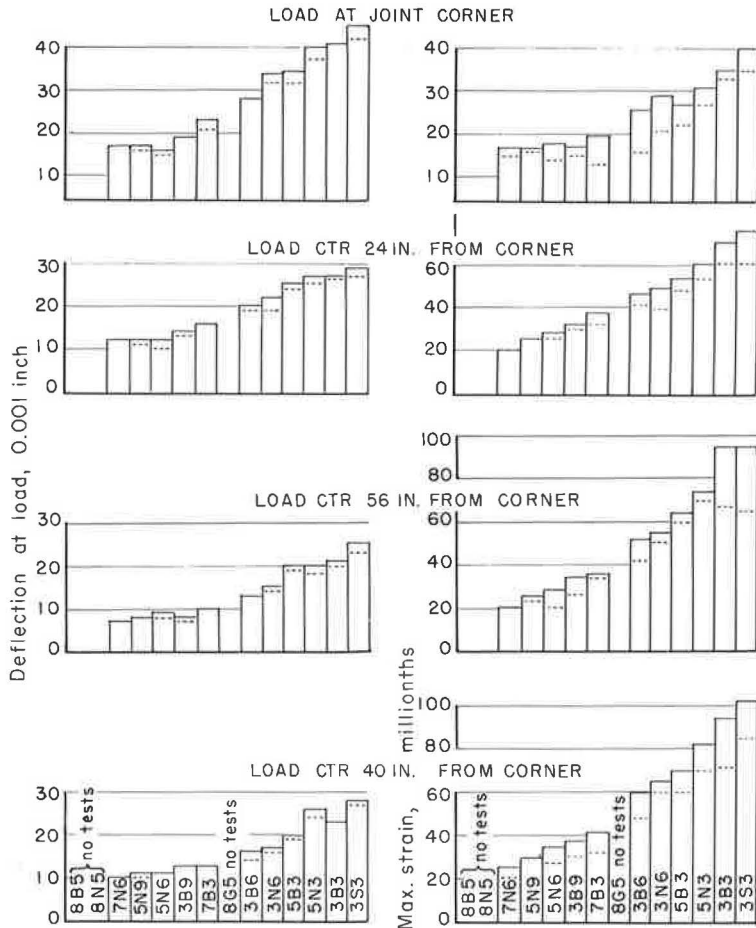
Figure 12.   Undoweled joint of 5-in. concrete slab on 6-in. cement-treated subbase.

was greater than 90 percent for all combinations and there was no significant difference in effectiveness between doweled and undoweled joints.

Relative Effect of Each Pavement Layer.—Although the evaluation study of concrete on a cement-treated subbase is not complete, the data in Figure 10 are sufficient to permit the construction of 3-point curves showing the effect of concrete thickness on deflections and strains when the subbase thickness was constant, and the effect of subbase thickness when the concrete thickness was constant. Figure 15 shows the influence of 3-, 5- and 7-in. concrete on 3-in. bonded and 6-in. unbonded CTS, and the effect of 3-, 6- and 9-in. CTS on 3- and 5-in. concrete.

For both the 3-in. bonded CTS and the 6-in. unbonded subbase, deflections and strains decreased significantly with increasing concrete thickness. For example, as concrete thickness was increased from 3 to 5 in., deflection reductions on the 3-in. bonded subbase averaged 45 percent and those on the 6-in. unbonded subbase 47 percent. Similarly, strain reductions on the 3-in. CTS averaged 40 percent, and those on the 6-in. CTS 45 percent. As concrete thickness was increased from 3 to 7 in., deflection reductions averaged 69 and 65 percent, respectively, on the 3-in. and 6-in. subbases, and strains were reduced 62 and 64 percent.

When the top layer of the pavement was 3-in. or 5-in. concrete, a 6-in. CTS reduced deflections 26 percent and strains 20 percent, on the average, below those of pavements
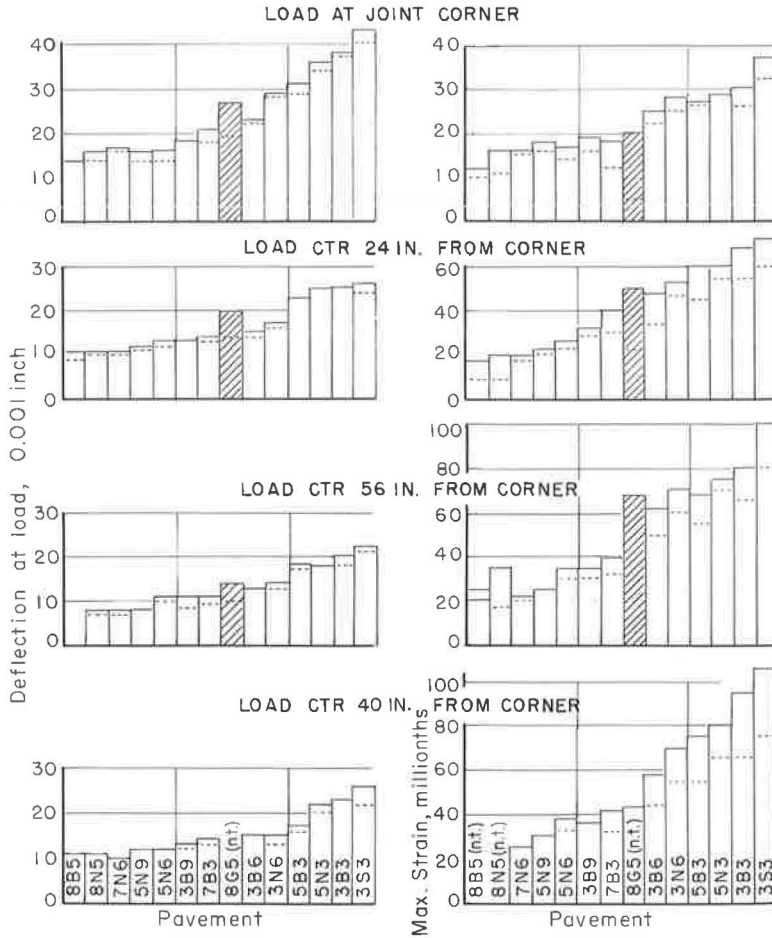
Figure 13.   Deflections and strains at undoweled joint.

TABLE 4

JOINT DEFLECTIONS AND LOAD TRANSFER EFFECTIVENESS

Pavement	Distance to Load (in.)	Deflection				Effectiveness	
		Undoweled Joint		Doweled Joint		Undoweled (%)	Doweled (%)
		Load (in.)	Opp. (in.)	Load (in.)	Opp. (in.)		
5N6	0	0.016	0.015	0.016	0.014	97	93
	56	0.009	0.008	0.011	0.010	94	95
7B3	0	0.023	0.021	0.021	0.018	96	92
	56	0.010	0.010	0.011	0.009	100	100
3B3	0	0.041	0.041	0.038	0.037	100	99
	56	0.021	0.020	0.020	0.018	98	95

LOAD AT JOINT CORNER

LOAD CTR 24 IN. FROM CORNER

LOAD CTR 56 IN. FROM CORNER

LOAD CTR 40 IN. FROM CORNER

Note: Dashed height = value across joint from load.
(n.t.) = no test   Load = 9 kips on 16 in. plate.

Figure 14.   Deflections and strains at doweled joint.

with 3-in. CTS. Subbases 9 in. thick resulted in deflection and strain reductions of 38 and 29 percent, respectively, below those when the subbase was 3 in. On a unit thickness basis, it is evident that the stronger material (concrete) reduced deflections and strains to a greater degree than the CTS.

Strength factors contribute also to the advantages of CTS over granular subbases in a pavement system. Load studies of concrete slabs on gravel (3) showed that gravel subbases in 5-, 10-, and 15-in. thicknesses reduced deflections at loaded edges of 8-in. concrete slabs by 7, 12, and 16 percent, respectively, below the values recorded when there was no subbase, and reduced edge strains 4, 10, and 13 percent, respectively. A 5-in. layer of unbonded CTS reduced deflections and strains about 50 percent. Thus, the 5-in. CTS was much more effective in increasing load capacity of 8-in. concrete pavements than 15 in. of gravel.

A tentative method for estimating combinations of concrete and CTS with equivalent load capacity is given in Figure 16. Maximum deflections caused by 9-kip loads at interior and free edge positions were expressed in terms of those of the 3B3 combinations. These values, in percent, were plotted as ordinates above the appropriate concrete thickness and CTS thickness. Trends for 3- and 6-in. subbases were estimated by curves on the left, and for 3- and 5-in. concrete by curves on the right. Ordinates for
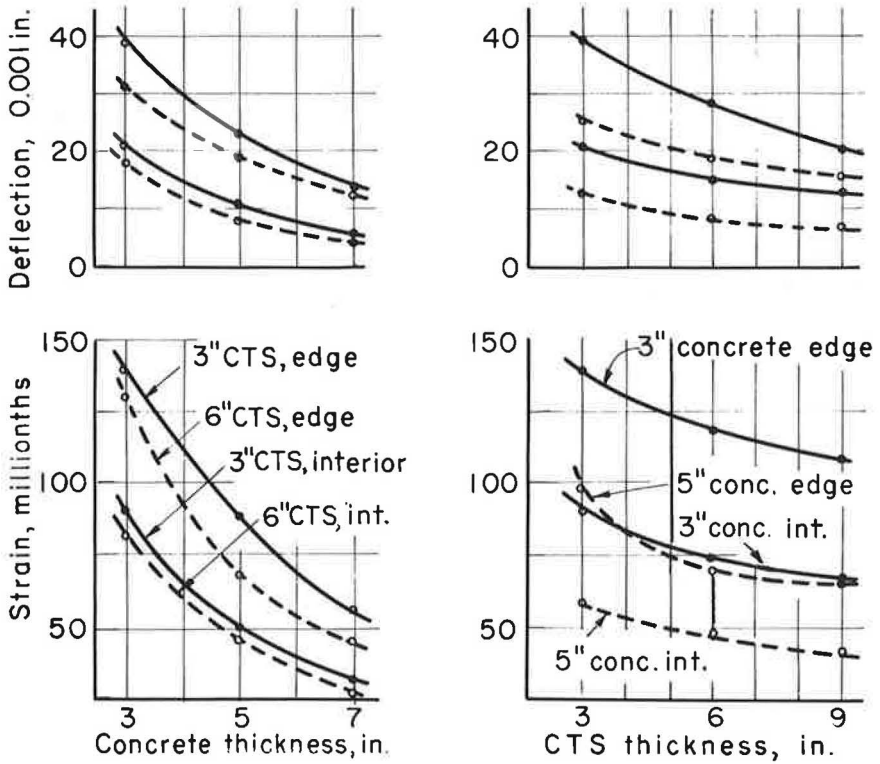
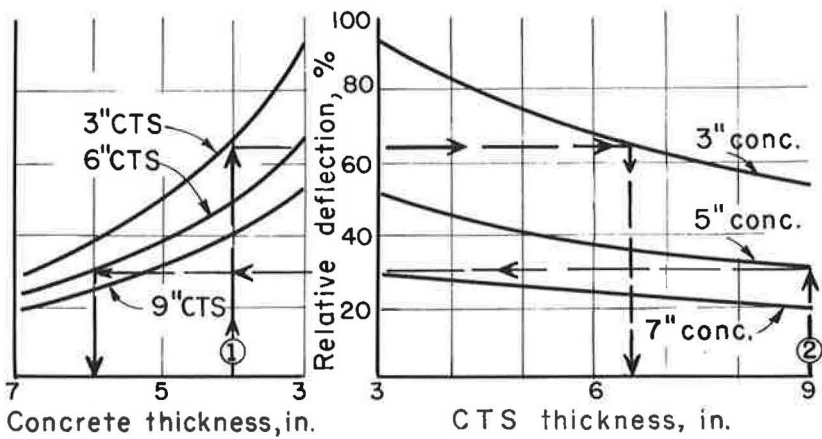Figure 15.   Influence of layer thickness.

Figure 16.   Pavements with equal deflections.

3- and 5-in. concrete on 9-in. CTS were transferred to the left to estimate the 9-in. CTS curve, and ordinates for 7-in. concrete on 3- and 6-in. subbase were brought to the right for the 7-in. concrete curve.

Examples of equivalent combinations of concrete and CTS are indicated by the arrows. Example 1 shows 4-in. concrete on 3-in. CTS to be equivalent to 3-in. concrete on $6\frac{1}{2}$-in. subbase. Example 2 indicates that 9 in. of CTS under 5 in. of concrete is about equal to 6 in. of concrete on 6 in. of subbase.

Effect of Interlayer Bond on Deflections and Strains.—Four of the pavement structures were tested with interlayer bond and without bond. The deflection and strain data from edge and interior tests, as shown in Figure 10, reveal that bond at the interlayer reduced pavements deflections below those of unbonded pavements. The data in Table 5 indicate that when subjected to 9-kip loads, deflections and strains of bonded layers ranged from 85 percent to 92 percent of the corresponding value for unbonded layers.

Reductions in deflection or strain of 8 to 15 percent due to the bond were not sufficient to change the deflection response of a weaker pavement system to that of the next stronger system tested. This is apparent in Figure 10. The significance of measure-

TABLE 5

EFFECT OF INTERLAYER BOND

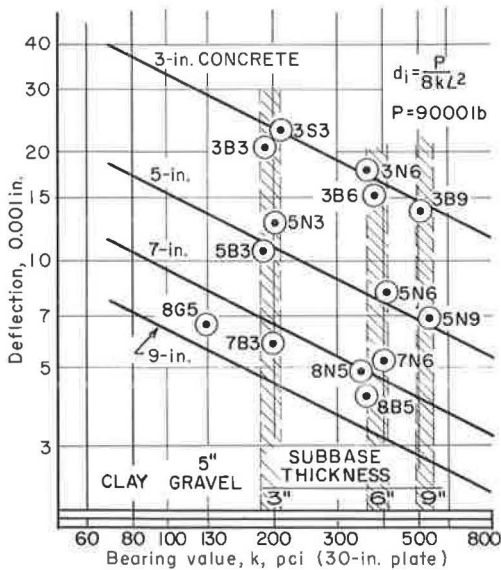| Pave-ment	Deflection (in.)		Strain (10^{-6})		Bonded vs Unbonded			
					Deflection (%)		Strain (%)	
	Interior	Edge	Interior	Edge	Interior	Edge	Interior	Edge
8B5	0.0042	0.009	21	36	87	86	92	86
8N5	0.0048	0.0105	23	42	-	-	-	-
5B3	0.0105	0.023	50	88	85	90	86	89
5N3	0.0123	0.0255	58	99	-	-	-	-
3B6	0.015	0.0285	74	118	86	92	90	91
3N6	0.0175	0.031	82	130	-	-	-	-
3B3	0.0205	0.039	90	139	89	88	92	90
3S3	0.023	0.044	98	155	-	-	-	-

Figure 17. Comparison of experiment data and theory at interior load position.
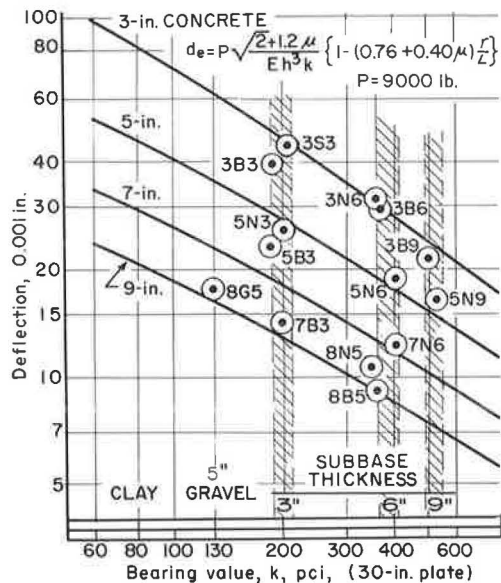

Figure 18. Comparison of experiment data and theory for load at slab edge.

ment reductions due to bond in terms of thickness of concrete is shown in Figures 17 and 18.

It should be noted that bond was obtained in the laboratory without difficulty by the application of cement-sand grout to the surface of the subbase. Cleansing alone or the application of an asphaltic emulsion did not guarantee bond. Weathering tests on beams of concrete and CTS bonded with cement grout showed negligible loss of bond.

Curled Slabs

After the static loadings of test pavements were completed, the ponding water was drained and the top surface of the concrete was allowed to dry. Corner and edge movements were recorded, and when corners moved upwards 0.025 in., or apparently stabilized at some lesser level, the static load tests were repeated. The time lapse between tests on flat and curled slabs varied from 10 to 20 days, depending on temperature and relative humidity.

Changes in Slab Shape.—The test slab surfaces became concave upward; Table 6 gives changes in elevation at joint corners, mid-joint, free edge, and interior locations. The amount of curl generally reached approximate stability in each panel, after which elevations varied a few thousandths of an inch on either side of the tabulated value. It is noted that corners of the thinner pavements tended to curl upward more than the thicker combinations.

Effect of Curl on Response to Load.— When 9-kip loads were applied to curled slabs, deflections were usually greater than those of flat slabs except at interior positions. Table 7 gives these deflection changes for six load locations: two joint corners, two mid-joints, a free edge, and an interior position. Trends in the data are difficult to perceive, but it is noted that the increase in deflection of the loaded side of joints is greater than that of the opposite side in most cases.

Changes in transverse strain along the joint and longitudinal strain at the free edge and interior are shown in Table 8. Strain on the loaded side of a joint usually increased more than that on the opposite side, but there were also some instances

TABLE 6

SLAB ELEVATION CHANGES IN INCHES

Pave-ment	Undoweled Corner	Doweled Corner	Free Edge	Interior
8B5	0.026[a]	0.016	0.005	-0.010
8N5	0.030[a]	0.026	0.007	-0.009
7N6	0.027	0.026	0.009	-0.009
5N9	0.034	0.031	0.012	-0.007
7B3	0.030	0.018	0.004	-0.010
5N6	0.040	0.028	0.006	-0.009
8G5	0.035[a]	0.028	0.012	-0.003
3B9	0.016	0.015	0.008	-0.007
5B3	0.028	0.025	0.013	-0.008
5N3	0.042	0.031	0.015	-0.010
3B6	0.046	0.035	0.024	-0.012
3N6	0.051	0.039	0.029	-0.012
3B3	0.053	0.040	0.020	-0.012
3S3	0.060	0.045	0.030	-0.013

[a]Indicates free corner with no adjacent slab.

TABLE 7

DEFLECTIONS OF CURLED SLABS UNDER 9-KIP LOADS

Pave-ment	Increase or Decrease in Deflection over Flat Slab Deflection (in.)									
	Undoweled Joint				Doweled Joint				Free Edge	Interior
	Corner		Mid-Joint		Corner		Mid-Joint			
	Load	Opp.	Load	Opp.	Load	Opp.	Load	Opp.		
8B5	-	-	-	-	0.008	0.006	0.002	0.002	0.001	0.001
8N5	-	-	-	-	0.014	0.010	0.004	0.003	0.006	0.001
7N6	0.010	0.008	0.007	0.006	0.007	0.005	0.006	0.005	0.005	0.001
5N9	0.012	0.009	0.006	0.005	0.017	0.015	0.007	0.005	0.006	0
7B3	0.007	0.005	0.006	0.004	0.005	0.003	0.003	0.004	0	0
5N6	0.006	0.005	0.003	0.004	0.010	0.007	0.001	0.001	0.006	0
8G5	-	-	-	-	0.008	0.004	0.001	-0.001	0.007	0
3B9	0.005	0.004	0.009	0.009	0.005	0.001	0.002	0.004	0.003	-0.002
5B3	0.010	0.001	0.007	-0.002	0.012	0.009	0.008	-0.003	0.004	-0.002
5N3	0.020	0.007	0.004	-0.003	0.018	0.016	0.005	0.001	0.008	0.002
3B6	0.004	-0.002	0.002	0	0.001	0.001	0.001	0	0.004	-0.002
3N6	0.024	0.011	0.012	0.014	0.007	0.014	0.009	0.009	0.024	0.001
3B3	0.020	0.008	0.015	0.008	0.006	0.002	0.007	0.004	0.004	0
3S3	0.024	0.023	0.013	-0.001	0.025	0.023	0.020	0.016	0.016	0.001

TABLE 8

TOP SURFACE STRAINS IN CURLED SLABS UNDER 9-KIP LOADS

Pave-ment	Increase or Decrease in Strain over Flat Slab Strain (in.)								Free Edge	Interior
	Undoweled Joint				Doweled Joint					
	Corner		Mid-Joint		Corner		Mid-Joint			
	Load	Opp.	Load	Opp.	Load	Opp.	Load	Opp.		
8B5	-	-	-	-	0.006	0.002	0.007	0	0	0
8N5	-	-	-	-	0.012	0.003	0.007	0.002	-0.003	-0.002
7N6	0.012	0.010	0.010	0.005	0.005	0.005	0.005	0	0	0.003
5N9	0.015	0.012	0.012	0.009	0.010	0.008	0.008	0.004	-0.005	-0.003
7B3	0.002	-0.001	0.005	-0.007	0.006	-0.001	0.006	-0.001	-0.008	-0.004
5N6	0.002	0.004	0.011	-0.001	0.011	-0.005	0.015	0.001	-0.006	-0.001
8G5	-	-	-	-	0.005	0	-0.006	0.005	-0.007	0
3B9	0.013	0.008	0.013	0.008	0.010	-0.008	0.012	0.012	-0.008	-0.010
5B3	0.006	-0.005	-0.008	-0.009	0.011	0.007	-0.004	-0.002	-0.006	-0.004
5N3	0.016	0.005	0.014	-0.008	0.014	0.002	0	-0.004	-0.002	0.005
3B6	0.004	-0.002	0.020	-0.009	0.011	0	0.003	-0.004	-0.020	-0.007
3N6	0.019	0.019	0.023	-0.007	0.020	0.013	0.019	0.023	0.005	0.009
3B3	0.010	0.004	0.020	0.010	0.019	0.010	0.014	-0.010	0.019	-0.013
3S3	0.014	-0.001	0.025	-0.018	0.017	0.016	0.004	0	0.030	0.003

of decreased strain. At the free edges and interior locations there were more cases of strain reduction than of strain increase.

Influence of Curl on Joint Effectiveness.—It was noted that increases in deflection due to loads at joints were greater for the loaded side than across the joint. The effectiveness ratios were computed for all combinations from the data in Figures 13 and 14 and Table 7. It was found that the effectiveness of undoweled joints varied from 77 to 98 percent in curled slabs as compared with 93 to 100 percent in flat slabs. Also, doweled joint effectiveness ranged from 80 to 98 percent in curled slabs as against a range of 83 to 100 percent in flat slabs. Although joints on curled slabs were slightly less effective than those in flat slabs in these static load tests there was excellent load transfer across the joint in both flat and curled slabs.

Comparison with Theory

Data from these tests on flat concrete pavements on CTS were checked by Westergaard's interior (8) and free edge (9) deflection formulas. These are relatively simple expressions and require only an evaluation of the elastic modulus of the concrete and the bearing value of the supporting base. A second method based on soil pressures may be used, but analysis by pressures in layered systems requires knowledge of the elastic constants of the materials under load restraints. Moment analysis, a third method, may be used to check strain measurements if the distribution of stresses through the layers is known.

A comparison of experimental measurements and theory is shown by Figure 17. A logarithmic plot of theoretical relations between interior slab deflection, d_i, and bearing modulus, k, of the subbase was constructed for slab thicknesses, h, equal to 3, 5, 7, and 9 in. from the Westergaard formulas:

$$d_i = \frac{P}{8kL^2} \tag{1}$$

in which

$$L^4 = \frac{Eh^3}{12(1 - \mu^2)k} \tag{2}$$

For these computations load P = 9,000 lb, E = 5×10^6 psi, and μ = 0.15.

Nominal subbase thicknesses were superimposed on the abscissa at locations determined from Table 1. Experimental deflections due to 9-kip interior loads were plotted

as ordinates above the proper bearing value. These points were circled and labeled to identify the pavement.

The experimental points cluster about appropriate theoretical lines. Although deflections of bonded pavements are shown, the analysis assumes no horizontal stress due to interlayer friction, therefore, it is not directly applicable to bonded pavements. The combinations with 3-in. concrete compare more closely with the theory than those with thicker concrete, but in general the agreement is reasonable. The advantage of bond may be estimated to be equivalent to an added concrete thickness of from $\frac{1}{2}$ to 1 in.

A second comparison was accomplished in a similar manner using Westergaard's edge equation

$$d_e = P\sqrt{\frac{2 + 1.20\mu}{Eh^3k}} \left[1 - (0.76 + 0.40\mu)\frac{r}{L}\right] \tag{3}$$

in which the loading plate radius $r = 8$ in. A logarithmic plot was drawn and experimental edge deflection points were located above appropriate bearing values as shown in Figure 18.

As in the case of interior loading, the experimental data for unbonded combinations fell reasonably close to the theoretical curves. Resistance of pavment 3B6 to edge deflection was slightly less than anticipated, but in other combinations bond at the interlayer improved deflection resistance as much as $\frac{1}{2}$ to 1 in. of additional concrete.

SUMMARY AND CONCLUSIONS

Cement-treated subbases were built on silty clay subgrades of relatively low bearing value and were covered with concrete surfaces. Deflections, strains, and pressures were measured when static loads were applied to the concrete slabs. Pavements were built with and without interlayer bond and the principal variables were subbase thickness and concrete thickness. Each structure included a doweled transverse joint, and all combinations except 8-in. concrete on 5-in. CTS included a transverse joint without dowels.

Progress toward accomplishing the objectives of the study was made as follows:

1. The ability of concrete pavements on CTS to support load was rated relative to that of 8-in. concrete on 5-in. gravel. Based on constant edge deflection, an 8-in. concrete slab bonded to 5-in. CTS was able to support 200 percent of the load carried by the standard 8-in. slab on 5-in. gravel, and a slab of 3-in. concrete on 3-in. CTS, unbonded, was able to support a load equal to 45 percent of the standard. At this same deflection other combinations were able to support loads distributed between these limits.

2. A cement-sand grout on the subbase surface prior to casting concrete effectively bonded the concrete and CTS layers. Load capacities of bonded pavements were equivalent to unbonded pavements with the concrete thickness increased by $\frac{1}{2}$ to 1 in. Corner movement due to curl was less for bonded pavements than for those without the bonding treatment.

3. Experimental deflection data were in good agreement with values computed by the Westergaard deflection formulas.

Instrumentation and test procedures provided an opportunity for the following observations incidental to the primary objectives:

1. Pressures on the subgrade directly under interior 9-kip loads increased with decreasing pavement thickness and varied from 2 to 6 psi for all combinations tested. Under edge loads, subgrade pressures were approximately 50 percent greater than under interior loads.

2. Edge deflections and strains were reduced as the load was moved inward from the slab edge. At the 24-in. position, edge deflections of the thicker pavement combinations with load-carrying ability equal to or greater than the standard 8-in. slab on

58

5-in. gravel averaged about 75 percent, and those with lesser ability about 60 percent of the edge deflections due to edge loads. Edge strains of the thicker pavement combinations were reduced almost $\frac{1}{2}$ for the 24-in. load position, and strains were reduced by greater amounts on the thinner pavements. Edge strains produced by inward loads on thin pavements are not necessarily critical and there is evidence to suggest that maximum strains on thin pavements are at the load plate in a transverse direction.

3. The deflections at both doweled and undoweled transverse joints were maximum when the load was at the outer corner; but for this load position top surface compressive strains at the load were sometimes exceeded by tensile strains parallel to the joint at 40 to 56 in. from the edge. The highest strains measured at joints were compressive at the load when the load center was at least 40 in. from the free edge of the concrete. At this location of maximum joint edge strain, the strains were always less than those caused by a free edge load but greater than those at the free edge caused by a load 24 in. inward from the edge. Therefore, the critical strain in a pavement due to a moving truck may be at a free edge or at a joint, and its location will be determined by the position of the wheel with respect to the free edge.

4. Joints in concrete pavements on cement-treated subbases effectively transferred load. Doweled joints offered very little advantage over joints without dowels in flat pavements of concrete on cement-treated subbases.

5. The concrete was approximately 3 times as effective in limiting deflections and strains as the CTS. In the range of layer thicknesses studied, and additional 2-in. thickness of concrete resisted slab deflections to the same degree as an additional 6 in. of CTS. Previous studies also have shown that a 5-in. CTS subbase under 8-in. concrete offered more resistance to deflection than 15 in. of gravel.

6. The combination slabs curled due to drying of the top surface in much the same manner as slabs on granular subbases, and the greatest movement occurred in pavements of low load capacity. Slabs with bonded interlayers curled slightly less than those without bond.

7. Deflections due to 9-kip loads on flat slabs were less than those for similar load positions on curled slabs except at interior locations. Top surface strains in flat slabs were usually less than corresponding strains in curled slabs except at free edges and interiors.

<div align="center">REFERENCES</div>

1. Colley, B. E., and Nowlen, W. J., "Performance of Subbases for Concrete Pavements Under Repetitive Loading." HRB Bull. 202, pp. 32-58 (1958).
2. Childs, L. D., and Nussbaum, P. J., "Pressures at Foundation Soil Interfaces Under Loaded Concrete and Soil-Cement Highway Slabs." Proc. ASTM 62 (1962).
3. Childs, L. D., and Kapernick, J. W., "Tests of Concrete Pavement on Gravel Subbases." Journal of the Highway Division, Proc. ASCE 84, HW 3 (1958).
4. Abrams, M. S., "Laboratory and Field Tests of Granular Soil-Cement Mixtures for Base Courses." ASTM Spec. Tech. Pub. 254 (1959).
5. "Soil-Cement Laboratory Handbook." Portland Cement Association, Chicago, p. 34 (1959).
6. Felt, E. J. and Abrams, M. S., "Suggested Method of Making and Curing Soil-Cement Compression and Flexure Test Specimens in the Laboratory." ASTM Proc. for Testing Soils p. 475 (1958).
7. Teller, L. W. and Sutherland, E. J., "A Study of the Structural Action of Several Types of Transverse and Longitudinal Joint Design." Public Roads, 7(7) (Sept. 1936).
8. Westergaard, H. M., "Stresses in Concrete Pavements by Theoretical Analysis." Public Roads, 7(2) (Apr. 1926).
9. Westergaard, H. M., "New Formulas for Stresses in Concrete Pavements for Airfields." ASCE Proc., 73 (1947).

Moving Load Test on Experimental Prestressed Concrete Highway Slab

JOHN R. SMITH and RICHARD K. LIGHTHOLDER
Department of Civil Engineering, University of Pittsburgh

This investigation was initiated to determine the behavior of an experimental prestressed slab when subjected to moving loads over an extended period of time. Details of the design and construction of the slab and the results of static and creep load tests were reported in HRB Proceedings, Vol. 37 (1958).

The tests were conducted on a 75-ft slab that included one of the rubber expansion joints. The load was applied by a specially designed vehicle having axles spaced 20 ft apart and carrying 14 tons each. The vehicle was positioned on the slab so that the curb wheels traveled in a straight line about 6 in. from the edge of the slab. Determination of the longitudinal and transverse stresses, deflection of the slab, and settlement of the slab, were made with appropriate instrumentation. The test extended over a $2\frac{1}{2}$-month period, September 19 to December 1, 1962 and comprised more than 580,000 repetitions applied at the rate of about 10,000 per day.

The performance of the slab was excellent. There was no serious damage done to either the slab or the joint. The test did indicate, however, that more attention should be directed towards the longitudinal cracks over the tendons and the elimination of pumping at the expansion joint. It is recommended that a test pavement of this type be incorporated as a part of the construction of an actual highway for further study under normal highway conditions.

•IN FEBRUARY 1957 the Jones and Laughlin Steel Corp. completed the construction of an experimental section of prestressed concrete highway pavement, 5 in. thick by 12 ft wide by 530 ft long. The project was initiated "not only to provide technical data on the strutural action of prestressed concrete highway pavements but also to provide reliable information on the feasibility of construction and the relative economics involved."

The test program was conducted in the spring and summer of 1957. Sixteen static load tests were made at three loading stations. Load deflection curves were obtained for dual wheels mounted with 10 by 20 truck tires with loads up to 40,000 lb and for a steel bearing plate with loads up to 66,000 lb. Sixteen creep speed load tests were taken for an axle load of 23,000 lb.

These tests were significant in determining the stresses and deflections of the pavement under a very limited number of load applications. They do not indicate the effect of the loss of subgrade support due to ironing effect, compaction of the subgrade, and pumping action that takes place under extended repetition of moving loads.

The pavement was designed for prestressing in the longitudinal direction only. There is no transverse reinforcing. This has raised some questions as to how the pavement would perform under normal traffic conditions.

PURPOSE AND SCOPE OF RESEARCH

The purpose of this investigation was to determine the behavior of an existing pre-stressed concrete highway slab when subjected to repeated applications of moving loads over an extended period of time. The project was carried out under a grant sponsored jointly by the Pennsylvania Department of Highways and the U. S. Bureau of Public Roads. The existing slab was donated by the Jones and Laughlin Steel Corp. for the purpose of this investigation.

There are five factors in this investigation that served to accelerate the test: (a) the subgrade was designed to meet the minimum standards of AASHO in order to create the least favorable, but acceptable conditions; (b) the vehicle traveled as close to the edge of the slab as practicable to produce maximum deflection at the edge of the slab; (c) each axle carried about 28,000 lb, 25 percent overload for Pennsylvania load limits; (d) the maximum speed of the vehicle was about 10 ft/sec, permitting greater deflections than would take place under normal velocities; and (e) the loads were applied at the rate of about 8 per min, so that the subgrade had little opportunity to recover after each load application. These contingencies made the tests more severe than would be expected under normal traffic conditions. On this basis it was felt that 500,000 repetitions would be adequate to evaluate the pavement.

TEST SECTION

The east end of the slab appeared to be the more logical area on which to set up the test. This end was chosen because there were no apparent cracks in the slab. It also contained an expansion joint and was removed from areas where previous testing had taken place.

A study of the oscillographs for the deflections under creep loads presented in the Jones and Laughlin report indicated that it would be desirable to place the axles of the vehicle 20 ft apart so that the deflections under one set of wheels would not affect the readings under the second set. It was also considered desirable to mount the strain gages at two cross-sections so that failure of a gage would not necessitate shutting down the operation. This permitted a degree of flexibility for the scheduling of gage replacement during fair weather and at times when the vehicle was shut down for maintenance. The dual setup would also serve as a cross-check to verify the readings.
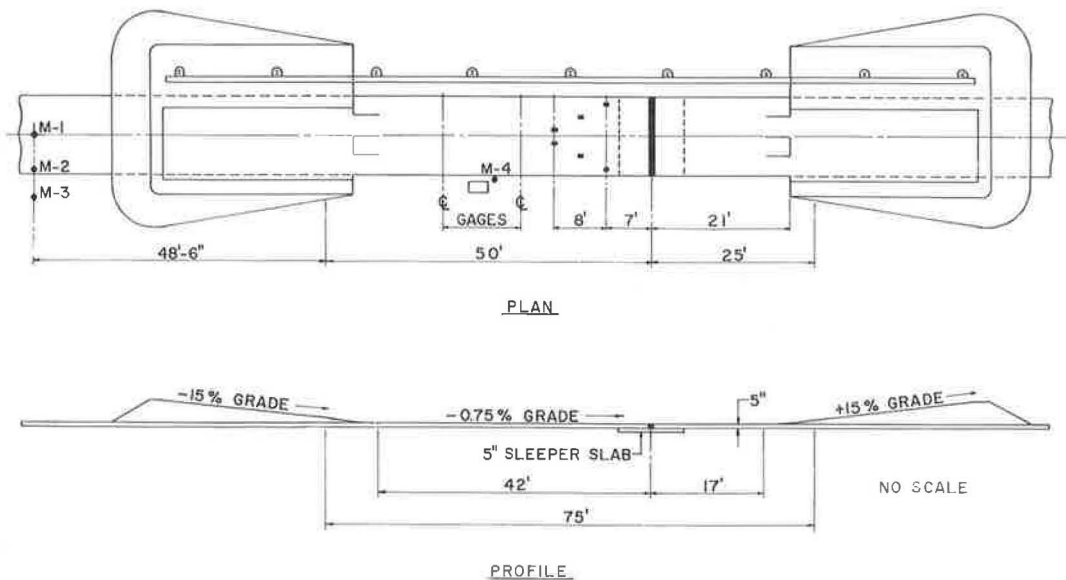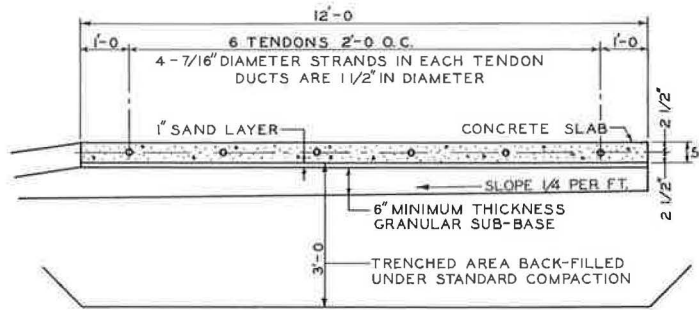

Figure 1. Test strip.

Figure 2. Typical site cross-section.

Figure 1 shows the plan and profile of the test area. The ramps were designed with a 15 percent grade to absorb the energy of the vehicle when it had attained a velocity of 10 ft/sec. The two strain gage stations were located 20 and 32 ft from the centerline of the expansion joint. The points M-1 to M-4 indicate the location of the thin-walled steel tubing that was driven into the ground for the nuclear moisture-density probe.

Figure 2 shows a typical cross-section of the site. The soil used in the subgrade is classified as an A-7-6 clay with a group index of 20. The T-99 unit weight of the clay varied from 90 to 95 pcf with average values of 93 pcf and an optimum moisture of 27 percent. It was compacted to within the range of 95 to 100 percent of the T-99 maximum with moisture contents at or above the optimum.

A natural sand-gravel mixture meeting the requirements of AASHO, Type 1, Grading B was used for a granular subbase. The compacted thickness of this base was 6 in. covered by a 1-in. leveling layer of washed sand and a layer of slater felt to reduce friction.

The concrete mix for the pavement was Pennsylvania Department of Highways' Class AA. The cement was air-entrained. The aggregate was stone with a maximum size of $2\frac{1}{2}$ in. Maximum water was 5.3 gal per sack. The concrete had an average cylinder strength of 4,483 psi at 28 days.

The $\frac{7}{16}$-in.-diameter strands used in the tendons were typical stress relieved prestressing strands with an average ultimate strength of 268,000 psi and an average elongation of 10 percent. The average prestress in the concrete after the release of the jacks varied from 360 to 470 psi and that of the tendons from 116,000 to 151,000 psi.

VEHICLE

The vehicle, shown diagrammatically in Figure 3, consists of a 28-ft trailer bed with the rear axle mounted on a frame that is connected to the bed with a king pin. The forward end is supported on a heavy-duty truck chassis in the same manner. The axles are 20 ft apart and carry dual wheels mounted with 10 by 20 truck tires. The tire pressure was maintained at 80 psi.

The vehicle was driven by an electric motor through the transfer case and the differential that came with the truck chassis. The maximum velocity of the vehicle was 10 ft/sec.

Forward and reverse movement of the vehicle was accomplished with a magnetic definite-time control that operated on a first come first served basis. The control was activated by staggered collector rails mounted at the side of the pavement. Current was supplied to the vehicle through similar collector rails.

The vehicle was made to travel in a straight line by means of a floating guide frame that engaged pins at each end of the frames on which the wheels were mounted. The guide frame was held in alignment with crane wheels that were mounted between two guide rails at the edge of the slab. The crane wheel housings were hinged to the guide frame by A-frames. The guide frame was moved back and forth with a pneumatic cylinder to engage the proper pins and thus guide each set of wheels in the proper direction.
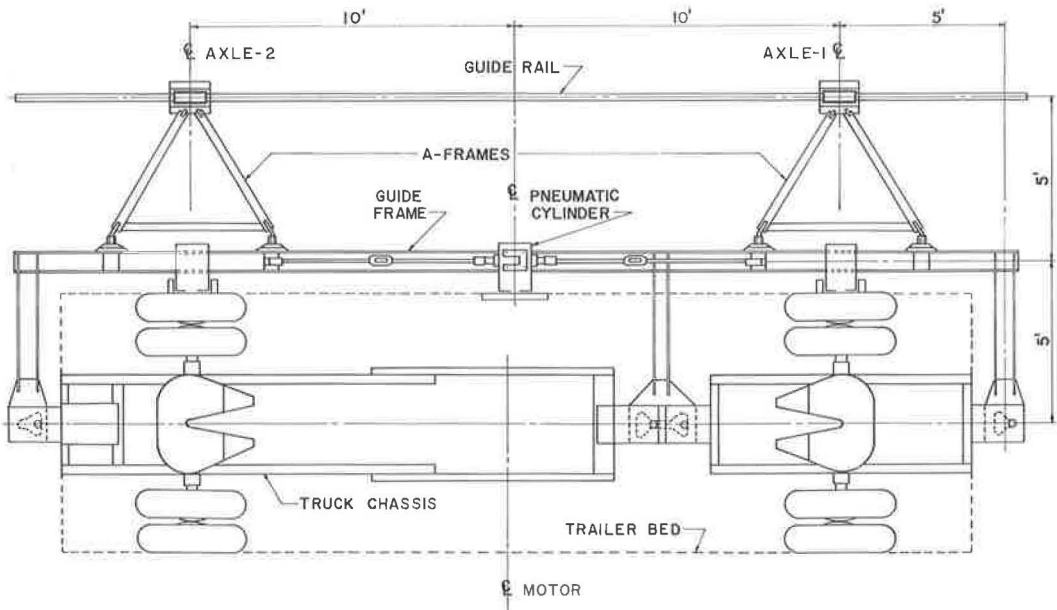
62

Figure 3. Test vehicle.

Figure 4. Assembled vehicle in operation.

A number of pressure switches, microswitches, and relays were wired into the electrical circuit to insure fail-safe operation.

The brakes were used for emergency stops. Reversing the direction of motion was accomplished on the ramps at each end of the test strip.

Figure 4 shows the assembled vehicle in operation. The vehicle is descending the east ramp. Mounted on the center of the bed is the control box with the compressor to the left of it. The compressor supplies air at 120 psi to the pneumatic cylinder and the brakes. The guide rails and collector rails are shown on the far side of the vehicle. The guide frame is shown engaging the guide pin on the near end of the chassis.

INSTRUMENTATION

Strain gage and deflectometer locations are shown in Figure 5. The gages were SR-4, Type A-9. Gages 1, 3, 4, 6, 8, and 9 were mounted at right angles to the longitudinal axis of the slab. Gages 2 and 7 were originally installed as transverse gages located 5 ft from the south edge of the pavement. They were rendered inoperative due to a longitudinal crack which developed through their position and were remounted as longitudinal gages 6 ft from the edge of the slab. Temperature-compensating gages 11, 12, and 13 were mounted on an unstressed block of concrete formed at the time the pavement was poured. The readings for the strain gages were recorded on a two-channel oscillograph.

Vertical deflections due to the passage of wheel loads were recorded at the edge of the slab. Deflectometers U-1 through U-5 were fastened at mid-depth to the side of the pavement. Deflectometers L-3, L-4 and L-5 were fastened to the side of the sleeper slab. Maximum readings were taken with a dial indicator. Readings were also recorded on the oscillograph with a cantilever-beam deflectometer.

Figure 6 shows the grid that was established on the slab for determining changes in elevation. Elevation of these points was taken periodically with a wye level and recorded to the nearest 0.001 ft. Line A was along the loaded edge of the pavement and Line D was along the unloaded edge.
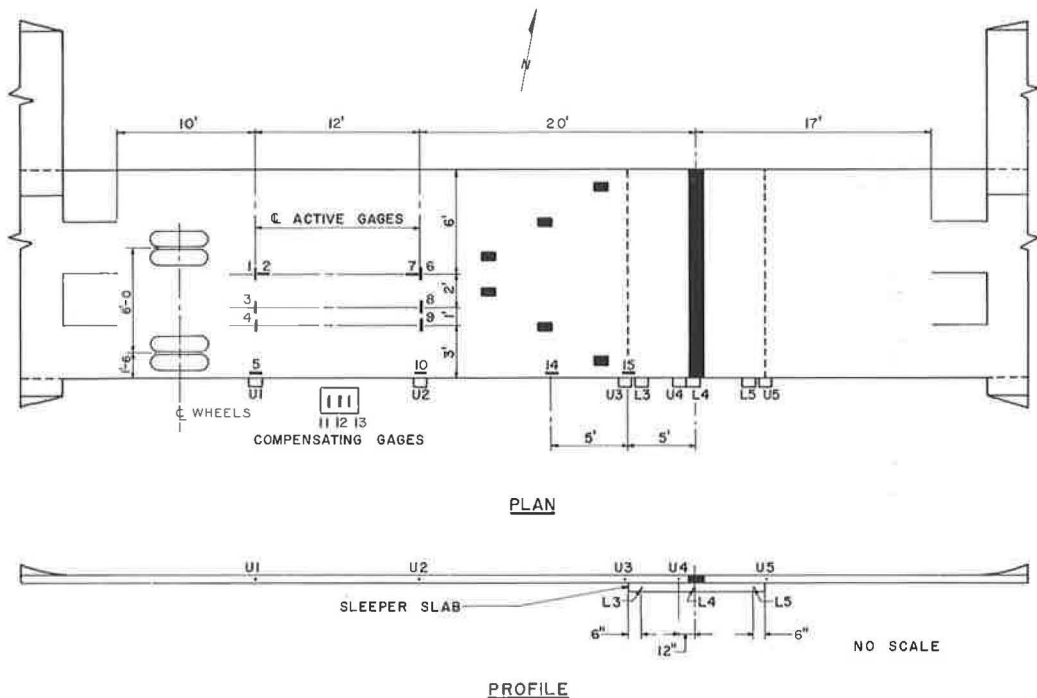

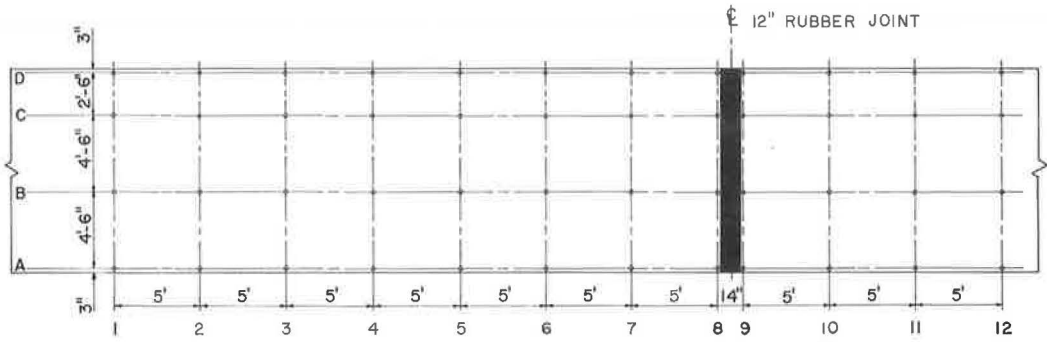Figure 5. Location of instrumentation.
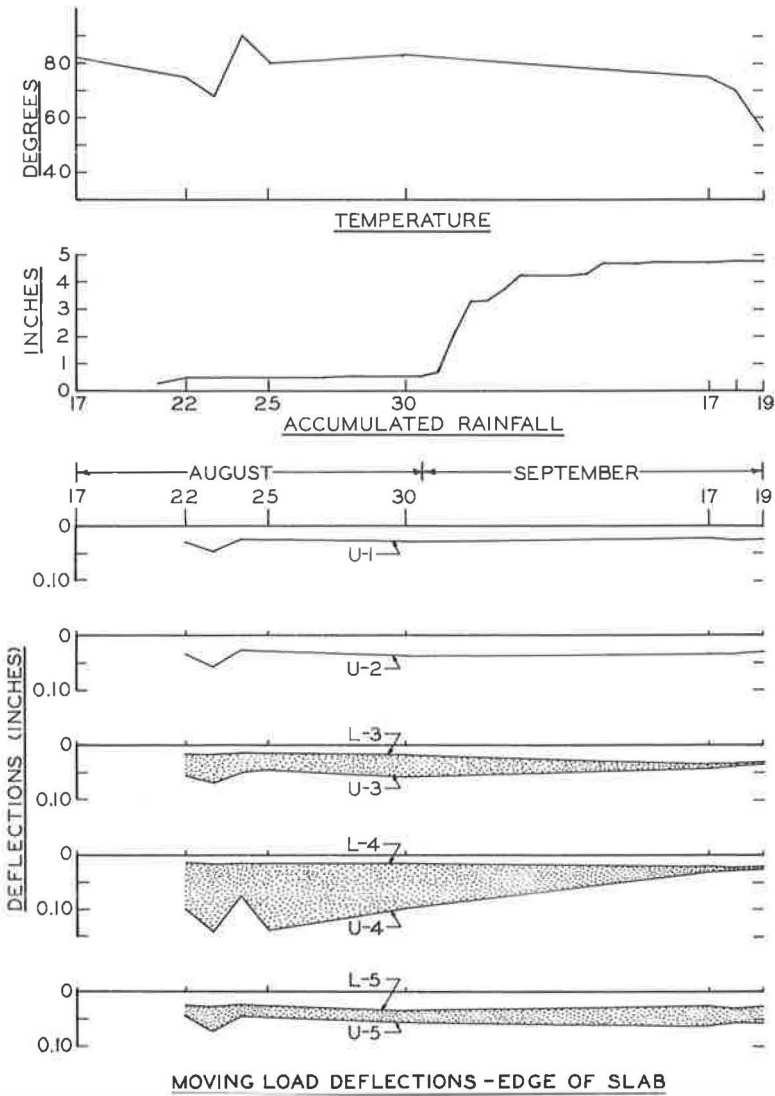
Figure 6. Stations for elevations.

MOVING LOAD DEFLECTIONS – EDGE OF SLAB

Figure 7. Pretest data for deflectometers.

PREPARATION FOR TESTS

Three thousand repetitions were applied to the slab while the vehicle and the instrumentation were being adjusted. During this time, the deflectometers indicated a separation between the sleeper slab and the main slab. This amounted to about 0.123 in. on the west side of the joint and 0.043 in. on the east side. It was decided to bring the main slab in contact with the sleeper slab on the west side of the joint by grouting the separation.

The pretest data for the deflectometers are shown in Figure 7. The separation between the two slabs is illustrated by the shaded area between U-3, L-3; U-4, L-4; and U-5, L-5. The readings for September 17 show the effect of the grouting operation. The relative movement between the main slab and the sleeper slab is negligible. The temperature and rainfall data shown at the top of the graph are of importance only to indicate the weather conditions which preceded the tests.

DEFLECTIONS AT EDGE OF SLAB

Figure 8 shows the range in temperature for each day and the accumulated rainfall during the test period that extended from September 19, 1962 to December 1, 1962, and resulted in approximately 580,000 passes of the axle loads over the slab. The bar graph at the bottom of Figure 8 shows the periods when the vehicle was shut down for repair or adjustment.

The majority of the deflections were recorded from 4 to 5 P.M. The oscillographs shown in Figures 9 and 10 are typical for the deflections at points U-1, U-2, U-3, and L-3. The variation in the width of the peaks was caused by a variation in the velocity. This also accounts for the somewhat higher readings at the broad peaks because lower velocity would cause a greater deflection.

The graphs in Figure 11 are a plot of the maximum peaks on the oscillographs. In a few cases these readings were supplemented with values obtained from the maximum reading deflectometers. In all but a couple of cases the two instruments agreed reasonably well with each other. It can be seen that the deflections of the slab at U-1, U-2, U-3, and L-3 were relatively consistent and amounted to about 0.030 in.

At points U-4, L-4, U-5, and L-5, the effect of the loss of subgrade support can be seen. The shaded area is representative of the separation between the main slab and the sleeper slab. The live load deflection of the sleeper slab averaged about 0.02 in. at L-4 and varied from 0.02 to 0.04 in. at L-5. The deflection of the main slab varied from 0.02 to 0.04 in. at U-4 and from 0.03 to 0.074 in. at U-5. The last readings, taken on December 1, 1962, indicated theat the separation was becoming less as pumping reduced the support under the east ramp.
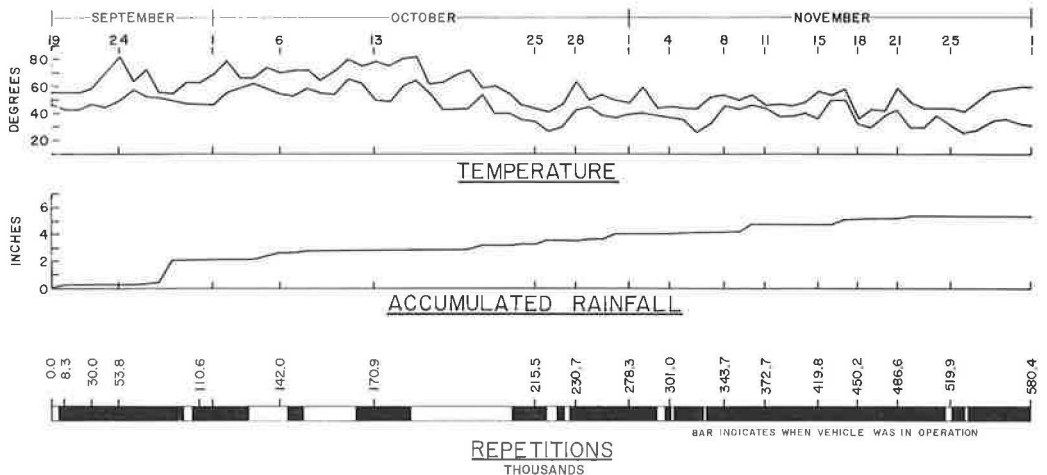

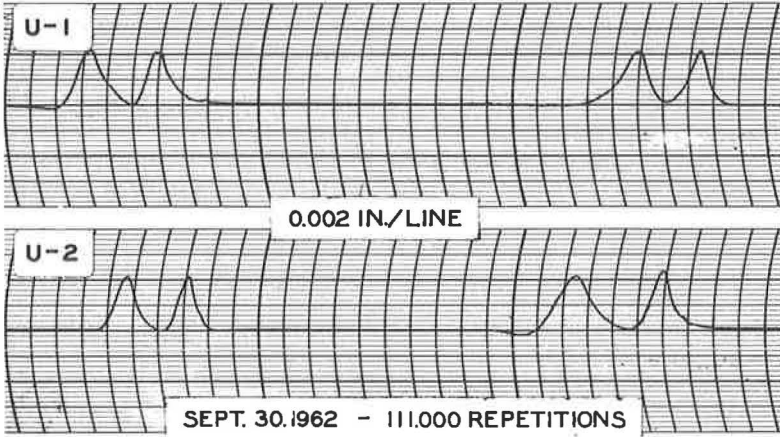Figure 8. Weather data and vehicle operation.

66

Figure 9. Typical deflections as recorded by oscillographs at U-1 and U-2.
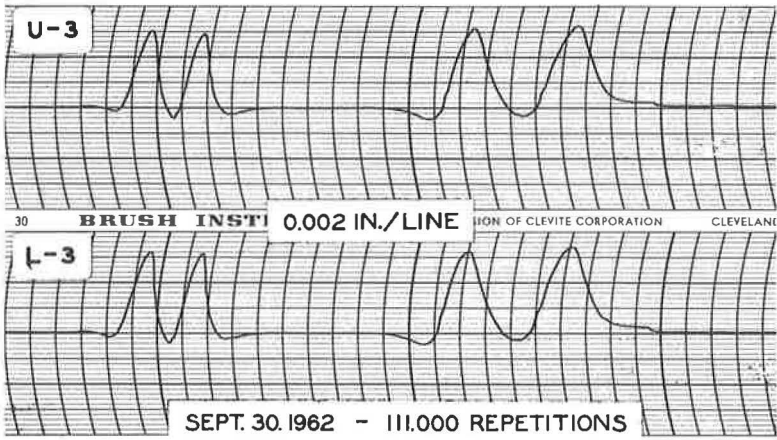

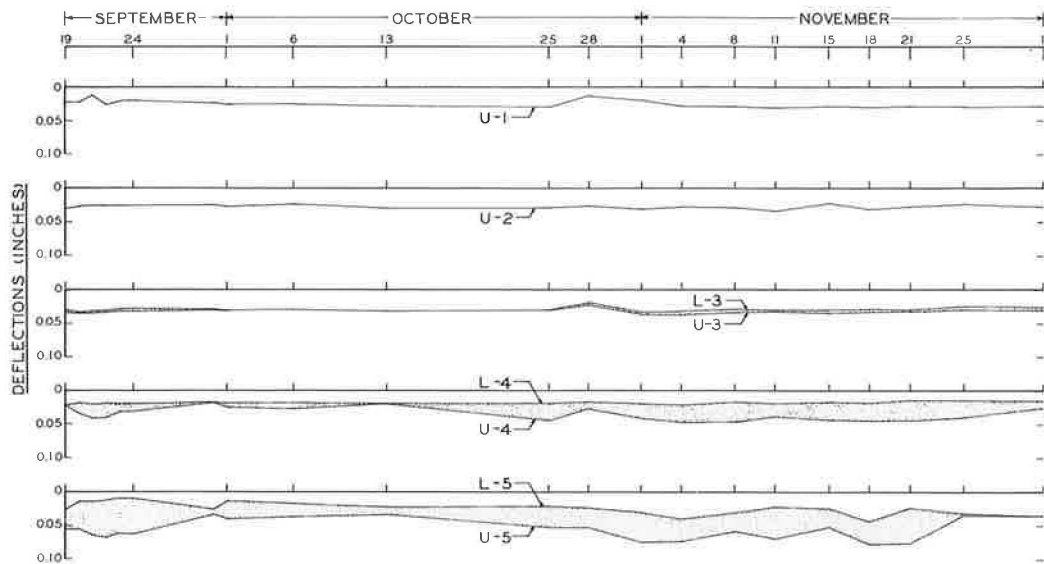Figure 10. Typical deflections as recorded by oscillographs at U-3 and L-3.

Figure 11. Moving load deflections—edge of slab.

Figure 12. Pumping at U-5, L-5—Oct. 30, 1962.

68

Figure 13. Pumping at U-5, L-5—Nov. 10, 1962.

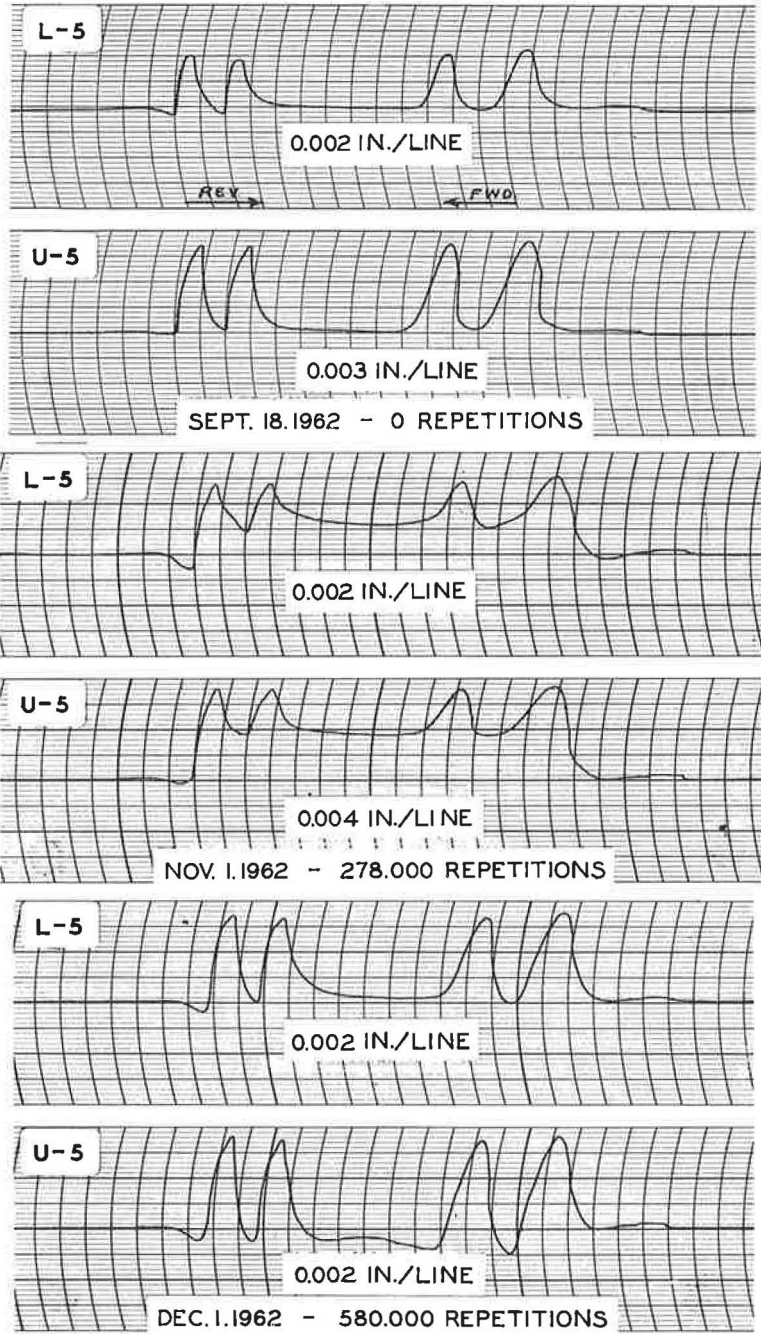Figure 14. Pumping at bottom of east ramp—Nov. 10, 1962.
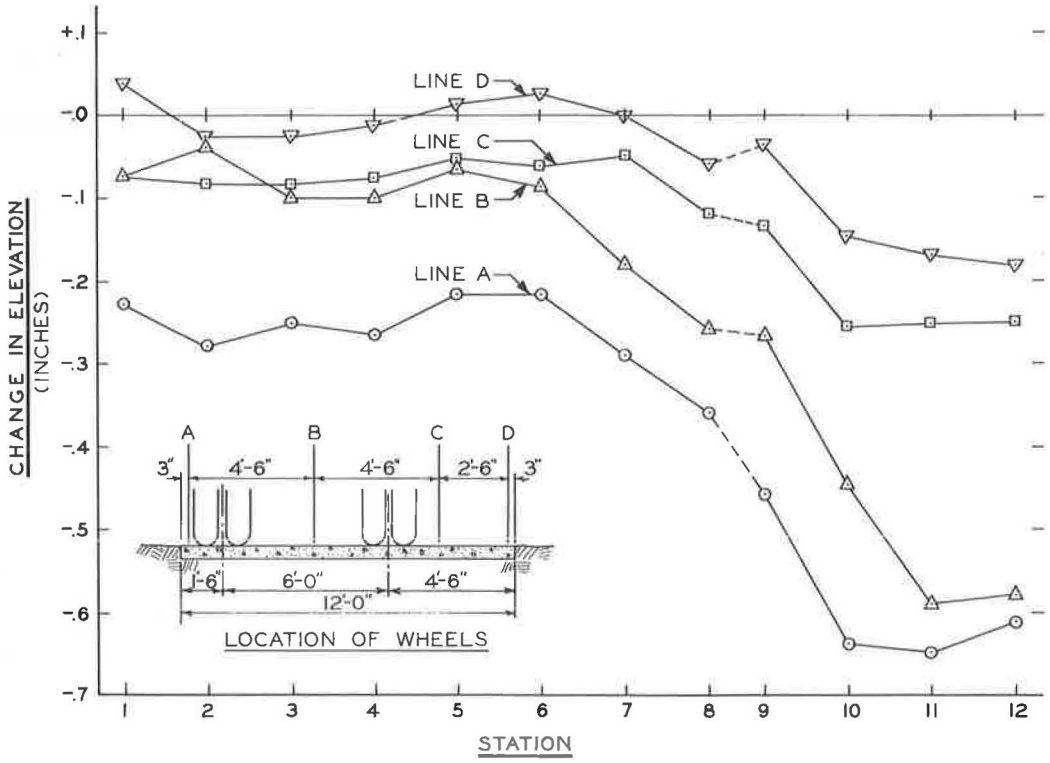
69

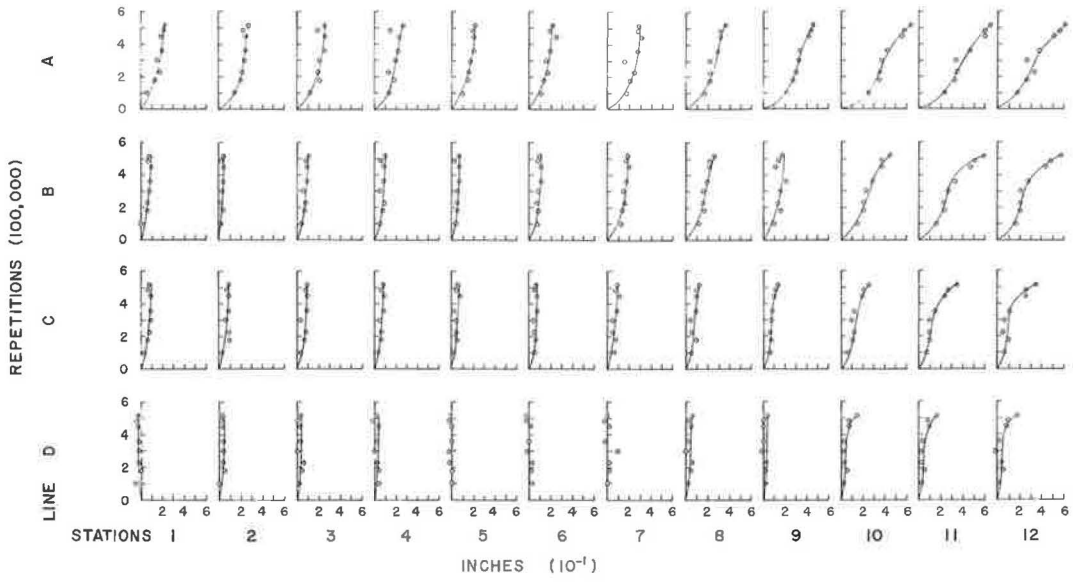Figure 15. Oscillographs at U-5 and L-5.

70

Figure 16.   Change in elevation, 580,000 repetitions.

Figure 17.   Change in elevations.

PUMPING

The first evidence of pumping was witnessed about 7 P.M. September 27, and it continued until about 10 A.M. the following morning. Two cubic feet of well-graded sand was pumped out at U-5, L-5. On October 30 about 1.5 cu ft of sand was pumped at U-5, L-5 (Fig. 12). In both cases there was no evidence of pumping at any other location.

On November 9 and 10 there was heavy pumping at the edge of the slab from the U-5, L-5 position to the bottom of the east ramp (Figs. 13 and 14). There was a substantial amount of fines pumped into the U-4, L-4 position and a somewhat lesser amount at U-3, L-3. The only other evidence of pumping was a slight trace of fine sand under the counter hose about 5 ft east of the west ramp.

On both November 17 and 21 pumping occurred along the edge of the slab from the expansion joint to the east ramp with fines accumulating at both U-3 L-3 and U-4 L-4. No pumping was found elsewhere. During the November 21 rain, water was seen pumping through the cracks that had developed in the slab east of the expansion joint.

The oscillograph charts shown in Figure 15 graphically illustrate what had occurred at U-5, L-5 due to the pumping action. The September 18, 1962 chart shows the deflections as the vehicle passes over the points and ascends the ramp, then reverses itself and returns across the point to the main slab. While the vehicle was up on the ramp, the deflections at U-5, L-5 returned to zero.

The November 1, 1962 chart was taken after 278,000 repetitions and a considerable amount of pumping. Here the slab appeared to be acting as a supported cantilever that maintained a reaction on the sleeper slab while the vehicle was on the ramp.

On December 1, 1962, after 580,000 repetitions and additional pumping, the slab appeared to have settled to the subgrade again because the deflections had nearly returned to zero while the vehicle was on the ramp. Figure 16 tends to reinforce this line of reasoning. The graph shows the change in elevation of the points shown in Figure 6, after 580,000 repetitions. The sketch in the lower left of the figure shows the relative location of the wheels and the points. The change in elevation between stations 1 and 7 is relatively consistent. Line A at the loaded edge of the slab has moved downward about 0.25 in. while line D on the opposite edge shows little change in elevation. Station 7 marks the west edge of the sleeper slab. Stations 8 and 9 are on the west and east sides of the rubber joint, respectively, and station 10 is at the east edge of the sleeper slab.

The pavement at the east edge of the sleeper slab has settled about 0.64 in. on line A and about 0.14 in. on line D. The pavement between the sleeper slab and the bottom of the ramp has settled about 0.65 in. on line A and 0.18 in. on line D.

Figure 17 shows the graphs for each point at which a record of the elevations was made. The graphs were plotted with repetitions on the ordinates and deflections on the abscissas; the effects of the pumping from Station 8, just to the west of the expansion joint, to Station 12 can be seen.

The principal cause of pumping was poor subbase drainage. Moisture tests indicated that the moisture content of the base material was about 24 percent. Rain had little effect on these readings. Water appeared to collect in the sand layer and during the early storms was forced in and out of the separation between the pavement and the sleeper slab. Much of the water and sand was forced out of the separation into the hole along the edge of the slab at deflectometers U-5, L-5. As the volume of sand under the slab was reduced, the pumping extended along the edge of the slab—first to the bottom of the east ramp and then back to the U-4, L-4 position at the rubber joint.

STRESSES

Most of the strain readings were recorded from 5 to 6 P.M. The transverse stresses are of questionable value because of the longitudinal cracks that developed through the strain gage stations. Typical oscillographs for the transverse stresses are shown in Figure 18. The maximum readings from these charts were plotted against repetitions to develop the graphs in Figure 19. The maximum transverse stress recorded was 105 psi at gage 8. This was based on an elastic modulus of 4,400,000 psi.
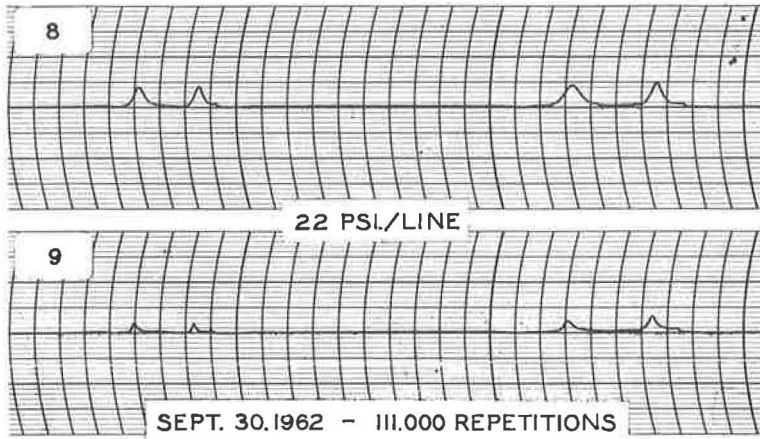
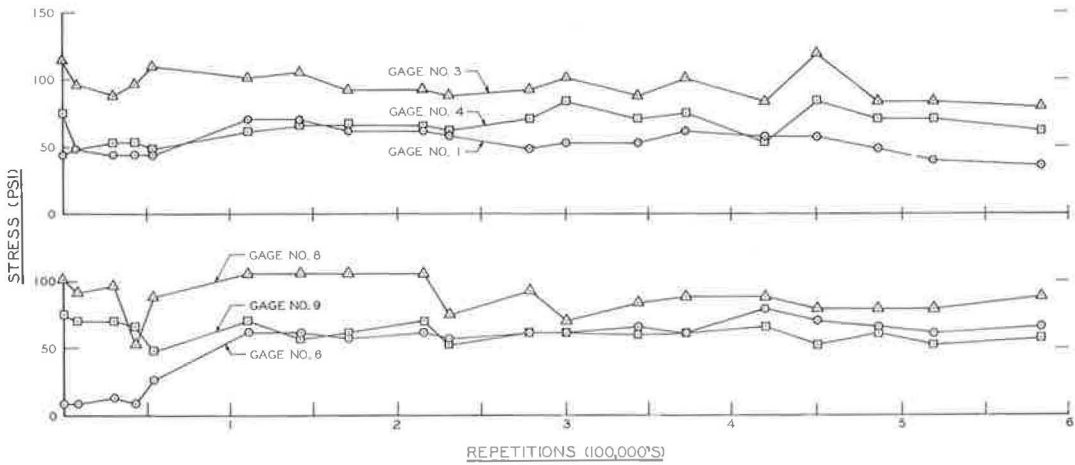Figure 18. Oscillographs for transverse gages 8 and 9.
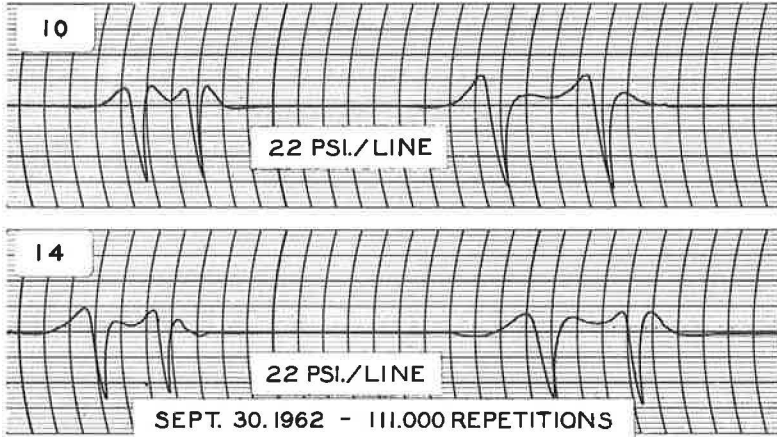

Figure 19. Transverse stresses.

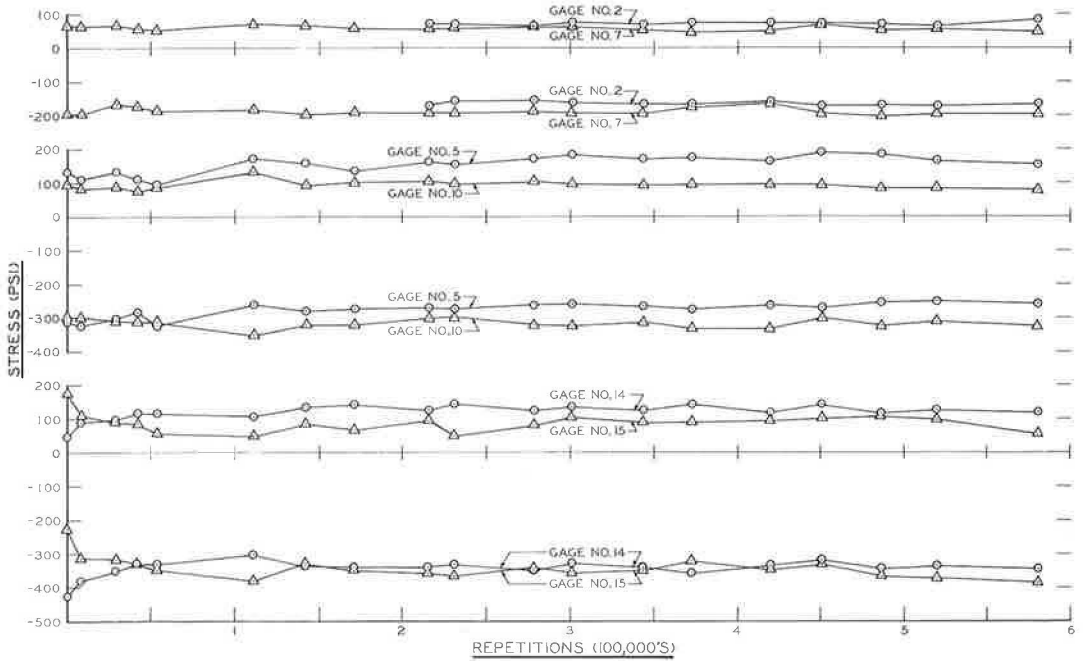Figure 20.   Oscillographs for longitudinal gages 10 and 14.

Figure 21.   Longitudinal stresses.

The oscillographs shown in Figure 20 for gages 10 and 14 are typical for the longitudinal gages. Figure 21 shows the maximum stresses recorded for the longitudinal gages. Gages 2 and 7 were located 6 ft from the edge of the slab and recorded a maximum tensile stress of 70 psi and a maximum compressive stress of 190 psi. The longitudinal gages along the edge of the slab show a maximum tension of 125 psi for gage 14 located 5 ft west of the edge of the sleeper slab and a maximum compression of 350 psi for gage 15 located at the west edge of the sleeper slab.

CRACKS

Longitudinal cracks were first discovered on August 22, 1962 during the initial compaction runs. These cracks are shown in Figure 22 and represent the condition that existed at the beginning of the test. They are located over the prestressing tendons. The relative position of the wheels is shown in the figure.

A record of the final cracks, after 580,000 repetitions, was made on December 2, 1962. These are shown in Figure 23. West of the joint the cracks at F-1 and F-4 increased in length only a few inches. Fifty thousand repetitions of the load caused an
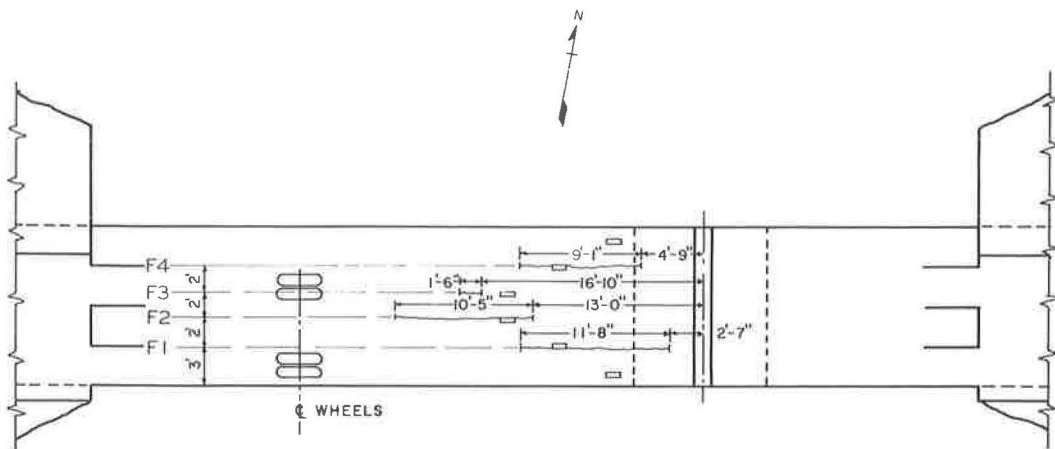
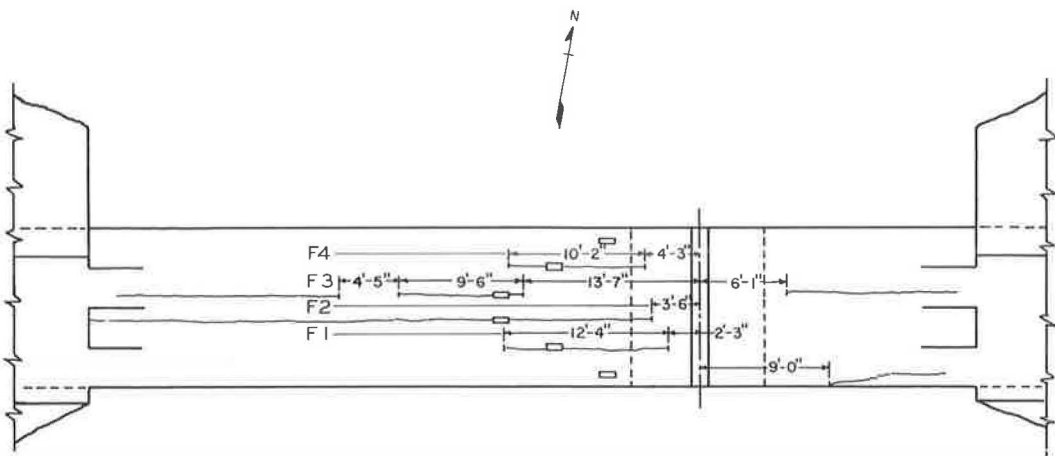

Figure 22. Longitudinal cracks, Aug. 22, 1962.

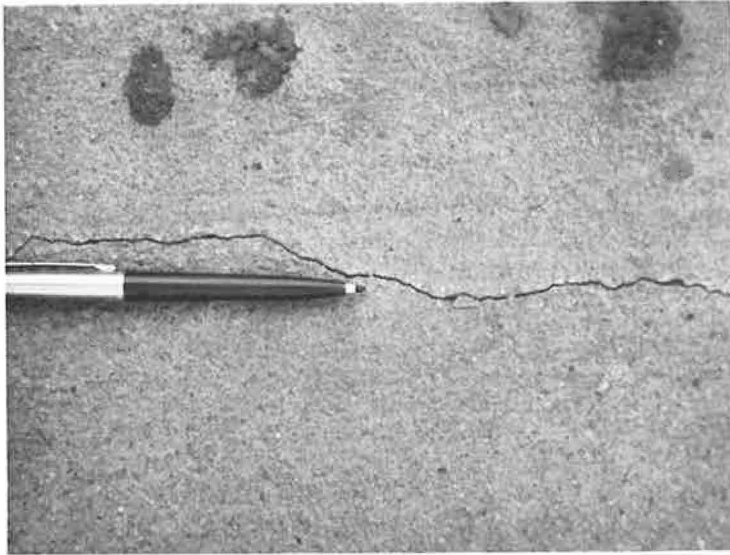Figure 23. Longitudinal cracks, Dec. 2, 1962.

Figure 24. Longitudinal crack at F-2.

extension of the crack F-2 from the west ramp to within 5 ft of the rubber joint. At the same time, a crack 8 ft long was found extending from the west ramp in line with F-3. Three hundred fifty thousand repetitions brought these two cracks on line F-3 within 7 ft of each other.

The cracks east of the joint developed during the rain on November 9 at 350,000 repetitions. When they were originally discovered, the crack along F-4 was within 8.5 ft of the expansion joint, and the crack at the edge of the pavement was 12.75 ft from the joint.

Toward the end of the tests, the edge of the slab was exposed for about 12 ft extending west from the west edge of the sleeper slab.

This was painted with whitewash to determine whether or not transverse cracks had developed on the bottom of the slab. After 25,000 repetitions an inspection was made and no evidence of cracks was found.

An examination of the test site in the summer of 1963 revealed that the crack at F-3 had extended the entire length of the slab to a point 3.5 ft west of the expansion joint. All the other cracks remained essentially the same as they were at the end of the tests.

A close-up of the crack at F-2 is shown in Figure 24. The picture was taken at what appears to be the widest crack in the test section. At this point it was 0.043 in. wide.

CONCLUSIONS

Wheel loads were applied to the slab at the rate of 500 repetitions per hr. Except for breakdowns, maintenance, and reading of the instruments this was a 24-hr operation. The 580,000 repetitions were accomplished in two and one-half month period from September 19, 1962 to December 1, 1962. During this time, the vehicle was shut down for maintenance and repairs or due to malfunction of the controls for a total of 21 days.

During the test the downward movement of the slab west of the joint increased to 0.25 in. at the loaded edge. In spite of this, the stresses shown in Figures 19 and 21 and the moving load deflections shown in Figure 11 were nearly constant for the pavement. The longitudinal stresses were well below the cracking stress and an investigation of the loaded edge of the slab revealed no transverse cracks.

The downward movement east of the joint was considerably greater. The loaded edge of the slab subsided about 0.65 in. This was caused by the excessive pumping in this area.

The project was initiated as a test of the prestressed slab. The data accumulated on the subgrade condition developed as a part of the investigation. It should be emphasized that in spite of the adverse foundation conditions the components of the pavement performed remarkably well. There was no serious damage done to either the slab or the rubber joint. The structural performance was excellent. Longitudinal cracks were evident over the tendons and should be considered in future designs. The appearance of similar cracks after grouting the tendons during slab construction, leads to the belief that these cracks were not entirely a result of the moving loads. The reduction of the cross-section due to the tendons was also a contributing factor.

While this test indicates the fine performance of the pavement under relatively extreme conditions, it is felt that further testing under normal highway conditions is necessary. It is recommended that a test pavement of this type be incorporated as a part of the construction of an actual highway. Particular attention should be given to the design and drainage of the subgrade, the placing of the slab on the sleeper slab, and the reduction or elimination of the longitudinal cracks by redistributing the prestressing strands, and, if practicable, the inclusion of transverse reinforcement.

Load Tests on Thin Pretensioned Pavement Slabs

A. P. CHRISTENSEN and R. L. JANES
Respectively, Development Engineer and formerly Senior Development Engineer,
Research and Development Laboratories, Portland Cement Association,
Skokie, Illinois

An investigation of the load response of prestressed concrete pavement slabs is in progress at the PCA Research and Development Laboratories. The first published result of this investigation was a theoretical procedure for determining the magnitude and distribution of stresses and deflections in prestressed concrete pavements beyond conditions to which the elastic theory is applicable. The theoretical procedure is specifically applicable to a centrally loaded infinite slab supported by a "dense liquid" foundation and prestressed equally in longitudinal and transverse directions.

To test the validity of the assumptions made in the analysis and to compare theoretical and measured data, three reduced scale prestressed concrete slabs supported on a spring subgrade and loaded through circular plates were tested to failure. Measurements of strain and deflection were made at a number of locations and load increments. Test variables included size of loading plate and magnitude of prestressing force.

Comparisons between test data and theory indicated fair agreement in values of deflection; however, measured strains were significantly smaller than predicted by theory. The theoretical assumption that the moment-curvature relationship can be represented by two straight lines—an elastic portion with a constant slope, followed by a plastic portion in which curvature may increase with no moment increase— is shown to be conservative for the static type of loading used. Under traffic load conditions, however, wherein a pattern of bottom surface cracks occurs, the theoretical moment-curvature assumption may be more closely approached. It is planned as part of the future testing program to investigate prestressed pavement response to repetitive moving loads.

•AN INTERIOR load of greater magnitude than one causing bottom surface cracking may be permitted on a prestressed concrete highway or airfield pavement. In the design of such pavements, it is therefore necessary to determine stresses and deflections for conditions not covered by the elastic theory. A theoretical procedure (1) was developed for this purpose at the PCA Research and Development Laboratories. This procedure is specifically applicable to a centrally loaded infinite slab supported by a "dense liquid" foundation and prestressed equally in longitudinal and transverse directions. It provides a method for predicting the distribution of moments and deflections in a prestressed concrete pavement for any load magnitude equal to or less than that causing top surface cracking if the radius of the loading plate, the cracking moment, the radius of relative stiffness, and the subgrade modulus are known. The location of

---

the top surface crack also can be estimated. In the development of this theoretical procedure, it was assumed that (a) the intensity of the subgrade reaction at each point of the bottom surface of the slab is proportional to the deflection of the slab at the point; (b) the moment-curvature graph is represented by two straight lines, i.e., an elastic portion with a constant slope, followed by a plastic portion in which curvature may increase with no moment increase; and (c) the radial cracks in the bottom surface of the concrete slab extend from the center of the load within a circular area that becomes larger as the load is increased. To determine the validity of these assumptions and to compare theoretical and measured data, a program of testing reduced scale precast prestressed concrete slabs was initiated.

OBJECTIVES AND SCOPE OF PROGRAM

The test program was designed to study the behavior of prestressed concrete slabs when subjected to interior loads sufficiently to cause both bottom and top surface cracking. While numerous variables deserve investigation, the reported tests are limited to slabs restrained to simulate infinite extent on a subgrade having an unvarying k value. Controlled variables included size of loading plate and magnitude of prestress.

The specific objectives of the program were (a) to compare measured deflected surface contours with theoretical values, (b) to compare stresses computed from measured strains with theoretical values, (c) to observe the manner in which bottom and top surface cracking occurred, and (d) to evaluate the assumptions made in developing the theoretical procedure.

TEST FACILITIES AND MATERIALS

Data are reported from load tests on three concrete slabs 8 ft by 8 ft by 1 in. thick. Prestressing was accomplished with pretensioned high-strength No. 12 steel wire. The slabs were precast, placed on an artificial coil spring subgrade, and load tested.

Prestressing

Uncoated stress-relieved steel wire was used for applying prestress at the mid-depth of the slabs. The wire diameter was 0.1055 in., area 0.00875 sq in., modulus of elasticity 27,600,000 psi, and ultimate strength 260,000 psi. The wire was tensioned in the frame shown in Figure 1. Two sides of the frame were formed by reinforced concrete beams anchored to the floor by post-tensioned steel bolts. Friction forces developed between the beams and the floor prevented movement due to tensioning of the wires. The wires were inserted through openings provided in these beams at 4-in. intervals along their lengths. The remaining two sides of the prestressing frame were formed by pairs of steel channels between which the wires were inserted. These channels reacted against the ends of the concrete beams.

Each prestressing wire was tensioned individually by a telescoping threaded spacer. The force in the wire was measured by a transducer (2) placed between the wire grip and the reaction frame at the side opposite the spacer. After tensioning the wires, a minimum of one day was allowed before casting the concrete slab. The force in each wire was checked and adjusted, if necessary, to the selected magnitude prior to casting.

To insure full prestress over as much of the slab as possible, a 1-in. split steel cube was fastened to each wire at the point where the wire entered the side forms. The two halves of the cube were grooved slightly undersize for the wire used and were clamped on the wire by countersunk machine screws.

Each slab was stressed equally in the longitudinal and transverse directions. The spacing between wires, amount of tensile force in each wire, and resultant concrete prestress are given in Table 1A.

Casting of Concrete

The cement factor of the concrete was 7.5 sk/cu yd; water-cement ratio was 0.45 by weight, and the sand-aggregate ratio was 0.59 by weight. Type 3 cement was used to obtain a high early strength, and the maximum size of gravel aggregate was $\frac{3}{8}$ in. The
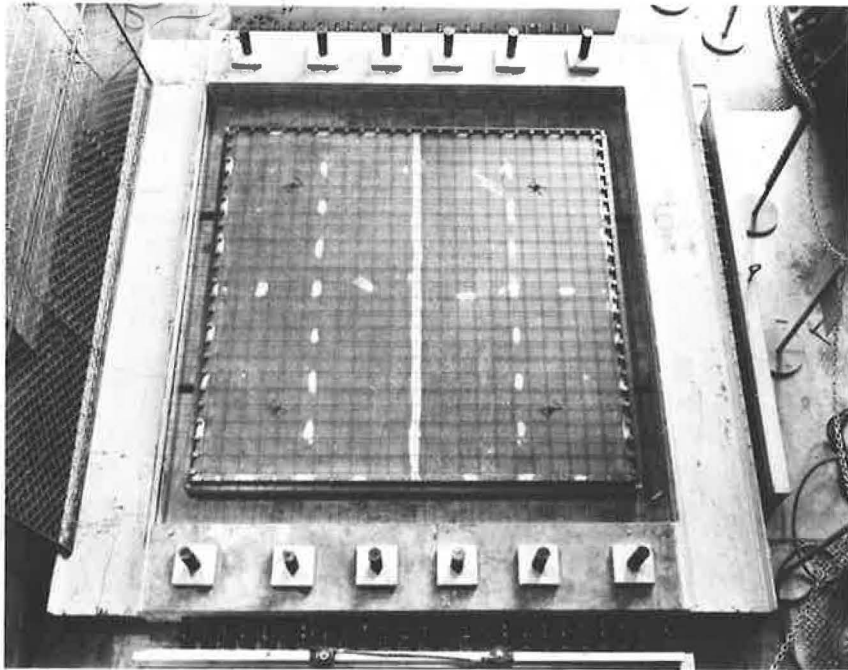
Figure 1. Casting bed.

slump averaged 4 in. and vinsol resin was added to provide an average air content of 5 percent.

Beams (6 by 6 by 30 in.) and cylinders (6 by 12 in.) were made at the time of casting. These were cured in a 70 F, 100 percent relative humidity room until the slabs were load tested, a period of from 8 to 10 days. As determined from tests on the beams and cylinders, the average compressive strength of the concrete was 5,770 psi, modulus of rupture 630 psi, and elastic modulus 3,500,000 psi.

After casting, each slab was covered with polyethylene sheeting and cured at a temperature of 70 to 75 F until the concrete had attained sufficient strength to permit release of the tension in the steel wires. Both top and bottom surfaces were then coated with a curing compound to reduce moisture losses and thereby minimize curling. Strain gages were then cemented to the slab surface at the desired locations.

Spring Subgrade

The artificial subgrade was composed of 121 coil springs, $5\frac{1}{2}$-in. diameter and

TABLE 1
EXPERIMENTAL AND THEORETICAL DATA

A. Experimental Properties[a]

Slab No.	Wire Spacing (in.)	Wire Tensile Force (lb)	Concr. Prestr. (psi)	a (in.)	Mod. of Rupture (psi)	σ_c (psi)	m_c (in. lb/in.)	L (in.)	α
1	4	1,200	300	3	630	930	155	9.54	0.315
2	4	1,200	300	5	630	930	155	9.54	0.525
3	4	600	150	3	630	780	130	9.54	0.315

[a]Symbols used are
  a = radius of loading plate, in.;
  σ_c = cracking stress = modulus of rupture plus prestress;
  m_c = cracking moment = $\sigma_c h^2/6$;
  h = thickness of slab, 1 in.;
  L = radius of relative stiffness $\sqrt[4]{\dfrac{E h^3}{12(1 + \mu^2) k}}$;
  E = elastic modulus, 3,500,000 psi;
  μ = Poisson's ratio, assumed 0.15;
  k = subgrade modulus, 36 pci; and
  α = a/L.

B. Experimental Values[b]

Slab No.	a (in.)	Prestress (psi)	Cracking Loads		b (in.)	c (in.)	Punching Failure Load (lb)
			Bottom (lb)	Top (lb)			
1	3	300	880	4,140	$11\frac{1}{2}$	14	9,000
2	3	300	1,220	4,820	$11\frac{1}{2}$	14	12,500
3	3	150	850	4,180	$12\frac{1}{4}$	14	8,000

[b]Symbols used are
  a = radius of loading plate, in.;
  b = average distance bottom radial cracks extended from load center at top cracking load, in.; and
  c = average radius of initial top circular crack, in.

C. Theoretical Values

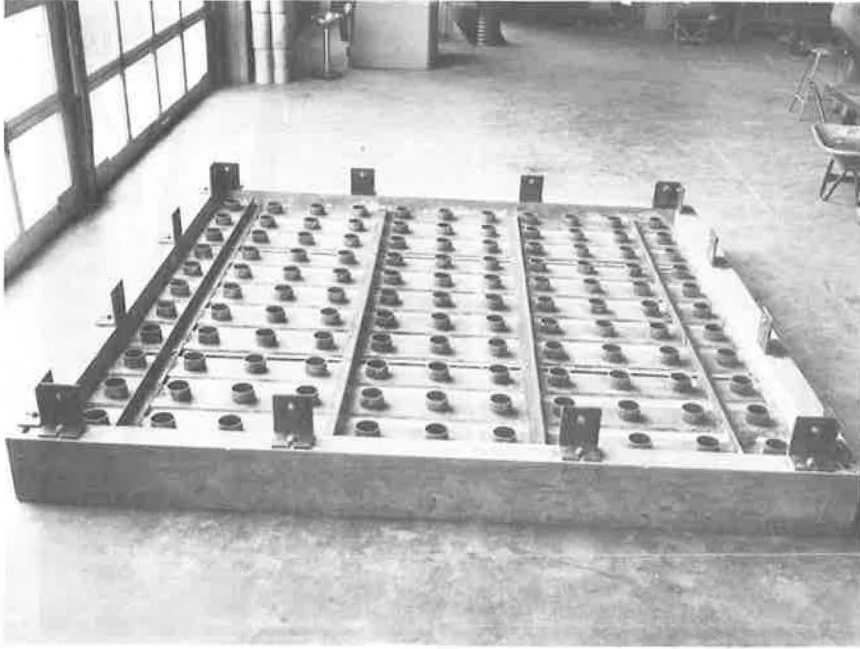| Slab No.	Cracking Loads		Radius of Top Crack (in.)
	Bottom (lb)	Top (lb)	
1	900	2,950	8.5
2	1,270	3,570	11.5
3	780	2,470	8.5

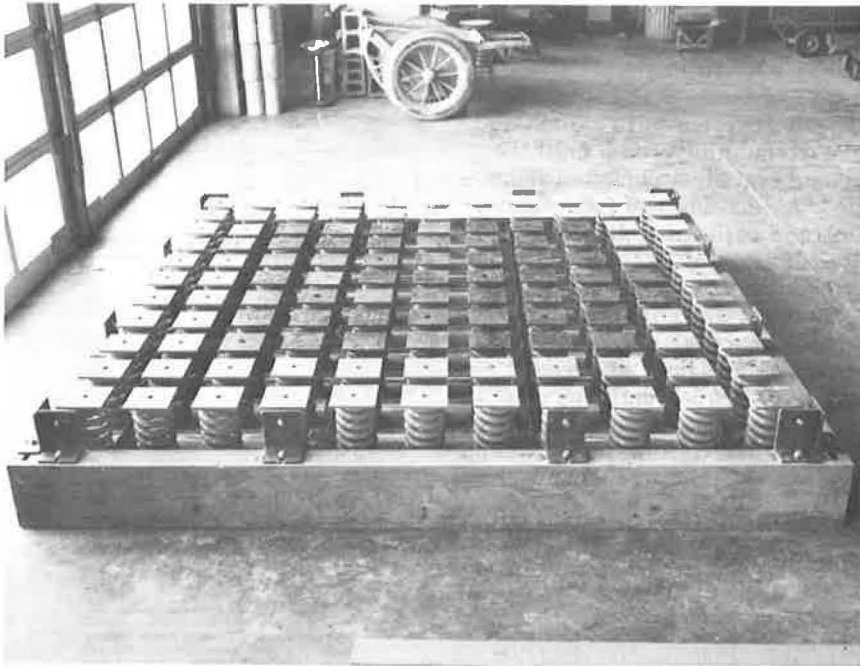Figure 2. Concrete box before coil spring placement.

Figure 3. Concrete box with coil springs and top plates in place.

Figure 4. Load test on concrete slab.

8 in. long. Load-deflection tests conducted on eight randomly selected springs indicated that the spring constant was 2,915 lb per in. of deflection. The springs were placed at 9-in. centers in the concrete box shown in Figures 2 and 3. Short lengths of pipe connected to the bottom of the box positioned the springs and prevented lateral movement during load testing. Similar short lengths of pipe welded to 6-in.-square plates were placed in the top of each spring.

Prior to each slab test, a small quantity of mortar was placed between the polyethylene sheets on top of each spring plate; the slab was then lowered carefully into place compressing the mortar slightly and providing uniform contact over all springs. From the spring constant and spring spacing, the average subgrade modulus over the area of the slab was 36 pci.

Load Application

Loads were applied to the concrete slabs through centrally located circular plates of 3- or 5-in. radius (Table 1A). The concrete box holding the springs was designed to fit on the platen of a 1 million lb testing machine. A surcharge of lead weights, shown in Figure 4, totaling 6,400 lb was placed uniformly over the top surface of the slab to satisfy the requirements of model scaling and to permit the slab to act as an infinite plate.

INSTRUMENTATION

A typical instrumentation plan is shown in Figure 5. SR-4 type A9-2 strain gages 4 in. long were cemented to the top surface of each slab to measure the maximum compressive strain at the load and the distribution of radial and tangential strains at various distances from the load. Strains were recorded continuously throughout a load test.

The deflection pattern of each slab was determined by twenty-eight 0.001-in. dial indicators attached to a wooden bridge that rested on the machine platen. Deflection measurements were noted at each load increment.
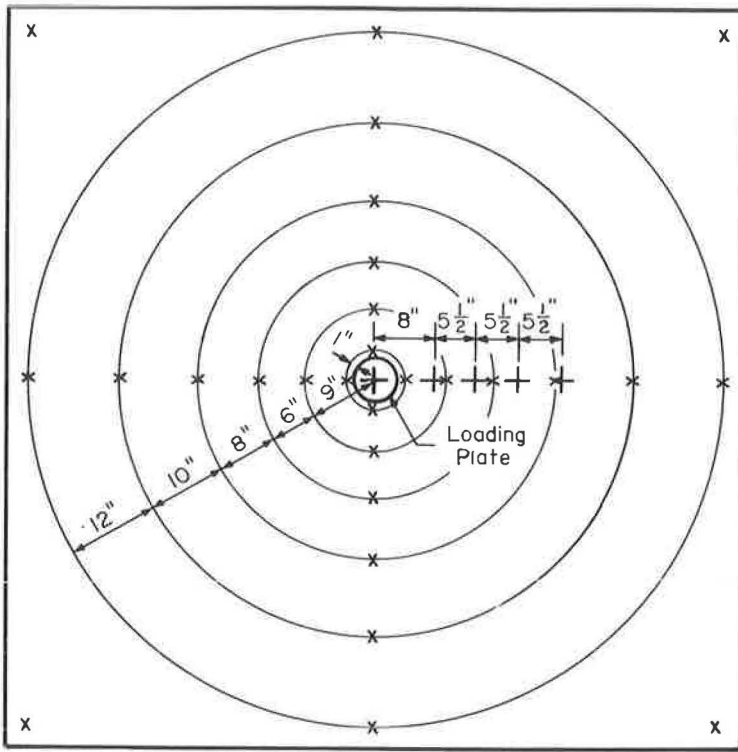
— Top Surface Strain Gage Location
X Deflection Dial Location

Figure 5. Typical instrumentation plan.

RESULTS

Load was increased in increments of 250 to 1,000 lb until the circular plate punched through the slab, failing the concrete in shear but leaving the prestressing wires intact. The punching failure loads were 9,000, 12,500, and 8,000 lb for Slabs 1, 2, and 3, respectively. Prior to punching failure, a number of concentric circular cracks were observed in the top surface. The initial top cracks were not visible until the load was about 7,000 lb; the radius was about 14 in. for all three slabs. After completion of test and release of load, the top cracks closed to such an extent that they were difficult to locate. A brittle coating of polyester resin applied in the later tests aided in locating cracks after release of load. A photograph of a top slab surface with the cracks outlined by black ink is shown in Figure 6. The bottom surface was also examined after completion of test. As shown in Figure 7, bottom cracks extended about 12 in. in radial directions from the load center.

Loads causing bottom and top surface cracking were those that produced tensile stresses at crack locations equal to cracking stresses. The cracking stress of each slab was assumed to equal the summation of the concrete modulus of rupture and the amount of prestress. As given in Table 1A, the cracking stress was 930 psi for Slabs 1 and 2 and 780 psi for Slab 3. Stresses in a radial and tangential direction computed from the measured strains by Eqs. 1 and 2 are shown in Figure 8.

$$\sigma_r = \frac{E}{1 - \mu^2} (e_r + \mu e_t) \qquad (1)$$
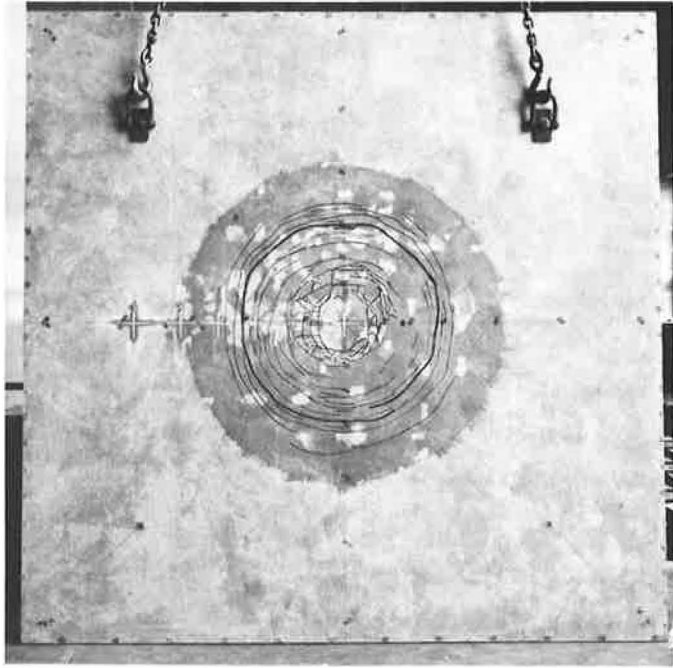
Figure 6. Top surface cracking after test of Slab 2.
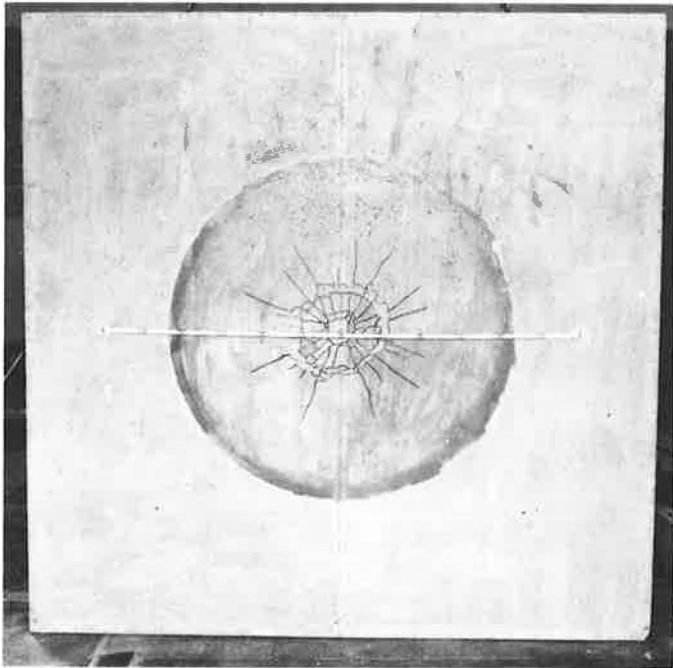
Figure 7. Bottom surface cracking after test of Slab 2.
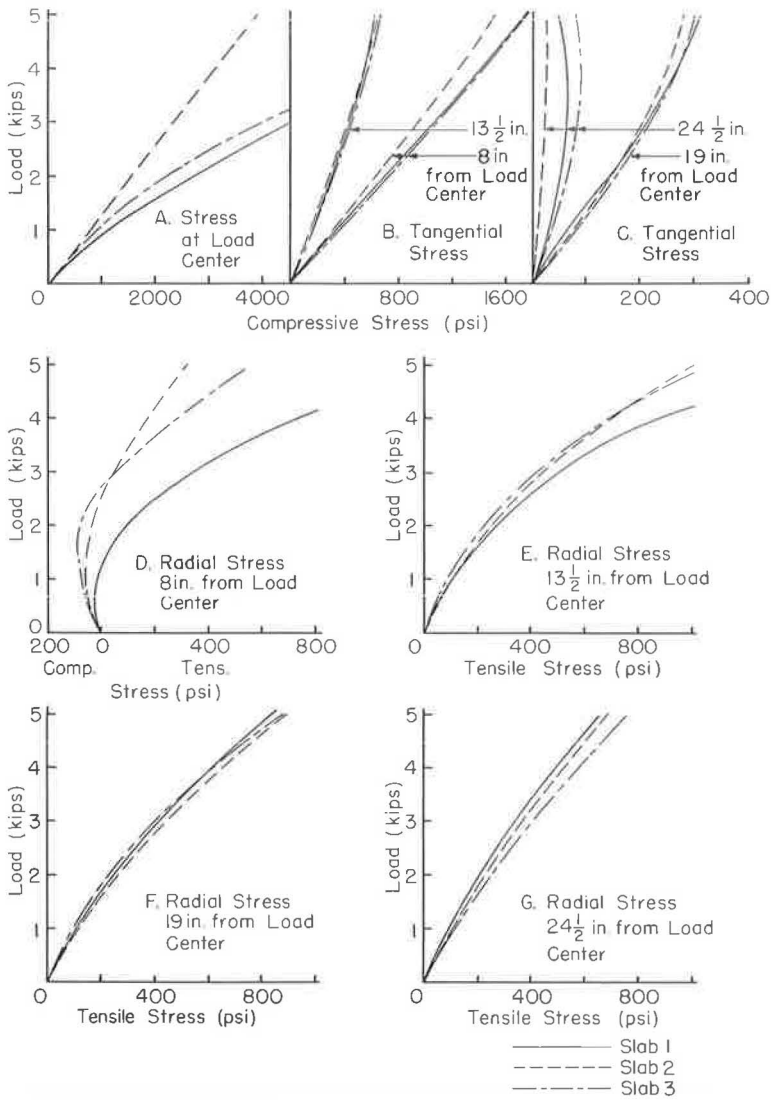
Figure 8. Top surface stresses.

$$\sigma_t = \frac{E}{1 - \mu^2} (e_t + \mu e_r) \tag{2}$$

in which

σ_r = radial stress,
σ_t = tangential stress,
e_r = measured radial strain,
e_t = measured tangential strain,
E = concrete modulus of elasticity, 3,500,000 psi, and
μ = Poisson's ratio, assumed 0.15.

Assuming the neutral axis to be at the mid-depth of the slab, top surface compressive stresses at the load center (Fig. 8A) were used to determine bottom surface crack-
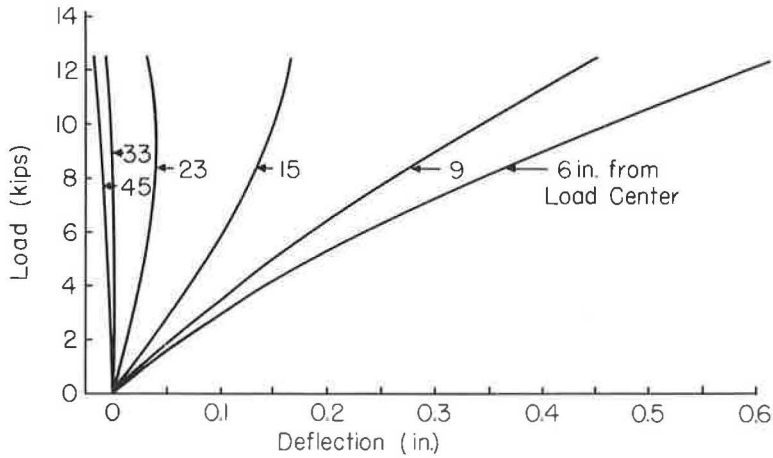
Figure 9. Deflection of Slab 2.
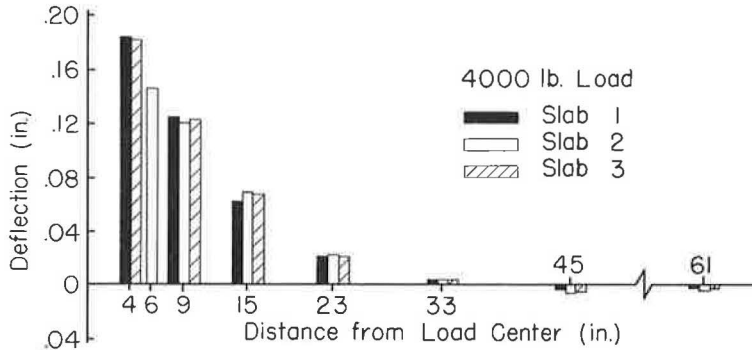
Figure 10. Comparison of slab deflections.

ing loads. Top surface radial tensile stresses $13\frac{1}{2}$ in. from the load center (Fig. 8E) were used to determine top surface cracking loads. Bottom and top surface cracking loads computed from these stress diagrams are given in Table 1B.

Cracking loads were compared to determine the influence of prestress and loading plate size. Slab 2 with the same prestress as Slab 1 was loaded with a larger plate and had greater cracking loads. Slab 3 with less prestress than Slab 1 was loaded with the same plate size and had nearly the same cracking loads. Therefore, the test slab cracking loads were influenced more by loading plate size variations than by the difference in prestress.

The extended distance of bottom surface radial cracks from the load center were estimated by determining where the tangential stresses (Figs. 8B and 8C) exceeded the cracking stresses. Table 1B lists these distances, b, for the load that produced top surface cracking. This distance was slightly greater for Slab 3, which had the smallest amount of prestress.

Deflections were measured incrementally at seven different distances from the load center with a total of 28 indicators as shown in Figure 5. At each distance from the load center, the four indicators spaced 90° apart provided similar deflections at each load increment throughout a test. This indicated that the pressure under the load plate was symmetrically distributed and that the coil spring subgrade responded properly.

Average deflections measured during the load test of Slab 2 are shown in Figure 9. These are typical of all three slabs. There was no abrupt change in the rate of deflec-

tion increase per unit load when either bottom or top surface cracking occurred. A comparison between deflections for the three slabs at a load of 4,000 lb is shown in Figure 10. This load approaches the magnitude causing top surface cracking. Deflections of the three slabs were similar, indicating only minor influence of variations in prestress and size of loading plate.

THEORETICAL VALUES

Experimental data were compared with values determined by the theoretical procedure (1) developed at the PCA Research and Development Laboratories for a centrally loaded infinite slab supported by a "dense liquid" foundation and prestressed equally in longitudinal and transverse directions. The explicit parameters necessary for the computation of theoretical values are cracking moment, subgrade modulus, and the ratio of
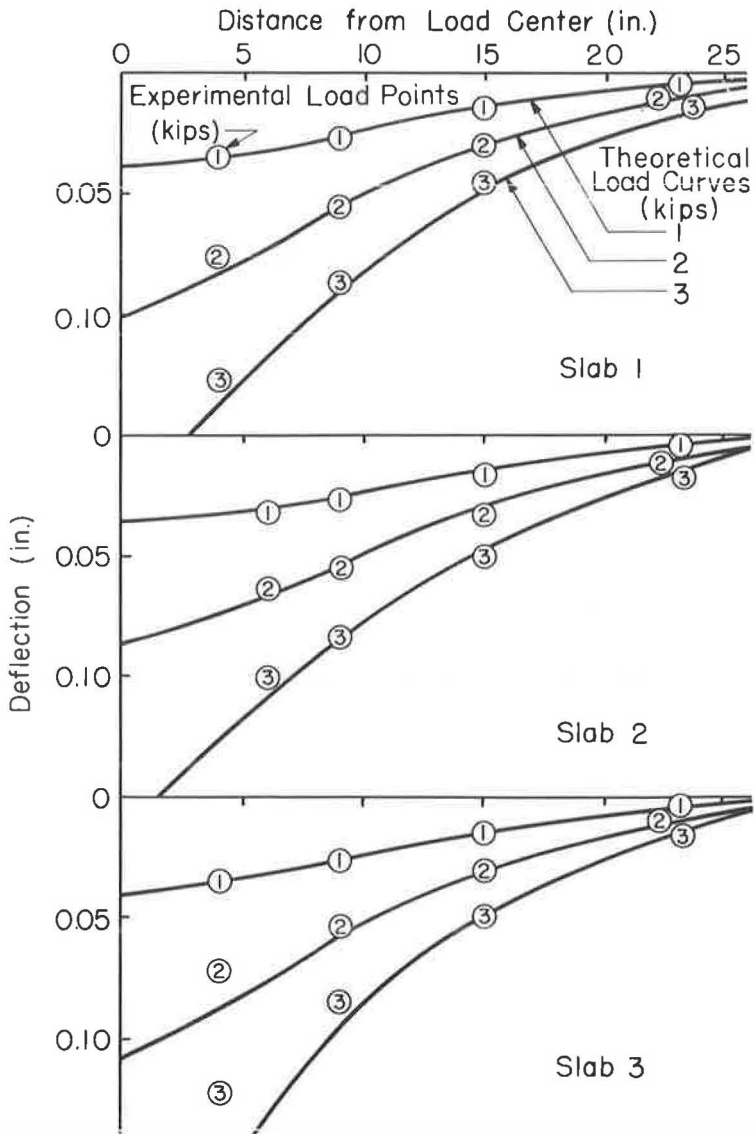
Figure 11. Comparison of experimental and theoretical deflections.
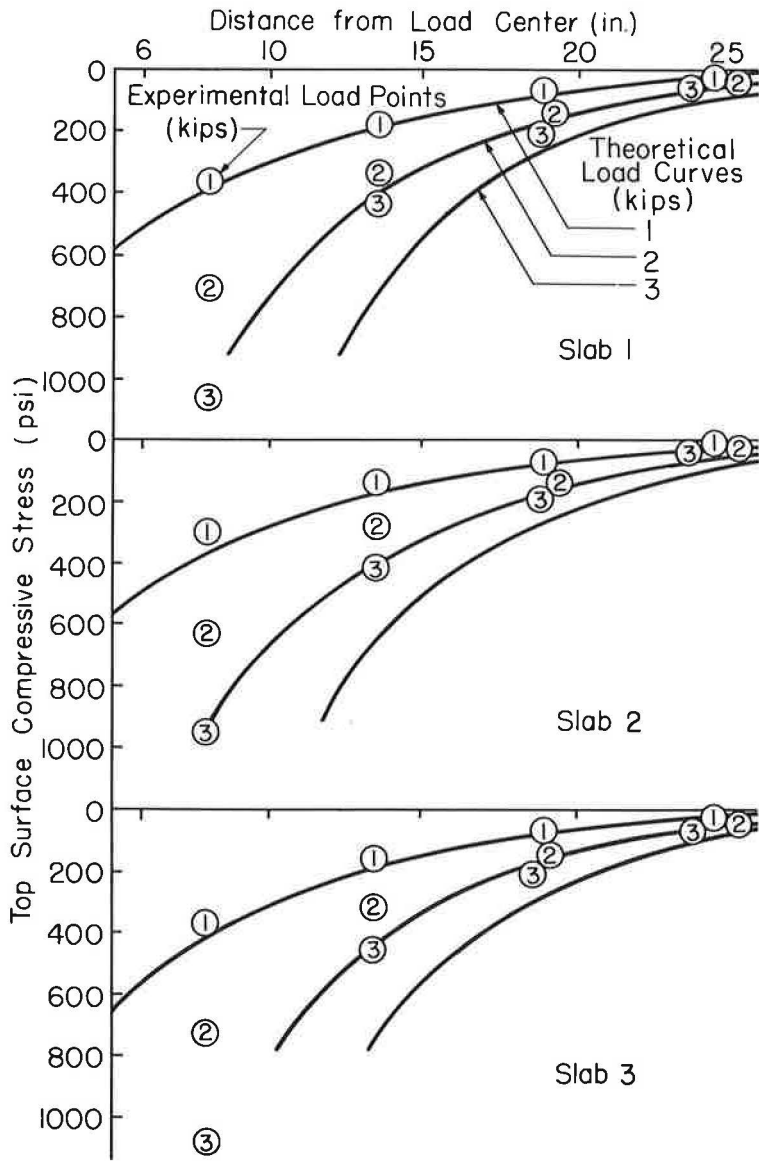
Figure 12. Comparison of experimental and theoretical tangential stresses.

the radius of the loading plate to the radius of relative stiffness. These quantities for the three slabs are given in Table 1A.

Theoretical deflection, tangential stress, and radial stress are shown by the curves in Figures 11, 12, and 13, respectively, for load applications of 1,000, 2,000, and 3,000 lb on each slab. The numbered circles are experimental results. The influence that prestress and loaded area size have on stresses and deflections predicted by the theoretical procedure was determined from these figures. Slab 2 had the same pre-stress as Slab 1 but was loaded with a larger plate. Slab 3 was loaded with the same plate size as Slab 1 but had less prestress. According to the theoretical treatment, increased deflections, tangential stresses, and radial stresses should result from a decrease in either the prestress or loaded area size. Experimental tangential stresses
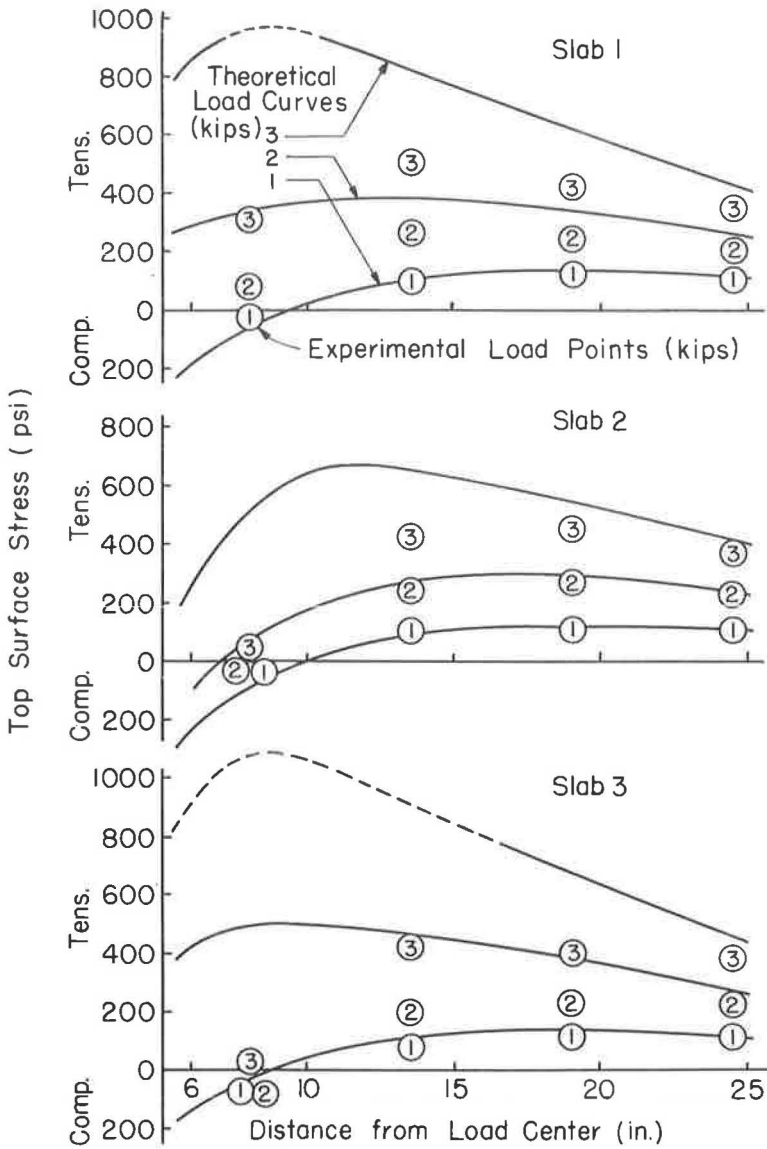
Figure 13. Comparison of experimental and theoretical radial stresses.

were influenced in this manner with Slab 3 showing the largest values and Slab 2 the smallest values. However, experimental deflections and radial stresses varied only slightly with changes in prestress and loaded area size.

Good agreement was found between experimental and theoretical data for the 1,000-lb load. At greater loads, the experimental deflections were in fair agreement with the theoretical values, but the experimental stresses especially those in the radial direction were smaller than the theoretical values. As a result of the radial stress differences, the experimental and theoretical loads for top cracking differed considerably.

Theoretical cracking loads and radii of top circular cracks are given in Table 1C. A comparison with Table 1B indicates that experimental and theoretical bottom cracking loads were in excellent agreement but that experimental top cracking loads and

radii of top circular cracks were greater than the theoretical values. Theoretical bottom cracking loads were computed by methods based on the elastic theory, and their agreement with experimental values indicated elastic slab behavior prior to cracking. Reasons for the disparity beyond elastic conditions were investigated.

A possible discrepancy between theory and experiment could result from the manner in which the load was distributed between the load plate and the test slab. Although a $\frac{1}{2}$-in. rubber pad was placed between the steel plate and concrete slab to aid in obtaining uniform load distribution, at higher magnitudes of load the combination of large slab deflections and a relatively stiff loading plate might have concentrated the load around the periphery of the plate.

Stresses at locations beyond the loading plate area resulting from a peripheral concentration of load would theoretically be equivalent to those resulting from a uniform load distributed through a plate having a radius of about 1.5 times as large. To explore this conjecture, the experimental values of Slab 1 were compared with theoretical values determined for a uniformly loaded plate of $4\frac{1}{2}$-in. radius. As shown by the tangential and radial stresses in Figure 14, there was better agreement between experimental and theoretical values for the peripheral loading condition than for the uniformly loaded 3-in. radius plate condition shown in Figures 12 and 13. However, the differences between experimental and theoretical stresses remained greater than magnitudes that might be attributed to test conditions. Therefore, the assumptions used in the development of the theoretical procedure were examined to obtain an explanation for the differences.
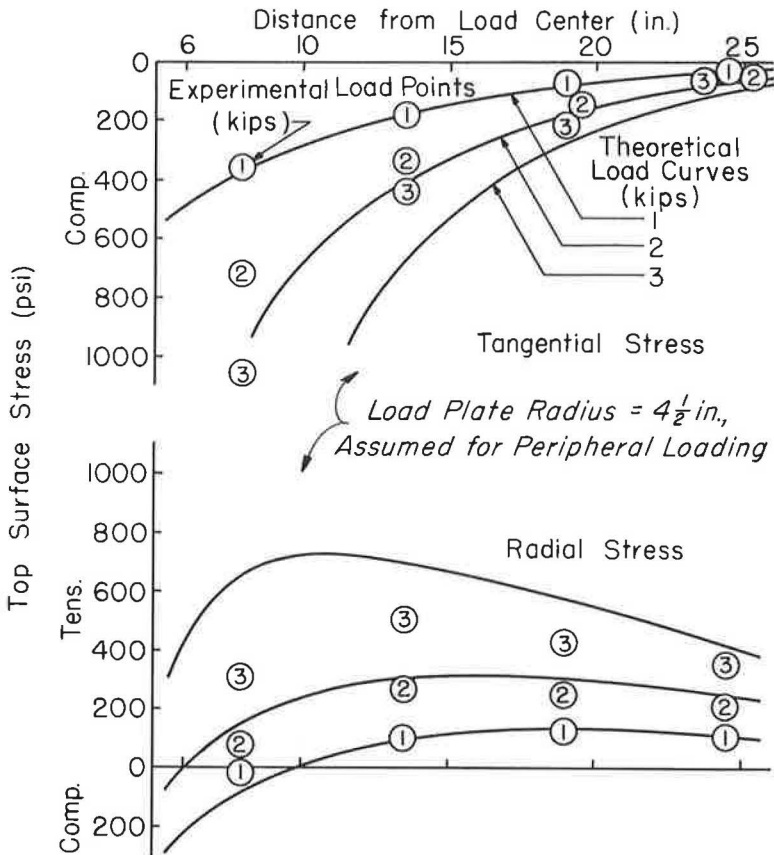
Figure 14. Comparison of experimental and theoretical stresses of Slab 1.

Three assumptions were involved: (a) that the intensity of subgrade reaction at each point of the bottom surface of the slab was proportional to the deflection of the slab at that point; (b) that the radial cracks in the bottom surface of the concrete slab extended from the center of the load within a circular area that became larger as the load was increased (Fig. 15A); and (c) that the relationship between moment and curvature was represented by two straight lines (Fig. 15B), that is, an elastic portion with a constant slope followed by a plastic portion in which curvature increased with no moment increase. The first assumption was fulfilled by the use of a coil spring subgrade, and the

— First Radial Crack
— Extended Crack
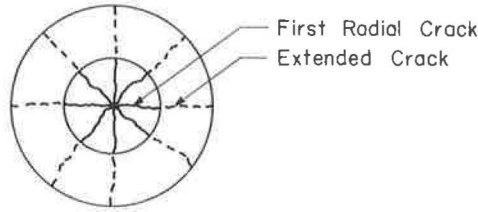
A. Assumed Bottom Surface Crack Pattern
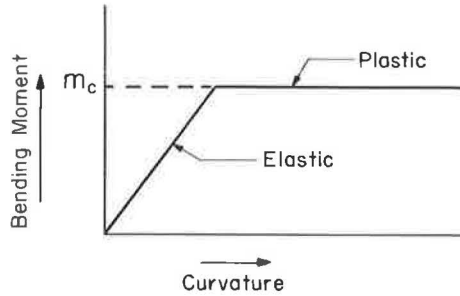
B. Assumed Moment-Curvature Relationship

Figure 15. Theoretical assumptions.
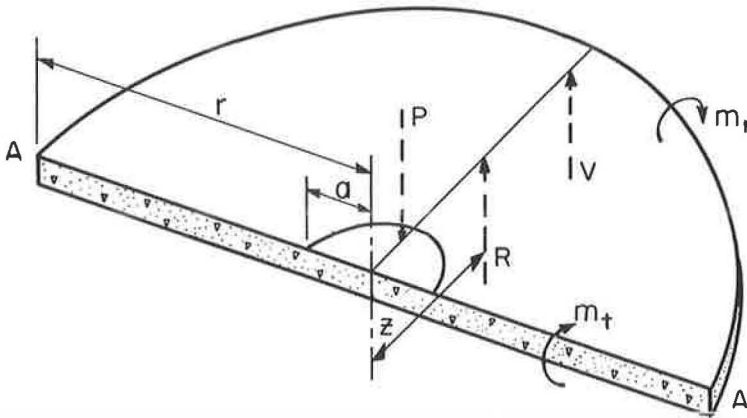
Figure 16. Semicircular portion of concrete slab with interior load.

second assumption was confirmed by the experimental data. To determine the accuracy of the third assumption, the following analysis of a free-body diagram of a loaded slab was undertaken.

The analysis was developed for a large concrete slab loaded at an interior location with a force of 2P uniformly distributed over a circular area of radius a. A semicircular section of this slab including half the loaded area is shown in Figure 16. The resultant applied load on this section is labeled P, the resultant subgrade reaction R, and the resultant shear force V. The moments consist of the radial moment per unit length, m_r, and the tangential moment per unit length, m_t. The shear and radial moments were assumed to be uniformly distributed along the circular arc of radius r measured from the center of the load.

Moments were summed about diameter A-A. The moment arm of the resultant applied load P is equal to $4a/3\pi$ assuming uniform distribution of load over the semicircular area of radius a. The moment arm of the resultant shear force V is equal to $2r/\pi$ assuming uniform distribution along the circular arc of radius r. The moment about A-A of the unit radial moment, m_r, is $2r\,m_r$. The average unit tangential moment along the diameter 2r is $\overline{m_t}$, and its moment about A-A is $2r\,\overline{m_t}$. The sum of moments about diameter A-A must equal zero as shown by Eq. 3.

$$\Sigma M_{AA} = O = P\left(\frac{4a}{3\pi}\right) - Rz - V\left(\frac{2r}{\pi}\right) + 2r\,(m_r + \overline{m_t}) \tag{3}$$

The resultant subgrade reaction R can be computed for any semicircular section of radius r by multiplying the displaced volume as determined from the measured deflections by the known subgrade modulus. Its moment arm z can be computed by locating the centroid of the displaced volume. The difference between the load and subgrade reaction forces is equal to the resultant shear force. Therefore, diagrams of $\overline{m_t} + m_r$ vs r can be determined for each increment of load applied to a test slab by using the measured deflection profile and the subgrade modulus.

The accuracy of the moment-curvature relationship assumed in the theoretical procedure was determined by the combined use of $\overline{m_t} + m_r$ diagrams and measured strain data. An example of the method employed before the occurrence of bottom surface cracking is given in Figure 17 using the data obtained when a 500-lb load was applied to Slab 1. As shown in Figure 17A, the deflection profile was obtained by drawing a smooth curve through the measured experimental values. This profile was used with the analysis outlined in the previous paragraph to obtain the $\overline{m_t} + m_r$ diagram shown in Figure 17B. As the slab reacted elastically before the occurrence of bottom cracking, the ratio of a $\overline{m_t} + m_r$ diagram to a $(\overline{\sigma}_t + \sigma_r)/E$ diagram was equal to the elastic modulus multiplied by the unit section modulus. Using the elastic modulus of 3,500,000 psi that was determined from beam and cylinder test specimens and 1/6 for the unit section modulus, the curve in Figure 17C was obtained from Figure 17B. Profiles of σ_t/E and σ_r/E were also obtained (Fig. 17D) by drawing smooth curves through values computed from the measured strains by Eqs. 1 and 2 rewritten to give σ_r/E and σ_t/E in terms of the strains. The σ_t/E profile was used to compute a profile of cumulative average tangential stress divided by elastic modulus or $\overline{\sigma}_t/E$. For this computation, average values for 2-in. increments were summed and divided by the number of increments. Differences between the σ_r/E and $\overline{\sigma}_t/E$ profiles in Figure 17D at locations of computed experimental values are represented by the points shown in Figure 17C. There was good agreement in Figure 17C between the points determined from the strain data and the curve determined from the deflection data using the elastic modulus of 3,500,000 psi from beam and cylinder tests. As similar good agreement was obtained for Slabs 2 and 3, the experimental data and method of analysis were considered to be reliable.

An example of the method employed after the occurrence of bottom surface cracking is shown in Figure 18 using the data obtained when a 3,000-lb load was applied to Slab 1. The $\overline{m_t} + m_r$ diagram computed with the use of the deflection profile is shown by curve A. Radial strains measured at distances of 8, $13\frac{1}{2}$, 19, and $24\frac{1}{2}$ in. from the load center were used to compute radial stresses. These stresses, which were less than the cracking stresses, were multiplied by the unit section modulus to obtain unit
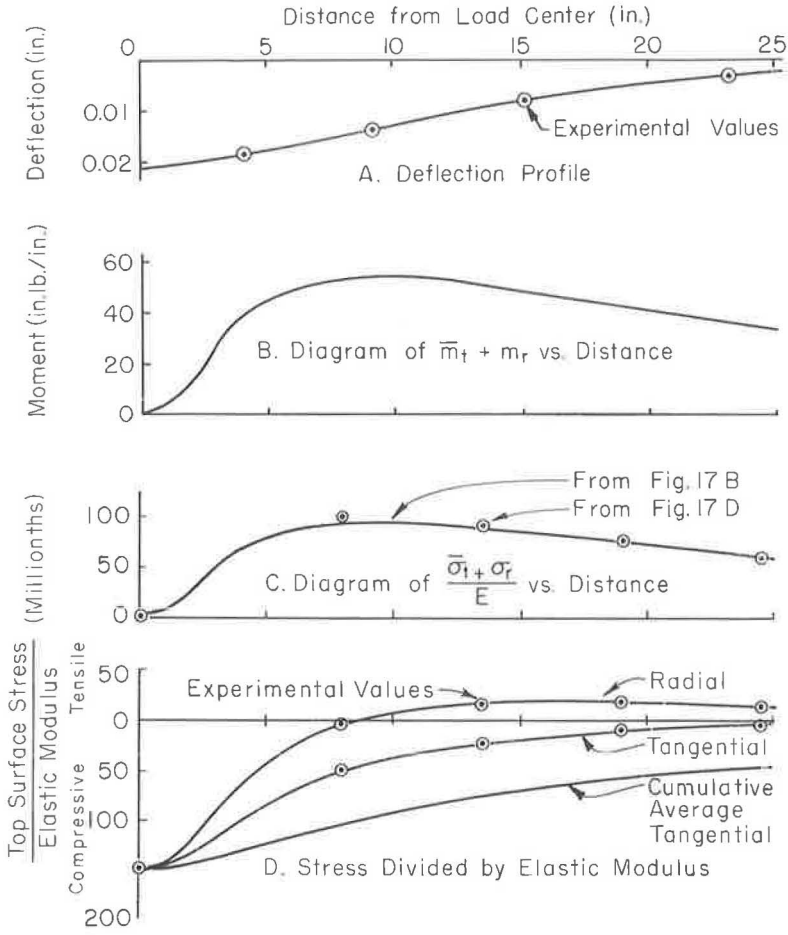
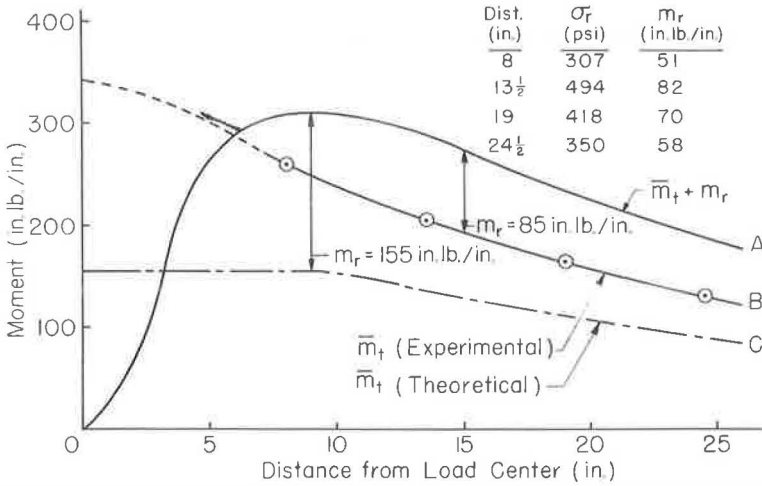Figure 17.   Diagrams for 500-lb load on Slab 1.

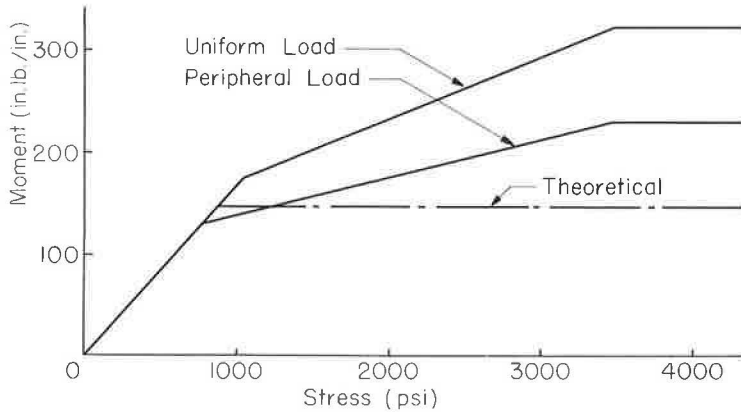Figure 18.   Moment diagrams for 3,000-lb load on Slab 1.

Figure 19. Moment-stress diagrams.

radial moments. These unit radial moments, m_r, were subtracted from the $\overline{m}_t + m_r$ diagram shown by curve A to obtain the average unit tangential moment, $\overline{m}_t$, diagram shown by curve B.

The cracking moment of Slab 1 was 155 in. lb/in. If the loaded slab had reacted according to the moment-curvature assumption used in the theoretical method, the maximum unit tangential moment would equal the cracking moment and the $\overline{m}_t$ diagram would be as represented by curve C. A comparison of the experimental and theoretical $\overline{m}_t$ diagrams indicated that tangential moments greater than those causing initial cracking occurred in the test slabs.

The example in Figure 18 was used to demonstrate that the occurrence of moments greater than those causing initial cracking was the major reason for differences between experimental and theoretical data. The maximum negative radial moment determined from the difference between curves A and B occurred 15 in. from the load center and equaled 85 in. lb/in. or 55 percent of the cracking moment of 155 in. lb/in. These values were for a load of 3,000 lb. Top surface cracking occurred at 4,140 lb with a radius of 14 in. as given in Table 1B. The maximum negative radial moment determined from curves A and C occurred 9 in. from the load center and equaled the cracking moment of 155 in. lb/in. at this 3,000-lb load. As given in Table 1C, the theoretical procedure predicted top surface cracking at 2,950 lb with a radius of 8.5 in. Therefore, the test slabs would have cracked approximately as predicted by the theoretical procedure if they had reacted in accordance with the theoretical moment-curvature assumption.

Average unit tangential moment, $\overline{m}_t$, diagrams obtained as shown by the example in Figure 18 were used to compute unit tangential moment, m_t, diagrams. By comparing m_t diagrams with tangential stress profiles determined from experimental strain data, moment-stress diagrams were obtained. The moment-stress diagrams (Fig. 19) were composed of the three connecting straight lines that provided the best agreement between moment and stress profiles of the three slabs for all loads less than those causing top surface cracking. A moment-stress diagram was determined for both the uniformly loaded area condition and the peripheral load condition previously described. Both diagrams were determined by the same procedure except that the moment arm of the resultant applied load as given in Eq. 3 was $2a/\pi$ for the peripheral load condition instead of $4a/3\pi$ as used for the uniformly loaded area. The moment-stress diagram resulting from the moment-curvature assumption of the theoretical procedure is also shown in Figure 19. A comparison of these diagrams indicates again that moments greater than the initial cracking moments occurred in the test slabs. Therefore, the slabs did not react in accordance with the assumption that the moment-curvature relationship can be represented by two straight lines with the maximum moment equaling the cracking moment.

CONCLUSIONS

Three reduced scale prestressed concrete slabs supported on a coil spring subgrade were loaded to failure through centrally located circular plates. Measurements of strain and deflection were made at a number of locations with a number of load increments. Test variables included loading plate size and prestressing force magnitude. The following conclusions were drawn:

1. Initial slab cracking occurred in the bottom surface under the loaded area. As the load was further increased, the bottom cracks extended in radial directions. At load averaging 4.4 times the bottom cracking load, a circular top surface crack occurred with a radius of 1.5 times the radius of relative stiffness. At load averaging 10.0 times the bottom cracking load, the loading plate punched through the slab failing the concrete in shear but leaving the prestressing wires intact. An increase in the size of loaded area caused an increase in the cracking loads. Additional prestress had little influence on the cracking loads.

2. A comparison between experimental data and values determined by a theoretical procedure developed at the PCA Research and Development Laboratories indicated the following: (a) experimental and theoretical bottom surface cracking loads were in excellent agreement; experimental deflection and stress profiles at bottom cracking loads were similar to theoretical profiles; (b) experimental top surface cracking loads were about 48 percent greater than theoretical values; at the top cracking loads, the experimental and theoretical deflections were in fair agreement, but the experimental stresses especially those in a radial direction were less than the theoretical values; and (c) observed radii of top surface circular cracks were greater than predicted by the theory.

3. An analysis of a free-body diagram of a loaded test slab indicated that moments greater than the initial cracking moment occurred after bottom surface cracking. Therefore, the slabs did not react in accordance with the assumption made in the theoretical procedure that the moment-curvature relationship can be represented by two straight lines with the maximum moment equaling the cracking moment. This was the major reason for greater experimental top cracking loads than theoretically predicted. The theoretical moment-curvature assumption is therefore conservative for static type loading. Under traffic load conditions, however, wherein numerous bottom surface cracks occur, the theoretical assumption may be more closely approached.

REFERENCES

1. Osawa, Y., "Strength of Prestressed Concrete Pavements." Jour. of the Structural Div., ASCE Proc., PCA Dev. Dept. Bull. D57 (Oct. 1, 1962).
2. Hanson, N. W., "Load Cells for Structural Testing." Jour. of the PCA Res. and Dev. Labs., PCA Dev. Dept. Bull. D33 (Jan. 1959).

Load Tests on Post-Tensioned Pavement Slabs

A. P. CHRISTENSEN
Development Engineer, Research and Development Laboratories, Portland Cement
Association, Skokie, Illinois

This paper reports data from static load tests conducted on
three concrete slabs post-tensioned with steel strands. Each
slab was 30 ft long, 12 ft wide, and 5 in. thick. The principal
variable was the amount of prestress. Two slabs had only longi-
tudinal prestress, one of 180 psi and the other of 360 psi. The
third slab had 360 psi longitudinal prestress and 70 psi trans-
verse prestress.

Data from interior loadings indicated that transverse pre-
stress may be required to prevent bottom surface cracks from
extending to the top surface. This suggests that if the structural
contribution of prestressing is to be utilized fully both longitu-
dinal and transverse prestress may be required for airport pav-
ing. For edge loadings none of the bottom surface cracks extend-
ed to the top. This suggests that longitudinal prestress may be
sufficient for highway pavements.

These comments on the mode of failure are based on static
load tests using one dual-plate assembly to simulate a dual-tire
wheel load.

•PRESTRESSED concrete pavements have been constructed in many localities during
the past 15 years. Prestress application methods may be classified into two groups.
One group utilized either post-tensioned or pretensioned steel cables placed in long in-
dividual slabs; the other group utilized either expanding flat jacks or wedges placed in
the joints between long slabs with the reactions absorbed by end abutments. Useful in-
formation has been reported concerning the relative merits of construction methods,
but little data have been developed on which a rational method of design can be based.

The principal items of uncertainty concern the behavior of a prestressed concrete
pavement when loaded and the mode of failure. In some of the early discussions of
these items, the limiting load on a prestressed concrete pavement was related only to
cracking in the bottom surface of the slab. The increase in load-carrying capacity
attained by prestressing would then be only the amount which the prestress added to
the flexural strength of the pavement. Subsequent studies (1, 2) have shown a much
greater increase in load-carrying capacity, and the occurrence of top surface cracking
has been suggested as the criterion for failure. In the design of a prestressed con-
crete pavement with the top surface cracking failure concept, it is necessary to deter-
mine stresses and deflections beyond conditions to which the elastic theory is applica-
ble. To provide a better understanding of the stresses and deflections that develop in
a prestressed concrete pavement when loads are applied after the occurrence of bottom
surface cracking, load tests were conducted on three prestressed concrete slabs con-
structed at the Portland Cement Association (PCA) Research and Development Labora-
tories.

SCOPE AND OBJECTIVES

Three concrete slabs were constructed in an outdoor environment and were pre-
stressed with post-tensioned steel strands. Each slab was 30 ft long, 12 ft wide, and

5 in. thick. The slab cross-sections were selected to be suitable for highway design. A thickness of 5 in. has been used for prestressed concrete highways in other experimental installations, and a width of 12 ft corresponds to a highway traffic lane. The length of 30 ft was sufficient to allow the development of moments equal to those in a pavement of infinite length when loaded at edge locations.

The amount and direction of prestress were varied for the three slabs. Two of the slabs had only longitudinal prestress, one of 180 psi and the other of 360 psi. The third slab had 360 psi longitudinal prestress and 70 psi transverse prestress. Static loads were applied at both interior and edge locations with magnitudes sufficient to determine slab deflection and moment characteristics in both the elastic and plastic range. Measurements were made to determine strain and deflection profiles of the slab and the pressure on the subgrade.

Specific Objectives

The objectives of the program are (a) to determine the effect of prestress level on strains and deflections causing bottom and top surface cracking for edge and interior loading, and (b) to interpret the significance of these data relative to the criterion for failure of a prestressed pavement.

MATERIALS AND PREPARATION

The slabs were constructed in an outdoor environment with the following materials and preparation.

Subgrade Material

The subgrade material for all slabs was a sandy clay loam with an AASHO classification of A-4. Subgrade characteristics are given in Table 1.

The subgrade modulus was determined from plate bearing tests made prior to the construction of each slab. The average value of Westergaard's subgrade modulus, k, as determined with a 30-in. diameter plate at 0.05-in. deflection was 140 pci.

Friction Reducing Layer

A friction reducing layer was used under all slabs to reduce to a minimum stresses resulting from restraint to horizontal slab movement. This layer consisted of $\frac{1}{4}$ in. of fine uniform sand covered with waterproof paper. All of the sand passed the No. 30 sieve, 30 percent passed No. 50, and all was retained on No. 100. The sand was compacted at its optimum moisture content by hand tamping.

Steel Prestressing Strand and Conduit

The post-tensioning strands were composed of uncoated stress-relieved steel wires. Dimensions and properties were diameter, $\frac{7}{16}$ in.; area, 0.1089 sq in.; minimum ult. str., 27,000 lb; and approx. mod. of elast. 26,000,000 psi.

Openings for the strands were provided by $\frac{3}{4}$ in. I.D. flexible conduit made from interlocking 0.010-in.-thick strip steel. As shown in Figure 1, the longitudinal conduit was placed at the slab mid-depth. For the slab with transverse prestress, the transverse conduit was placed alternately above and below the longitudinal conduit.

Concrete Slabs

The concrete mix used for the three test slabs contained 564 lb of cement per cu yd; water-cement ratio was 0.48 by

TABLE 1

SUBGRADE PROPERTIES

	Particle Size (mm)	Percent	Pcf	Pci
Material				
Gravel	76.2 -2.0	1	-	-
Coarse sand	2.0 -0.42	6	-	-
Fine sand	0.42 -0.074	41	-	-
Silt	0.074-0.005	27	-	-
Clay	below 0.005	25	-	-
Liquid limit	-	23.1	-	-
Plasticity index	-	7.3	-	-
Maximum dry density				
(AASHO stand)	-	-	114.5	-
Optimum moisture	-	13.2	-	-
Modulus of subgrade				
reaction, k	-	-	-	140

T = Transverse Spacing of Steel Strand
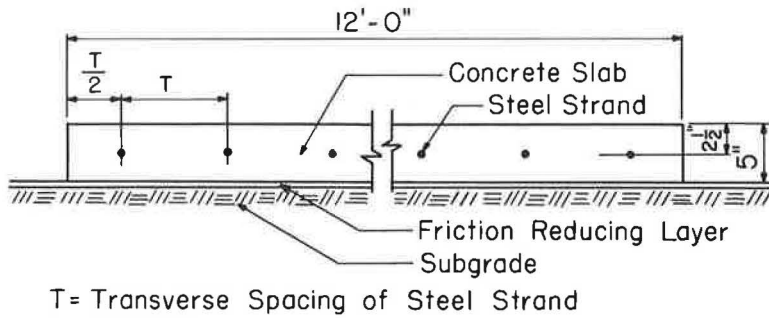
Transverse Section (All Slabs)

L = Longitudinal Spacing of Steel Strand
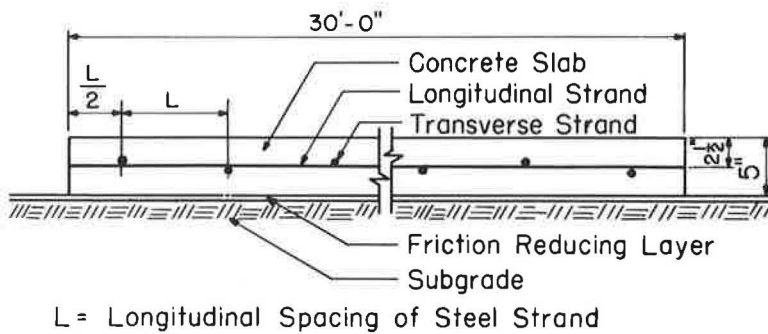
Longitudinal Section (Slab 3 Only)

Figure 1. Prestressed concrete slab cross-sections.

weight; maximum size gravel aggregate was $1\frac{1}{2}$ in., and the sand-aggregate ratio was 37 percent by weight. The slump averaged 4 in., and the air content averaged 5 percent.

Beams, 6 by 6 by 30 in., were made at the time of casting and were tested after 28 days of moist curing at 73 F and 100 percent relative humidity. In addition, data were obtained from 5-in. wide beams cut from the slabs after load testing was completed. The concrete properties as determined from these beams are shown in Table 2. For computing stresses from measured strains, a value of 5 million psi was used for the concrete modulus of elasticity for each test slab.

During placing of the concrete steel chairs were used to keep the conduits at the required depth, and $\frac{5}{8}$-in. diameter deformed reinforcing bars were inserted through the conduits prior to casting to provide greater rigidity against bending. For Slabs 1 and 2, a wood spacer that was notched at the proper steel locations was moved ahead of the concrete as it was placed. In Slab 3 with transverse pre-

TABLE 2

CONCRETE PROPERTIES

Slab No.	A-Beams[1]		B-Beams[2]	
	Mod. of Rupture (psi)	Sonic Modulus (10^6 psi)	Mod. of Rupture (psi)	Sonic Modulus (10^6 psi)
1	580	5.06	700	6.14
2	520	4.70	640	5.75
3	540	4.61	660	5.88

[1] A-Beams (6 by 6 by 30 in.) made at time of casting and tested after 28 day moist curing.
[2] B-Beams (5 by 5 by 30 in.) cut from slabs after load testing was completed at an average period of 15 months after construction.
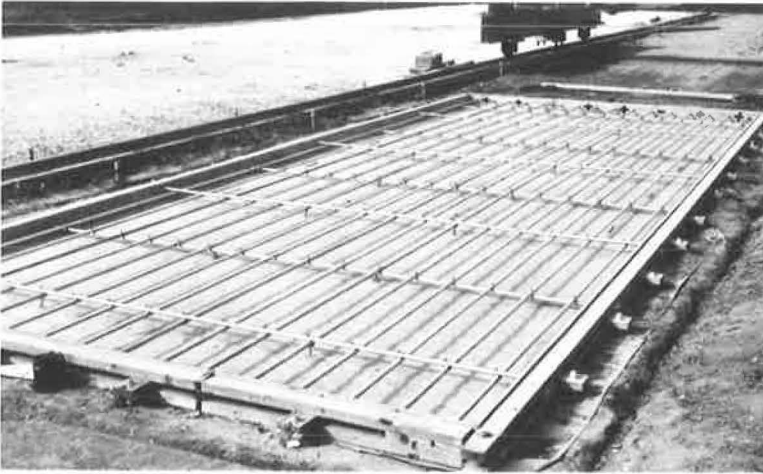
98

Figure 2. Grid of flexible conduit prepared for slab with two-way prestress.

TABLE 3

PRESTRESSING VALUES

Slab No.	Steel Spacing (in.)		Concrete Prestress (psi)	
	Longitudinal	Transverse	Longitudinal	Transverse
1	18	0	180	0
2	9	0	360	0
3	9	45	360	70

stressing, the longitudinal conduits were tied to the transverse conduits as shown in Figure 2. All of the methods used to keep the conduits in alignment were judged to be satisfactory because the losses from friction between the strands and the conduits were negligible during tensioning.

Prestressing and Grouting

After the concrete had cured for a minimum of 28 days, the slabs were prestressed. Before inserting the steel strands, the conduits were cleaned with water and air under pressure. The strands were stressed individually using a hydraulic ram at one end of the slab. They were held at the required stress by means of a grip at each end. The load on each strand was carefully measured using a load transducer (3) between the strand grip and the concrete slab.

After stressing each strand to 150,000 psi or 16,290 lb, the conduits were filled with grout. A minimum period of 24 hr elapsed between stressing and grouting, and the stress on each strand was adjusted if necessary just prior to grouting. The spacing of the steel strands and the magnitude of concrete prestress for each slab are given in Table 3.

The grout consisted of neat cement with a water-cement ratio of 0.5 by weight. Aluminum powder in the amount of 2.0 gm per 100 lb of cement was added to reduce shrinkage.

LOADING DEVICES

Loads were applied to the slabs by a 50-ton hydraulic ram reacting against a steel beam as shown in Figure 3. Rails on each side of the test area for the entire length facilitated the positioning of the steel beam. This beam was held in position during a load test by soil anchors spaced along the rails permitting the application of loads up to 100,000 lb.

Loads were applied through two plates in the shape of rectangles with semicircular ends simulating dual tires. Each plate had an area of 100 sq in. with a length of 13.83 in. and a width of 8.30 in. During load testing the plates were spaced 13.0 in. apart measured between the centerlines. The magnitude of load was measured by a pair of transducers (3) with electrical response sensed by strain indicators.

Figure 3.   Outdoor test area showing the loading device.

INSTRUMENTATION

The instrumentation plan was not the same at all test locations. Instrumentation was provided to measure strain and deflection of the concrete slab and pressure on the subgrade at various load increments.

Strain measurements were made using 6 in. long SR-4 type A9 gages cemented to the concrete at a number of top surface and vertical edge locations. Deflections were measured with 0.001-in. dial indicators attached to a wooden bridge that was supported independently of the slab. Pressures at the top of the subgrade during edge load tests were measured with Carlson stress meters (4). These meters had a $7\frac{1}{4}$-in. diaphragm plate and were installed in a mortar bed with the stem downward. A length of sponge rubber weather stripping material was wrapped around the circumference of the diaphragm to assure unrestricted action. Instrument constants were furnished by the manufacturer, and check tests on the calibration curve were made after the stress meter had been installed.

EDGE LOAD TESTS

Static loads were applied at the longitudinal slab edges. The dual loading plates were positioned with the outer edge of one of the plates tangent to the longitudinal edge of the slab at a minimum distance of 10 ft from a transverse edge. Loads applied along one edge of each slab were sufficient to cause only bottom surface cracking. Along the opposite edge the loads were sufficient to cause top surface cracking. In this way the response of the test slabs to load was determined after a number of either bottom or top surface cracks had formed.

Bottom Surface Cracking

The magnitude of load causing bottom surface cracking was determined from strain and deflection data obtained during an initial load test on each slab. The initial load was applied at a longitudinal edge midway between slab ends. After application and release of the initial load, loads of the same maximum magnitude were applied both at the initial location and also at 6-in. intervals for a distance of 2 ft along the edge. Sufficient time elapsed between each load application to permit recovery of the slab and subgrade.

Loads were applied in 4-kip increments at the positions shown in Figure 4 with measurements made at each increment to determine compressive strain, tensile strain, and deflection at the load.

Initial Loadings.—The data obtained from the initial edge load tests on the three slabs are shown in Figures 5 through 7. The slabs were uncracked at the time of loading. Figure 5 shows the strains measured by the gage on the top surface and the gage on the vertical edge near the bottom surface of each slab. A linear strain distribution was assumed, and straight lines connecting these measured strains passed through zero strain near the mid-depth of the slabs before bottom surface cracking occurred. After cracking there were larger strain changes per unit load; the strains measured near the bottom surface increased more than the top surface strains, and the locations of zero strain occurred above the mid-depth of the slabs. The true bottom surface cracking loads were difficult to determine but were estimated at 18,000 lb for Slab 1 and 20,000 lb for Slabs 2 and 3. The additional longitudinal prestress resulted in an increase in the load causing bottom surface cracks that extended in a generally transverse direction inward from the edge.
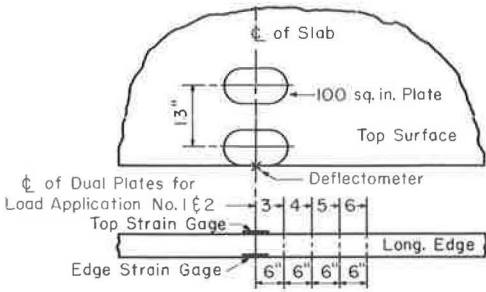
Figure 4.   Bottom cracking load positions and instrumentation.
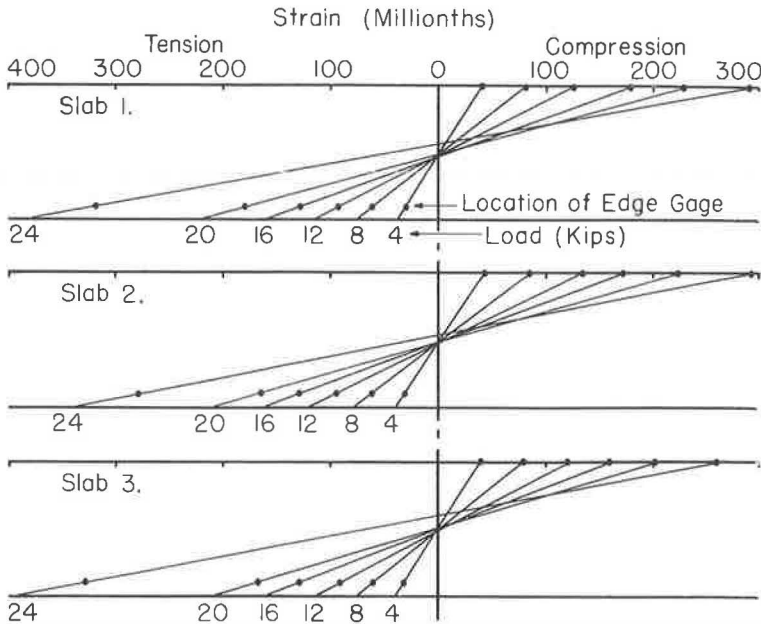
Figure 5.   Edge strain diagrams.

Top surface longitudinal edge stresses at the load were computed by multiplying the measured compressive strains by the concrete elastic modulus using a value of 5 million psi. These stresses are shown in Figure 6 with the corresponding edge deflections shown in Figure 7. These figures indicate that the compressive stress and deflection at the edge were nearly proportional to the applied load before bottom surface cracking occurred. Values computed by methods based on the elastic theory are also shown on these figures. For this purpose, influence charts (5) were used with a value of 140 pci for the subgrade modulus, 5 million psi for the concrete elastic modulus, and 0.15 for Poisson's ratio. The load test compressive stresses and deflections averaged 16 per-
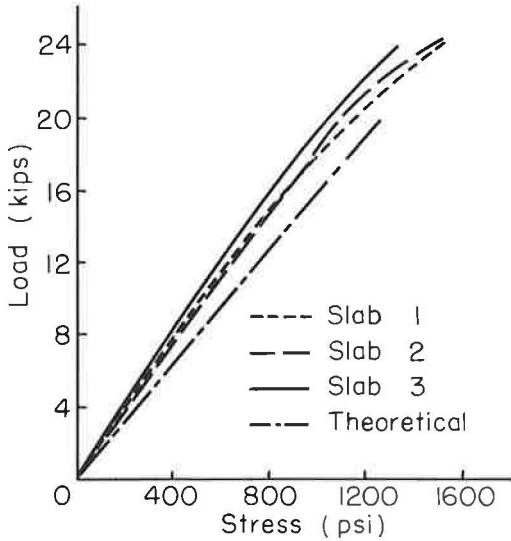
Figure 6. Top surface compressive edge stresses.
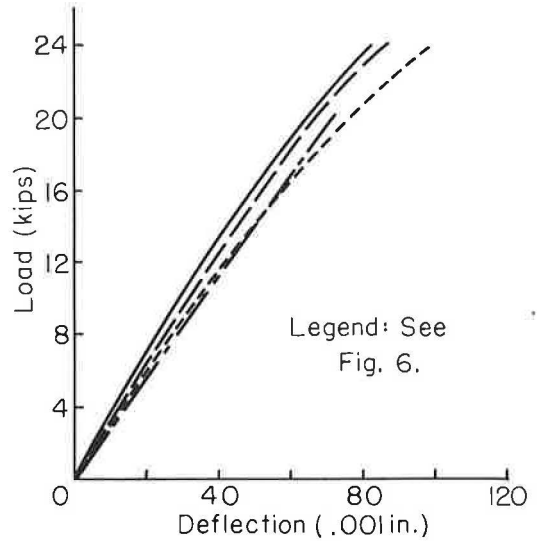
Figure 7. Edge deflections.
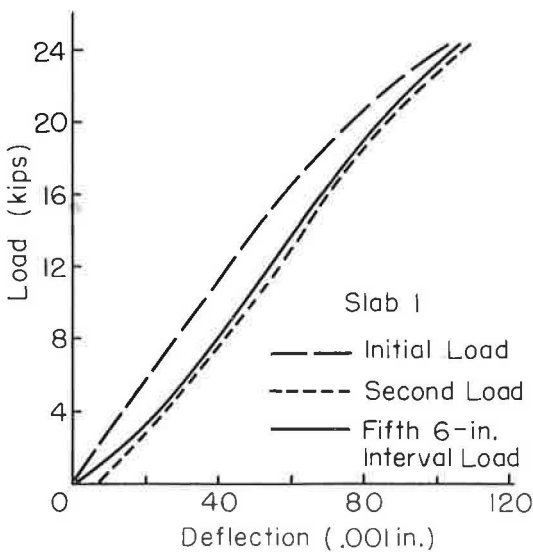
Figure 8. Edge deflections.
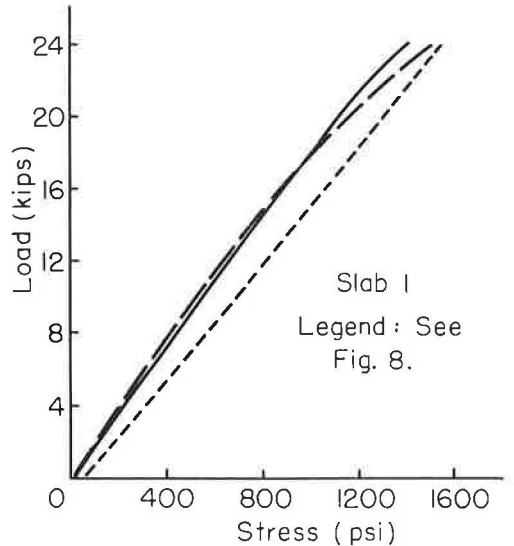
Figure 9. Top surface compressive edge stresses.

cent and 5 percent, respectively, less than the theoretical values before cracking occurred.

Second and Interval Loadings. —The maximum load initially applied on each of the three slabs was 24 kips. This load was also maximum for the second application of load at the initial location and for loads applied successively at 6-in. intervals along the edge of each cracked slab. The results from the second load application and the fifth 6-in. interval load application on Slab 1 are shown in Figures 8 and 9.

The data from the second load application on Slab 1 are representative of those obtained from tests on all three slabs after bottom cracking had occurred. Residual deflection was measured after each load was applied and released. Only residual edge deflection after the initial load was released is reported as shown by the no load deflection of the second load curve in Figure 8. Averaging the data for the three slabs, the residual deflections were 5 percent of the initial 24-kip load deflections. During the second load application on the three slabs, the ratios of deflection to load were nearly constant throughout the entire range from the residual values at no load to values at the 24-kip load that were about 5 percent greater than those resulting from the initial load applications. As shown in Figure 9, the ratio of compressive stress to load was also nearly constant throughout the entire range of the second application. The stresses in the three slabs at loads of 24 kips averaged 3 percent greater during the second load application than during the initial application.

The data from the load tests at 6-in. intervals showed variations due to small differences in the distance between bottom surface cracks. The results of the fifth 6-in. interval load application on Slab 1 as shown in Figures 8 and 9 are typical of most of the tests. As shown in Figure 8, the deflections for the interval and second load applications were similar. The deflections of the three slabs at 24 kips averaged 4 percent greater for the interval applications than for the initial applications.

Of special interest during the 6-in. interval applications were the loads causing the development of new bottom surface cracks as determined from the edge stresses. As shown by Figure 9, the top surface longitudinal edge stresses at the load location were similar during the initial and interval load applications. However, the strains measured on the vertical edge near the bottom surface were slightly smaller during the interval applications than during the initial applications. There was probably some stress relief due to the proximity of bottom cracking. As a result, the loads causing bottom surface cracking during the 6-in. interval applications were usually larger by as much as 10 percent than those determined during the initial applications.

Top Surface Cracking

The initial load for each series of top surface cracking studies was applied midway between the slab ends at the opposite side from that tested for bottom surface cracking. The load was increased until top surface cracking was observed. After application and release of the initial load, a second load of the same maximum magnitude was applied at the initial location. Loads of a slightly greater magnitude were then applied at 6-in. intervals along the edge for a distance of 2 ft and continued at intervals of 1 ft for 3 ft more. Sufficient time elapsed between each load application to permit recovery of the slab and subgrade.

Loads were applied in 4-kip increments at the positions shown in Figure 10. Measurements were made at each increment to determine the longitudinal and transverse concrete strain and deflection profiles and the maximum intensity of pressure on the subgrade. The location of the top surface crack was also determined if one occurred.

Initial Loadings. —To illustrate the type of strain data obtained during these load tests, the results of the initial top surface cracking edge load test on Slab 1 are shown in Figures 11 and 12. Figure 11 shows the distribution of longitudinal strains measured on the top surface of the slab along the edge. Figure 12 shows the distribution of transverse and longitudinal strains measured on the top surface of the slab along the transverse center line of the loaded area.

These measured strains were used in the computation of stresses by the following equations:
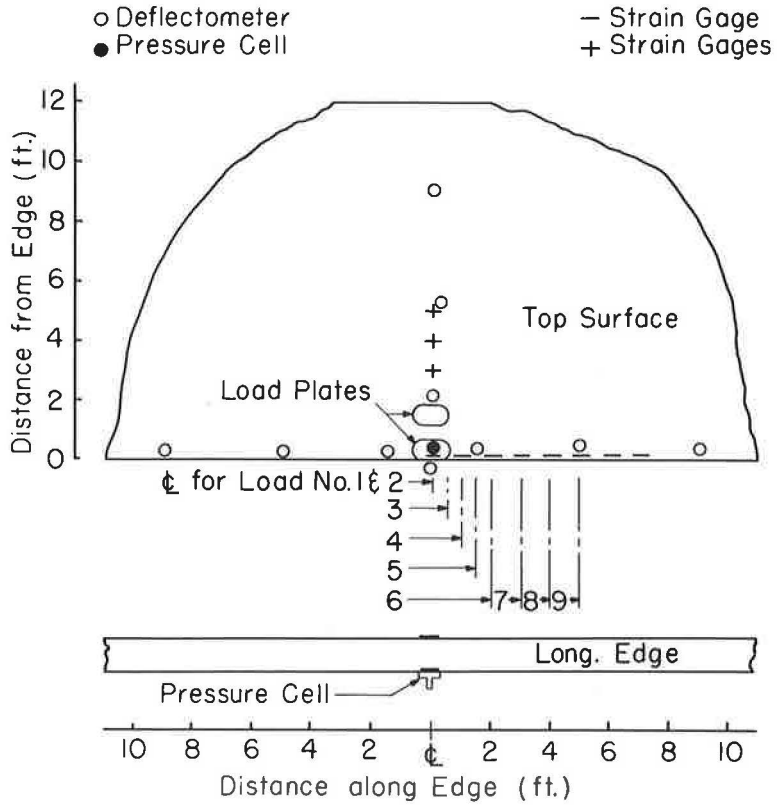
Figure 10. Top surface cracking load positions and instrumentation.
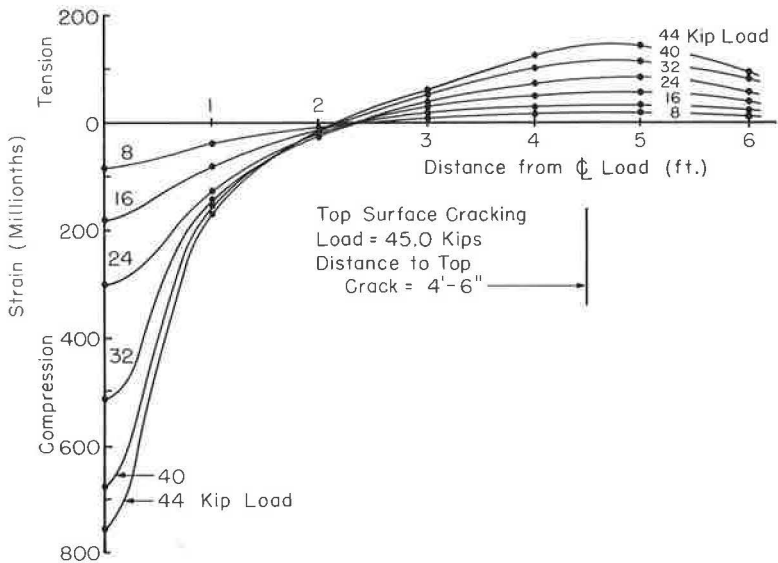
Figure 11. Distribution of top surface strains along edge of Slab 1.
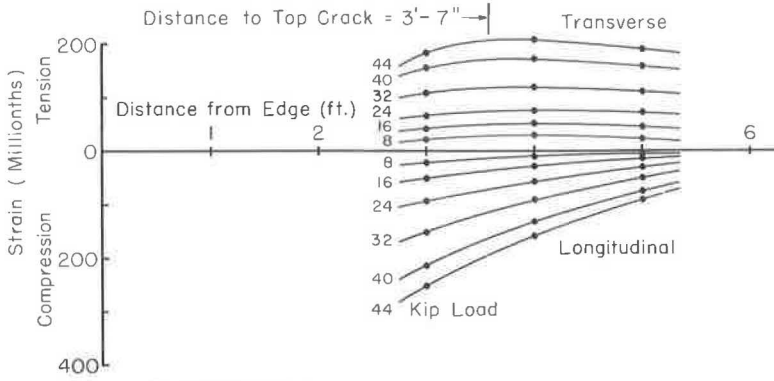
Figure 12. Distribution of top surface strains inward from edge of Slab 1.

$$\sigma_x = \frac{E}{1 - \mu^2} (e_x + \mu \ e_y) \tag{1}$$

$$\sigma_y = \frac{E}{1 - \mu^2} (e_y + \mu \ e_x) \tag{2}$$

in which

σ_x = longitudinal stress (psi),
σ_y = transverse stress (psi),
e_x = longitudinal strain (in./in.),
e_y = transverse strain (in./in.),
E = concrete elastic modulus (5,000,000 psi), and
μ = Poisson's ratio assumed as 0.15.

The maximum top surface tensile stresses in a longitudinal direction at the edge and in a transverse direction inward from the edge are shown in Figures 13 and 14, respec-
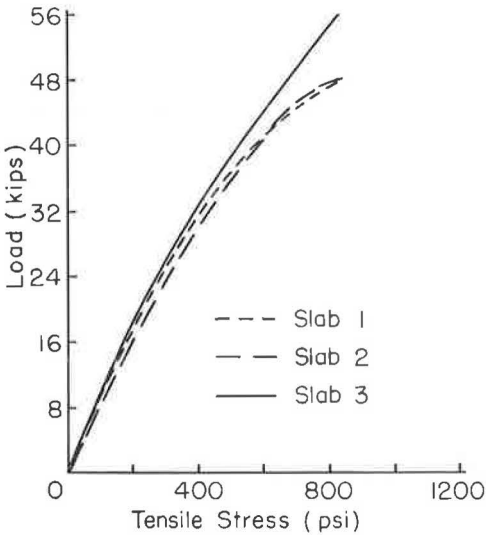
Figure 13. Maximum top longitudinal tension along edge.
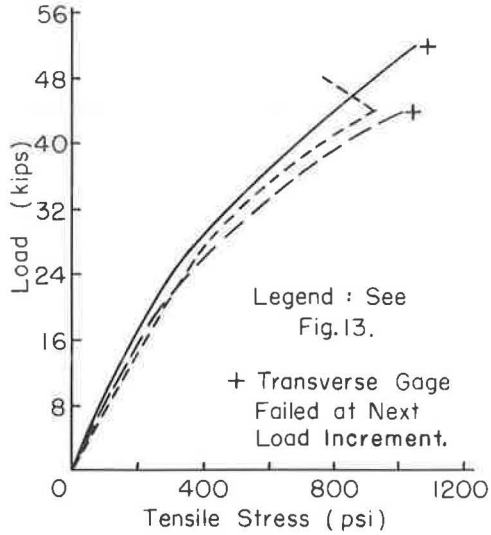
Figure 14. Maximum top transverse tension inward from edge.

tively. The maximum tensile stresses inward from the edge averaged 14 percent greater than those at the edge. When these tensile stresses were equal to the cracking stresses of the prestressed slabs, top surface cracking occurred.

From visual observations made during load testing, the top surface cracks appeared to form initially in the longitudinal direction at distances varying from 43 to 52 in. inward from the edge. With the top surface cracking load maintained, the crack progressed toward the edge of the slab. Top cracks occurred within 6 in. of the location of the maximum reading strain gage for load tests on all three slabs. The magnitude of load causing top surface cracking and the location of the cracks for the three test slabs are given in Table 4. The top cracking load was greatest for Slab 3 with both longitudinal and transverse prestress.

Top surface longitudinal compressive edge stresses and edge deflection at the transverse centerline of the loaded area are shown in Figures 15 and 16, respectively. When bottom surface cracking occurred, there was a slight increase in the rate of deflection change per unit load. When top surface cracking occurred, there was a relatively large increase in deflection at the load. Typical deflection profiles are shown in Figure 17 for increments of edge load on Slab 1. The distances from the load to the location of zero deflection were similar for all slabs and varied from about 8 to 10 ft.

The maximum subgrade pressures are shown in Figure 18. The slopes of these load pressure curves for the linear portions from 12 to 24 kips were used with load deflection ratios determined from Figure 16 for the same loading range to compute values of k. The computed values averaged 129 pci for the three slabs as compared with the value of 140 pci determined from plate bearing tests.

TABLE 4

TOP SURFACE CRACKING LOADS AND
LOCATIONS OF CRACKS

Slab No.	Top Surface Cracking Load (kips)	Distance to Top Surface Crack (in.)		
		A	B	C
1	45.0	52	54	43
2	45.0	80	94	52
3	54.0	66	58	46
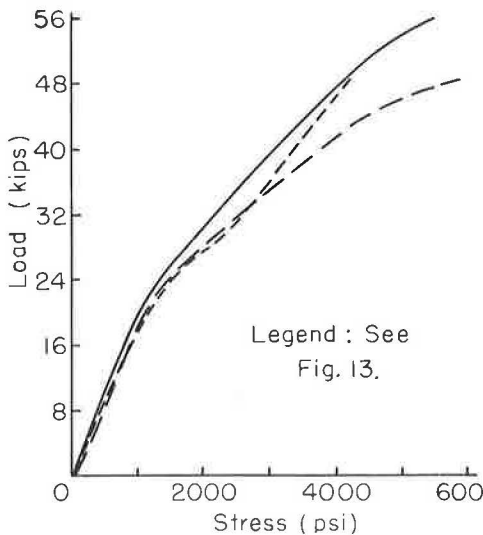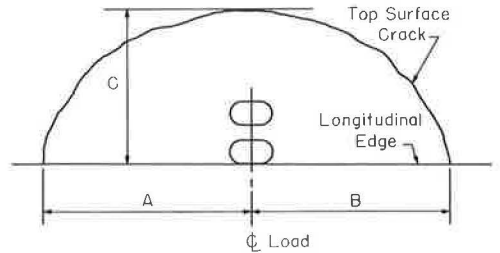
Figure 15. Top surface longitudinal compressive edge stress at load.
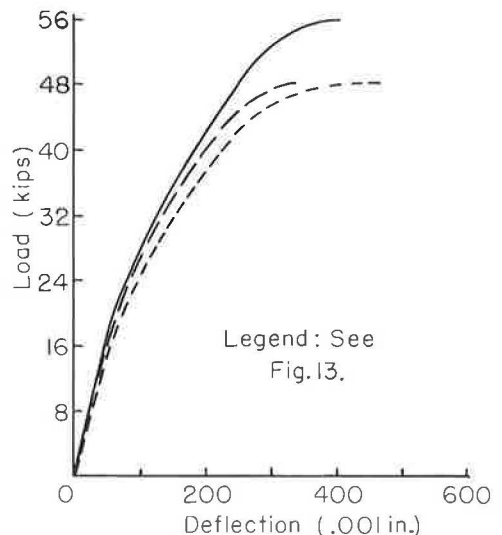
Figure 16. Edge deflections at load.
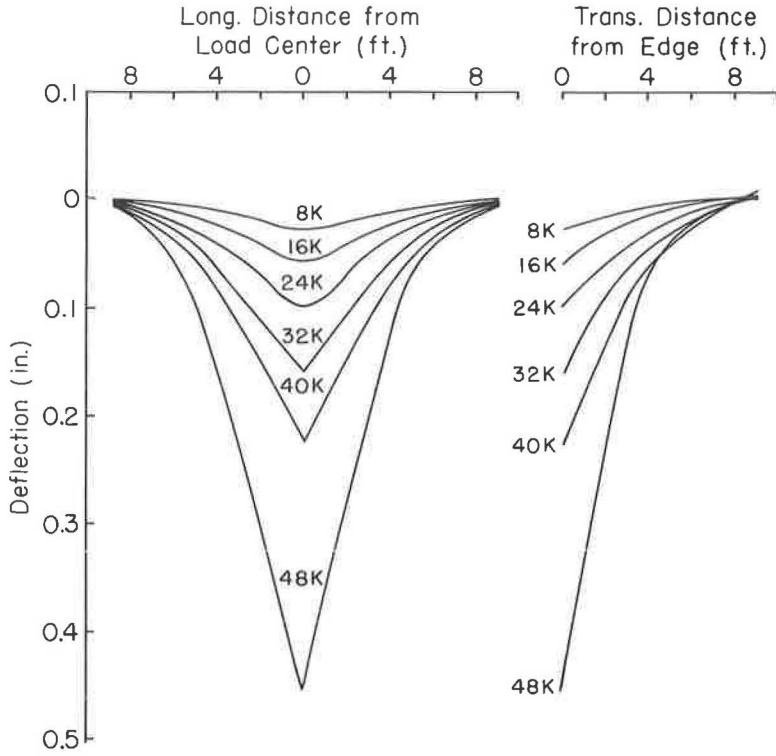
Figure 17. Typical deflection profiles, initial load, Slab 1.
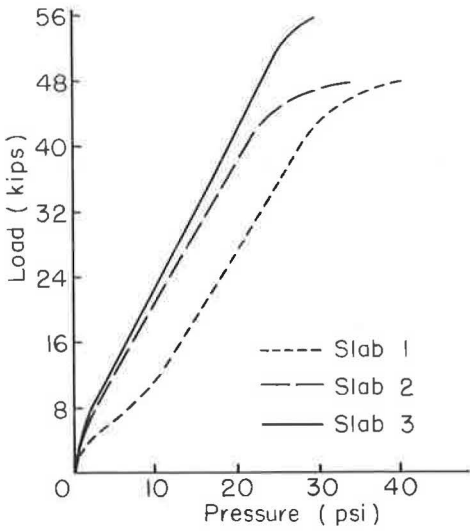
Figure 18. Maximum subgrade pressure at load.
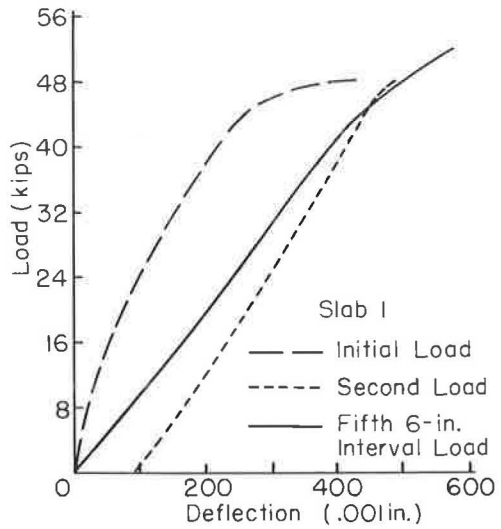
Figure 19. Edge deflection at load.

107
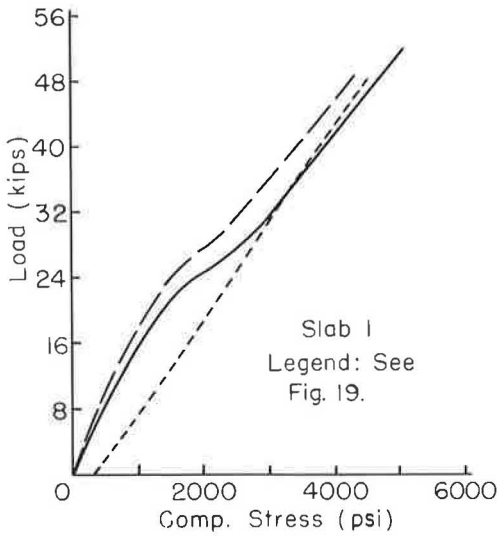
Figure 20. Top surface compressive edge
stress at load.
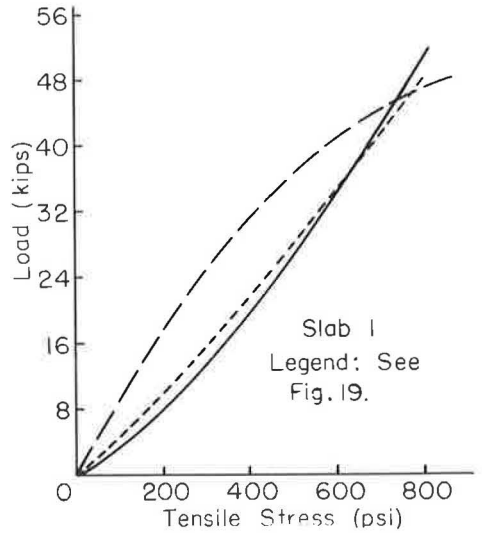
Figure 21. Maximum top surface longitudinal
tension along edge.
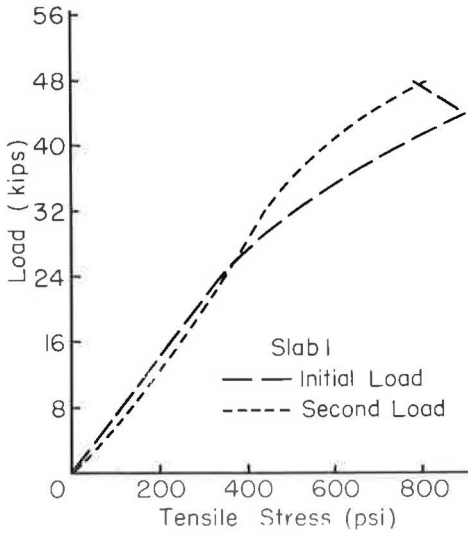
Figure 22. Maximum top surface transverse
tension inward from edge.
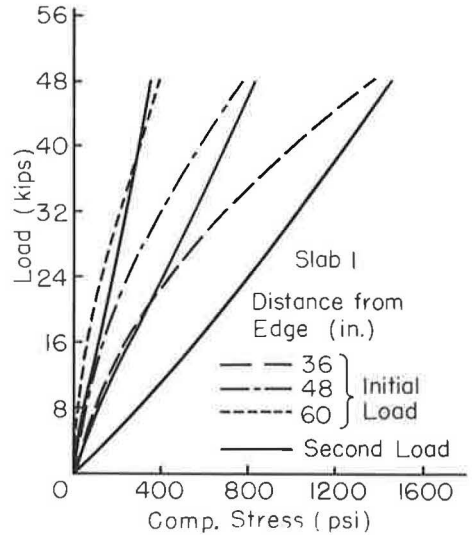
Figure 23. Top surface longitudinal com-
pressive stress inward from edge.

Second Loadings.—The maximum top surface cracking loads initially applied were 48, 48, and 56 kips for Slabs 1, 2, and 3, respectively. The same maximum loads were used for the second applications on the three slabs at the initial locations. The results from the second load application on Slab 1 as shown in Figures 19 to 23 were representative of those obtained from tests on all three slabs after top cracking had occurred.

After the initial load was removed some residual deflections remained in the slabs. The largest residual deflection occurred at the location of maximum deflection on the

108
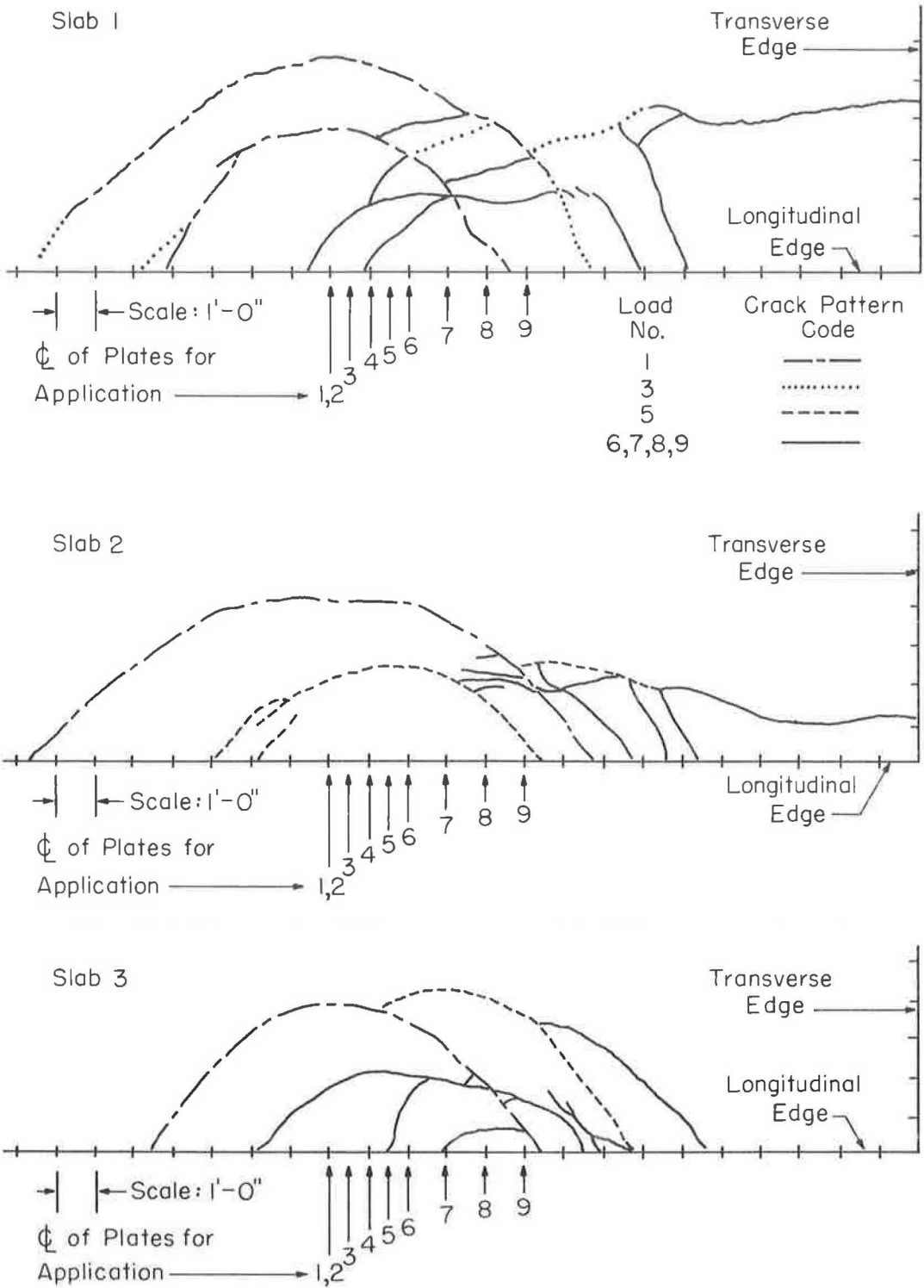
Figure 24. Top surface crack patterns for edge load tests.

slab edge adjacent to the load (Fig. 19). Averaging the data for the three slabs, the maximum residual deflections were 19 percent of the initial top cracking load deflections. Deflection profiles for second load applications showed an increase in the longitudinal distance and a decrease in the transverse distance from the load to the location of zero deflection compared to initial load applications.

During the second load applications, it was observed that the ratios of deflections and maximum stresses to load were rather constant throughout the entire range (Figs. 19-23). These ratios for the second load applications were generally slightly larger than those observed before bottom surface cracking during the initial applications. A comparison of stresses and deflections at the maximum load of the two applications indicated that variations were related to gage locations. Adjacent to the load, deflections and top surface longitudinal stresses averaged 14 and 8 percent, respectively, greater for the second applications than for the initial applications on the three slabs. Inward from the edge, the maximum top surface transverse tensile stresses were somewhat less for the second load applications due to the proximity of top cracking to the measuring gages. Stresses determined at other locations averaged the same at the maximum load for the two applications. Subgrade pressures are not reported for the second load applications because the pressure cells were inoperative after the high loads of the initial applications.

Interval Loadings. — The maximum loads applied at 6- and 12-in. intervals along the edge were 4 kips greater than those initially applied to insure a number of top surface cracks. They were equal to 52, 52, and 60 kips for Slabs 1, 2, and 3, respectively. Data from these tests showed variations due to differences in the distance between cracks. Results of the fifth 6-in. interval load application on Slab 1 (Figs. 19-21) are typical of most of the tests.

The loads causing the development of new bottom surface cracks (as determined from the edge stresses) were of interest during the top cracking interval applications. Before the formation of a new bottom surface crack, the maximum bending of the slab occurred at the previous bottom surface crack. However, as shown in Figure 20, the top compressive edge stresses at the load where the new crack developed were greater for the 6-in. interval load tests than for the initial load tests. This stress increase was probably due to the permanent subgrade deformation that developed during previous loadings and the loss of slab support. As a result, the loads causing bottom surface cracking during the 6-in. interval applications were usually smaller, by as much as 13 percent, than those determined during the initial applications.

The slabs were not instrumented to measure strains inward from the edge during the interval load applications. The maximum top surface tensile stresses along the edge during the interval load applications (Fig. 21) were similar to those determined from the second load applications. The load magnitudes causing new top surface cracking were the same for both the interval and initial load tests. A new top surface crack usually progressed from a former crack to the edge of the slab (Fig. 24). The top cracks remained visible after the loads were removed, and in a few cases after a number of loads had been applied along an edge the top cracks became enlarged.

As shown by the example in Figure 19, the ratios of maximum deflection to load were nearly constant throughout the entire range of interval applications. The maximum deflections at the top surface cracking loads of the three slabs averaged 17 percent greater during the interval applications than during the initial load applications. Deflection profiles for 6-in. interval applications showed that deflections along the slab edge were greater toward the locations of previous load applications. This illustrated the influence of permanent subgrade deformation developed during previous loadings.

INTERIOR LOAD TESTS

Static loads were also applied at an interior location of each slab. The dual loading plates were positioned midway between the longitudinal slab edges at a minimum distance of 8 ft from a transverse edge. The load was increased in 4-kip increments until either top surface cracks appeared or the loading equipment's safe limit was reached. At each increment measurements were made to determine the longitudinal and trans-
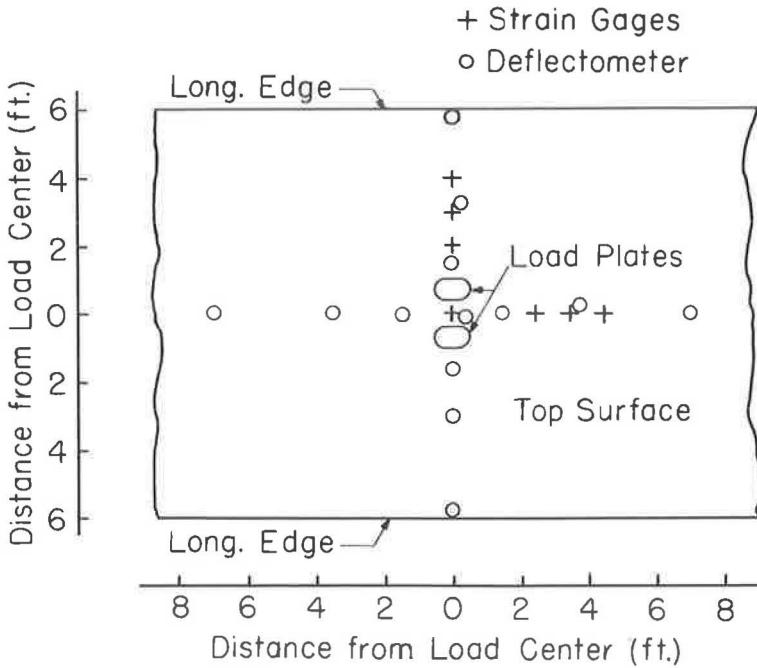
Figure 25.   Interior load instrumentation plan.

verse concrete strain and deflection profiles with the instrumentation shown in Figure 25.   The location of the top surface crack was also determined if one occurred.

Stresses at interior locations were computed by Eqs. 1 and 2 using the measured longitudinal and transverse strains.   Top surface longitudinal and transverse compressive stresses midway between the dual loading plates are shown in Figures 26 and 27, respectively.   These stresses were nearly proportional to the applied load before bottom surface cracking occurred and the transverse stress averaged 79 percent of the longitudinal stress.   A comparison was made between the load test stresses prior to cracking and the values obtained using influence charts (5).   For these computations, 140 pci was used for the subgrade modulus, 5 million psi for the concrete elastic modulus, and 0. 15 for Poisson's ratio.   The load test stresses averaged 16 percent less than the theoretical values before cracking occurred.

The magnitude of load causing bottom surface cracking was estimated from the stress diagrams shown in Figures 26 and 27.   Assuming that bottom surface cracking occurred when either the top surface longitudinal or transverse compressive load stress was equal to the summation of the concrete modulus of rupture and the amount of longitudinal or transverse prestress, it was computed that the interior bottom surface cracking loads were 28. 0, 26. 0, and 31. 2 kips for Slabs 1, 2, and 3, respectively.   After cracking, the stress changes per unit load increased especially in the longitudinal direction.

Top surface cracks were visible in Slabs 1 and 2 (no transverse prestress) when interior load magnitudes were 72 and 68 kips, respectively.   For each of these slabs, a longitudinal crack began between the dual loading plates and progressed to the nearest transverse edge.   This was a full depth crack that probably originated as a bottom surface radial crack.   It was not caused by large radial top surface tensile stresses.

No top surface cracking was observed in Slab 3 (longitudinal and transverse prestress) when a load of 100 kips was applied twice at the same interior location.   A greater load could not be applied as this was the safe limit of the reaction beam and soil anchor system.   As shown in Figure 28, the maximum top surface radial tensile stresses in the longitudinal direction were greater than in the transverse direction,
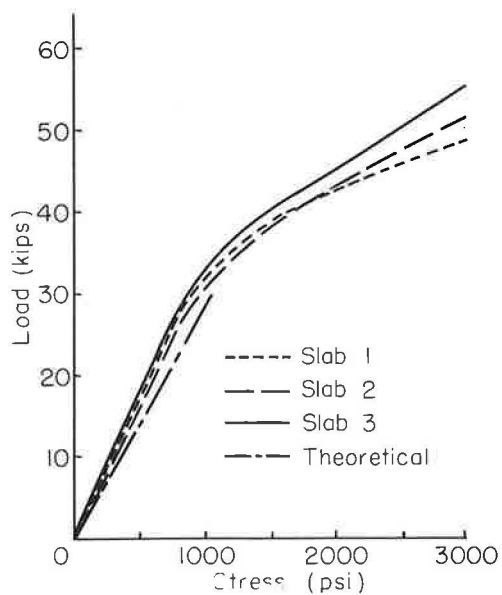
Figure 26. Top surface longitudinal compressive stress at load.
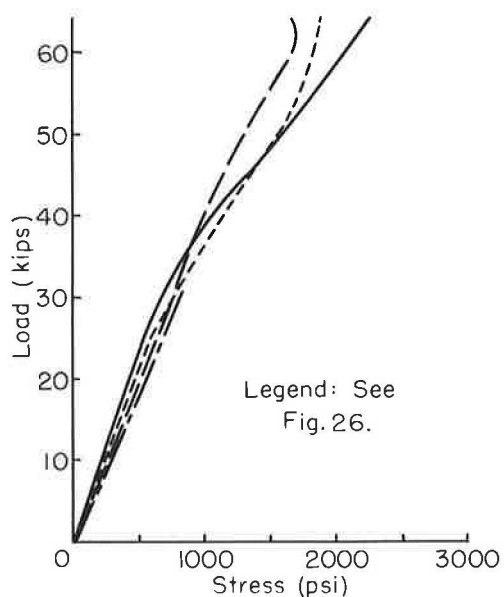
Figure 27. Top surface transverse compressive stress at load.
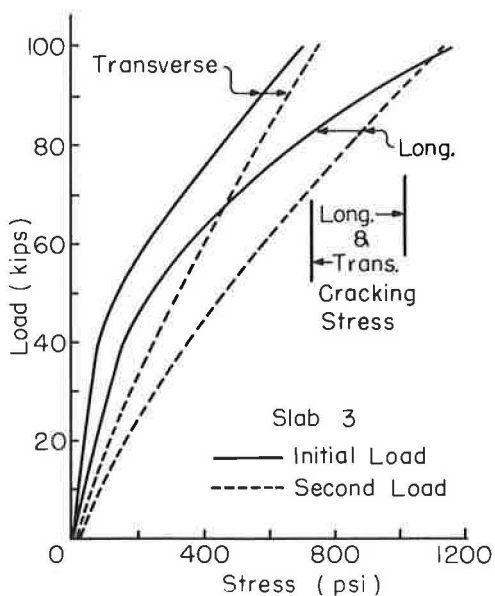
Figure 28. Maximum top surface radial tensile stress.
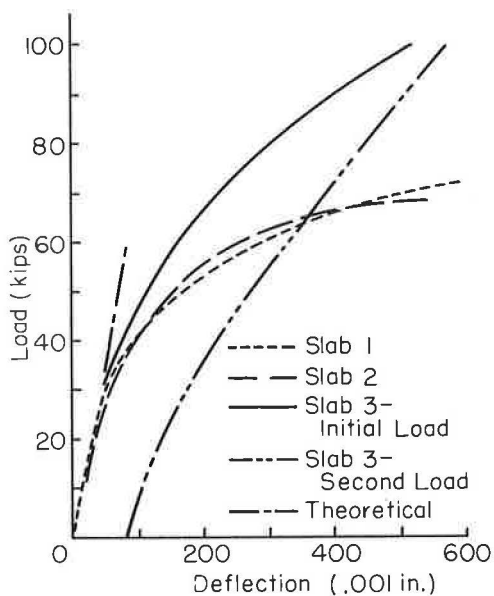
Figure 29. Interior deflection at load.
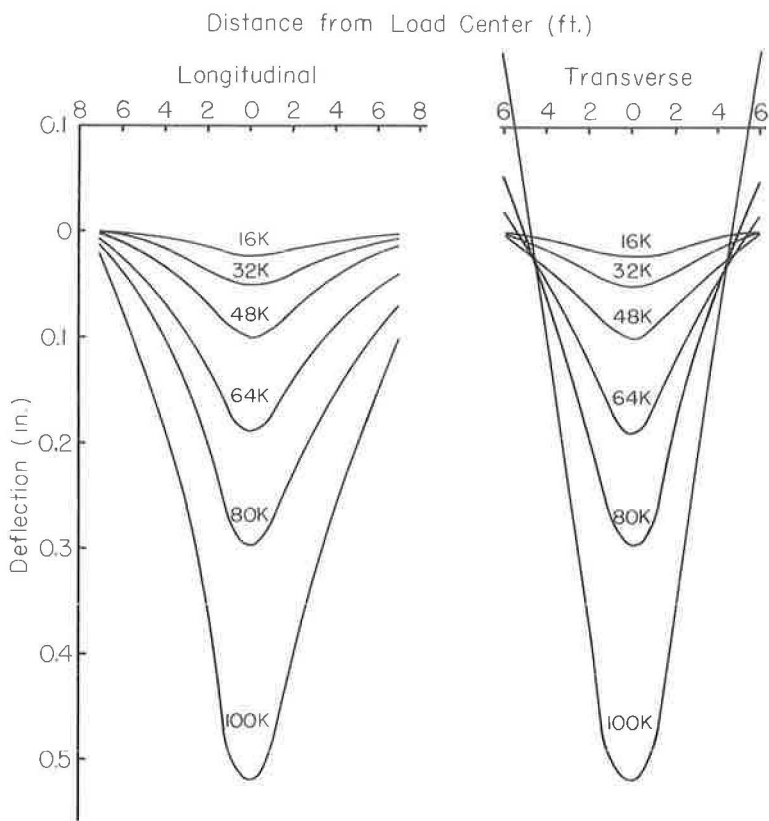
Figure 30. Deflection profiles, interior load, Slab 3.

indicating some influence from the proximity of the longitudinal slab edges. The ratios of the maximum radial tensile stresses to the applied load increased when bottom cracking occurred during the initial application but were nearly constant throughout the entire range during the second application. At a load of 100 kips, the stresses were very nearly the same for the second application as for the initial application. Assuming the cracking stress to be the summation of the concrete modulus of rupture and the amount of longitudinal or transverse prestress, it was computed from Figure 28 that top surface cracking should occur at a load near 100 kips.

The interior deflections at the load are shown in Figure 29. Prior to cracking, the measured deflections averaged 6 percent greater than the theoretical values determined from influence charts (5). After bottom surface cracking there was a progressive increase in the rate of deflection change per unit load especially for tests on Slabs 1 and 2 (no transverse prestress). After the initial load on Slab 3 was released there was a residual deflection of 0.080 in. or 15 percent of the initial 100-kip value. During the second application, the deflection to load ratio was more nearly constant throughout the entire range, and there was a 10 percent increase in the second 100-kip load deflection.

The proximity of the longitudinal slab edges influenced the load deflection profiles as shown by the typical example in Figure 30 for Slab 3 interior load increments. The longitudinal edges deflected upward at higher load magnitudes. The distances from the load to the location of zero deflection varied from about 7 to 9 ft in the longitudinal direction and from about 5 to 6 ft in the transverse direction. Obviously, the slabs were not behaving as though they were of infinite extent. No comparison was made between measured and theoretical stresses and deflections due to interior load magnitudes greater than those causing bottom cracking because the theoretical methods for determining these values assume infinite extent.

SUMMARY

The following observations apply to edge load tests:

1. The top surface longitudinal compressive edge stress at the load, the maximum top surface longitudinal tensile stress at the edge, the maximum top surface transverse tensile stress inward from the edge, and the edge deflection at the load were nearly proportional to the applied load before bottom surface cracking occurred. After cracking there were slight increases in the rate of change of these stresses and deflections per unit load.

2. Prior to bottom cracking, the edge deflection and the top surface longitudinal compressive edge stress at the load were slightly less than values determined by methods based on the elastic theory.

3. Bottom surface cracking originated at the slab edges adjacent to the load when the bottom surface tensile stress was equal to the cracking stress.

4. During load application, the maximum top surface transverse tensile stress inward from the edge was greater than the maximum top surface longitudinal tensile stress at the edge. Top surface cracking occurred when these tensile stresses were equal to the cracking stress. The top surface cracks formed initially in the longitudinal direction and progressed toward the longitudinal edge of the slab while the top cracking load was maintained.

5. When top surface cracking occurred, there was a relatively large increase in edge deflection at the load.

6. The distances from the load to the location of zero deflection varied from about 8 to 10 ft during initial applications on the uncracked slabs.

7. The ratio of the measured subgrade pressure to the slab deflection was nearly equal to the subgrade modulus determined from plate bearing tests.

8. After application and release of 24-kip loads (slightly greater than those causing bottom surface cracking in the three test slabs) the maximum residual deflections averaged 0.005 in. or 5 percent of the maximum 24-kip load deflections. After application and release of loads causing top surface cracking in the three test slabs, the maximum residual deflections averaged 0.073 in. or 19 percent of the maximum top cracking load deflections.

9. When a second load was applied after the occurrence of bottom surface cracking, the top surface longitudinal compressive edge stress at the load, the maximum top surface longitudinal tensile stress at the edge, the maximum top surface transverse tensile stress inward from the edge, and the edge deflection at the load were nearly proportional to the applied load when the magnitude was less than or equal to the maximum initially applied value. These quantities were slightly greater for equal loads than those observed before bottom surface cracking during the initial applications.

10. When loads having magnitudes sufficient to cause bottom surface cracking were applied at 6-in. intervals along the edge, the maximum bending of the slab occurred at the previous bottom surface crack until the formation of a new bottom surface crack. The loads causing bottom surface cracking during the 24-kip 6-in. interval applications were usually greater by as much as 10 percent than those that caused initial cracking. The loads causing bottom surface cracking during the 52- and 60-kip, 6-in. interval applications were usually smaller, by as much as 13 percent, than those that caused the initial cracking. There was little change in the loads causing top surface cracking during the 6-in. interval top cracking applications.

The following observations apply to interior load tests:

1. The top surface longitudinal and transverse compressive stresses midway between the dual loading plates, the maximum top surface radial tensile stresses in both a longitudinal and transverse direction from the load, and the interior deflection at the load were nearly proportional to the applied load before bottom surface cracking occurred. The ratio of transverse compressive stress to longitudinal compressive stress at the load averaged 79 percent before cracking. After cracking, there were increases in the rate of change of these stresses and deflections per unit load.

2. Prior to bottom cracking, the interior deflection at the load was slightly greater and the top surface longitudinal and transverse compressive stresses at the load were less than the values determined by methods based on the elastic theory.

3. Bottom surface cracking originated at the load when the bottom surface tensile stress was equal to the cracking stress.

4. A full depth longitudinal crack developed between the dual loading plates and progressed to the nearest transverse slab edge when an interior load averaging 2.59 times the bottom cracking load was applied to the two test slabs with only longitudinal prestress. No top surface cracks were observed in the slab with both longitudinal and transverse prestress at an interior load of 3.20 times the bottom cracking load. The maximum top surface radial tensile stresses in the longitudinal direction from the load were greater than in the transverse direction. This lack of symmetry resulted primarily from the proximity of the longitudinal slab edges.

5. Longitudinal and transverse deflection profiles also indicated that the 12-ft wide slabs did not behave similarly to one of infinite surface area when loaded at interior locations.

6. After the application and release of a load equal to 100 kips or 3.20 times the bottom cracking load on the slab with both longitudinal and transverse prestress, the maximum residual deflection was equal to 0.080 in. or 15 percent of the maximum 100-kip load deflection. When the load was applied for the second time at the same location, the top surface longitudinal and transverse compressive stresses midway between the dual loading plates, the maximum top surface radial tensile stresses in both a longitudinal and transverse direction from the load, and the interior deflection at the load were nearly proportional to the applied load for the entire 100-kip range. These quantities were greater for equal loads than those determined before bottom surface cracking during the initial application.

INTERPRETATION OF RESULTS

The three test slabs reacted similarly during initial load applications. An increase in the amount of longitudinal prestress resulted in an increase in the load causing bottom surface cracking during edge applications. The use of both longitudinal and transverse prestress resulted in an increase of the load causing bottom surface cracking during interior applications and the load causing top surface cracking during edge applications on the two slabs with only longitudinal prestress; whereas, no top cracking was observed in the slab with both longitudinal and transverse prestress when the interior load was equal to the highest magnitude obtainable with the loading equipment.

Bottom surface cracks did not develop into full depth cracks during any edge load test at intervals of 6 in. along the longitudinal edges of all three slabs or during the interior load test of the slab with both longitudinal and transverse prestress. Bottom surface cracking had no apparent detrimental effect on the ability of the three slabs (including the two with only longitudinal prestress) to support the edge loads applied in the test program. Bottom surface cracking also had no apparent detrimental effect on the ability of the test slab with both longitudinal and transverse prestress to support an interior load.

When top surface cracking occurred during an edge load application, there was a large increase in slab deflection at the load. The top cracks remained visible after the loads were removed, and after a number of loads had been applied along an edge there was a general deterioration of the pavement and subgrade. There was also a large increase in slab deflection at the load when a full depth longitudinal crack occurred during interior load application on each of the two slabs with only longitudinal prestress. This crack, which probably originated as a bottom surface radial crack, was visible in the top surface at a load much greater than that causing bottom surface cracking during the single static load application. It seems likely that this full depth crack might occur at a load close to that causing bottom surface cracking during repeated moving load applications. Therefore, until additional information is obtained on the effect of traffic conditions, load applied at interior locations of a concrete highway or airfield pavement prestressed only in the longitudinal direction might be limited to that causing bottom surface cracking.

The results of the load test program therefore suggest that the criterion for failure of a prestressed pavement is occurrence of a top surface crack. Bottom surface cracking may be allowed if prestress is applied properly to prevent the bottom cracks from developing into full depth cracks. With this criterion for failure, a prestressed concrete pavement can support a substantially greater load than a conventional concrete pavement of the same thickness. Part of this additional load capacity is due to the increase in allowable stress causing pavement cracking by the amount of prestress applied to the pavement in a direction perpendicular to the cracking. Most of the additional load capacity is a result of the allowance of loads greater than those causing bottom surface cracking. Therefore, the load-carrying advantage obtained by prestressing a concrete pavement is due principally to a change in the criterion for failure from a bottom surface crack to a top surface crack. This justified change in failure criterion has more significance than the amount of prestress that is applied.

In the design of a prestressed concrete pavement it is necessary to determine whether prestress should be applied in more than one direction. To fully utilize the load-carrying advantage obtained by prestressing, the prestress should be applied in directions that make it possible to allow bottom surface cracking. The results of the static load test program suggest that to allow the application of bottom surface cracking loads, two-directional prestress is necessary for interior load applications but longitudinal, prestress is sufficient for edge load applications. Another advantage obtained by prestressing a concrete pavement is the elimination of weakened plane type transverse contraction joints. This is accomplished by applying sufficient prestress to overcome pavement tensile stresses that result from subgrade friction, warping, curling, and a nonlinear temperature or moisture differential throughout the depth of a pavement. Both concrete airport and highway pavements will require longitudinal prestress to reduce the number of transverse joints. Airport pavements may require transverse prestress to allow the application of interior loads greater than those causing bottom surface cracking.

While both longitudinal and transverse prestress may be required for airport pavements, it may be possible and also desirable for reasons of economy to construct a prestressed concrete highway pavement with only longitudinal prestress. Transverse prestress may not be needed to obtain a joint-free pavement or to allow the application of loads greater than those causing bottom surface cracking at edge locations. The maximum load on a concrete highway pavement prestressed only in the longitudinal direction is probably limited to that causing bottom surface cracking when applied at interior locations. If two-directional prestress is used, the maximum load is probably limited to that causing top surface cracking when applied at edge locations. Therefore, the use of transverse as well as longitudinal prestress results in a further increase in load-carrying capacity. This factor should be considered in deciding whether transverse prestress is worthwhile in a concrete highway pavement.

It should be emphasized that only half-axle conditions were represented in the test program. No attempt was made to combine stresses and deflections for full axle conditions. Only static load tests were conducted, and the conclusions may be subject to some modification when the effects of repeated traffic loads are considered especially in the determination of the failure criterion.

REFERENCES

1. Carlton, P. F., and Behrmann, R. M., "Model Studies of Prestressed Rigid Pavements for Airfields." HRB Bull. 179, pp. 32-50 (1958).
2. Moreell, B., Murray, J. J., and Heinzerling, J. E., "Experimental Prestressed Concrete Highway Project in Pittsburgh." HRB Proc. 37:150-193 (1958).
3. Hanson, N. W., "Load Cells for Structural Testing." Jour. of PCA Res. and Dev. Labs., PCA Dev. Dept. Bull. D33 (Jan. 1959).
4. Carlson, R. W., and Pirtz, D. G., "Development of a Device for the Direct Measurement of Compressive Stress." ACI Proc. (Nov. 1952).
5. Pickett, G., Raville, M. E., Janes, W. C., and McCormick, F. J., "Deflections, Moments and Reactive Pressures for Concrete Pavements." Bull. 65 and Supplement, Kansas State College Experimental Station (Oct. 1951).

Tests of Reinforcement Splices for Continuously-Reinforced Concrete Pavement

HENRY A. LEPPER, JR., and JAI B. KIM
University of Maryland, College Park

Lap splices in reinforcement for continuously-reinforced concrete pavements were tested under longitudinally-applied static axial tensile loading to failure. Twenty-eight specimens, 8 in. thick, 13 in. wide, by 20 ft long were reinforced with two hardgrade No. 5 deformed bars (average yield strength 64,000 psi) and twenty-four specimens of similar size were reinforced with a strip of welded-wire fabric having 5/0 longitudinal wires (average yield strength 81,000 psi).

Observations were made for openings of the preformed crack under load, together with the occurrence and opening of additional cracks and the mode of failure. Results were evaluated in terms of several criteria that are significant to the function of reinforcement in continuously-reinforced pavement.

●THE LONGITUDINAL reinforcement in continuously-reinforced concrete pavement consists of many lengths of either high-strength deformed bars or welded-wire fabric. Continuity of reinforcement in the longitudinal direction is provided by overlapping the ends of the steel to form a splice. The lapped splice transfers force from one bar to another through the surrounding concrete by bond and, in the case of welded-wire fabric, by bond and the anchorage offered by the transverse wires.

Laboratory experiments were made to evaluate the load-deformation characteristics of lap splices in deformed-bar and in welded-wire fabric reinforcement. Although laboratory tests cannot duplicate all conditions encountered in the field, such tests yield valuable information indicating the optimum splice length required to maintain reinforcement continuity. Static load tests to fracture, made at early concrete ages, constitute the most severe strength test of the splices and were chosen to cover the most critical conditions that might occur in the field.

The basic requirement for reinforcement in continuously-reinforced concrete pavement is to hold tightly closed all transverse cracks that may form. When cracks are prevented from opening more than 0.01 or 0.02 in., the subgrade is protected and spalling or deterioration at such cracks does not occur. When reinforcement is adequate to cause additional transverse cracks to form without allowing existing ones to open excessively, stresses will be relieved and a stable condition is reached. If reinforcement is overstrained at a crack so that yielding occurs, the crack may open enough to deteriorate. Obviously, if the reinforcement fails in tension or a splice opens all continuity is lost.

The splice must be capable of performing as well as the unspliced reinforcement. Three criteria for judging the adequacy of a splice are used in this investigation:

1. Is the lap length sufficient to produce other cracks away from the splice at all ages of concrete?

2. Is the lap sufficient to develop the yield strength of the reinforcement?

3. Is the splice strong enough to develop the ultimate strength of the reinforcement, or short of this, to cause other cracks to open to 0.1 in. or more?

It is recognized that the third criterion represents a condition that does not occur in pavements in actual service. However, it does serve to compare the strength of splices with the strength of unspliced reinforcement under the conditions of these tests.
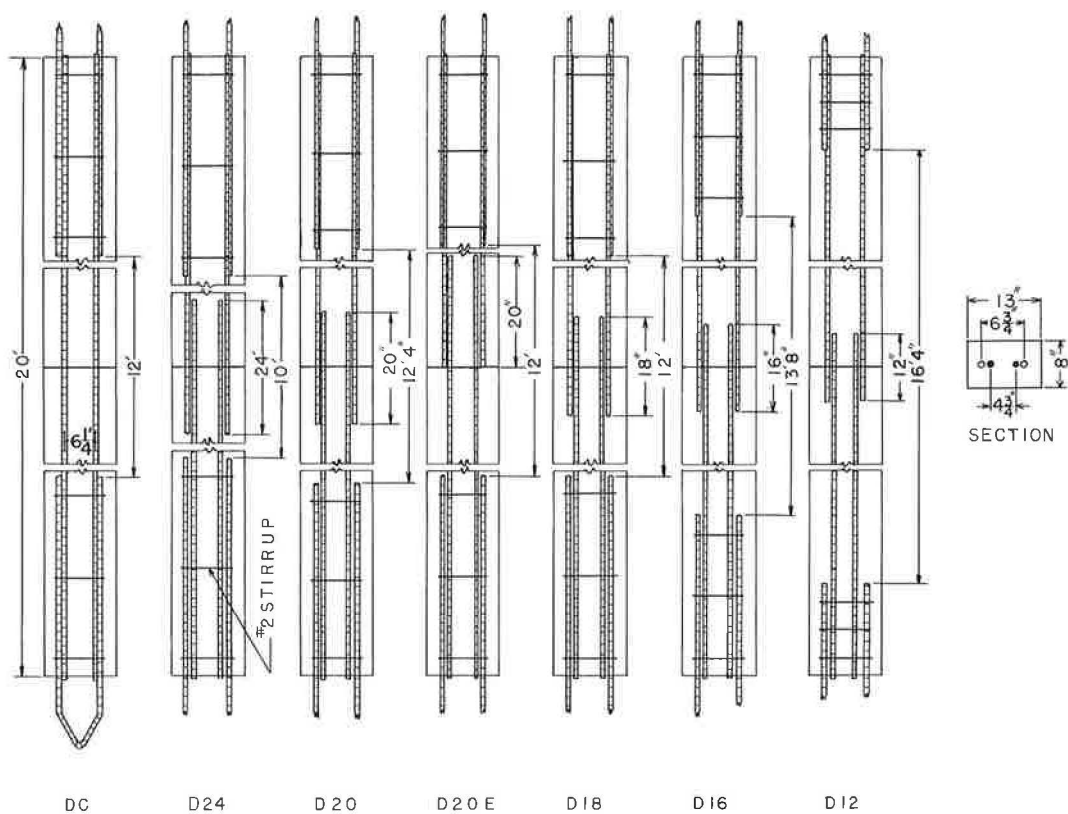
Figure 1. Deformed-bar specimens, series D.

PROGRAM OF TESTS AND TEST SPECIMENS

Two series of tests were made: (a) 28 specimens were reinforced with high-strength deformed bars, and (b) 24 specimens with welded-wire fabric. Six splice arrangements were tested and compared with an unspliced control in the deformed-bar series; five splices and an unspliced control were tested in the welded-wire fabric series. Four identical specimens for each splice arrangement were cast from one concrete batch for test at 1-, 3-, 7-, and 14-day ages. A single class of concrete was used. The test specimens were 8 in. deep by 20 ft long, with 0.6 percent steel reinforcement located at mid-depth. The specimens were designed to represent a length of pavement containing a transverse crack at the lap splice. The crack was formed by inserting a sheet metal separator at the splice to prevent load transmission through the concrete at this point.

Details of the specimens reinforced with deformed bars, series D, are shown in Figure 1. Specimen width was 13 in. to accommodate two No. 5 bars (0.57 percent steel). Unspliced control specimens, DC, had a 12-ft test length between ends of yokes, with separator at midlength. Splice lengths of 24, 20, 18, 16, and 12 in., with separator at midlength of splice, were tested in specimens D24, D20, D18, D16, and D12, respectively. Specimen D20E had a 20-in. splice with separator at the end of the splice. Reinforcement was placed symmetrically in plan to avoid eccentricity of load. Test lengths between the yokes varied from 10 ft to 16 ft 4 in. The shorter yoke embedments were sufficient for the lower loads resisted by the shorter splices. No transverse reinforcement was used within the test length. Stirrups were used around the yokes to prevent failure in the yoke regions.

The welded-wire fabric reinforcement, series WWF, consisted of four 5/0 gage longitudinal wires on 3-in. centers welded to No. 1 gage transverse wires on 12-in. centers. The longitudinal wires extended 6 in. beyond the last transverse wire. Specimens of this series
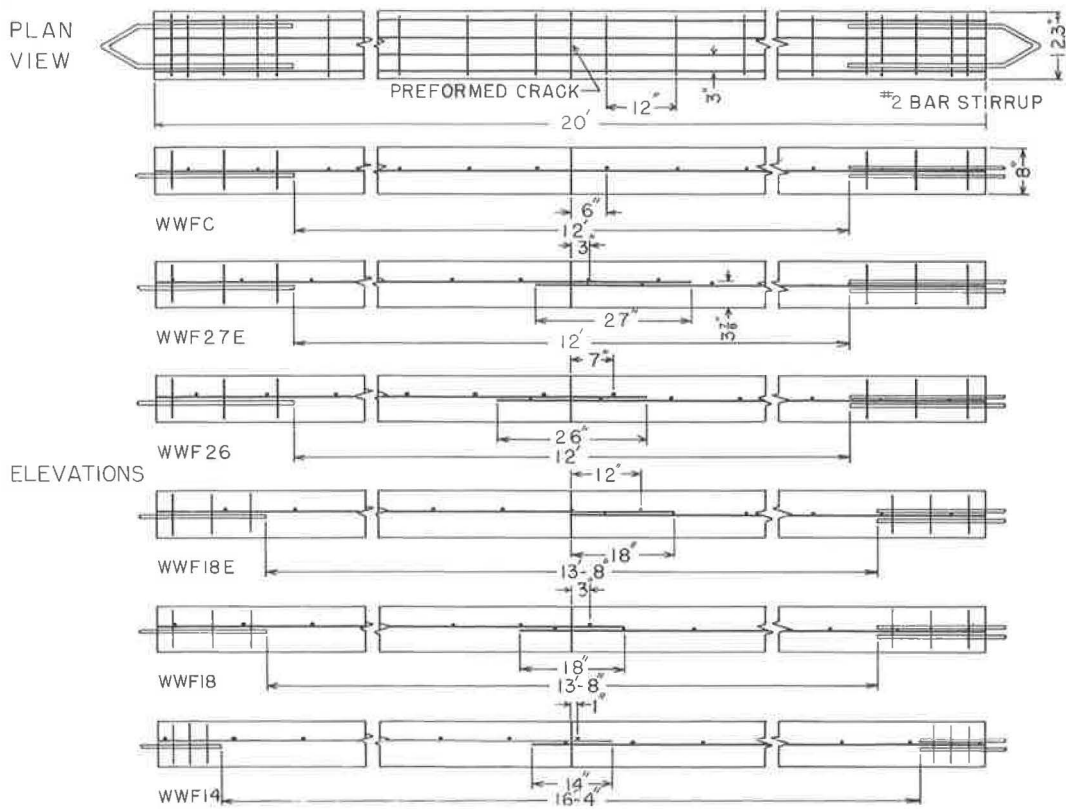
Figure 2. Welded-wire fabric specimens, series WWF.

were 12.3 in. wide (0.60 percent steel) with transverse wires cut to the full width.

Unspliced control specimens, WWFC, were reinforced with a single length of fabric at mid-depth, Figure 2. The separator for the preformed crack was located at mid-length, and was midway between transverse wires. Specimen WWF27E was made with a 27-in. splice, with the preformed crack located at the end transverse wire of one length of reinforcement. The overlapped reinforcement length was thus anchored by two transverse wires beyond the preformed crack, the second wire from the end of the fabric being 3 in. from the crack. WWF26 had the end transverse wires of each fabric length 7 in. beyond the preformed crack. In WWF18E, the end transverse wires lap 6 in., with the preformed crack at the second transverse wire of one fabric length and at the end of the other fabric length. WWF18 and WWF14 had 6-in. and 2-in. laps between end transverse wires, respectively, and corresponding embedments of 3 in. and 1 in. beyond the preformed crack.

MATERIALS

The concrete mix was designed for 4,000-psi compressive strength at 28 days, 6.25 sacks of cement per cu yd, with $2\frac{1}{2}$-in. slump and 5 percent entrained air. Concrete was made from high-quality quartz-sand fine aggregate, well-graded quartz-gravel coarse aggregate and Type I portland cement. Maximum aggregate size was $\frac{3}{4}$ in. An air-entraining agent was added to the mixing water. Measurements made on the concrete batches at the time of casting specimens and standard strength tests results on 6- by 12-in. compression cylinders, 6- by 6- by 20-in. flexure beams and 3- by 6-in. splitting tension cylinders are given in Table 1.

Deformed-bar reinforcement was furnished in two lots. The results of tensile

TABLE 1
PROPERTIES OF SERIES D AND WWF CONCRETE

Batch	Slump (in.)	Air (%)	Test Age (day)	Compressive Strength (psi)	Modulus Rupture (psi)	Splitting Tensile Strength (psi)
DC	2.4	4.0	1	1,715	339	223
			3	3,320	533	474
			7	4,350	679	584
			14	5,075	695	584
D24	6	4.0	1	1,052	235	151
			3	2,360	446	296
			7	3,583	519	385
			14	4,410	544	382
D20	2.1	5.2	1	1,798	377	207
			3	2,644	495	330
			7	3,392	521	376
			15	4,268	564	440
D20 E	3	3.5	1	1,650	378	326
			3	2,635	467	440
			7	3,200	532	453
			14	3,995	620	473
D18	2.5	5.8	1	1,897	475	285
			4	3,060	567	458
			7	3,800	594	352
			14	4,138	608	446
D16	3	5.5	1	1,123	274	147
			3	2,478	486	326
			7	3,406	555	458
			14	3,864	607	378
D12	2.5	4.6	1	1,418	315	212
			3	2,504	453	332
			7	3,390	512	454
			14	3,855	553	460
WWF C	3.5	6.5	1	1,261	288	199
			3	2,810	498	405
			7	3,628	609	414
			14	4,041	644	480
WWF 27E	6	6.7	1	1,660	335	260
			3	3,006	507	377
			7	3,519	580	373
			14	3,961	642	505
WWF 26	3	5.8	1	1,001	271	179
			3	2,785	485	404
			7	3,589	573	453
			14	4,028	566	470
WWF 18E	3	5.9	1	1,469	328	262
			3	2,894	451	384
			7	3,953	573	424
			14	4,050	568	468
WWF 18	5	6.0	1	1,519	328	198
			3	2,508	455	427
			7	3,555	528	409
			14	4,163	550	506
WWF 14	3	5.6	1	1,541	320	214
			4	2,880	508	319
			7	3,329	563	387
			14	3,688	587	367

TABLE 2
PROPERTIES OF REINFORCEMENT NO. 5 DEFORMED BARS, SERIES D

Test No.	Area (sq in.)	Yield Point (psi)	Yield Strength 0.2% Offset (psi)	Tensile Strength (psi)	Modulus of Elasticity (psi)	Elongation (% in 2 in.)
First Lot Used in Specimens DC, D24, D20, D12						
1	0.295	65,080	65,100	109,830	31,200,000	—
2	0.295	65,080	65,100	110,060	31,300,000	24
3	0.295	65,080	65,150	110,850	31,900,000	25
Avg.		65,080	65,120	110,250	31,500,000	24.5
Second Lot Used in Specimens D20E, D18, D16						
1	0.295	63,390	64,100	104,750	30,300,000	27
2	0.295	62,710	63,050	105,080	28,300,000	19
3	0.295	62,710	63,050	104,070	31,200,000	26
Avg.		62,940	63,400	104,630	29,900,000	24
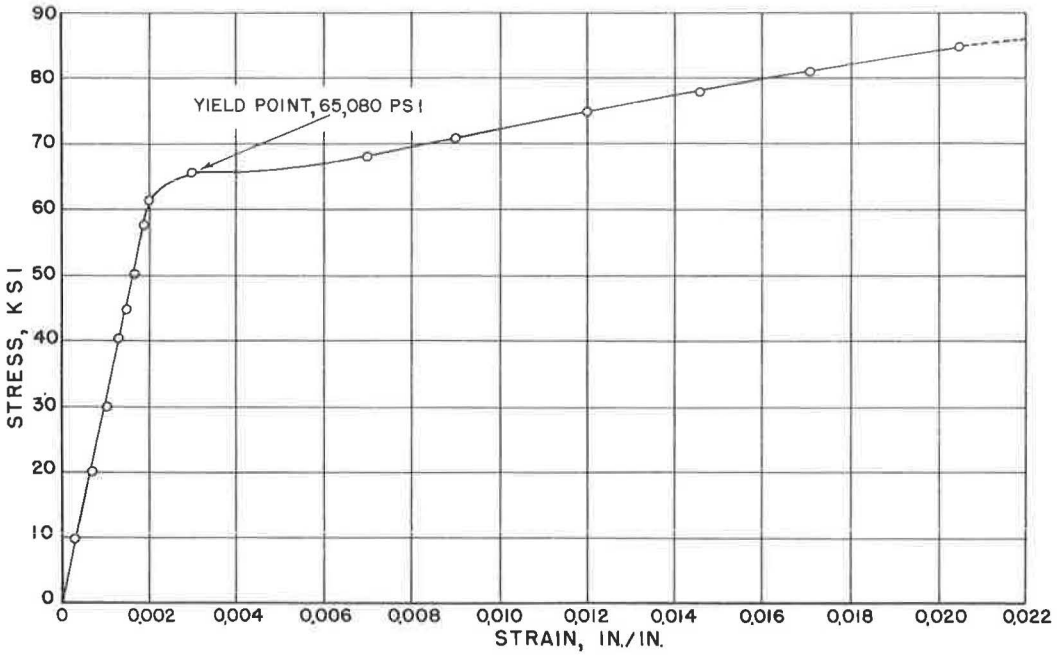
Figure 3. Initial portion of stress-strain curve, No. 5 deformed bar.
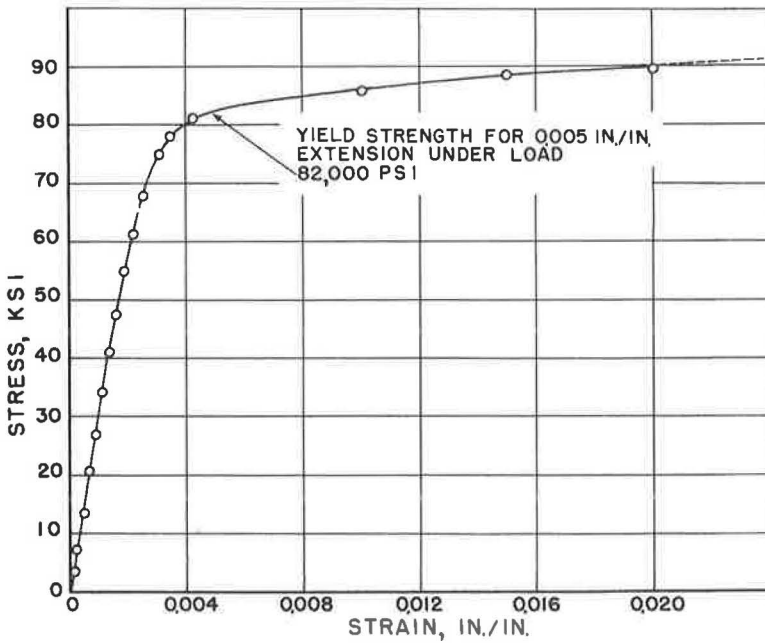
Figure 4. Initial portion of stress-strain curve, 5/0 wire.

TABLE 3

PROPERTIES OF WELDED-WIRE FABRIC

| Gage Length | Test No. | Area (sq in.) | Tensile Tests | | | | Weld Shear Tests | |
			Yield Strength 0.005 in./in. Ext. Under Load[1] (psi)	Tensile Strength (psi)	Modulus of Elasticity (psi)	Elongation (% in 2 in.)	Test No.	Shear Strength (lb)
Across Welds	1	0.147	82,000	87,990	27,800,000	6	1	2,640
	2	0.147	81,000	86,220	26,300,000	6	2	4,040
	3	0.147	81,500	88,940	28,600,000	10	3	2,600
	Avg.		81,500	87,720	27,600,000	7	4	3,600
							5	3,200
Between Welds	1	0.147	81,000	87,440	31,300,000	10	6	2,380
	2	0.147	80,000	85,880	28,600,000	–	7	2,540
	3	0.147	82,000	89,610	30,000,000	11	8	3,640
	Avg.		81,000	87,680	29,900,000	10.5	9	3,160
							10	3,140
							Avg.	3,094

[1]ASTM A82-61T.

strength tests on each lot are given in Table 2. A typical tension-test stress-strain curve for a sample from the first shipment is shown in Figure 3. Elongations measured in a 2-in. gage length are higher than the specification values based on 8-in. gage length.

The results of tensile tests of longitudinal wire samples cut from the welded-wire fabric are given in Table 3. Three samples were tested with the 2-in. gage length between welds, and three with the gage length spanning a weld. The transverse wire in the latter case was cut an inch away from the longitudinal wire, so that the weld was not disturbed prior to these tests. A typical stress-strain curve for the longitudinal wire between welds is shown in Figure 4.

Ultimate shear strength of welds was found by supporting the transverse wire on a bearing plate and pulling the longitudinal wire through a $5/8$-in. hole in the plate. Results of these tests (Table 3) probably are lower than would be obtained from tests made with a fixture that holds the transverse wire against rotation.

TESTING APPARATUS

The 20-ft specimens were tested under tensile loading applied in the longitudinal direction. Test loads were applied through yokes made of reinforcing bars embedded in the concrete at each end of the specimen. The loading frame was built of structural steel members (Fig. 5). Load was applied through a pulling head actuated by a hand-operated hydraulic jack. The yoke at one end of the specimen was connected to the
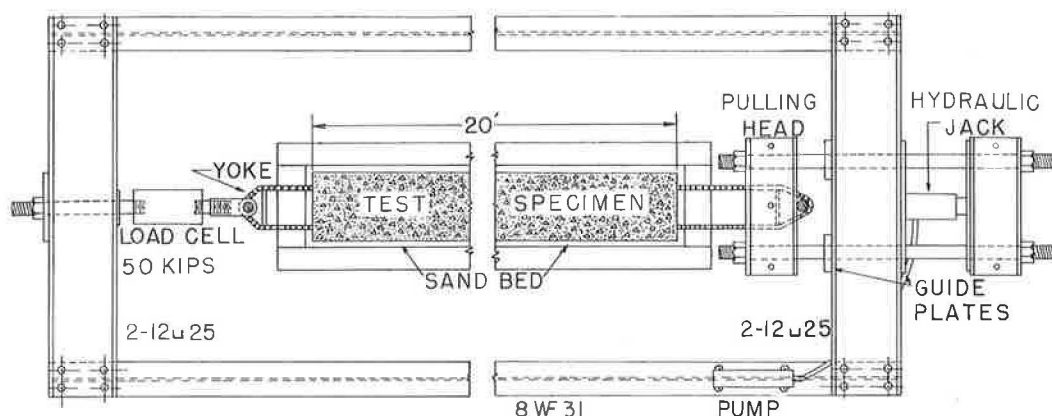
Figure 5. Plan of loading frame.

pulling head. The other end of the specimen was connected to the frame through a yoke, clevis, and strain-gage load cell. The load cell and the SR-4 strain indicator were calibrated in a universal testing machine.

Four 0.0001-in. dial gages, located symmetrically on the side faces of the specimen near the top and bottom were used to measure the preformed crack openings. They were mounted on brackets attached to bolts cast into the concrete 3 in. from the pre-formed crack. The widths of additional transverse cracks formed during the test were measured on the top surface of the specimen with a low-power microscope equipped with an optical scale.

The specimens were supported during testing on the base section of the form in which they were cast. A 1-in. thick bed of fine sand covered with two layers of 4-mil poly-ethylene sheeting below the specimen served to minimize frictional resistance.

FABRICATION OF SPECIMENS

Plywood forms were prepared for casting four specimens from each batch of con-crete. The base form was 2 ft wide and was supported on four 20-ft long, 2- by 6-in. timbers. A 1-in. bed of sand, graded to pass a No. 16 sieve, was carefully compacted in a recess in the top of the base form and brought to a smooth surface by a straight-edge. A 4-mil sheet of polyethylene stretched taut over the sand bed was stapled to the base form. A second sheet of polyethylene wide enough to wrap around the speci-men was spread over this base, and side forms were bolted on top of this second sheet to the edge of the base.

At midlength of the specimens, the side forms had 12-in. long removable plywood pieces. A sawed slot in these pieces held the $\frac{1}{16}$-in. thick sheet metal separator at the position of the preformed crack. Machine bolts ($\frac{1}{4}$- by 1 $\frac{1}{2}$-in.) were used to secure the dial indicator brackets to these pieces 3 in. away from the slot, with 1-in. length to be embedded in the concrete.

For deformed-bar test specimens, holes at the mid-depth of the sheet metal separator supported the reinforcement. The holes were drilled $\frac{1}{8}$ in. larger than bar diameter to allow wrapping the bar with a $\frac{1}{4}$-in. wide rubber ring to prevent possible locking of the bar deformations in the separator. For WWF specimens, 3 $\frac{3}{8}$-in. deep separators wide enough to be held in the slots were placed above and below the wire fabric and taped together.

At the ends of the specimens, the reinforcement and the yokes were supported on plywood end forms having holes for accurate steel location. Wire ties attached to the side forms supported the reinforcement at several points along the specimen length.

The welded-wire fabric was exposed to the weather to rust for four weeks to simulate the reinforcement surface conditions usually encountered in the field. To avoid using possibly damaged welds at the splice, a 25-ft length of wire fabric was cut in half and the interior ends were placed in the splice region of the test specimen. The specimen to be tested at 1-day age was cast in the loading frame. Other specimens were cast at nearby locations on the laboratory floor.

The concrete was supplied by a local ready-mix plant. The designated quantities of sand, cement, and gravel were delivered to the laboratory in a horizontal-axis truck mixer. Mixing water and the air-entraining agent were added at the laboratory. Inas-much as it was not possible to determine the exact moisture content of the aggregate at the plant, the following mixing procedure was adopted. A portion of the mixing water and all air-entraining agent were placed in the mixer and the concrete was mixed suffi-ciently to permit making a slump test; slump was invariably low. Water was then added to bring the slump to the desired value, and the concrete was thoroughly mixed.

The concrete was cast directly into the forms from the truck mixer. An internal vibrator was used to consolidate the concrete in the forms. Specimens were finished by striking off the top surface, covering with wet burlap, and wrapping in the polyethyl-ene sheet. Within 24 hours the side forms were removed so that the specimens could be covered closely with wet burlap and polyethylene wrapping. Occasional spraying with water served to keep the specimens thoroughly wet. Curing temperatures were the ambient laboratory temperatures.

At intervals during the placing process, concrete was taken from the truck discharge to form a composite batch sample for preparation of the specimens for concrete strength tests. This concrete was remixed by hand to obtain uniformity. The air content was measured by air meter. Cylinder and beam test specimens were cast in metal forms following standard procedures. At 24 hours, the forms were stripped and the samples placed in a 70 F, 100 percent humidity curing room.

TEST PROCEDURE

Two to three hours before testing, the curing wrapping was removed and the poly-ethylene sheeting beneath the specimen was cut free from the base form. A coat of whitewash was then applied to the top and side surfaces of the specimen to permit easy crack detection. The specimen was moved into the testing frame on the base form, which was lifted by slings with an overhead crane. The lifting points were located in the form at the quarter points of the specimen length to avoid bending at the splice. To center the specimen in the testing frame, the base was adjusted by shims.

The specimen was moved longitudinally to break the initial restraint of the sand bed on the bottom surface and to minimize the frictional resistance during test. Using a small hydraulic jack, the specimen was twice pushed about $\frac{3}{8}$ in. in each direction with the final movement being toward the load cell end. Thus, protruding irregularities in the bottom of the specimen moved into recesses in the sand bed as the specimen was strained during test.

Frictional resistance was measured on 11 specimens. Load readings were taken from a proving ring placed between the small hydraulic jack and one end of the speci-men; movement readings were obtained by a 0.001-in. dial indicator at the other end of the specimen. After a consistent relationship between frictional resistance and movement had been established, these measurements were discontinued.

After breaking the initial sand bed restraint, the specimen was connected to the testing frame and dial gages were attached. The longitudinal tensile loading was begun in 1,000- to 2,000-lb increments, depending on specimen strength. The dial gages were read at each increment. When transverse cracks or any signs of splice failure devel-oped, the test was stopped and load value recorded. Specimen conditions were noted and measurements of openings of all transverse cracks were made. The loading was then resumed until the next increment was reached or additional cracks developed. Following this procedure, the load was increased until the specimen failed. The final crack pattern was recorded in detail and photographs of the splice region were taken. The cracked concrete around the failed splice was removed to examine the failure pattern and to detect weld failures when such occurred with welded-wire fabric. Strength tests of concrete control samples were made immediately before or after testing each specimen.

TEST RESULTS

Frictional Resistance

The results of a typical set of measurements for frictional resistance between speci-men and sand bed are shown in Figure 6. These curves show the forces required to produce the movements indicated on the abcissae. The direction of motion was toward the jack end for the first movement, 1, and was away from the jack for the last move-ment, 4. The curves show that the frictional resistance at sliding became fairly steady at 940 lb during the fourth movement. This corresponds to a coefficient of sliding friction of 0.45 for the specimen weight of 2,090 lb. Table 4 shows the results of the eleven sliding friction measurements made.

Typical Behavior Under Load

Curves showing load as a function of preformed crack opening were plotted from the log of each test. Typical examples of such curves are shown in Figures 7, 8, 9, 10, and 11. Each crack is indicated by a number or letter on the curve at the point where it occurred, and the same symbol locates the crack on the sketch on the curve
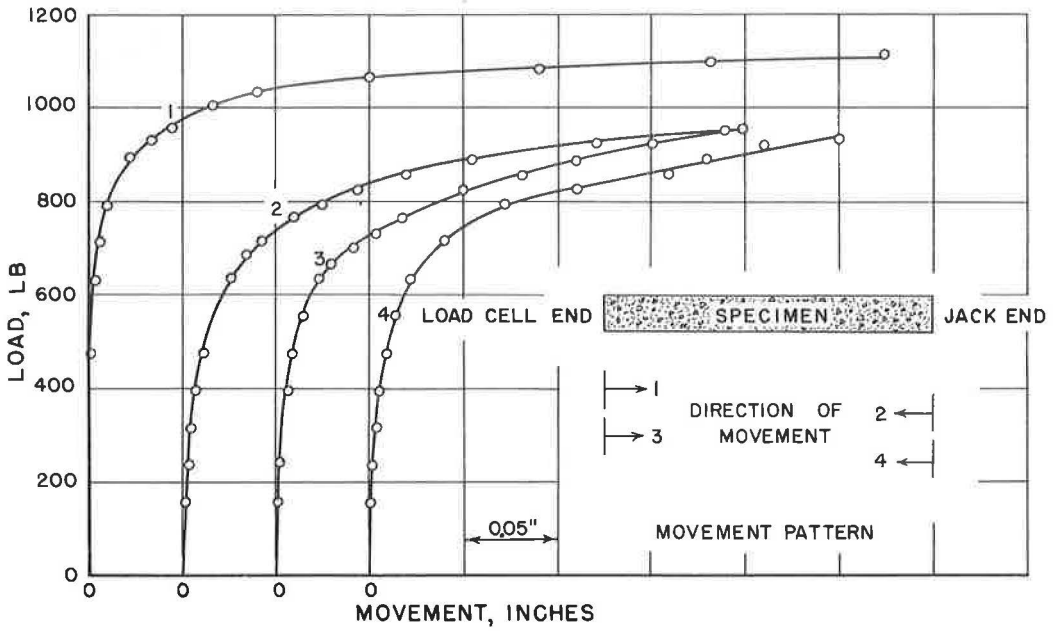
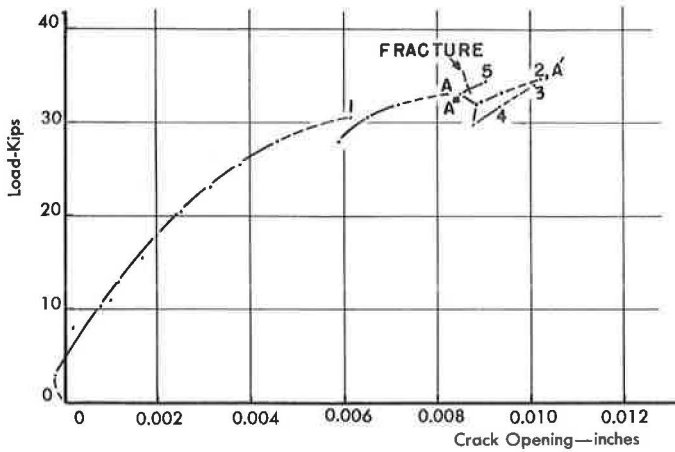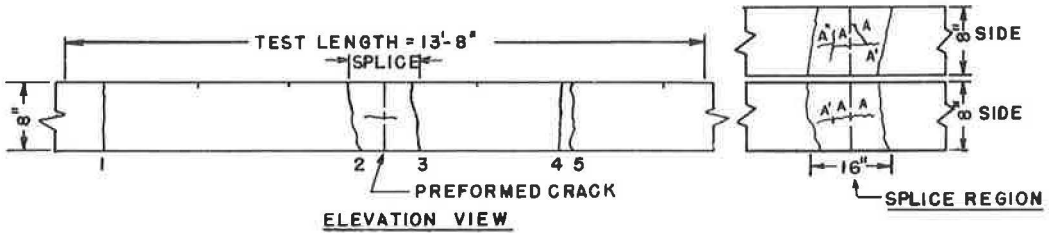Figure 6. Frictional resistance, specimen D16-14.
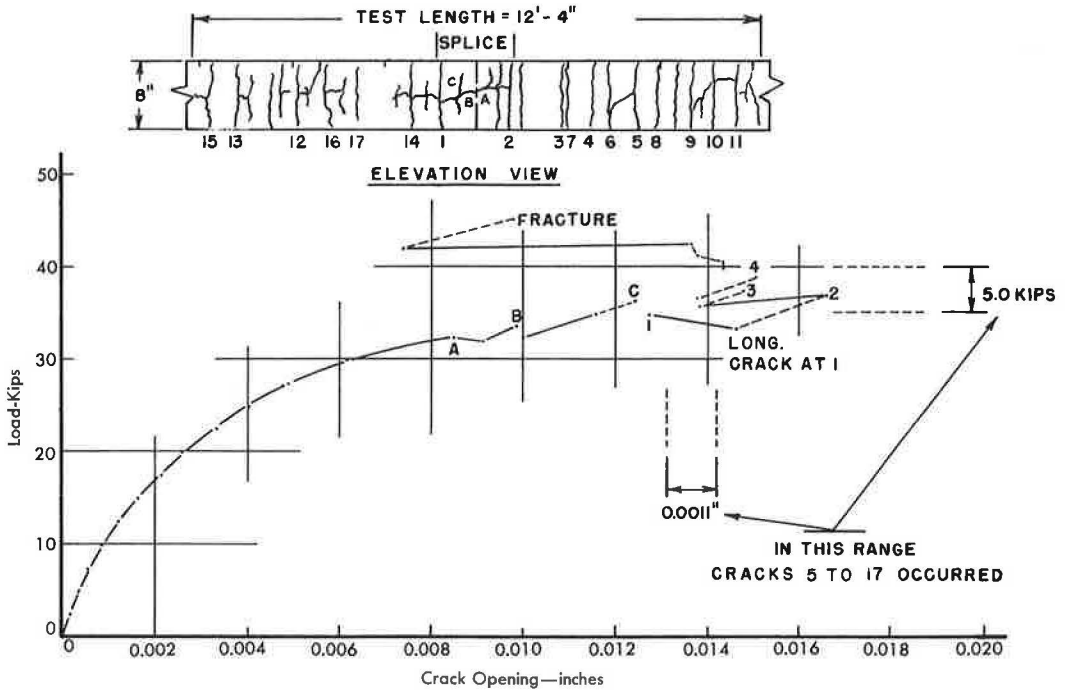

Figure 7. Test record, specimen D16-7.
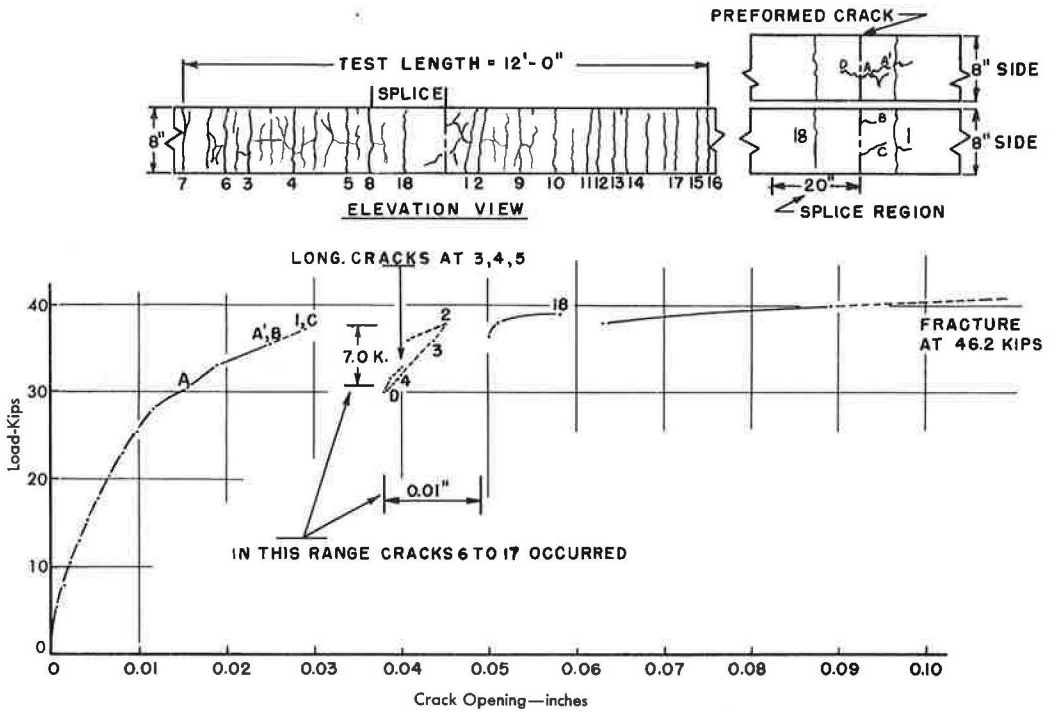
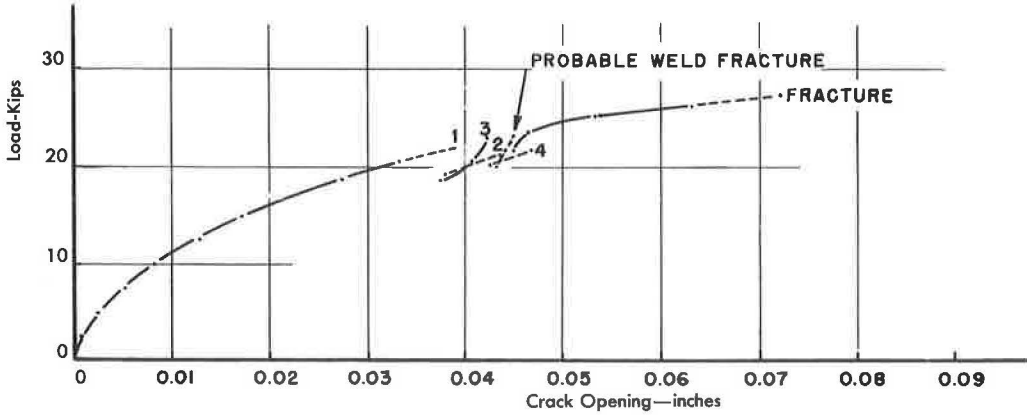Figure 8. Test record, specimen D20-15.

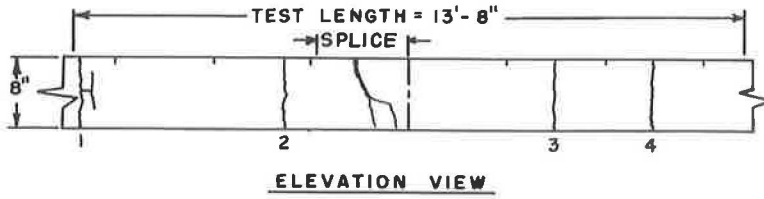Figure 9. Test record, specimen D20E-14.
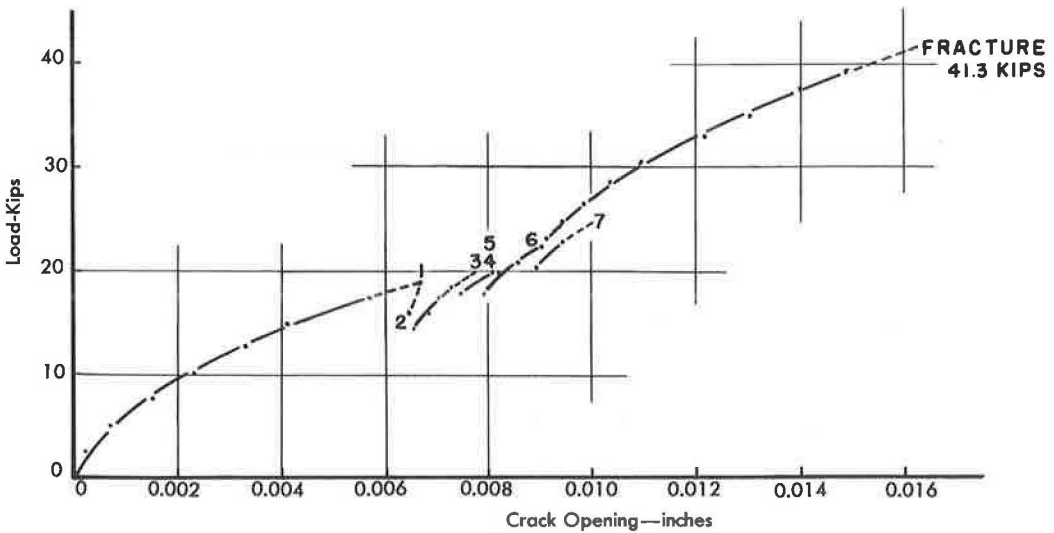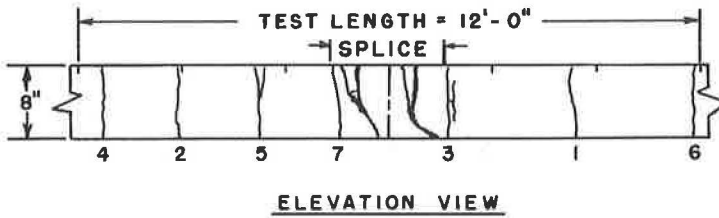
Figure 10. Test record, specimen WWF18E-1.

Figure 11. Test record, specimen WWF26-1.

sheet. Numbers represent transverse cracks in the order of appearance, and letters denote longitudinal horizontal cracks. Primes indicate extension of existing cracks.

Specimen D16-7, 16-in. lap, 7-day concrete (Fig. 7), is representative of a relatively weak deformed-bar splice. Some initial adjustment in the dials at early stages of loading accounts for the small (0.0005 in.) zero error. The preformed crack opened at increasing rate until the first transverse crack (1) occurred 6 ft from the preformed crack at 30.2 kips and 0.006-in. opening of the preformed crack. Load dropped slightly and the preformed crack closed a little because the transverse crack released some of the strain on the specimen.

Continued straining led to the development of longitudinal horizontal cracks (A), on both sides of the preformed crack at 32.8 kips (steel stress 55.6 ksi). Load dropped to 31.7 kips but the preformed crack opened to 0.0089 in. At 34.5 kips a transverse crack (2) developed at the end of the splice, together with extension of the longitudinal cracks. Further straining, but at loads less than 34.5 kips, caused a crack at the other end of the splice (3) and two additional transverse cracks, as indicated by isolated points (4, 5) on the curve. During this stage, it was apparent that the concrete had broken out on one side of the preformed crack and all load transfer was through the remaining half of the splice on the other side. Because the concrete between the preformed crack and crack (2) had broken free, the dials indicate a partial closing of the preformed crack. This occurred in many cases of splice failure. Fracture occurred at 35.3 kips (steel stress 59.8 ksi) with a sudden complete longitudinal crack on the previously unbroken side of the splice. Figure 12a shows a fracture at the splice that is typical of the shorter splices in deformed bars.

Specimen D20-15 is typical of a stronger deformed-bar splice (Fig. 8). When the load reached 32.5 kips, longitudinal splitting (A) occurred in the splice, extending 3 in. on one side of the preformed crack. At the same time, the preformed crack opened another 0.0006 in. At 34.0 kips, crack (A) lengthened and a longitudinal crack (B) started on the other side of the splice. Vertical cracks (C) developed from the ends of these longitudinal cracks, about 4 in. from the preformed crack, at 36.5 kips. Load decreased, and with straining a transverse crack (1) formed at one end of the splice at 35.1 kips. The second transverse crack (2) developed at 37.1 kips (opening 0.0167 in.) accompanied by secondary cracking shown on the sketch. Following this crack the preformed crack opening decreased to 0.014 in.

Fifteen additional transverse cracks formed at loads between 35.0 and 40.1 kips (67.8 ksi steel stress) and preformed crack opening between 0.0131 and 0.0142 in. Some of these natural cracks opened as much as 0.04 in., and longitudinal cracks developed in several locations between closely spaced transverse cracks (Fig. 12b). The steel was stressed to the yield range at the higher loads in this stage. Further straining caused increased opening of all cracks, the widest attaining 0.132 in., with load rising to 43.0 kips. Because of the cracks in the splice region, the dials indicated a closing of the preformed crack. Fracture occurred at 45.3 kips, with large separation at the splice (Fig. 12c).

Specimen D20E-14 (Fig. 9) represents the deformed-bar specimens that exhibited large preformed crack openings (DC and D20-E). Longitudinal crack, (A), developed at 30.3 kips on the unspliced side of the preformed crack, extending 2 in. from the crack. At 35.3 kips the crack, (A) extended further both vertically and longitudinally, (A'), and a longitudinal crack (B) occurred 2 in. below top surface in the opposite side of the specimen. With further increase of load to 37.1 kips (steel stress 62.9 ksi), a transverse crack (1), formed and another longitudinal crack (C) extending 4 in., occurred $3\frac{1}{2}$ in. below the crack (B). At this stage, no longitudinal cracks were observed on the spliced side of the preformed crack. The load decreased to 35.8 kips, and the preformed crack opened another 0.012 in. After forming additional transverse cracks (2) at 37.7 kips, (3) at 35.9 kips and (4) at 31.9 kips a longitudinal crack, (D), developed on the spliced side, extending 3 in. from the preformed crack.

Fourteen additional transverse cracks formed at loads between 30.0 and 38.9 kips and at preformed crack openings between 0.0378 and 0.0631 in. Longitudinal cracks developed at some of the transverse cracks, but cracks (A), (B), and (D) did not extend further in this stage. As the load was further increased, no additional cracks formed
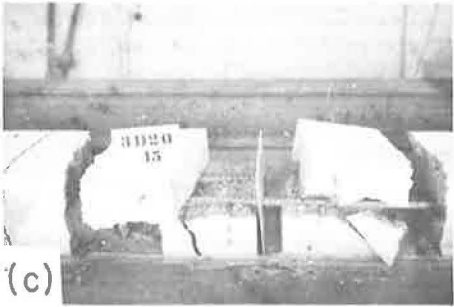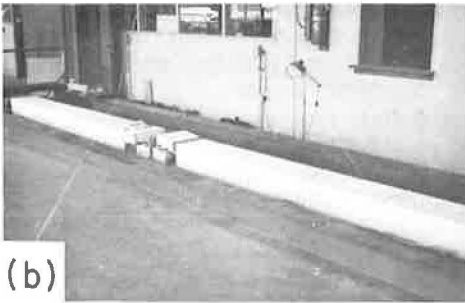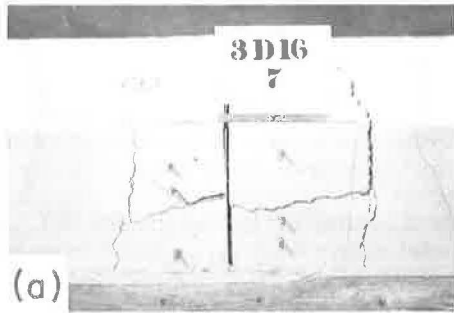
Figure 12. Fracture patterns: (a) specimen D16-7, (b) D20-15, and (c) D20-15.

Figure 13. Fracture patterns: (a) specimen WWF18E-1 and (b) WWF26-1.

but the transverse cracks as well as the preformed kept opening with extension of the longitudinal cracks until sudden fracture of the splice at 46.2 kips (steel stress 78.2 ksi). Some transverse cracks opened as much as 0.2 in. just prior to fracture.

Specimen WWF18E-1 (Fig. 10) represents a relatively weak welded-wire fabric splice. At 21.6 kips (steel stress 36.7 ksi) a transverse crack, (1), formed. The load dropped to 19.0 kips and the preformed crack closed a little. Three additional transverse cracks formed between 18.6 and 22.8 kips and preformed crack openings of 0.0375 to 0.0470 in. At 22.9 kips, a noise was heard, probably indicating failure of one weld at the second transverse wire from the preformed crack. With further increase of load, the transverse and preformed cracks continued to open until fracture occurred at the splice at 27.2 kips (steel stress 46.2 ksi). Cracks appeared at the second transverse wire from the preformed crack (Fig. 13a). Just prior to the fracture, some transverse cracks opened 0.06 in.

Specimen WWF26-1 (Fig. 11) is typical of stronger welded-wire fabric splices. The first transverse crack (1) formed at 18.5 kips (steel stress 31.4 ksi). As the load dropped to 15.7 kips and the preformed crack closed a little, a second transverse crack (2) formed. Five additional transverse cracks formed at loads between 14.1 to 24.4 kips and preformed crack openings 0.0065 to 0.01 in. Beyond this stage, both preformed and transverse cracks continued to open but no additional cracks occurred prior to fracture of the splice at 41.25 kips (steel stress 70.0 ksi). The fracture was

accompanied by cracks at sections between the first and second transverse wires on both sides of the preformed crack (Fig. 13b). The maximum transverse crack opening was 0.12 in.

Summary of Tests

The principal results of the tests are summarized for deformed-bar reinforcement (Table 5) and for welded-wire fabric reinforcement (Table 6). Load and preformed crack opening at the formation of the first natural transverse crack within the test length are given, and cases in which the first transverse crack formed at the end of the splice are indicated.

TABLE 4
FRICTIONAL RESISTANCE

Specimen	Age (day)	Maximum Frictional Resistance in the Fourth Movement (lb)	Frictional Coefficient
D16	1	1,030	0.49
D16	3	910	0.44
D16	7	950	0.45
D16	14	940	0.45
D12	1	1,070	0.51
D12	3	810	0.39
D12	7	870	0.42
D12	14	760	0.36
WWF14	1	950	0.48
WWF14	4	860	0.43
WWF14	7	830	0.42
Avg.		907	0.44

Load and preformed crack opening at first observation of a longitudinal crack are also given in Table 5. Most of the longitudinal cracks were first observed at the preformed cracks as previously described; those observed first at natural transverse cracks are indicated.

The number of transverse cracks before fracture is given in both Tables 5 and 6. Fracture data (Table 6) include load, maximum preformed and natural transverse

TABLE 5
TEST RESULTS DEFORMED-BAR REINFORCEMENT

Speci-men	Age (day)	First Trans. Crack		First Long. Crack		No. of Transverse Cracks Before Fracture	Fracture			
		Load (kip)	Preform. Crack Open. (in.)	Load (kip)	Preform. Crack Open. (in.)		Load (kip)	Maximum Crack Opening Observed		Type
								Preformed (in.)	Transverse (in.)	
DC	1	21.3[a]	0.0115	28.8[b]	0.0181	15	45.0	0.1356	0.2080	Test ter-
DC	3	31.9[a]	0.0183	34.8[b]	0.0200	20	46.3	0.1066	0.1360	minated
DC	7	27.4[a]	0.0120	31.3	0.0191	21	46.8	0.1338	0.2180	with no
DC	14	35.0	0.0300	30.0	0.0150	23	46.9	0.1325	0.1940	fracture
D24	1	18.8	0.0047	30.8[b]	0.0083	12	42.1	0.0116	0.0880	Longitu-
D24	3	30.0	0.0077	30.0	0.0076	17	44.2	0.0137	0.0560	dinal
D24	7	36.3	0.0093	31.3	0.0067	17	48.2	0.0132	0.1000	crack in
D24	14	36.4	0.0093	36.4	0.0092	25	48.9	0.0153	0.1840	splice
D20	1	18.3	0.0020	29.5[b]	0.0056	14	42.3	0.0120	0.1320	Longitu-
D20	3	31.0	0.0094	27.0	0.0062	16	45.2	0.0130	0.1600	dinal
D20	7	35.0[c]	0.0130	26.1	0.0056	6	37.9	0.0218	0.0360	crack in
D20	15	36.5[c]	0.0131	32.5	0.0085	22	45.3	0.0166	0.1520	splice
D20E	1	28.6	0.0157	31.2[b]	0.0170	14	41.3	0.0980	0.1080	Longitu-
D20E	3	20.4	0.0084	29.1	0.0157	23	42.0	0.1150	0.1200	dinal
D20E	7	35.0	0.0267	30.1	0.0144	31	44.4	0.1200	0.1200	crack in
D20E	14	37.1	0.0290	30.3	0.0154	23	46.2	0.1700	0.1680	splice
D18	1	22.5[a]	0.0064	29.9	0.0124	13	33.5	0.0184	0.0260	Longitu-
D18	4	31.5	0.0091	31.5	0.0126	6	35.2	0.0223	0.0360	dinal
D18	7	35.0[c]	0.0175	33.4	0.0104	20	40.0	0.0184	0.0900	crack in
D18	14	34.4[c]	0.0105	34.4	0.0105	25	50.0	0.0149	0.1140	splice
D16	1	23.4	0.0104	27.1	0.0130	8	27.2	0.0130	0.0200	Longitu-
D16	3	27.8	0.0073	29.0	0.0093	1	29.4	0.0146	0.0300	dinal
D16	7	30.2	0.0061	32.8	0.0080	5	35.3	0.0103	0.0220	crack in
D16	14	32.9[c]	0.0149	32.9	0.0150	4	36.6	0.0168	0.0260	splice
D12	1	18.8	0.0128	23.1	0.0186	3	23.1	0.0186	0.0118	Longitu-
D12	3	22.5[c]	0.0098	23.3	0.0320	1	23.3	0.0322	—	dinal
D12	7	25.3[c]	0.0129	26.3	0.0129	1	27.4	0.0165	—	crack in
D12	14	28.9[c]	0.0095	28.9	0.0114	1	29.2	0.0125	—	splice

[a]Located at the end of yoke.
[b]Located at natural transverse crack.
[c]Located at end of splice.

TABLE 6

TEST RESULTS WELDED-WIRE FABRIC REINFORCEMENT

| Specimen | Age (day) | First Trans. Crack | | No. of Transverse Cracks Before Fracture | Fracture | | | |
| | | Load (kip) | Preform. Crack Open. (in.) | | Load (kip) | Maximum Crack Opening Observed | | Type[a] |
						Preformed (in.)	Transverse (in.)	
WWFC	1	17.5[b]	0.0158	7	50.7	0.2400	0.176	A
WWFC	3	35.0	0.0436	6	53.3	0.1510	0.256	A
WWFC	7	41.3	0.0435	6	51.3	0.0740	0.100	A
WWFC	14	39.5	0.0475	7	50.0	0.1150	0.160	A
WWF27E	1	20.5	0.0185	9	35.5	0.0700	0.046	B
WWF27E	3	30.5	0.0281	7	52.5	0.1150	0.224	A
WWF27E	7	32.9	0.0288	5	51.5	0.0625	0.140	A
WWF27E	14	32.9	0.0267	7	54.5	0.0650	0.126	B
WWF26	1	18.5	0.0067	9	41.3	0.0162	0.124	C
WWF26	3	27.5	0.0078	7	47.7	0.0198	0.096	B
WWF26	7	37.5[b]	0.0132	7	48.5	0.0155	0.174	D
WWF26	14	35.0	0.0101	8	52.3	0.0186	0.108	B
WWF18E	1	21.6[b]	0.0360	4	27.2	0.0720	0.060	B
WWF18E	3	25.1	0.0394	6	31.0	0.2318	0.080	B
WWF18E	7	27.5	0.0395	3	33.5	0.2512	0.076	B
WWF18E	14	39.4	0.0450	8	47.9	0.0825	0.200	B
WWF18	1	20.7	0.0070	7	23.9	0.0230	0.136	B
WWF18	3	24.9	0.0058	10	41.2	0.0109	0.084	B
WWF18	7	28.2	0.0087	6	37.2	0.0140	0.280	B
WWF18	14	31.1	0.0078	10	38.8	0.0230	0.100	B
WWF14	1	-	-	-	14.6	0.0453	-	C
WWF14	4	-	-	-	20.6	0.0309	-	C
WWF14	7	-	-	-	23.4	0.0100	-	C
WWF14	14	-	-	-	29.9	0.0100	-	C

[a]Failure types:
   (a) Longitudinal wire tension,
   (b) Weld and concrete at splice,
   (c) Concrete at splice, and
   (d) Weld and longitudinal wire tension.
[b]Located at end of yoke.

crack openings, and type of failure. The maximum crack openings were measured at the last load increment prior to fracture. "Weld and concrete at splice" (footnote a under fracture type in Table 6) indicates fracture by cracking of concrete in the vicinity of the transverse wires of the spliced region accompanying the weld failures (Fig. 13b).

DISCUSSION OF RESULTS

First Transverse Crack

First transverse cracks occurred in the uniformly reinforced test length between the yokes and the ends of the splice in 33 out of 52 cases. In 8 of the 28 deformed-bar specimens the first crack developed at one end of the splice. In 7 other cases in both series D and WWF, it developed at the end of the yoke bars. No transverse cracks developed in specimens WWF14. In all cases, the load required to cause the second crack was but little greater than at first crack. Apparently there is no significant stress concentration in the concrete at the end of a reinforcing bar to cause early cracking at this place.

Test results for series D (Fig. 14) are grouped by age, because cracking is a function of concrete strength. At 1-day age, load at first crack varied from 18.3 to 28.6 kips, whereas at 14 days the range was between 28.9 and 37.1 kips. The preformed crack opening when the first transverse crack occurred was between 0.0020 and 0.0157 in. at 1-day age, and between 0.0093 and 0.0300 in. at 14-day test age. Larger preformed crack openings appeared in DC and D20E, in which only two reinforcing bars cross the preformed crack.

All splice lengths of 16 in. or greater in deformed-bar reinforcement were capable of resisting loads great enough to break the concrete in tension in unspliced regions at
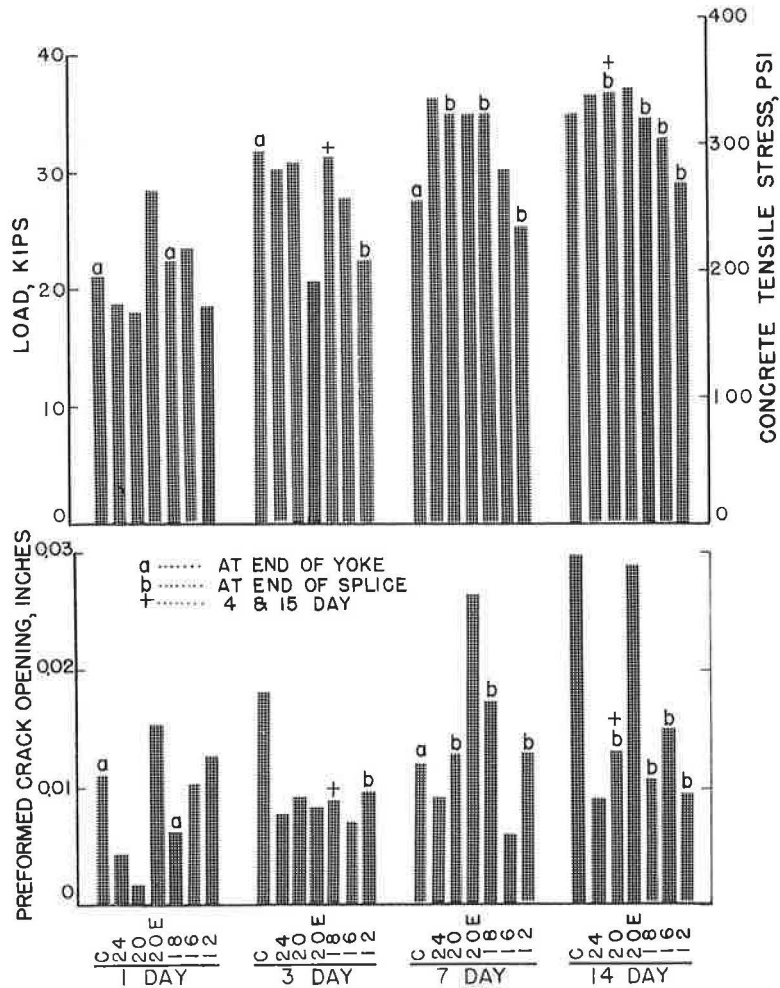
Figure 14. First transverse cracks, series D.

all ages. Preformed crack openings within or at the end of these splices were held to small values as the additional transverse cracks developed.

In specimens D12-3, -7, and -14, the only transverse cracks occurred at the end of the splice, and load at fracture was but little greater than load at first crack. Although these were transverse cracks, they appear to be part of the breakdown of the splice and not independent cracks as occurred with longer splices.

First transverse crack data for welded-wire fabric are given in Table 6 and Figure 15. At 1-day age, load at first crack varied from 17.5 to 21.6 kips, and from 31.1 to 39.5 kips at 14-day test age. Preformed crack openings were 0.0067 to 0.0360 in. at 1-day and 0.0071 to 0.0475 in at 14-day age. The openings were greater for WWFC and WWF27E because four longitudinal wires from one fabric only were effective across the preformed crack. All lap lengths tested except 14 in. were strong enough to hold preformed cracks within the splice from opening excessively prior to the formation of additional transverse cracks.

The average values of the first transverse crack openings measured immediately after the cracks formed were 0.0159 in. for deformed-bar and 0.0292 in. for welded-wire fabric specimens. These measurements were made on all specimens.

Concrete strength varied somewhat from batch to batch (Table 1) and increased with age. A comparison was made, therefore, between concrete tensile stress at formation
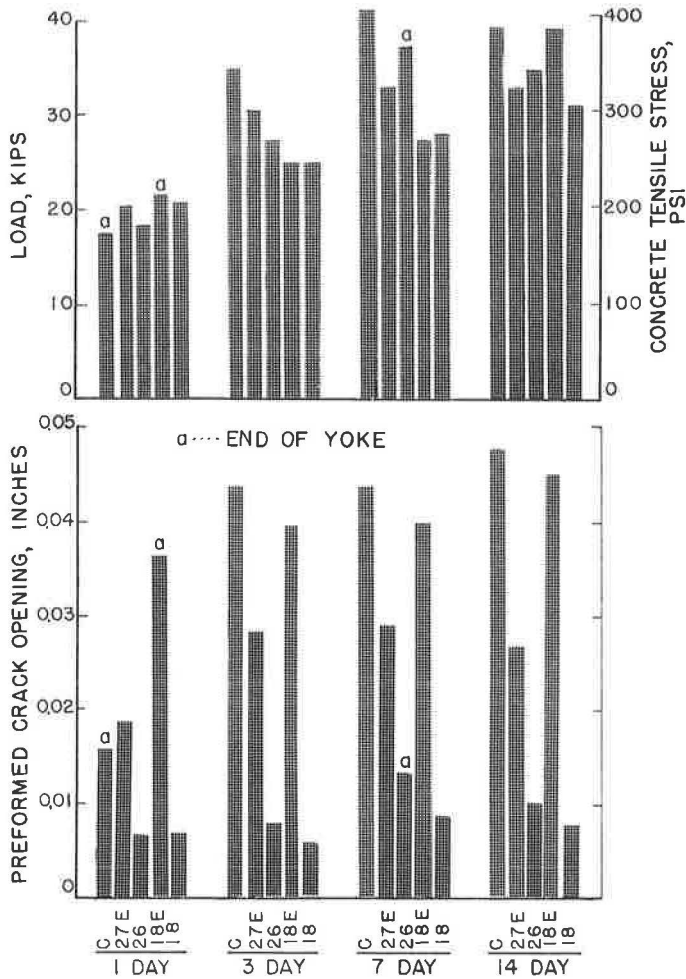
Figure 15. First transverse cracks, series WWF.

of the first transverse crack and strength measurements from the control samples. Concrete tensile stresses were calculated by dividing the test loads by the transformed area of cross-section. Modulus of elasticity of concrete was measured on nine compression test cylinders from different batches and an average value of 4,130,000 psi for all ages was used to transform steel to equivalent concrete area.

Concrete tensile stresses at formation of the first transverse crack are given in Table 7. These values varied with age, as would be expected. The ratio of concrete tensile stress to modulus of rupture and the ratio of concrete tensile stress to the square root of compressive strength at the same age were calculated. Average values of these ratios are

$$\sigma_c = 0.57\ M_r \quad \text{and} \quad \sigma_c = 5.20\ \sqrt{f_c}$$

Number of Transverse Cracks Before Fracture

The ability of a splice to withstand loads sufficient to produce transverse cracks at unspliced sections is important to the satisfactory functioning of reinforcement in continuous pavement. The number of transverse cracks formed before fracture (Tables

TABLE 7

CONCRETE TENSILE STRESS AT FIRST TRANSVERSE CRACK

	Deformed Bar				Welded Wire Fabric				
Specimen	Age (day)	Concrete Tensile Stress σ_c (psi)	$\dfrac{\sigma_c}{M_r}$	$\dfrac{\sigma_c}{\sqrt{f_c}}$	Specimen	Age (day)	Concrete Tensile Stress σ_c (psi)	$\dfrac{\sigma_c}{M_r}$	$\dfrac{\sigma_c}{\sqrt{f_c}}$
DC	1	198[a]	0.58	4.78					
D24	1	174	0.74	5.37	C	1	172[a]	0.60	4.84
D20	1	170	0.45	4.01	27E	1	201	0.60	4.93
D20E	1	265	0.70	6.53	26	1	182	0.67	5.75
D18	1	209[a]	0.44	4.80	18E	1	212[a]	0.65	5.53
D16	1	217	0.80	6.99	18	1	203	0.62	5.21
D12	1	174	0.55	4.63	14	1	-	-	-
Avg.		201	0.61	5.30	Avg.		194	0.63	5.25
DC	3	296[a]	0.56	5.14					
D24	3	278	0.62	5.73	C	3	343	0.69	6.47
D20	3	288	0.58	5.60	27E	3	299	0.59	5.45
D20E	3	189	0.40	3.68	26	3	270	0.56	5.11
D18	4	292	0.51	5.28	18E	3	246	0.55	4.18
D16	3	258	0.53	5.19	18	3	244	0.54	4.87
D12	3	209[b]	0.46	4.18	14	4	-	-	-
Avg.		259	0.52	4.97	Avg.		280	0.59	5.22
DC	7	254[a]	0.37	3.84					
D24	7	337	0.65	5.63	C	7	405	0.67	6.72
D20	7	325[b]	0.62	5.58	27E	7	323	0.56	5.44
D20E	7	325	0.61	5.74	26	7	368[a]	0.64	6.14
D18	7	325[b]	0.55	5.28	18E	7	270	0.47	4.29
D16	7	280	0.50	4.79	18	7	277	0.52	4.64
D12	7	235[b]	0.46	4.04	14	7	-	-	-
Avg.		297	0.54	4.99	Avg.		329	0.57	5.45
DC	14	325	0.47	4.56					
D24	14	338	0.62	5.09	C	14	388	0.60	6.10
D20	15	339[b]	0.60	5.19	27E	14	323	0.50	5.13
D20E	14	344	0.55	5.44	26	14	343	0.61	5.40
D18	14	319[b]	0.52	4.96	18E	14	387	0.68	6.08
D16	14	305[b]	0.50	4.90	18	14	305	0.55	4.72
D12	14	268[b]	0.48	4.32	14	14	-	-	-
Avg.		320	0.53	4.92	Avg.		349	0.59	5.49
Grand Avg.			0.55	5.05	Grand Avg.			0.59	5.35

[a]Crack at end of yoke.
[b]Crack at end of splice.

5 and 6) indicates the ability of the splice to produce transverse cracks. Eighteen-inch or longer splices in both deformed-bar and welded-wire fabric specimens produced numbers of cracks comparable with the unspliced specimens (DC and WWFC).

First Longitudinal Cracks—Series D

Longitudinal cracks appearing in the 8-in. faces in the plane of reinforcement are evidence of bond failures in the deformed-bar test specimens. They are caused by tensile splitting forces in the concrete acting perpendicular to the reinforcement. Beyond the adhesion stage, the bond strength depends chiefly on bearing of reinforcement deformations against the concrete, and the tensile splitting forces are thus induced.

In more than half of these tests, the first transverse cracks were observed before the formation of the longitudinal crack (Table 5). The 12 cases in which the first longitudinal cracks formed before, or at the same time as, the first transverse cracks involved later-age test specimens. It seems that the occurrence of the first longitudinal crack is a function of the preformed or transverse crack opening as well as concrete strength, whereas the first transverse crack depends on concrete strength alone. While these longitudinal cracks extended gradually, many additional transverse cracks developed before complete longitudinal splitting at the splice took place at fracture.

In most cases, the first longitudinal crack occurred at preformed cracks. The 5 cases in which the first longitudinal cracks developed elsewhere were early-age test specimens either unspliced or having relatively longer splices. The openings of the preformed cracks, except DC and D20E, never exceeded 0.015 in. unless the splice was in final process of fracture. The preformed cracks opened as much as 0.02 in before the first longitudinal cracks were observed in DC and D20E.

The steel stresses at which longitudinal cracks occurred in unspliced portions of the test length are given in Table 8. These cracks were in the plane of the steel and developed from previously formed transverse cracks or from the preformed crack in DC and D20E. These longitudinal cracks are apparently associated with steel stresses of about 50 ksi or greater, and are somewhat dependent on concrete age.

The occurrence of longitudinal cracks within the splice at the preformed crack is more significant than splitting at other transverse cracks. Crack opening, steel stress (based on 0.6 percent steel) and bond stress are given in Table 9.

Splitting within the splice occurred at preformed crack openings between 0.0052 and 0.0150 in. in all cases (except D12) having four bars across the crack. Openings for specimens DC and D20E are larger, since there is but half as much steel stiffening the crack.

Steel stresses of about 40 ksi or higher were required to start splitting in the splice. There is some tendency toward higher stresses for longer splices and later ages. Sixteen-inch or longer splices were capable of developing steel stresses of 44 ksi or more at all test ages before the first longitudinal cracks were observed. These steel stresses are comparable to the steel stresses developed by unspliced specimens, DC. The 12- and 16-in. splices developed longitudinal cracks only within the splice, at loads near fracture (Fig. 16).

Bond stress is computed as the average unit bond stress on the total embedded bar surface area at the splice. Bond stresses increase with age in general. The bond stresses are lower for the longer splices. It is recognized that the bond stress distribution along the splice is not uniform; rather, splitting begins at a higher than average bond stress adjacent to the preformed crack. The higher values of average bond stress for the shorter splices (Table 9c) are probably near the unit bond stress attained locally along the splice when a longitudinal crack forms. However, the average bond stresses for the initiation of longitudinal cracks in the longer splices may be of use in estimating the likelihood of such occurrences in other splices of these proportions made with similar materials.

TABLE 8

LONGITUDINAL CRACKS IN UNSPLICED REGIONS
(Series D)

Specimen	Steel Stress at Trasverse Crack			
	1-Day	3-Day	7-Day	14-Day
DC	48.8	59.0	53.1	50.8
D24	51.7	57.3	63.6	65.9
D20	50.0	55.1[a]	60.2[a]	62.9[a,b]
D20E	51.9	49.3	51.0[a]	59.8[a]
D18	–	55.9[a,c]	59.3[a]	61.7[a]
D16	–	–	–	–
D12	–	–	–	–
Avg.	50.5	55.3	57.4	60.3

[a]Crack at end of splice.
[b]Fifteen-day age.
[c]Four-day age.

TABLE 9

CONDITIONS AT LONGITUDINAL CRACK
FORMATION AT THE PREFORMED CRACK
(Series D)

Specimen	Age at Test			
	1-Day	3-Day	7-Day	14-Day
(a) Preformed Crack Opening (in.)				
DC	0.0242	0.0286	0.0191	0.0150
D24	0.0112	0.0076	0.0067	0.0092
D20	0.0063	0.0062	0.0052	0.0085[a]
D20E	0.0269	0.0157	0.0144	0.0154
D18	0.0124	0.0126[b]	0.0104	0.0105
D16	0.0130	0.0093	0.0080	0.0150
D12	0.0186[c]	0.0320[c]	0.0129	0.0114
(b) Stress in Steel (ksi)				
DC	55.1	61.5	53.1	50.8
D24	67.8	50.8	53.1	61.7
D20	51.7	45.8	44.2	55.1[a]
D20E	60.3	49.3	51.0	51.3
D18	50.7	53.4[b]	56.6	58.5
D16	45.9	49.2	55.6	55.7
D12	39.2[c]	39.5[c]	44.6	48.9
(c) Bond Stress (psi)				
DC	–	–	–	–
D24	432	324	338	393
D20	395	350	338	421[a]
D20E	461	377	390	393
D18	430	453[b]	481	495
D16	439	470	531	533
D12	499[c]	503[c]	568	624

[a]Fifteen-day age.
[b]Four-day age.
[c]At fracture.

Figure 16. First longitudinal cracks, series D.
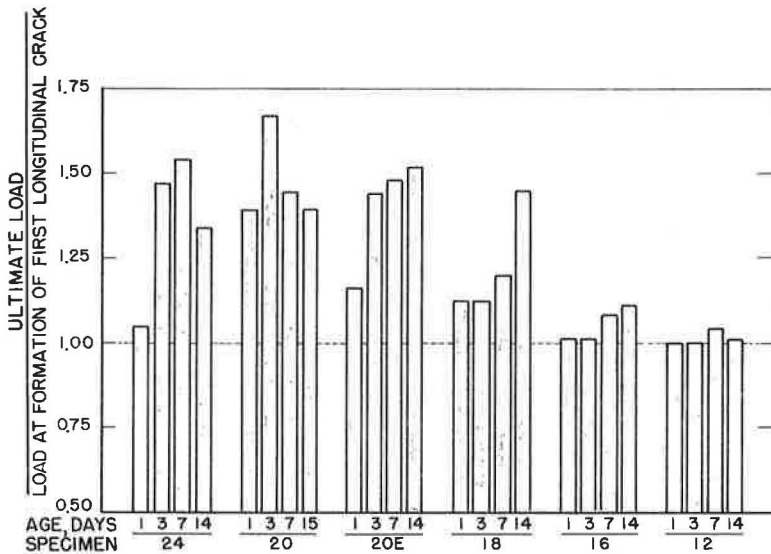
Figure 17. First longitudinal crack at the preformed crack, series D.

The ratios of fracture load to load at the formation of the first longitudinal cracks at the preformed crack are shown in Figure 17. These ratios indicate the reserve strength of a splice after the formation of the first longitudinal cracks. The first longitudinal cracks that developed at the preformed crack continued to extend with further straining of the specimen, and eventually contributed to the complete splitting of the splice at fracture. In the meantime, additional transverse cracks developed and existing ones continued to open. The ability of a splice to resist increased load after starting a longitudinal crack is important. Eighteen-inch or shorter splices are definitely inferior to 20-in. or greater splices in this respect.

TABLE 10

STEEL STRESS FOR 0.05- AND 0.10-IN. CRACK OPENINGS (Series D)

Specimen	Test Age (day)	Crack Opening			
		0.05 In.		0.10 In.	
		Steel Stress (ksi)	No. of Transverse Cracks Formed	Steel Stress (ksi)	No. of Transverse Cracks Formed
DC	1	63.6	10	72.2	10
DC	3	59.0	6	77.1	14
DC	7	62.5	8	72.2	15
DC	14	62.5	5	72.9	20
D24	1	56.2	9	67.8	9
D24	3	67.8	13	-	-
D24	7	63.6	5	72.0	14
D24	14	63.8	2	72.0	14
D20	1	50.0	8	69.8	10
D20	3	59.3	10	72.3	15
D20	7	-	-	-	-
D20	15	70.0	19	72.9	19
D20E	1	53.3	11	65.2	13
D20E	3	50.3	2	63.2	11
D20E	7	59.3	1	62.2	6
D20E	14	64.0	3	66.0	17
D18	1	-	-	-	-
D18	4	-	-	-	-
D18	7	59.3	4	64.4	14
D18	14	61.7	3	72.7	21

TABLE 11

STEEL STRESS FOR 0.05- AND 0.10-IN. CRACK OPENINGS (Series WWF)

Specimen	Test Age (day)	Crack Opening			
		0.05 In.		0.10 In.	
		Steel Stress (ksi)	No. of Transverse Cracks Formed	Steel Stress (ksi)	No. of Transverse Cracks Formed
WWFC	1	38.2	5	57.3	6
WWFC	3	59.5	1	63.7	3
WWFC	7	70.2	2	81.0	7
WWFC	14	67.2	4	68.0	4
WWF27E	1	57.5	7	-	-
WWF27E	3	56.2	2	84.8	8
WWF27E	7	68.5	2	68.5	3
WWF27E	14	60.2	3	68.8	6
WWF26	1	37.2	6	58.5	7
WWF26	3	56.2	2	73.3	7
WWF26	7	63.8	2	65.2	6
WWF26	14	66.5	5	75.8	7
WWF18E	1	37.8	2	-	-
WWF18E	3	47.8[a]	1	50.0[a]	5
WWF18E	7	46.8	2	53.5[a]	2
WWF18E	14	47.0	2	67.0	3
WWF18	1	37.4	2	37.8	4
WWF18	3	44.7	1	63.6	7
WWF18	7	49.0	2	63.3	6
WWF18	14	59.5	6	59.5	7

[a]At preformed crack.

Longitudinal cracks were not observed in the specimens reinforced with welded-wire fabric, except at fracture. In WWF14, 18, and 18E, the concrete above the reinforcement and between the transverse wires in the splice region split apart at fracture (Fig. 13a).

Large Crack Openings

In addition to the ability of a splice to produce transverse cracks in the region away from the splice, the splice should also be capable of opening these transverse cracks in the unspliced region amounts comparable with the crack openings in the unspliced control specimens. A splice is considered satisfactory when it withstands loads at an arbitrary 0.10-in. opening of any transverse crack without opening the preformed crack such amounts. The highest steel stresses (based on 0.6 percent steel) attained and number of transverse cracks formed prior to 0.05- and 0.10-in. openings of any crack are given in Tables 10 and 11. The cases in which the preformed cracks opened 0.05 and 0.10 in. before any other transverse crack opened these amounts are indicated in Table 11. Test specimens WWF14, D12 and D16 fractured before any transverse crack opened 0.05 in. (Tables 5 and 6).

Exclusive of splices at imminent fracture, 0.10-in. cracks did not occur until the stresses exceeded about 60 ksi for both kinds of reinforcement. Steel stresses of 50 ksi or greater in the deformed-bar series and 40 ksi or greater in welded-wire fabric caused 0.05-in. cracks.

Twenty-inch or longer splices in deformed bar and 18-in. or longer in welded-wire fabric were capable of opening some of the transverse cracks to 0.10 in. The number and opening of transverse cracks in the test lengths of specimens having these splices were comparable to the cracking in the control specimens.

Ultimate Strength

In specimens with the preformed cracks located at center of the splices, the preformed cracks opened less than 0.03 in. for deformed-bar and 0.045 in. for welded-wire
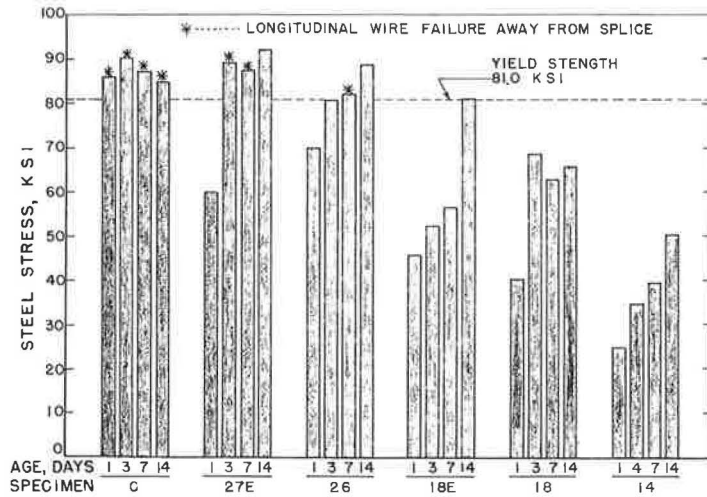
Figure 18. Ultimate strengths, series D.
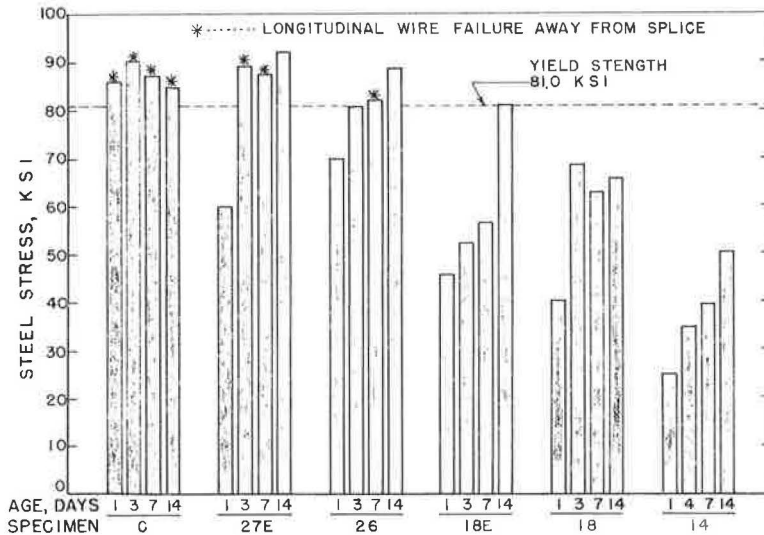
Figure 19. Ultimate strengths, series WWF.

fabric reinforcement. For preformed cracks at the end of the splice and unspliced controls, some preformed cracks opened as much as 0.17 in. for deformed-bar (DC and D20E) and 0.24 in. for welded-wire fabric (WWFC and WWF27E) reinforcement (see Tables 5 and 6). In all specimens reinforced with deformed bars, the preformed crack within the splice opened less than natural transverse cracks until fracure occurred. This was true also of specimens WWF18 and WWF26. Preformed cracks at the ends of the splices in both series behaved like transverse cracks in unspliced reinforcement.

Steel stresses at cracked sections in unspliced regions, series D, were computed from the fracture loads (Fig. 18). Splices 20 in. or longer in deformed bars developed the yield strength of the reinforcement before fracture. Eighteen-inch splices developed

TABLE 12

UNIT BOND STRESS AT ULTIMATE LOAD
(Series D)

Specimen	Age at Test			
	1-Day	3-Day	7-Day	14-Day
D24	454	477	520	528
D20	548	586	491	587[a]
D20E	535	544	575	598
D18	482	507[b]	576	720
D16	440	476	572	593
D12	499	503	592	630
Avg.	493	516	554	609

[a] Fifteen-day age.
[b] Four-day age.

slightly less than the yield strength at one and three days. Ultimate loads for all series D specimens except DC (unspliced) occurred upon fracture of the splice. Transverse crack openings greater than 0.1 in. were obtained for all but three cases of the 20- and 24-in. splices. Tests of specimens DC were terminated at crack openings of 0.1 in. or greater. Thus, only the second part of the third criterion was used in evaluating these splices.

Specimens WWFC, WWF27E-3 and -7, and WWF26-7 failed by tensile fracture of the longitudinal wires in the unspliced region (Fig. 19). WWF26-7 failed at the welds in the splice region on two longi-tudinal wires and the other two of the same fabric failed in tension at a transverse crack away from the splice. WWF14 and WWF26-1 (Fig. 13b) failed by concrete cracking at the transverse wires in the splice. Fractures in the rest of the WWF specimens oc-curred by cracking of the concrete at the transverse wires in the splice accompanying the weld shear failures at the transverse wires. The weld failures were observed by removing broken concrete from the splice area after test. The first part of criterion three (develop ultimate strength of reinforcement) applied only to some of the WWF specimens.

Except at 1-day age, 26- and 27-in. splices developed the yield strength of the reinforcement. The shorter splices were unable to attain the yield strength (Fig. 19).

Average unit bond stresses at ultimate load in series D are given in Table 12. These bond stresses were less sensitive to splice length than the bond stresses at the forma-tion of the first longitudinal cracks at the preformed crack. The average values of the ultimate bond stresses for all splice lengths were 493 psi at 1 day, 516 at 3 days, 554 at 7 days, and 609 at 14 days.

SUMMARY OF RESULTS

Tensile cracking strength of the reinforced concrete slab can be estimated by $0.57 M_r$ or by $5.20 \sqrt{f_c}$ in pounds per square inch, where M_r and f_c are modulus of rupture and compressive strength of the concrete at the time of interest, respectively. Stresses are calculated for the transformed area of the reinforced section.

Horizontal longitudinal cracks occurred in the plane of the reinforcement in speci-mens reinforced with deformed bars. Such cracking originated at transverse cracks in the unspliced portions of the test specimens when steel stresses reached 50 ksi or greater with crack openings of 0.015 to 0.029 in. These longitudinal cracks are indi-cations of bond failure in regions where the tensile stress in the steel decreases sharply in the longitudinal direction from the high values at the transverse crack. The high tensile stress gradient requires high bond stresses in these regions. When bond failure occurs, the tensile stress gradient must decrease, and the strain in a greater length of steel contributes to marked increases in transverse crack opening.

Longitudinal cracking from the preformed crack in the splice appeared at about the same loads as the first natural transverse crack. In the longer splices, however, these longitudinal cracks were short and did not progress further until many additional transverse cracks had formed.

Ultimate average bond strength in deformed-bar splices between 12 and 24 in. in length varied from 493 psi at 1-day age to 609 psi at 14-day age. These values were obtained with average concrete compressive strengths of 1,470 psi at 1-day age to 4,100 psi at 14-day age.

Large openings of transverse cracks, except at fracture of shorter splices, did not occur until the reinforcement yielded. Such large openings were preceded by the de-velopment of many transverse cracks.

Cracks at splices do not open as wide as cracks at the end of splices or in unspliced reinforcement because there is twice as much steel in the splice area.

CONCLUSIONS

On the basis of the three stated criteria, the 20-in. splice length (D20 and D20E) in No. 5 deformed-bar reinforcement was adequate in all respects at all concrete ages. This is a 32-diameter lap. The 18-in. splice (D18), 29-diameter lap, was also adequate based on the first criterion but was on the borderline by the second criterion and did not meet the third at 1- and 3-day ages.

In welded-wire fabric of the size tested, the 26-in. splices (WWF26 and WWF27E) were adequate by all three criteria. The 18-in. splice (WWF18) met only the first criterion.

These experiments, in which loading was continued to failure at early concrete ages, constitute a most severe test of splice strength. Splices adequate by all three criteria will perform as well as the unspliced reinforcement when high stresses occur in the pavement.

ACKNOWLEDGMENTS

Behavior of Experimental Continuously-Reinforced Concrete Pavements In Mississippi

SILVIO J. SPIGOLON
Associate Professor of Civil Engineering and Assistant Director,
Engineering Experiment Station, University of Mississippi

The first two continuously-reinforced concrete pavements constructed by the Mississippi State Highway Department have been designated as experimental sections and are being observed by the University of Mississippi Engineering Station. These pavements contain several design features that are relatively new in this type of construction. This paper describes the performance of the pavements to date.

A description of the design features and the construction methods used for both pavements is presented. Longitudinal movements of the pavement and crack width changes have been measured periodically. Crack surveys have been performed particularly in the early weeks after construction. Data on end movements, crack widths, crack frequency, and methods used for obtaining the data are presented and discussed.

Both pavements are in excellent condition. On the basis of the limited, but very satisfactory, performance of these pavements, several new projects using continuously-reinforced concrete pavement are being constructed and others are being planned.

•THE MISSISSIPPI State Highway Department, with the cooperation of the U. S. Bureau of Public Roads, has designed and constructed several sections of continuously-reinforced concrete pavement. The first two projects were designated as experimental sections and are being observed by the University of Mississippi Engineering Experiment Station. Both pavements contain some form of terminal anchorage and both have been placed on cement-treated bases. In the spring of 1961, the first pavement was completed in De Soto County. The second was completed in April 1962 in Jones County.

DE SOTO COUNTY PROJECT

The De Soto County project is 5.3 miles long and is that portion of I-55 extending from the Tennessee state line southward. It is a four-lane dual roadway facility consisting of ten individual continuously-reinforced concrete pavements, each terminating at a bridge or adjoining pavement. The pavement at the north terminus is a jointed concrete highway constructed by the Tennessee Highway Department. At the south terminus is an asphaltic-concrete pavement. A schematic plan of the project is shown in Figure 1. The lengths of the individual continuous sections, starting at the south end of the project, are 5,164 ft, 6,781 ft, 8,178 ft, 4,756 ft, and 724 ft, respectively, in the west pavement. For the east pavement, the lengths are 5,004 ft, 6,703 ft, 8,256 ft, 4,756 ft, and 724 ft, respectively, from south to north.

Experimental Features

The major experimental features incorporated in the De Soto County project were (a) the use of cast-in-place concrete piles as anchorages to inhibit the seasonal longi-
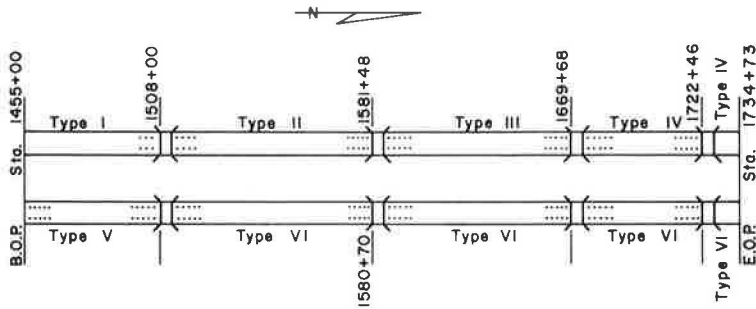
Figure 1. Plan of De Soto County project.

tudinal movements of the ends of the pavement, (b) a comparison of three combinations of pavement thickness and steel percentage, (c) a comparison of four sizes and spacings, of transverse reinforcement, and (d) the use of a cement-treated base.

Table 1 gives the significant characteristics of the various pavement sections. Details of the concrete anchor piles are shown in Figure 2. Ten piles were used at all pavement ends with the following exceptions: (a) eight piles were placed at the south end of the Type II pavement; (b) six piles were used at the north end of the Type I pavement; and (c) the south end of the Type I and the north end of the Type VI, at station 1734+73, were left without pile restraint. This arrangement was used to determine the effectiveness of the various sizes of pile groups.

At each pavement terminus where a pile anchorage was used, a series of eight 20-ft slabs separated by 1-in. doweled expansion joints was placed between the continuously-reinforced concrete pavement and the adjoining bridge or pavement. The slabs were individually reinforced with the same size, arrangement, and percentage of steel reinforcement as the adjoining continuous pavement. Figure 3 shows the arrangement of the pile groups and the terminal slabs. The diameter, depth, and configuration of the piles were originally suggested by Zuk (1) on the basis of model tests.

The spacing of the chair supported transverse rods was varied (Table 1). The transverse reinforcement serves to preserve the integrity of the longitudinal center joint and as a support platform for the longitudinal steel at the slab mid-depth during construction. The objective of field observations at the time of construction, and of subsequent measurements of behavior, was to evaluate the effect of the varied spacings and to determine, if possible, an optimum spacing.

This pavement is located a few miles east of the Mississippi River and roughly parallel to the floodplains bluffs. The surface soils on the bluffs are geologically classified as loess (a wind-blown, clayey silt). Underlying the loess is a layer of sandy gravel of undefined thickness. The loess thickness varies from about 20 ft to zero, depending on local erosion. Because lumping of the loessial subgrade has been a serious problem in this area, a cement-treated base was used.

In cross-section, the roadway consists of a 6-in. cement-treated subgrade, 13 or 14 in. of sand-gravel base, the upper 6 in. of which was cement-treated, and 7 or 8 in. of concrete slab. The total structure thickness, slab and base, is 21 in. All longitudinal reinforcement is No. 6 deformed bars, intermediate or hard grade, 40 ft - 0 in. long, placed at the mid-depth of the slab. Continuity of the reinforcement was obtained by overlapping successive bars 15 in. All overlaps were in line in the transverse direction. The steel was maintained continuous through all construction joints. All of the construction joints also contained a series of 15-in.

TABLE 1

PAVEMENT CHARACTERISTICS

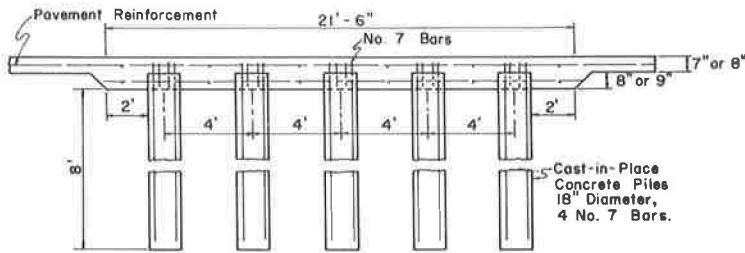| Pavement Type	Thickness (in.)	Longitudinal Reinforcement (%)	Transverse Reinforcement
I	7	0.7	No. 4 bars at 24 in.
II	8	0.6	No. 4 bars at 24 in.
III	8	0.7	No. 3 bars at 18 in.
IV	8	0.7	No. 4 bars at 30 in.
V	8	0.7	No. 4 bars at 36 in.
VI	8	0.7	No. 4 bars at 24 in.

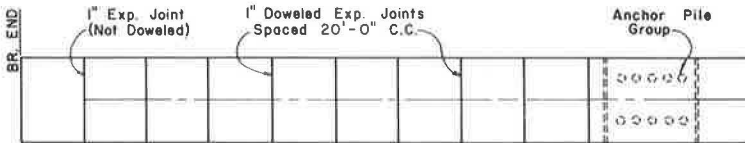Figure 2. Typical detail of pile anchorage (De Soto County).

Figure 3. Typical plan of jointed slabs at pavement ends (De Soto County).

long, 1-in. diameter smooth dowel bars spaced 16 in. center-to-center in the plane of the continuous reinforcement. The construction specifications required that no construction joint could be placed within 5 ft of an overlap in the longitudinal steel.

Two layers of longitudinal reinforcement were used at the anchor pile caps (Fig. 2). The anchor pile reinforcement protruded above the piles and was tied to the pavement reinforcement steel.

Construction Methods and Materials

Cement treatment of the subgrade was started in the summer of 1960. Following the subgrade treatment, a sand-gravel base material was hauled into place. The lack of binder in the granular base was the source of a major construction difficulty. Haul trucks and other construction equipment traversed the unstabilized base only with great difficulty.

Paving was started in October 1960 at station 1628+91 of the west pavement. This point was nearest to the contractor's batch plant and base treatment was only partially completed. Paving proceeded southward in the normal manner, with two Koehring 34-E dual-drum pavers, one on each shoulder. Side forms, chair-supported transverse steel, and longitudinal steel were maintained 500 to 1,000 ft in advance of paving. The concrete was placed through the reinforcing steel to the full depth and full width of the slab. The finishing unit following the spreader provided full-width vibration to the fresh concrete. A split, wooden header board served to form the daily construction joint.

The poor trafficability condition existed until the base cement treatment was completed in the east pavement. The contractor then elected to stop paving at station 1554+07 and moved his operations to station 1455+00 of the west pavement. The two paving mixers were placed in tandem on the east base and the concrete was transported across the median in open buckets by crawler-mounted cranes operating on the shoulders. This method of construction (Fig. 4) was used throughout the remainder of the project.

On December 3, 1960, the project was closed down for the winter. Paving had been completed on the entire west pavement and had progressed from station 1456+60 to station 1491+82 of the east pavement. Work was started again on April 6, 1961, and was completed on May 2, 1961. A typical rate of paving for the major portion of the project was 150 to 180 lin ft per hr.

The anchor piles were emplaced in advance of construction. Holes were bored to
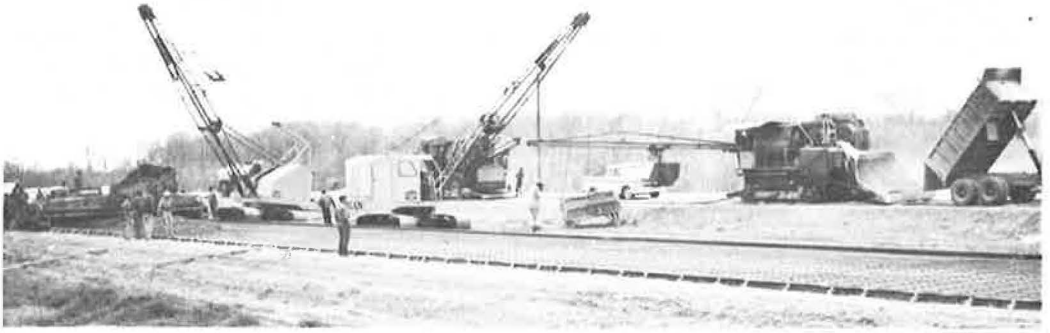
Figure 4. Method used for transport of concrete across median (De Soto County).

18-in. diameter and 8-ft depth by a truck-mounted earth auger. The four No. 7 reinforcing bars were formed in a cage by spiral windings at the top and bottom. The portion of each pile which was to extend into the 16-in. pavement section was formed by the use of a removable sheet metal form. Concrete for the piles was obtained from a local ready-mix concrete supplier and was delivered by mixer truck. Construction traffic was routed around the pile groups at all times. Where cement treatment of the base was not completed before anchor pile placement, mechanical mixing and compaction of the soil-cement were greatly hampered.

Two brands of portland cement were used for the concrete and the soil-cement—Marquette and Missouri Portland. The granular base was treated with 5% cement by volume and was compacted by a tractor-drawn steel-wheel vibratory roller followed by a rubber-tired roller. The concrete mix used was 1:2:3.75. Recorded slumps ranged from 1 to $2\frac{1}{2}$ in. Fine and coarse aggregates were obtained from local borrow pits in the Mississippi River terrace deposits. A white liquid membrane was sprayed on the completed concrete surface for curing. The yield points for eight samples of the No. 6 reinforcing bars ranged from 50,200 to 56,100 psi.

Compression tests of soil-cement cylinders, made from the base material and tested at 28 days, typically ranged from 100 to 400 psi. Concrete cores taken from the pavement had compressive strengths ranging from 4,000 to 8,500 psi at an age of 270 days with an overall average of about 6,000 psi. The modulus of rupture for test beams at 28 days ranged from 550 psi to 800 psi.

Observations of Behavior

The major observations being made on the De Soto County pavement are (a) longitudinal movements, (b) crack widths, and (c) crack spacing.

The seasonal longitudinal movements of the ends of each pavement and of selected points in the interior of several sections are being measured to the nearest 0.01 in. Each measurement point consists of a 10-ft deep, concrete encased pipe monument placed 1 ft from the pavement edge and a pair of brass gage plugs imbedded in the pavement surface. A measurement device is located on the gage plugs and leveled. A movable arm from the device is extended out to a vertical extension inserted in the pipe monument. At the end of the movable arm is a cross bar to which a vernier caliper is attached. Longitudinal movements are recorded as the movement of the device, and of the pavement, relative to the monument.

Over 100 cracks in the entire project have been gaged for observation of seasonal changes in surface crack width. Gage plugs were imbedded in the pavement surface on each side of each designated crack in the manner prescribed in HRB Circular 372 (2) and measurements have been made with a Soiltest multi-position strain gage. All measurements are referenced to a standard invar steel bar. Initial, absolute crack

widths have been measured at the surface with a microscope containing an etched objective lens.

Periodic crack surveys were started for each pavement section soon after its construction. The location of every crack in the entire project has been located to the nearest 0.1 ft at the outside pavement edge. As each new crack was located, it was marked with a small spot of traffic marking paint at the outside pavement edge, thereby removing the need for re-measurement in subsequent surveys.

Visible transverse cracks began appearing on the pavement surface and sides as soon as 3 days after construction of a slab section. In the west pavement (placed from October to December 1960), the average crack spacing ranged from 5 ft to 10 ft for the various sections. The east pavement (placed in spring 1961) showed a slower rate of cracking during the first few months after construction. This was undoubtedly due to the lack of cold weather. After two or more years in place, and two or three winter seasons, crack spacings have apparently stabilized so that the effect of placement season cannot be differentiated. Table 2 presents the results of a crack survey performed in the spring of 1963. With the possible exception of the zones within 1,000 ft from the pavement ends, all sections and pavement types show approximately the same average crack spacing.

For each pavement type, groups of four cracks were gaged (a) in the center of a day's pour near the center of a pavement section, (b) following a construction joint, and (c) 400 to 500 ft from an end. The first three cracks from each pavement end were also gaged. For the short (724-ft) sections at the north end of the project, six cracks were gaged near the center of the slab lengths.

The variation of crack width with temperature and time for the four gaged locations for the two southernmost sections in the east and west pavements is shown in Table 3. Values are for the average of the three or four gaged cracks at each location.

Each value (Table 3) is the result of two separate types of measurement: (a) establishment of the "true" surface crack width at one time by the use of a direct reading microscope, and (b) observation of changes in the "true" surface crack width by measurement of changes in distance between gage plugs on each side of the crack. Of the two measurements, the crack width change is by far the more reliable. The establishment of a "true" surface crack width was hampered by the indistinct surface edges and by the apparent lack of uniformity in width over even short lengths of each crack. Each microscope measurement used was the average of ten readings in the line of the gage plugs. Moreover, crack width is not uniform with depth. In several instances, observations of cores taken from cracks showed that the cracks extended downward only to the depth of the reinforcement. In most of the cores, however, the cracks extended the full depth of the slab.

Recognizing such limitations in the data, several tentative, general conclusions can be drawn regarding crack widths. All surface crack widths measured are reasonably small. No significant differences can be shown between the crack widths for the various experimental pavement designs. This is undoubtedly due, in great part, to the relatively small variation in the pavement design variables compared to the larger, normal variation in width of the individual cracks or groups of cracks. A variation in crack width occurs as a function of ambient temperature. However, there is also a distinct trend for the average crack widths to increase with time. The temperature effect may be seen, for example, by comparing the readings for January 1963 and March 1963. The time effect may easily be seen by comparing the width changes from August 1961 to August 1962 to June 1963, all of which were measured at about the same air temperature. Whether or not this trend will continue remains to be seen.

The effectiveness of the concrete piles as terminal anchorages is shown by the end movement measurements (Fig. 5). A comparison is made of the observed longitudinal movements of the ends of selected pavement sections. The air temperature recorded at the time of the individual measurements is also shown. All movements have been referenced to an initial "zero" reading in May 1961. The effect, or lack of effect, of the end movements on the crack pattern adjacent to the end is shown in Figure 6, in which the actual location of each visible crack has been plotted to scale for the first 300 ft of several pavement ends. No conclusions regarding the effect of end movement on cracking have been made.

TABLE 2

CRACK SURVEY RESULTS

Pavement Type	Station Limits	Date Paved	Paving Temperature (°F)	Avg. Crack Spacing (ft)	Avg. Crack Spacing for Type (ft)
I	1455+00 – 1459+19	10/29/60	42 – 64	4.1	
	1459+19 – 1468+22	10/31/60	40 – 62	4.0	
	1468+22 – 1482+14	11/ 1/60	45 – 72	4.0	
	1482+14 – 1495+82	11/ 2/60	45 – 72	4.6	
	1495+82 – 1506+64	11/ 3/60	45 – 65	4.7	4.3
II	1511+86 – 1526+22	11/ 4/60	40 – 65	5.8	
	1526+22 – 1530+44	11/ 5/60	40 – 60	5.0	
	1530+44 – 1541+90	11/ 7/60	44 – 60	5.6	
	1541+90 – 1554+07	11/ 8/60	40 – 58	3.9	
	1554+07 – 1564+44	10/24/60	45 – 78	5.6	
	1564+44 – 1575+86	10/22/60	40 – 71	4.6	
	1575+86 – 1579+68	10/21/60	40 – 63	7.5	5.1
III	1586+10 – 1592+58	10/20/60	40 – 54	5.0	
	1592+58 – 1599+78	10/18/60	55 – 83	5.3	
	1599+78 – 1613+22	10/17/60	58 – 78	4.6	
	1613+22 – 1621+08	10/15/60	68 – 77	5.1	
	1621+08 – 1625+00	10/13/60	75 – 82	4.9	
	1625+00 – 1628+91	10/12/60	68 – 78	6.4	
	1628+91 – 1639+76	11/14/60	50 – 62	5.3	
	1639+76 – 1655+60	11/15/60	47 – 70	5.1	
	1655+60 – 1663+98	11/16/60	42 – 64	4.9	
	1663+98 – 1667+88	11/17/60	50 – 77	5.8	5.1
IV	1673+11 – 1678+46	11/17/60	50 – 77	4.6	
	1678+46 – 1690+99	11/18/60	50 – 72	5.1	
	1690+99 – 1706+99	11/19/60	50 – 75	5.6	
	1706+99 – 1720+67	11/21/60	45 – 57	5.8	5.4
IV	1725+89 – 1733+13	11/22/60	50 – 72	5.8	5.8
V	1456+60 – 1463+50	11/25/60	45 – 63	7.4	
	1463+50 – 1475+44	11/26/60	41 – 59	5.4	
	1475+44 – 1480+22	12/ 2/60	45 – 52	7.5	
	1480+22 – 1491+82	12/ 3/60	50 – 61	5.0	
	1491+82 – 1495+48	4/ 6/61	45 – 55	3.8	
	1495+48 – 1503+07	4/ 7/61	44 – 64	5.0	
	1503+07 – 1506+64	4/ 8/61	45 – 55	10.8	5.5
VI	1511+86 – 1514+07	4/ 8/61	45 – 55	7.9	
	1514+07 – 1526+26	4/10/61	42 – 56	4.4	
	1526+26 – 1538+00	4/11/61	50 – 61	5.6	
	1538+00 – 1548+51	4/13/61	52 – 65	5.7	
	1548+51 – 1561+17	4/14/61	50 – 61	4.6	
	1561+17 – 1571+60	4/17/61	41 – 59	4.5	
	1571+60 – 1578+90	4/18/61	56 – 63	6.0	5.1
VI	1585+32 – 1587+70	4/18/61	56 – 60	4.9	
	1587+70 – 1603+56	4/19/61	60 – 75	5.3	
	1603+56 – 1621+56	4/20/61	58 – 78	5.0	
	1621+56 – 1640+06	4/21/61	59 – 78	6.1	
	1640+06 – 1657+06	4/24/61	54 – 78	8.5	
	1657+06 – 1667+88	4/25/61	58 – 82	5.8	5.9
VI	1673+11 – 1690+42	4/26/61	58 – 78	4.8	
	1690+42 – 1706+02	4/27/61	57 – 82	3.9	
	1706+02 – 1717+02	4/28/61	62 – 80	4.9	
	1717+02 – 1720+67	5/ 2/61	48 – 64	5.3	4.5
VI	1725+89 – 1733+13	5/ 2/61	48 – 64	6.0	6.0

The 1963 winter to summer movement for the unrestrained end of the short, Type VI section at the north end of the east pavement has been about 1.05 in. In all other respects, the movement pattern with time and temperature change has been the same as shown for station 1455+00 (west pavement, unrestrained south end of the Type I pavement). The difference in movement is probably due to the presence of the jointed concrete pavement at the north terminus as opposed to the asphalt pavement at the south end of the project. The movement patterns of all the pile restrained ends not shown in Figure 5 are quite similar in configuration and magnitude to those for the ends of the Type V pavement. The recorded end movements range from 0.30 to 0.75 in. In the overall pattern, there appears to be a trend toward a slight permanent elongation with time.

TABLE 3

CRACK WIDTH MEASUREMENTS, DE SOTO COUNTY

Pavement Type	Date and Air Temperature (°F)							
	Aug. 1961, 78-81	Nov. 1961, 45-50	Feb. 1962, 40-45	Aug. 1962, 76-89	Jan. 1963, 20-32	Mar. 1963, 67-74	June 1963, 88-90	Aug. 1963, 91-97
(a) Center of Day's Work in Center of Section (in.)								
I	0.016	0.016	0.012	0.008	0.020	0.015	0.014	0.018
II	0.010	0.008	-	0.006	0.014	0.011	0.012	0.012
V	0.011	-	-	0.013	0.024	0.017	0.016	0.017
VI	-	-	-	0.012	0.023	0.020	0.019	0.022
(b) Following a Construction Joint (in.)								
I	0.007	0.012	0.014	0.008	0.024	0.018	0.021	0.020
II	0.007	0.011	-	0.009	0.023	0.017	0.019	0.017
V	-	-	-	0.009	0.031	0.022	0.017	0.019
VI	-	-	-	0.008	0.015	0.012	0.013	0.010
(c) 400-500 Ft from End (in.)								
I	0.006	0.009	0.011	0.006	0.020	0.013	0.014	0.012
II	0.003	0.006	-	0.008	0.020	0.012	0.013	0.006
V	-	-	0.012	0.009	0.026	0.018	0.018	0.018
VI	-	-	-	0.008	0.022	0.016	0.016	0.020
(d) First Three Cracks from End (in.)								
I	-	-	-	0.011	0.023	0.018	0.024	0.023
II	0.007	0.009	-	0.010	0.020	0.016	0.024	0.019
V	0.006	-	0.011	0.006	0.020	0.013	0.018	0.014
VI	-	-	-	0.010	0.017	0.018	0.022	0.025
(e) Center of Short Sections at North End of Project (in.)								
IV	0.008	0.015	-	0.012	0.027	0.027	0.027	0.025
VI	-	-	-	0.011	0.022	0.024	0.023	0.019

All terminal joints appear to be functioning well except at station 1455+00 of the west pavement. Here the unrestrained pavement end occurs directly against an asphalt pavement with no joint filler or load transfer device used. Cold weather contraction causes the junction to open more than $1\frac{1}{2}$ in. In the summer heat, the juncture space is completely closed. The long-term effect of this condition can only be surmised at this time.

At an age of three years, the De Soto County project appears in very good condition. No extra-large cracks or other failures directly attributable to the pavement design or behavior have occurred. A road roughness survey performed when the pavement was one year old showed a surface smoothness rated at very good to excellent for riding qualities.
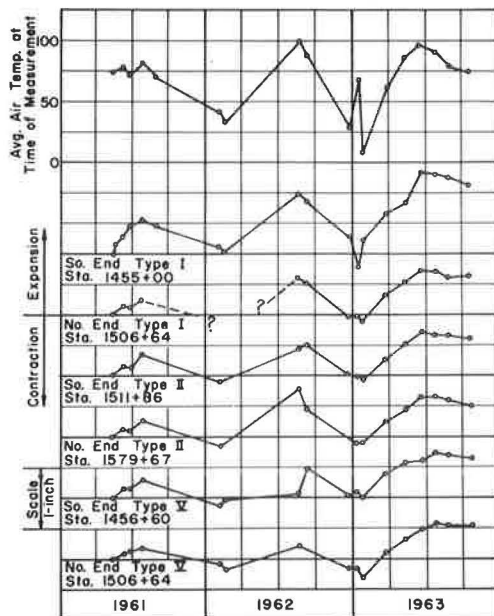

Figure 5. Measured longitudinal movements of various pavement ends (De Soto County).
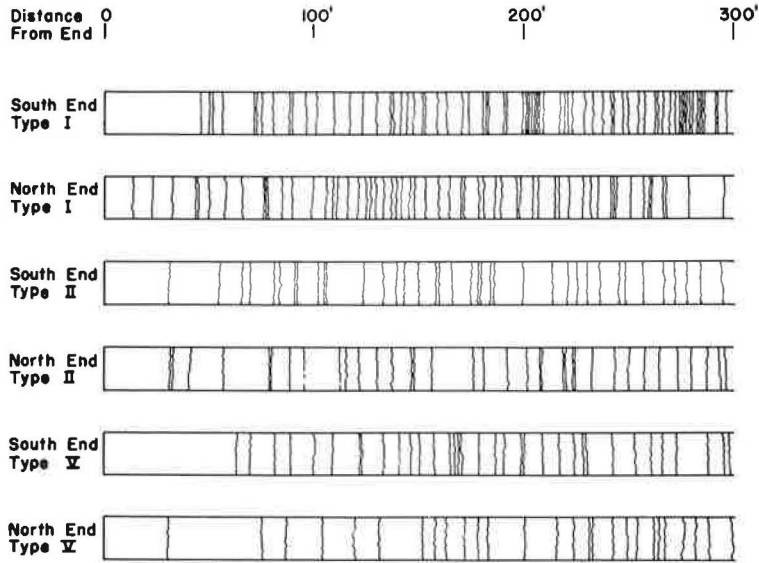
Figure 6. Crack pattern for first 300 ft for various pavement ends (De Soto County).

JONES COUNTY PROJECT

The second continuously-reinforced concrete pavement in Mississippi is in Jones County, in the south-central part of the State. This project is a 6.77-mi section of I-59 extending from Ellisville to Moselle. The project consists of two parallel, 24-ft pavements separated by a variable width median . Each pavement consists of two 12-ft wide traffic lanes. A uniform 8-in concrete thickness was used throughout the project. The experimental section begins at a jointed pavement at its south terminus and ends at a bridge at its north terminus. The pavement is continuous over the entire 6.77-mi length which, according to available information, makes this the longest section of unbroken, continuously-reinforced concrete pavement constructed to date.

Experimental Features

The major experimental features of the Jones County project were (a) use of concrete lug anchors as a means of terminal restraint; (b) a side-by-side comparison of wire-mesh and deformed-bar reinforcement, for each of three steel percentages; (c) use of a cement-treated base; and (d) use of a diagonal-lap configuration in the deformed-bar reinforcement.

The characteristics of the various pavement designs incorporated in the project are given in Table 4. The six pavement types are of equal lengths. A plan of the project is shown in Figure 7. The narrower median width was used where two local roads pass over the project.

TABLE 4
PAVEMENT CHARACTERISTICS, JONES COUNTY

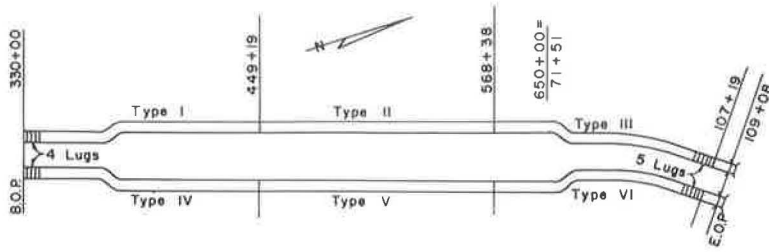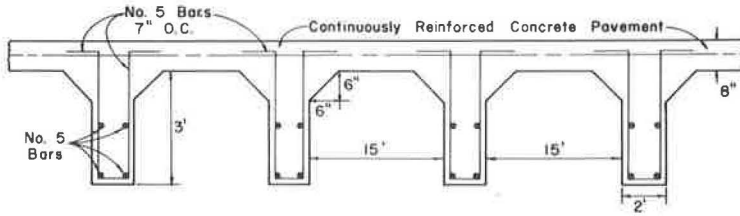| Pavement Type	Long. Reinf. (%)	Long. Reinf. Type	Transverse Reinf.
I	0.5	No. 6 bars	No. 4 bars at 30 in.
II	0.6	No. 6 bars	No. 4 bars at 30 in.
III	0.7	No. 6 bars	No. 4 bars at 30 in.
IV	0.5	No. 5/0 wire mesh	No. 1 wire at 12 in.
V	0.6	No. 5/0 wire mesh	No. 1 wire at 12 in.
VI	0.7	No. 7/0 wire mesh	No. 00 wire at 12 in.

Figure 7. Plan of Jones County project.

Figure 8. Typical detail of concrete lug anchors (Jones County).

The design of the full pavement-width lugs (Fig. 8) is very similar to that used (3) in several of Texas' continuously-reinforced concrete pavements. Four lugs were used at the south end of the project and five were used at the north, bridge end of both pavements. A series of eight 21-ft jointed slabs was placed between the bridge and the end of the continuously-reinforced concrete pavements at the north end of the project. The slabs were separated by 1-in. doweled expansion joints, had a uniform 9-in. thickness, and were reinforced with No. 00 ga. (longitudinal) and No. 4 ga. (transverse) wire mesh. The south end of the project abuts directly against a jointed concrete pavement. This pavement has the same thickness and reinforcement as the bridge-end terminal slabs except that the distance between the 1-in. doweled expansion joints is 63 ft 9 in. No contraction joints were provided. The slabs rest on a cement-treated base prepared in the same manner as that for the continuously-reinforced pavement. The arrangement of the anchor lugs at the pavement ends is shown in Figure 9.
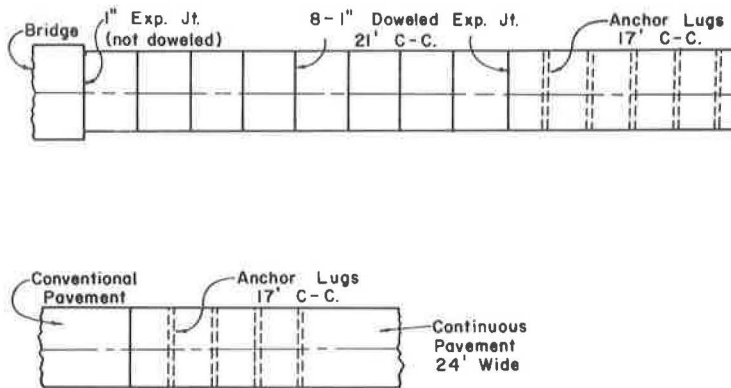

Figure 9. Typical plans at ends of pavement (Jones County).

In cross-section, the entire pavement consists of a uniform 8-in. concrete slab resting directly on a prepared subgrade, the upper six inches of which were cement-treated to form a base course. The west pavement is reinforced with No. 6 deformed bars, 40 ft 0 in. long, overlapped 15 in., and placed at the mid-depth of the slab. The wire mesh mats in the east pavement were 11 ft 6 in. wide and 24 ft 0 in. long, one in each traffic lane, overlapped 13 in., and placed 3 in. below the pavement surface. The effective overlap of the first cross-wires in the succeeding mats was 1 in.

Because of the possibility of failure at the overlaps in the bar reinforcement, the laps were formed at a 30° angle to the transverse steel rather than parallel to it as in the De Soto County project. The laps in the mesh reinforcement were in line across the pavement.

Construction Methods and Materials

The cement-treated base was mixed and compacted in fall 1961. Concrete paving was started on January 1, 1962, at the north end of the east pavement and proceeded southward until completion on February 27, 1962. The west pavement was placed (north to south) between March 5 and April 3, 1962.

The anchor lug trenches were dug by hand prior to concrete placement. After the lug reinforcing steel was in place, paving was started. Two concrete mixers were used in tandem. The forward paving mixer was a Koehring Tribatch, triple-drum mixer operating on the prepared base. The concrete was placed full width of the pavement and struck off 3 in. below the proposed pavement surface. A series of No. 4 deformed bars, 30 in. long, were spaced 30 in. apart across the centerline to tie the longitudinal joint. The rear mixer, operating on the shoulder, was a Koehring 34-E dual-drum unit used to place the remaining 3 in. of concrete. The combination spreader-finisher used on the project contained a series of submerged vibrators located on 3-ft centers.

The paving procedure for the bar-reinforced west pavement differed slightly from that used in the east pavement. The longitudinal reinforcement was tied to the chain-supported transverse bars and was maintained at least 500 ft in advance of concrete placement. The contractor's two paving mixers were operated simultaneously, in tandem, on the inside shoulder. As before, the anchor lugs were cast monolithically with the pavement. Placement of the reinforcing bars is shown in Figure 10. Concrete was placed in the full width of the pavement and to full depth through the reinforcement.
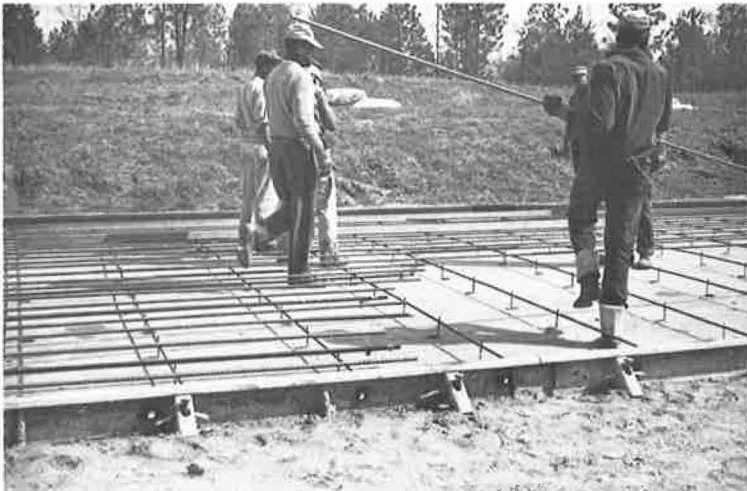

Figure 10. Placement of bar reinforcement in west pavement (Jones County).

Construction joints throughout the project were formed with a split, wooden header. No construction joint was allowed within 5 ft of any overlap in the longitudinal reinforcement. No additional longitudinal steel or load transfer devices were used at the construction joints.

The location of overlaps in the longitudinal reinforcement was measured and recorded for the entire project, for possible use in future studies of cracking tendencies at the laps.

The concrete mix used was 1:2.2:3.75. Recorded slumps ranged from 1 to 2 ½ in. Two brands of cement were used on the project—Ideal and Lone Star. Local sand and gravel were used as concrete aggregates. A white liquid membrane was sprayed on the completed concrete surface for curing.

The cement-treated base course was 28 ft wide and 6 in thick. Portland cement was added in the amount of 7 percent by volume. A mandatory 7-day curing period was used before traffic was allowed on the base. Curing was effected by a seal coat of asphalt emulsion.

Compression tests of concrete cores showed compressive strengths ranging from 6,000 psi to 10,500 psi at an age of 6 months. The overall average compressive strength was approximately 8,000 psi. The modulus of rupture for test beams at 28 days ranged from 750 psi to 1,150 psi.

Observations of Behavior

The field observations performed on this project are as follows: (a) longitudinal movements, (b) crack widths, and (c) crack spacing.

The measurement techniques and instrumentation are essentially the same as those used in the De Soto County project and were as previously described (2). The pavement ends and selected interior points are being measured for longitudinal, seasonal movements. Crack widths are being measured (a) 400 to 500 ft from each pavement end, (b) following a construction joint, and (c) in the center of a day's pour in the center of a test section for each of the six pavement designs. Cracks have been gaged in groups of four. Crack surveys are being performed on about 60 percent of the total project. Each individual survey section encompasses a complete day's pour.

Crack surveys were performed periodically for each designated section, starting immediately after construction. Visible cracks appeared in most sections within two or three days after construction. However, in the bar-reinforced west pavement, some sections did not show cracking for up to two weeks after construction. The west pavement was placed in warm, spring weather. Apparently, such shrinkage cracks as did form were so small as to be invisible to the naked eye. About 30 days after construction, most of the pavement sections showed crack spacings in the range of 8 to 15 ft for both pavements. Exceptions to this occurred at the pavement ends, the final 1,000 ft more-or-less, and at the north end of the mesh-reinforced pavement. This area was paved first, during an extremely cold winter. Several thousand feet of pavement in the interior of the Type VI showed almost no cracks even after 60 days.

By December 1963, the entire project had experienced at least one winter season. The results of a crack survey performed at this time are given in Table 5. The mesh-reinforced east pavement performed as expected; the crack frequency was greater for the higher steel percentage. On the other hand, the bar-reinforced west pavement showed average frequencies which indicate no effect of steel percentage. Whether this situation will persist with time remains to be seen.

Crack width measurements were accumulated in the same manner as for the De Soto County project. This information has not yet been developed to the point that definite trends can be established. The normal crack widths are, by visual inspection, of the same order of magnitude as those reported for the De Soto County project (Table 3).

The pattern and magnitude of longitudinal movements of the ends of the pavements are shown in Figure 11. The air temperatures were recorded at the time of the individual measurements. It is too early to estimate long-term trends. No reason can now be given for the difference in the behavior of the 4-lug and 5-lug ends. Possibly, the jointed concrete pavement at the 4-lug end offers a greater restraint than the bridge approach slabs and the bridge offer to the 5-lug end.

TABLE 5

JONES COUNTY CRACK SURVEY, DECEMBER 1963

Pavement Type	Station Limits	Date Paved	Paving Temp. (°F)	Avg. Crack Spacing (ft)	Avg. Crack Spacing for Type (ft)
I	330+00 - 334+53	4/ 3/62	50-55	6.0	
	334+53 - 347+70	4/ 2/62	50-63	4.9	
	364+53 - 381+97	3/29/62	66-85	8.3	
	381+97 - 400+39	3/28/62	58-82	5.9	
	400+39 - 420+90	3/27/62	50-76	6.0	
	420+90 - 440+60	3/26/62	56-73	6.6	6.2
II	440+16 - 464+32	3/23/62	52-75	7.8	
	464+32 - 484+05	3/22/62	54-65	5.2	
	484+05 - 508+13	3/21/62	60-80	6.4	
	524+46 - 540+54	3/19/62	52-75	8.6	6.7
III	560+69 - 571+36	3/14/62	48-51	5.0	
	589+05 - 606+10	3/12/62	45-68	6.5	
	606+10 - 622+88	3/ 9/62	64-78	7.4	
	644+35 - 86+88	3/ 7/62	39-56	6.6	
	100+09 - 107+19	3/ 5/62	42-51	5.1	6.2
IV	330+14 - 333+91	2/27/62	68-84	7.5	
	333+91 - 351+50	2/26/62	75-84	9.1	
	351+50 - 362+71	2/17/62	49-68	8.4	
	362+71 - 377+80	2/16/62	50-64	8.2	
	396+59 - 416+45	2/12/62	54-78	7.1	8.0
V	449+81 - 462+64	2/ 7/62	42-58	7.0	
	462+64 - 482+82	2/ 5/62	60-75	7.5	
	495+40 - 513+88	2/ 2/62	49-75	7.6	
	549+06 - 567+15	1/30/62	50-70	7.0	7.3
VI	587+35 - 601+05	1/24/62	50-70	6.0	
	607+67 - 621+44	1/17/62	40-53	6.4	
	621+44 - 626+93	1/ 9/62	35-47	5.1	
	626+93 - 639+52	1/ 8/62	42-57	3.0	
	77+42 - 91+94	1/ 3/62	26-58	7.3	
	97+00 - 103+65	1/ 2/62	26-51	4.1	
	103+65 - 107+19	1/ 1/62	37-42	3.3	4.9

With the exception of the extra-wide cracks, the entire project appears to be in excellent condition. No problems have been encountered in the bar-reinforced west pavement. Riding qualities of the project are very good to excellent on the basis of roughometer tests.

Extra-Wide Cracks

Soon after the construction of several sections of the mesh-reinforced east pavement, a series of ten abnormally wide cracks was located. Nine of the ten were located in the Type VI section which contains 0.7 percent steel. The other was found in the Type IV design, 0.5 percent steel. All of the cracks occurred at overlaps in the wire mesh and were typically $\frac{1}{4}$ in. or more wide. Repair of these sections was effected during the summer of 1962. In each instance, a 30-in. wide zone of concrete (full pavement width) was removed to the depth of the steel reinforcement. Half-inch deformed bars were welded to the mesh mats on both sides of the crack at each longitudinal wire. The entire opening, steel and concrete, was then coated with an epoxy cement and a high-early strength concrete was placed to fill the gap. After $1\frac{1}{2}$ yr, all of the repairs appear to be in excellent condition.

No reason can be given at this time for the occurrence of the cracks. At first appearance, the blame should be laid on the very short overlap of the mesh sheets. With a 13-in. overlap and 24-ft lengths, approximately 4.75 percent of the pavement length contains overlapped wires. Yet, of all the cracks that had been located at the time of the failures, only 3.3 percent occurred in overlapped areas. Moreover, of all the overlaps in the surveyed zones, only 6.2 percent of the laps had visible cracks in their lengths. With the exception of the 10 extra-wide cracks, all other cracks at laps appeared to be of the same size as those in the other sections. This highly simplified analysis would tend to indicate that there is no greater tendency for cracks to occur at the overlaps than anywhere else in the pavement.

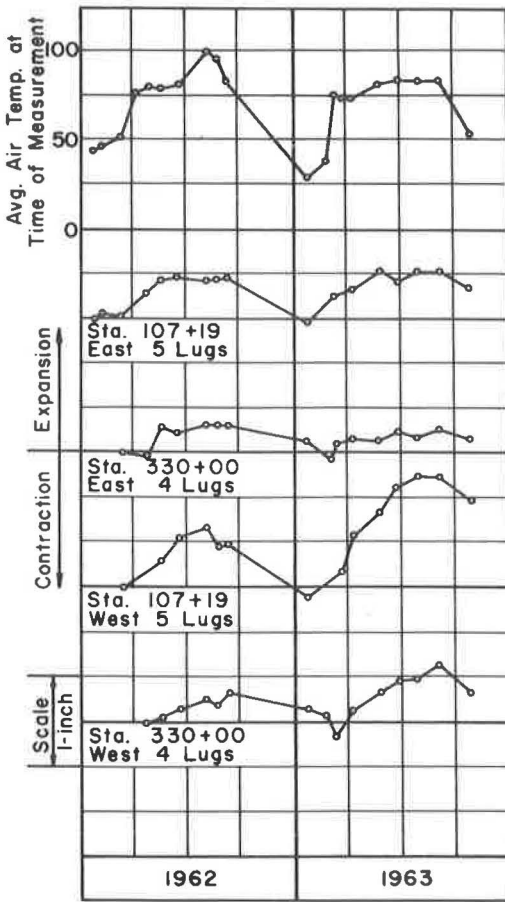Figure 11. Measured longitudinal movements of pavement ends (Jones County).

GENERAL DISCUSSION

The results of the measurements and general observations concerning the long-term behavior of the two Mississippi projects are being recorded and reported to the U. S. Bureau of Public Roads by the Mississippi State Highway Department as part of a nationwide correlation study of continuously-reinforced concrete pavements. Although other such pavements have furnished much valuable information, there are many questions still remaining which can only be answered by additional experimental pavements of the type Mississippi has constructed. In addition to the primary experimental features, there are several characteristics of the Mississippi projects which do not lend themselves to direct measurement. During certain periods in the winter season, the De Soto County pavement experiences almost daily freeze-thaw cycles in contrast to the more northern states where only a few such cycles occur in any one year. The southern states, including Mississippi, have a winter construction season. Continuously-reinforced concrete pavements placed in cold weather should experience lower tensile stresses and higher compressive stresses due to temperature change than pavements placed in the summer. Further more, it is believed that the Mississippi pavements are the first to be placed on a soil-cement base, and in De Soto County, the first to use concrete piles as a means of end anchorage.

On the basis of the short-term, but satisfactory, performance of the two projects discussed in this report certain general statements can be made.

1. The steel percentages and pavement thicknesses used in these projects have given satisfactory performance. Although differences in crack frequency have occurred due to varied steel ratios, no detrimental behavior due to insufficient steel percentage or pavement thickness has been found.

2. Because of the satisfactory performance of the De Soto County project, no valid argument can be presented for the diagonal-lap configuration of the deformed-bar reinforcement. However, the diagonal arrangement is no more costly than the straight-across configuration.

3. In the De Soto County pavement, no clear evidence can be found for using smaller transverse bar spacings than 36 in. It is probable that even larger spacings could be used, perhaps limited only by that distance that would allow significant vertical movements of the longitudinal bars during concrete placement.

4. The concrete anchor piles used in De Soto County appear to be restraining the slab ends satisfactorily. On the basis of the limited data available, it would appear that pile groups of 6 or 8 piles are sufficient to maintain reasonable end restraint.

5. The concrete anchor lugs used in Jones County appear satisfactory as a means of terminal restraint.

6. The 7-in. pavement thickness used in De Soto County appears to be serving as satisfactorily as the 8-in. pavements. This may be due to the presence of the cement-treated base. There is a possibility that even thinner pavements may be used provided they are placed on a strong base.

ACKNOWLEDGMENTS

REFERENCES

1. Zuk, William, "Analysis of Special Problems in Continuously-Reinforced Concrete Pavements." HRB Bull. 214, pp. 1-21 (1959).
2. "Recommendations for Experimental Continuously-Reinforced Concrete Pavements." HRB Committee on Rigid Pavement Design, Circular 372, (Nov. 1958).
3. Subcommittee VII, ACI Committee 325, "Second Progress Report—Continuously Reinforced Concrete Pavements." ACI Journal, Proc., 59:1569-86 (Nov. 1962).

Construction of a Continuously-Reinforced Concrete Pavement in South Dakota

ROBERT A. CRAWFORD and DONALD W. ANDERSON
   Assistant Physical Research Engineers, South Dakota
   Department of Highways, Pierre

•THIS REPORT is primarily concerned with the environment, design, construction, and testing program of two continuously-reinforced concrete test sections constructed in South Dakota in 1963.

The two sections, portions of Interstate Highway Project I90-9(11)395, are located approximately four miles northwest of Sioux Falls and are approximately 3,400 and 4,400 ft long. Figures 1 and 2 show the general location of the project and the location of the test sections within the project.

This project contains two experimental features: (a) the depth of longitudinal steel beneath the surface of the concrete, and (b) the method of controlling end movement. Pavement thickness and quantity of steel were held constant throughout both continuously-reinforced sections.

Section 1 was constructed as part of the eastbound lane and Section 2 the westbound lane. The opposite lanes paralleling the test sections were considered as control sections and were of standard South Dakota design. Both the test control sections were included in the same project and constructed by the same contractor.

Average daily traffic for 1958 was estimated at 4,576 vehicles, and for 1975 it was
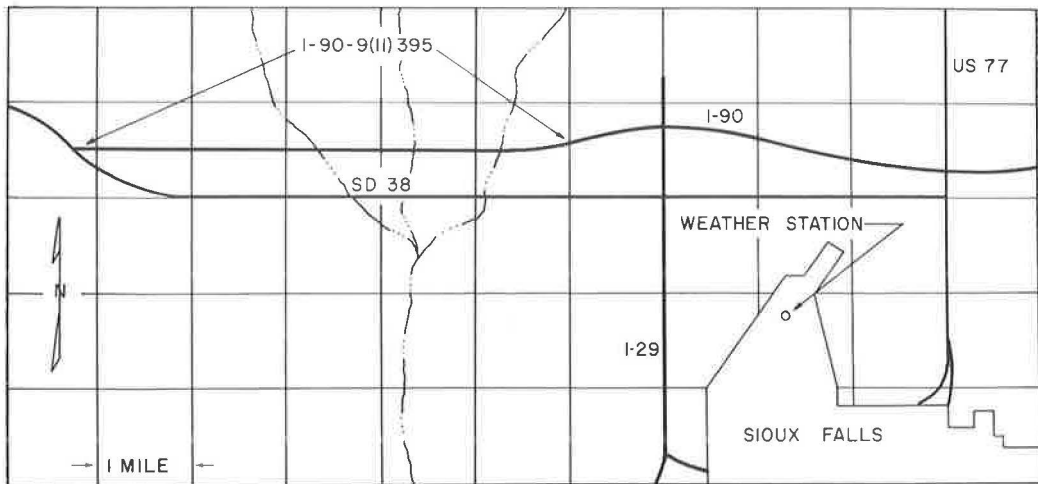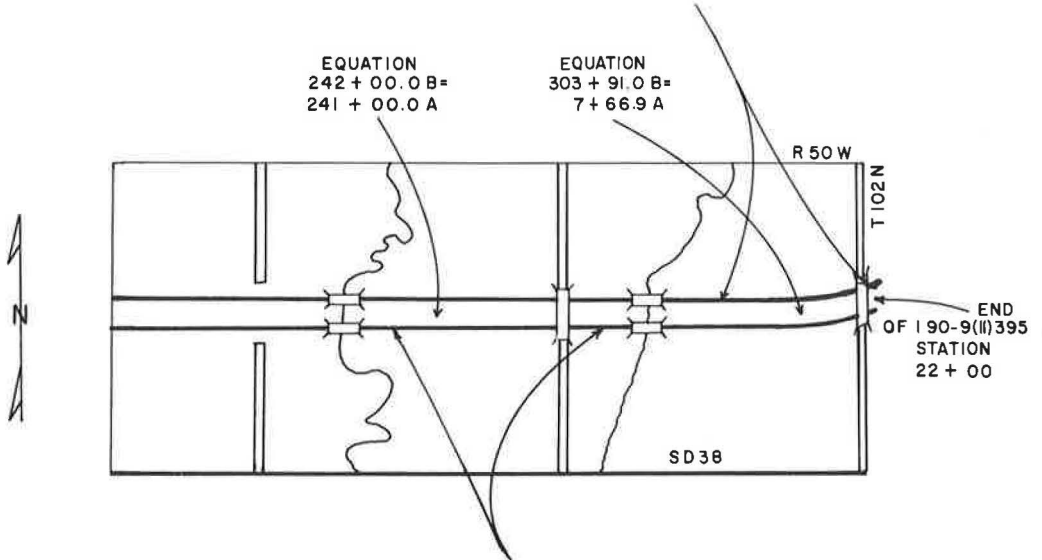

Figure 1. Location of project I-90-9(11)395 containing continuously-reinforced test sections.

CONTINUOUSLY REINFORCED CONCRETE PAVEMENT
TEST SECTION NO. 2
STATION 282 + 65.03 TO STATION 20 + 60.5
(WESTBOUND LANES)

Figure 2.   Location of test sections within project.

TABLE 1

TEST SECTION MATERIALS DATA

No. of Samples	AASHO Soil Group and Index	Passing 200 Sieve Range (%)	Passing 200 Sieve Avg. (%)	Liquid Limit Range	Liquid Limit Avg.	Plasticity Index Range	Plasticity Index Avg.	Geological and Pedological Description
25	A-6 (8) to A-7-6(16)	90-100	97	33-47	36	11-26	16	Moody-Nora silty clay loam
5	A-6 (9) to A-6 (11)	98-99	98	34-39	36	13-17	15	Nora-Crofton silt loam
1	A-6 (13)	91	91	40	40	22	22	Rowena silty clay loam
2	A-6 (9)	94-95	94	34	34	14	14	Local alluvial land, fans

(a) Subbase

Gradation Specifications (% passing)

2-In.	1-In.	¾-In.	¼-In.	No. 10	No. 40	No. 200	Liquid Limit	Plasticity Index
100	80-100	—	40-75	25-55	10-40	0-20	—	Less than 10
—	—	100	50-80	35-65	0-40	0-15	Less than 25	Less than 4

(b) Concrete

Aggregate Type Coarse	Aggregate Type Fine	Max. Size of Coarse Aggregate	Cement Factor	Air Entrained	Slump (in.) Range	Slump (in.) Avg.	Compressive Strength Age (days)	Compressive Strength Range	Compressive Strength Avg.	Flexural Strength Age (days)	Flexural Strength Range	Flexural Strength Avg.
Crushed stone quartzite	Sil. sand	2-in.	1.39 bbl and 1.39 lb pozzo-lith per cu yd	Yes 3-6%	1¼-3	1¾	28	4,735- 6,995	5,771	28	616- 783	726

(c) Longitudinal and Transverse Reinforcing Steel

Type	Grade	Bar Size	Tensile Strength Yield Point Range (psi)	Tensile Strength Yield Point Average (psi)	Percent Elongation Range	Percent Elongation Average
Billet	A-432-62T	No. 5	71,780-63,860	67,820	11.72-15.62	13.67

Figure 3. Water standing in poorly drained channel between sections.

estimated to be 10,799 vehicles per day including 8 percent commercial vehicles. (A 15-min, 16-mm color movie has been made showing all phases of construction. It is available through the Physical Research Division, South Dakota Department of Highways.

ENVIRONMENT

Soils throughout the project area are silt loams and silty clay loams developed from loess. Soil classification shows the majority of them to be A-6 with an occasional A-7-6. Group indexes ranged from 9 to 11. Liquid limits of the soils ranged from 30 to 50. A description of soil samples and their test results are given in Table 1.

Drainage is generally good throughout the test section areas. Natural slopes vary from 1 to 7 percent with the general drainage toward the south. A poorly drained channel crosses the project between the two continuously-reinforced sections and would possibly affect them in periods of above normal precipitation. Figure 3 shows undrained water standing in this channel approximately 24 hr after rain occurred during construction. The east end of Section 2 which had been completed at the time of the rain is visible.

Maximum frost penetration as calculated at the Sioux Falls weather station (3 miles from the project) is 66 in. Average annual precipitation is 25 in. of moisture, including 44 in. of snowfall. Table 2 gives the monthly rainfall, average temperatures, and other climatological data of the period from January 1961 through July 1963. This includes the entire construction period. Table 3 gives the daily weather records for the paving phase.

DESIGN

Subgrade design was according to standard South Dakota practice. Compaction of the soil was to a minimum of 92 percent of Standard Proctor, AASHO Designation T99-57, Method A, with the upper 12 in. of subgrade requiring a minimum density of 96 percent. Moisture content was held to within 2 percentage points above and 6 percentage points below optimum moisture.

Two types of subbase were used for a combined thickness of 9 in. throughout the continuously-reinforced sections. The lower 6 in. was 2-in. maximum size and the upper 3 in., "subbase cushion," was $3/4$-in. maximum size. Subbase specifications are given in Table 1. The material was produced from a local gravel pit and was manufactured largely by screening with a small amount of crushing. Tests on the material as it was placed on the project showed compliance with specifications. Compaction of the subbase was to a minimum density of 95 percent Standard Proctor, AASHO Designation T99-57 Method D.

For this project, a pavement thickness of 8 in. was chosen for the continuously-reinforced sections using concrete with a compressive strength of 5,000 psi and a flexural strength of 600 psi. The conventional pavement in the control sections had a thickness of 9 in. and used concrete of 3,000-psi compressive strength. Coarse

TABLE 2

SIOUX FALLS AREA CLIMATOLOGICAL DATA

Time Period	Max. Temp.	Avg. Daily Max. Temp.	Min. Temp.	Avg. Daily Min. Temp.	Avg. Monthly Temp.	Monthly Departure from Normal	Precipitation
Jan. 1961	45	25.7	-23	2.7	14.2	0	0.25
Feb. 1961	51	34.2	-13	12.9	23.6	+4.1	0.92
Mar. 1961	67	43.9	18	27.3	35.6	+3.6	1.14
Apr. 1961	81	53.3	17	30.4	41.9	-4.5	1.04
May 1961	86	65.7	25	44.2	55.0	-3.1	4.67
June 1961	98	80.9	43	56.7	68.8	+0.8	3.86
July 1961	95	84.7	52	59.6	72.2	-2.6	2.16
Aug. 1961	98	86.6	51	61.4	74.0	+1.6	1.79
Sept. 1961	92	70.5	28	48.0	59.3	-3.1	2.36
Oct. 1961	84	64.5	22	38.1	51.3	+1.3	2.66
Nov. 1961	62	42.8	13	23.9	33.4	+1.2	1.40
Dec. 1961	56	25.9	-16	6.1	16.0	-3.4	0.80
Jan. 1962	47	23.2	-22	2.3	12.8	-2.4	0.29
Feb. 1962	57	25.4	-31	9.0	17.2	-1.9	4.05
Mar. 1962	55	32.1	-16	17.1	24.6	-5.5	1.72
Apr. 1962	94	57.9	18	33.5	45.7	-0.2	1.70
May 1962	88	73.6	36	52.4	63.0	+4.7	6.07
June 1962	91	77.5	45	57.7	67.6	-0.5	3.98
July 1962	94	80.5	47	60.8	70.7	-3.6	5.50
Aug. 1962	94	83.8	48	59.3	71.3	-0.5	2.77
Sept. 1962	85	71.3	32	47.4	59.4	-2.4	3.58
Oct. 1962	82	64.6	19	40.7	52.7	+2.4	0.46
Nov. 1962	74	49.0	15	28.2	38.6	+6.0	0.16
Dec. 1962	61	33.0	-14	12.3	22.7	+1.6	0.19
Jan. 1963	54	16.6	-22	-3.3	6.7	-8.5	0.90
Feb. 1963	59	30.9	-13	8.7	19.8	+0.7	0.53
Mar. 1963	80	49.8	16	28.1	39.0	+8.9	1.16
Apr. 1963	86	61.5	20	37.3	49.4	+3.5	1.25
May 1963	89	70.6	27	48.2	59.4	+1.1	2.00
June 1963	99	85.0	50	62.0	73.5	+5.4	2.51
July 1963	98	87.1	58	64.5	75.8	+1.5	6.45

TABLE 3

CONSTRUCTION PERIOD WEATHER DATA

Date 1963	Temperature Max.	Temperature Min.	Precipitation (in.)	Wind Average (mph)	Sky Cover (tenths)	Construction Operation
5-25	70	54	Trace	14.5	9	Poured Section 2
5-26	72	57	Trace	13.5	10	Curing
5-27	66	54	Trace	12.0	10	Curing
5-28	74	50	Trace	12.0	5	Curing
5-29	81	44	0	9.2	1	Poured east end Section 1
5-30	87	51	0.20	11.9	9	Curing (holiday)
5-31	71	62	0.12	19.7	10	Completed Section 1
6-1	74	60	0.28	13.5	8	Curing
6-2	82	58	0.14	9.1	8	Curing
6-3	85	63	0	14.9	5	Curing

aggregate was 100 percent crushed quartzite, and the fine aggregate consisted of silicious sand having an average fineness modulus of 2.85. Specifications required 3 to 6 percent air entrainment and a slump of between 2 and 3 in. Type 1 cement was used for all concrete. The contractor on this project elected to use pozzolith, and job mixes using this admixture were designed. General information concerning the continuously-reinforced concrete is given in Table 1. The job mixes for the continuously-reinforced and conventional pavements within this project are given in Table 4.

Because of severe climatic conditions, it was decided to use over 0.6 percent longitudinal steel. This requirement was met with No. 5 deformed bars spaced on 6-in. centers. This provided longitudinal steel at the rate of 0.646 percent of the cross-sectional area of the slab. A further safety factor was the use of A-432 billet steel with a minimum yield point of 60,000 psi (Table 1). Specifications required the steel in 40-ft lengths as it was felt that this was the maximum length which could be easily handled. Transverse steel was also No. 5 deformed bars of the same billet steel spaced on 44-in. centers, 23 ft 10 in. long for a 24-ft pavement width. All longitudinal and transverse steel intersections were tied. Support chair placement under the intersection of every sixth longitudinal bar with every transverse bar provided one support chair ever 1.222 sq yd.

TABLE 4

CONCRETE MIXTURE DATA

| Material	Continuously-Reinforced	Conventional
Cement	523 lb	478 lb
Water	232 lb	225 lb
Fine aggregate	1,166 lb	1,216 lb
Coarse aggregate ($^3/_4$-No. 4)	1,209 lb	1,211 lb
Coarse aggregate ($1^1/_2$-$^3/_4$)	806 lb	807 lb
Air-entraining agent	1.85 oz	1.27 oz
Pozzolith	1.39 lb	1.27 lb

Figure 4. Support chairs for reinforcing steel.

Specifications required that the chairs (Fig. 4) be approved by the State engineers because it was important that the steel be maintained in its proper position during concrete placement.

An 18-in. overlap was specified for the longitudinal steel (approximately 29 diameters). To strengthen the pavement further, a staggered lap lime was chosen—the end of one 18-in. lap being even with the beginning of the adjacent lap. This resulted in the lap line being skewed approximately 18° from the centerline. All overlaps were tied twice to insure against slippage while placing concrete. Figure 5 shows the layout of the steel and the overlaps.

As a research feature, the depth to the center of the longitudinal steel was $2\frac{1}{2}$ in. in Section 1 and $3\frac{11}{16}$ in. in Section 2. The purpose of this variation was to determine if the steel depth has any effect upon crack pattern, depth, or width. A construction tolerance of $\pm \frac{3}{8}$ in. was allowed in both horizontal and vertical placement of the longitudinal reinforcing steel.

A frequent failure location in continuously-reinforced concrete is at the construction joints. To prevent failure and to furnish additional load transfer, additional steel was specified for construction joints. Longitudinal bars that did not extend 4 ft into the
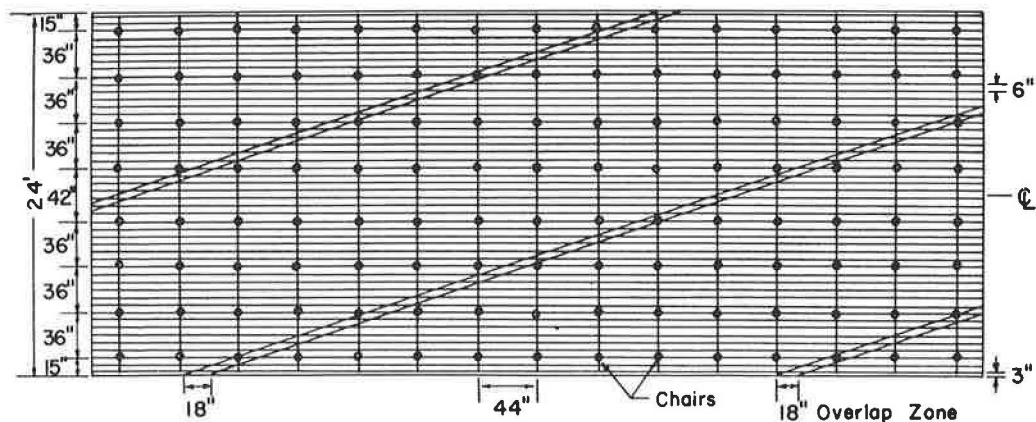
LONGITUDINAL STEEL — No. 5 x 40' Billet Steel A432 — 48 Deformed Bars for 24' Width Provides 0.646% of Cross Sectional Area

TRANSVERSE STEEL — No. 5 x 23' 10" Billet Steel A432 Deformed Bars Spaced on 44" Centers

CONCRETE— 8" Thick, 1 1/2" Max. Size Aggregate. 5000 P.S.I. Compressive Strength, 600 P.S.I. Flexural Strength at 28 Days

DEPTH OF LONGITUDINAL STEEL— Section 1— 2 1/2" and Section 2— 3 11/16" From Surface of Slab to Center of Longitudinal Steel

OVERLAP OF LONGITUDINAL STEEL— 18" Overlap Staggered as Shown (18" = 28.8 Diameters)

SPECIAL SUPPORTING CHAIRS— One Per 1.222 Sq. Yd.

Not To Scale

Figure 5. Plan showing steel and overlap layout.

back-slab or 6 ft into the fore-slab were spliced with additional 10 ft long No. 5 bars placed to extend 6 ft into the fore-slab. In addition, 18 in. long 1-in. dowel bars were placed on 24-in. centers, starting 12 in. from the edge of the slab. Figure 6 shows the steel placement at a construction joint.

Two different types of terminal joints were used (transverse lug end anchors and wide-flange joints). The wide-flange joints were used in Section 1 and consisted of a 10-in. wide-flange beam weighing 100 lb/ft and shaped to conform to the crown of the pavement. The beam was placed in a 8-in. thick reinforced-concrete sleeper slab. Figure 7 shows the I-beam and reinforcing steel in place prior to pouring the sleeper slab, and Figure 8 shows continuously-reinforced concrete in place against the beam. Steel plates were welded to each end of the beam to prevent the intrusion of subbase material between the beam and the pavement during cold weather pavement contraction. Figure 9 shows the design details of the sleeper slab and I-beam. The portion of the sleeper slab upon which the continuously-reinforced pavement rested was finished as smoothly as possible to prevent interlock of the pavement and the sleeper slab. Friction

Figure 6. Construction joint design.
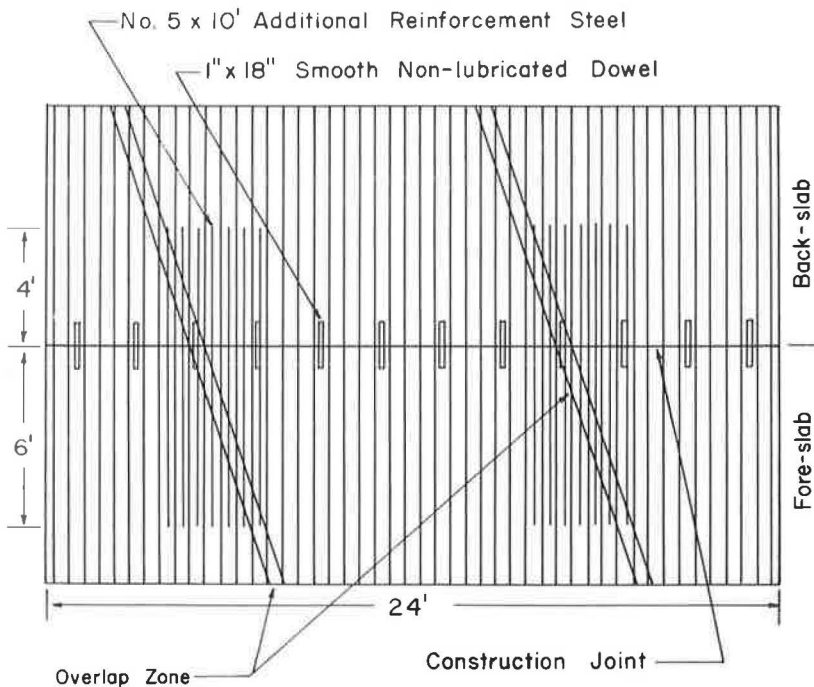
All No. 5 Deformed Longitudinal Bars Which do not normally extend at least 6 feet into the Fore-slab beyond a Construction Joint, or 4 feet into the Back-slab, are spliced with No. 5 deformed bars, 10 feet long, extending 6 feet into the fore-slab.

In addition, the Construction Joint is reinforced with 1" x 18" smooth dowels, non-lubricated, spaced 24" center to center and 12" from edge of pavement, and at one-half the depth of pavement.

Splice bars and dowels are of billet steel.

was further reduced by a coating of asphalt placed upon that side of the I-beam and slab prior to pouring the pavement. A rougher, nonlubricated surface was constructed on the side of the sleeper slab that held the conventional pavement.

Three end-anchor lugs were placed at each end of Section 2. The reinforced end anchors, 5 ft deep and 2 ft thick, were cast separately to the full width of the pavement. A keyway was formed into the top of each lug to aid in transmitting pavement stresses
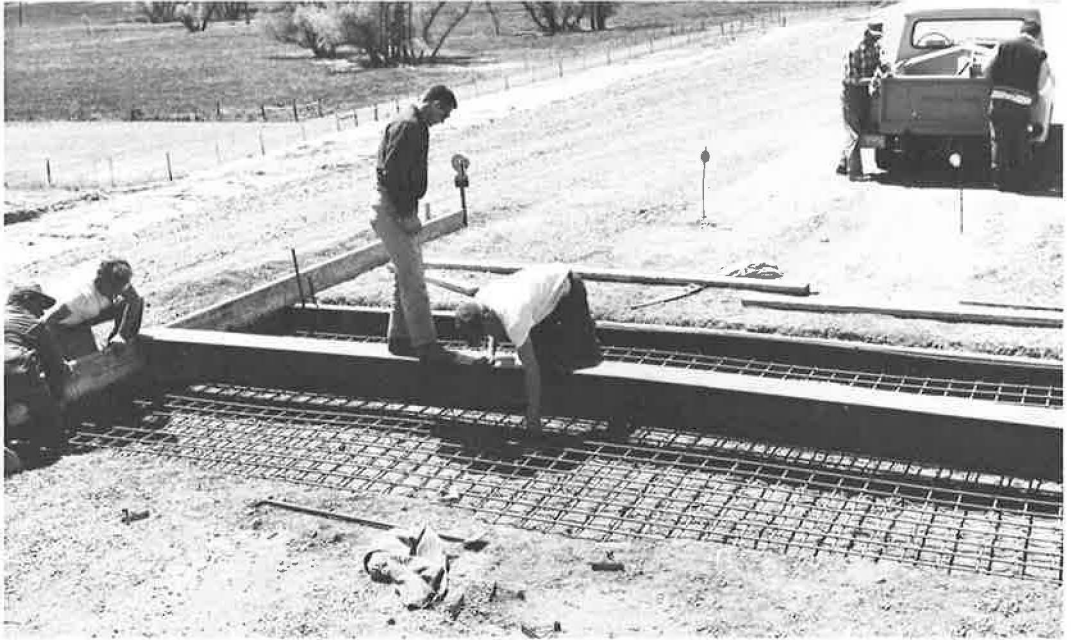

Figure 7. Wide-flange end joint prior to pouring sleeper slab.

Figure 8. Continuously-reinforced concrete in place against wide-flange beam.

to the anchor lug. A completed end-anchor lug is shown in Figure 10. The pavement thickness was increased to 10 in. in the region of the end anchor lugs. Figure 11 shows design details of the end anchors.

Three expansion joints with 46.5-ft spacing were placed in the conventional pavement at the ends of each section. These joints consisted of 1 in. of mastic with lubricated dowel bars $1\frac{1}{4}$ in. by 18 in. long spaced on 12-in. centers. The top of the joint was sealed with rubber asphalt filler.

As previously mentioned, the control sections were designed and built according to standard South Dakota pavement designs. Subgrade and subbase requirements were the same as the continuously-reinforced sections with the exception of subbase thickness. Standard design procedures specified different subbase thicknesses in the control sections, while a uniform 9-in. thickness was used in the test sections to limit the variables.

Figure 12 shows the total subbase thicknesses of both pavement designs. Conventional designs specify a 9-in. pavement thickness with welded-wire fabric reinforcement placed $2\frac{1}{2}$ in. below the surface. The reinforcement must weigh not less than 60 lb per 100 sq ft and consists of No. 1 longitudinal wires on 6-in. centers with No. 4 transverse wires on 12-in. centers. The ends of the mesh are lapped 12 in. Concrete having a compressive strength of 3,000 psi is used. Thirty-inch long No. 5 bars are placed every 48 in. across the pavement centerline as tie bars. One and one-fourth inch diameter are placed mid-depth in the pavement on 12 in. centers at contraction joints. These transverse joints are spaced at 46 ft 6 in. Expansion joints are normally specified only at structures.
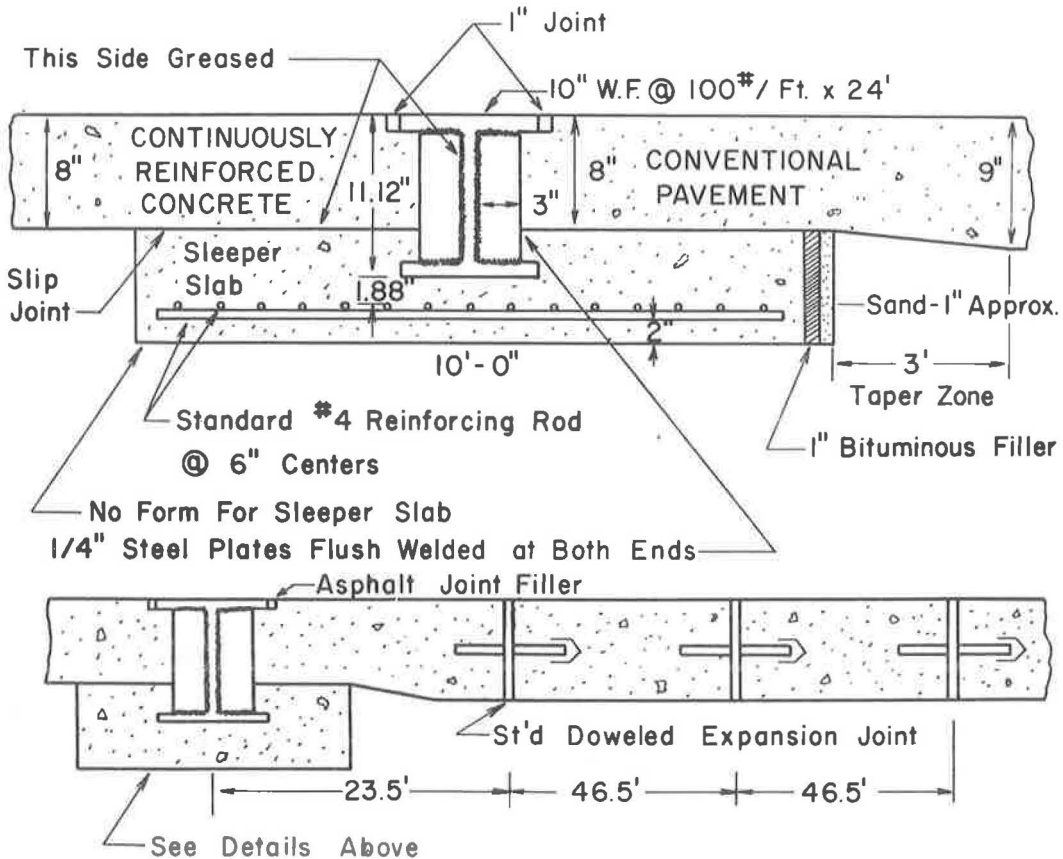

Figure 9. Wide-flange joint design details.

Figure 10. Completed end-anchor lug.

The longitudinal joint was sawed to one-fourth the depth of the pavement for both the conventional and continously-reinforced sections. Transverse joints on the conventional pavement were formed with steel contraction joint inserts that were later crimped for placement of the sealing compound.

Conventional shoulder design was used throughout a 4-ft inner and 10-ft outer shoulder, and both were covered with a 2-in. thickness of bituminous material.

CONSTRUCTION

Grading operations were carried out in 1961 and 1962. No unexpected difficulties were encountered, and this work was completed on schedule. The subbase was placed during the fall of 1962. Depth checks made subsequent to this showed plan thicknesses to be present.

The end-anchor lugs and I-beam sleeper slabs were constructed approximately a week prior to pouring the pavement. The lugs were simple to construct because no forms were required except to shape the top of the lug.

In order to maintain the wide-flange beam at the proper elevation in the sleeper slab, the contractor tack-welded the ends of the beam to paving forms that had previously been placed to grade (Fig. 7). The reinforcing steel was then placed under the beam, tied, set on chairs, and the concrete poured.
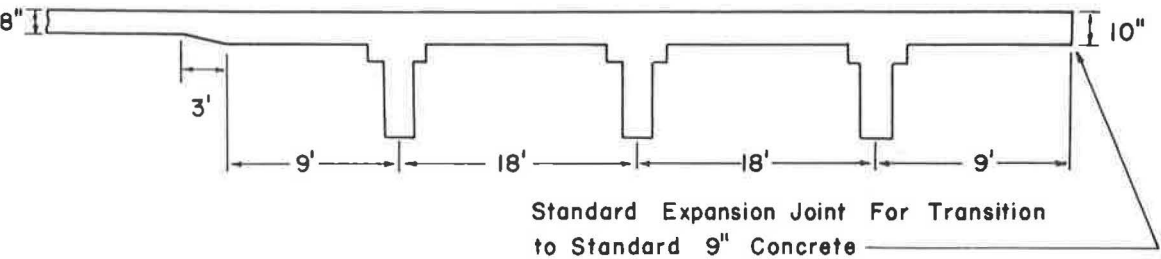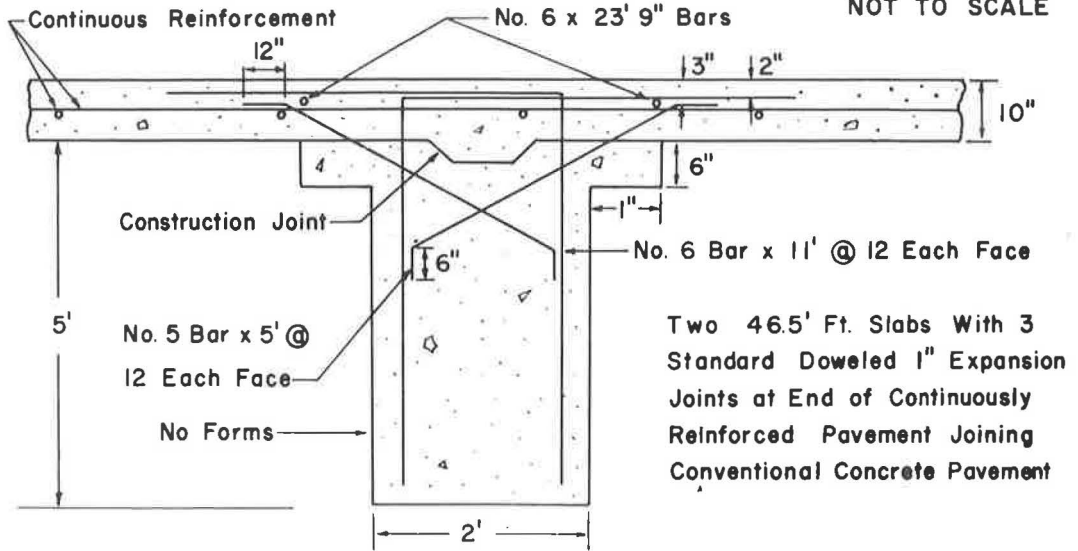
164

Figure 11. Design details of transverse lug end anchorage.
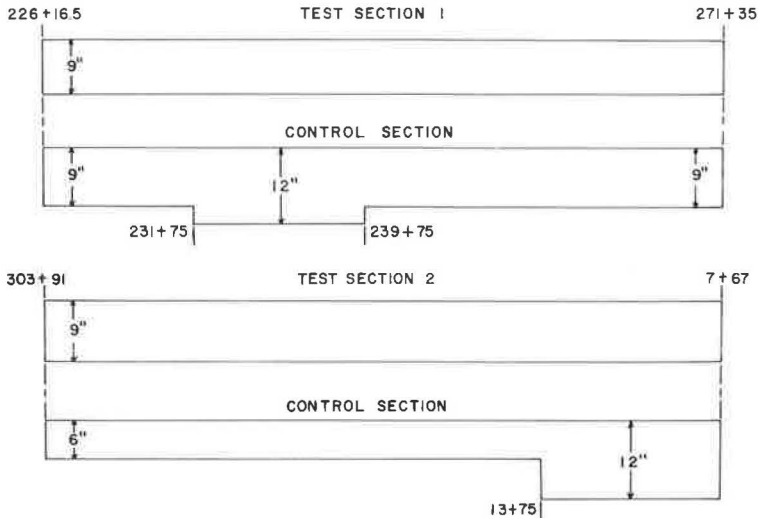

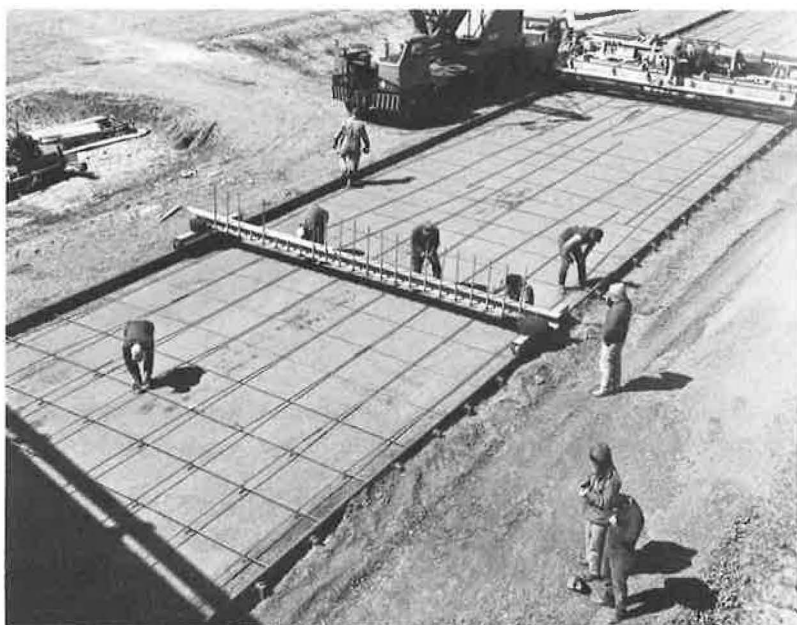Figure 12. Total gravel subbase thickness for both pavement designs.

Figure 13. Reinforcing steel operational sequence.

Fine-grading was completed and the forms were set in place before any steel was placed. The forms were then marked and the transverse steel was laid in position on the grade. Every sixth longitudinal bar was laid on top, and both the overlaps of this longitudinal steel and its intersections with the transverse steel were tied. Chairs were then placed under the transverse steel to lift it to its proper elevation. Figure 13 shows this operational sequence. The first eight longitudinal bars were spaced using steel rods welded on an old scratcher. The remaining bars were then carried into place and tied, spacing them from the original eight bars. As previously mentioned, all transverse and longitudinal steel intersections were tied, and all overlaps were tied twice. Figure 14 shows the steel in place before pouring concrete in Section 1.

Section 2 was paved on May 25, 1963. The paving train consisted of two 34-E dual-drum pavers, one spreader, one screed, one bull float, two finish men, a belting machine, and a burlap drag. Ten spud-type vibrators attached to the front of the screed were used to consolidate the concrete. Care was taken to prevent contact of the vibrators with the reinforcing steel because this would dampen their effect.

Section 1 was paved on May 29 and 31. The paving train was identical with the exception of an additional screed and the use of a pan vibrator instead of the spud-type vibrators. This was found to be necessary in this section because of the shallower steel that would not permit full immersion of the spud vibrators within the concrete.

Curing was accomplished with reflective plastic sheeting placed upon the slab for a minimum of 72 hr. The weather during the paving and curing period was variable (Table 3).

No movement of the steel was noticeable while placing the concrete. One 100-ft long section at station 17+00 to 18+00 where only every other transverse and longitudinal steel intersection was tied was observed to move excessively. This tie arrangement was used to see if it was possible to reduce the steel tying labor. When movement was observed, the practice was discarded. No difficulty was encountered in getting the concrete to flow around the reinforcing steel.

Figure 14. Reinforcing steel in place.

The stationing was marked in the pavement every 100 ft to facilitate observation and testing after construction.

Hourly temperature measurements were taken of the concrete as it left the paver. A maximum temperature of 72 F and a minimum of 60 F were recorded with an average concrete temperature of 66 F. Although the weather resulted in above normal temperatures during the curing period, the plastic during membrane reflected sufficient heat to keep the pavement quite cool. Upon removal of the plastic after 72 hr, there were no visible cracks other than a few shrinkage cracks. Transverse pavement cracking first began to appear the day after the curing plastic was removed.

TESTING PROGRAM

In addition to the previously mentioned construction testing, a testing program of indefinite duration is to continue. This program includes crack-width measurements, end movement surveys, and present serviceability index studies.

As rapidly as cracks developed, holes were drilled on each side of the crack and brass plugs cemented into the holes. These plugs were then drilled so that measurements of crack width and movements could be made with a 10-in. Whittemore strain gage. A minimum of 12 selected cracks in each end and central 500-ft section of both

TABLE 5

MAXIMUM CRACK WIDTH MEASUREMENTS

Section 1 (avg. 0.008 in.)			
West End (in.)	Center (in.)		East End (in.)
0.009	0.005	0.006	0.010
0.007	0.007	0.007	0.010
0.004	0.013	0.006	0.010
0.012	0.006	0.009	0.005
0.010	0.008	0.003	0.011
0.012	0.005	0.006	0.012
0.012	0.007		0.008
0.009 average	0.007 average		0.009 average

Section 2 (avg. 0.011 in.)			
0.008	0.010	0.006	0.010
0.015	0.012	0.014	0.011
0.007	0.015	0.010	0.021
0.012	0.012	0.009	0.013
0.013	0.013	0.010	0.009
0.011	0.007	0.010	0.013
0.010	0.009		0.006
0.011 average	0.011 average		0.012 average

continuously-reinforced sections will be measured. These measurements will be made during August and January of each year when the air temperatures are over 100 F and less than -20 F, respectively. Crack location surveys will be conducted in the same 500-ft sections during September, December, March, and June during the first year after construction and each fall thereafter.

Permanent reference points free from frost action have been placed at the ends of each continuously-reinforced section, and measurements will be made of pavement end movements during the hottest and coldest periods of each year to determine the range of end movement. The measurements will be made from the reference points with a transit, and the distance from the line of sight to a permanently established point in the pavement, approximately 6 in., will be measured with a ruler graduated to 0.02 in. In addition to continuously-reinforced sections' end movement, movement of the sleeper slab I-beam and the conventional pavement at the ends of Section 1 will also be measured.

Pavement temperatures will be taken at the time of the crack measurements. These temperatures will be obtained from mercury-filled temperature wells that were installed during pavement construction.

The present serviceability indexes of the test and control sections will be determined annually with a BPR-type roughometer. This roughometer has been correlated with CHLOE profilometers and a PSI formula developed. Traffic counts and axle-load weights will be obtained once each year.

In August 1963, four cores were drilled over cracks in the test sections. It was found that three of the four cracks followed transverse reinforcing bars. Longitudinal steel was found to be within $\frac{1}{4}$ in. of the plan depth within the slab. There was no apparent difference in the quality of vibration produced by the spud and pan vibrators. Some porosity was found in cores which had been vibrated by either method.

Although the crack patterns are not yet fully developed, a slight difference between the two sections is apparent. In Section 1, with the shallower steel, the average crack spacing exclusive of the section ends is approximately 2.3 ft. The majority of the cracks in this section are on a 1- to 2-ft spacing with occasional unbroken pavement 10 to 15 ft in length. The influence of the unrestrained pavement ends is shown by a diminishing crack pattern starting approximately 120 ft from the east end and 500 ft from the west end of Section 1. There are no cracks in the final 100 ft of either end of this section. Maximum measured movement of the pavement ends at the I-beams has

been 0.074 in. at the east end and 0.095 in. at the west end with a pavement temperature of 2 F.

Section 2 with the steel placed nearly at mid-depth has an average crack spacing of 3 ft. The crack frequency is somewhat less within 100 ft of the end-anchor lugs because of slight movement of the lugs. Measurements have shown this movement to be 0.068 and 0.046 in. on the east and west ends of this test section, respectively. However, cracks are present up to and between the anchor lugs.

Crack widths are small in both sections. The crack widths as measured by a 10-in. Whittemore strain gage are given in Table 5. The values listed are for the measured widths of 27 selected cracks at the 500-ft end and central portion of each test section. These measurements represent the maximum reading obtained for each crack since test section construction.